Biomechanical Analysis

of the

Achilles Tendon Enthesis Organ

A thesis submitted in partial fulfilment for the degree of PhD by:

Peter Theobald

Institute of Medical Engineering & Medical Physics,
Cardiff University, UK.

ProQuest LLC
789 East Eisenhower Parkway
P.O. Box 1346
Ann Arbor, MI 48106-1346

Summary

The tendon/ligament insertional region is a common site of injury, despite the protection offered by the surrounding tissues. These tissues, termed the enthesis organ, form a concept that has only recently been developed and thus has been the focus of only a few publications. The work in this thesis is the first study to perform a biomechanical analysis of the enthesis organ, providing information that may potentially improve injury management methods.

A thorough assessment of the enthesis organ biomechanics was made using a number of techniques. Dissecting room cadavers allowed for micro- and macroscopic examination, whilst magnetic resonance imaging and ultrasound provided *in vivo* images and movie files. Specially fabricated apparatuses were also developed to investigate the load bearing and lubrication regime.

A number of the structures within the enthesis organ were identified as being of biomechanical importance. The paratenon/deep fascia was recognised as influencing the insertional angle of the Achilles tendon, possibly in tandem with the superior tuberosity. It was Kager's fat pad, however, that appeared the most highly specialised and influential tissue. This is currently excised when performing arthroscopic ankle surgery, although microscopic examination revealed a highly specialised structure with 3 separate regions. These appeared to allow independent movement of its distal wedge into the retrocalcaneal bursa, a movement that was hypothesised to both equalise a pressure change and to lubricate the contacting surfaces of the enthesis organ.

This work concludes that the surgical removal of Kager's fat pad is likely to starve the Achilles tendon enthesis organ of a number of biomechanical functions performed by this tissue, and thus may influence pain relief post-operatively. The excision of the superior tuberosity, however, appears insignificant as it not believed to increase the likelihood of enthesis failure, although preservation of both the superior tuberosity and the deep fascia/paratenon would ensure continued regulation of the Achilles tendon insertion angle.

Acknowledgements

The work in this thesis has only been possible following the assistance of many people. I am grateful to Prof. Graeme Bydder (University of California, San Diego) and Dr. Neil Pugh (University Hospital of Wales, Cardiff) for their patience and efforts in collecting the clinical images required. Thanks are also due to Dr. Siva Kulasegaram & Dr. Terry Bennett for their assistance in producing a computational model of the Achilles tendon enthesis organ, and to Dr. Carl Byrne & Prof. Duncan Dowson for their ideas and suggestions in the development of the friction apparatus. The success of this and other rigs would not have been possible without the skill and experience of both the electrical and mechanical technicians, especially Mr. Alan Griffiths, Mr. Paul Farrugia & Mr. David Hobbs; the help and support of Dr. Sam Evans was also greatly appreciated.

I am indebted to the knowledge, advice and ideas of my supervisors: Prof. Len Nokes, Prof. Michael Benjamin & Prof. Colin Dent, without whom I would not be in this position. Of importance too have been Jonathan Haynes and Matthew House, both of whom have ensured my time outside of work has been most enjoyable.

My greatest thanks, however, are reserved for my family and Sarah. Without their support and encouragement, patience and advice, this thesis would never have completed.

Table of Contents

List of Figures

Chapter 2

Chapter 3

Chapter 4

Chapter 5

Chapter 5

List of Tables

Chaper 3

Abbreviations

A	Anterior aspect of Kager's fat pad
AR	Arm
AT	Achilles tendon
B	Ball bearing
BPW	Bursal protruding wedge
C	Calcaneus
D	Rotating disc
DP	Deep fascia/paratenon
DRF	Dorsiflexion
E	Enthesis
ECM	Extracellular matrix
EF	Enthesis fibrocartilage
EPP	Enthesis proximal point
FC	Femoral condyle
FHL	Flexor hallucis longus
GAG	Glycosaminoglycan

GS	Gastrocnemius/soleus muscle belly
H	Specimen holder
HA	Hyaluronic acid
K	Kager's fat pad
LM	Lateral malleolus
LVDT	Linear variable displacement transducer
M	Meniscus
MCP	Metacarpophalangeal joint
MM	Medial malleolus
MRI	Magnetic resonance imaging
Neut	Anatomical neutral position of ankle flexion
P	Posterior aspect of Kager's fat pad
PF	Periosteal fibrocartilage
PLF	Plantarflexion
PMMA	Polymethylmethacrylate
PR	Pillar
Ra	Average surface roughness

RCB	Retrocalcaneal bursa
S	Superior tuberosity
SF	Sesamoidal fibrocartilage
SP	Spring
ST	Superior tuberosity
t	Tidemark
TP	Tibial plateau
US	Ultrasound

Nomenclature

Symbol	Parameter	Units
A	Enthesis cross sectional area	m^2
AT_D	Perpendicular distance between ankle axis and the Achilles tendon	m
AT_F	Achilles tendon tensile load	N
D_H	Specimen holder to pivot distance	m
D_S	Spring mounting point to pivot distance	m
F	Achilles tendon tensile force	N
F_H	Specimen holder frictional force	N
F_S	Spring force	N
K	Spring constant	N/mm
L	Load	N
M_{ankle}	Ankle moment	N.m
n	Number of asperities	
N_H	Specimen holder reactant load	N
Ra	Surface roughness	μm

R^2	Coefficient of determination	
S	Reduced Sommerfeld number	$mm.s^{-1}/N$
V	Sliding speed	$mm.s^{-1}$
x	Spring extension	mm
z_i	Asperity amplitude	μm
ΔV	Potentiometer voltage change	V
θ	Angle of arm rotation	Degrees
τ	Enthesis shear stress	MPa
γ	Achilles tendon insertional angle	Degrees
μ	Coefficient of friction	

Glossary

Planes of imaging:

Sagittal	The plane that runs parallel to the longitudinal axis through the body, dividing it into left and right parts.
Coronal	The plane that runs parallel to the longitudinal axis through the body, dividing it into front and back parts.
Transverse	The plane of section that runs perpendicular to the longitudinal axis of the body, dividing it into upper and lower parts.

Anatomical orientation:

Medial	Towards the midline of the body
Lateral	Farther from the midline of the body
Superior	Towards the top of the body
Inferior	Farther from the top of the body
Anterior	Towards the front of the body
Posterior	Farther from the front of the body

Degrees of freedom of the ankle joint

Dorsiflexion	Upwards movement of the foot
Plantarflexion	Downwards movement of the foot

Miscellaneous:

Asymptote	A position on a graph where the differential (i.e. gradient) is equal to zero
Biotribology	The study of friction in biological systems
Diaphysis	The mid-section of a long bone
Eccentric	Lengthening of the muscle fibres caused by application of an external load
Epiphysis	The end of a long bone
Gold standard	A methodology/design that is used as a measure of success
In viva	Outside the human body
In vivo	Within the human body
Sample Point	A position where a number of histological sections are collected from
Section	A single histological slice
Tribology	The study of friction in mechanical systems

1, Introduction

1.1 Introduction

The concept of the Achilles tendon enthesis organ has recently been developed to describe a collection of neighbouring tissues that protect the Achilles tendon insertion site. This site, or enthesis, is the interface between the largest tendon in the body and the largest bone in the foot **[1]**. Through the Achilles tendon and across the interface, the contractile force generated by the gastrocnemius and soleus muscles of the lower leg is transferred to the calcaneus, serving to plantarflex the foot. The ability of the Achilles tendon to withstand loading >9kN **[2]** is indicative of the potential magnitude of this force.

Since the enthesis organ was first hypothesised **[3]**, a number of studies have further developed the concept, focussing mainly on the biological aspects of the enthesis organ **[4-13]**. Whilst a number of studies have alluded to the possible biomechanical functions of the enthesis organ, only studies investigating the biomechanics of individual components within the enthesis organ have been published. Therefore, the influence of these structures upon the gross biomechanics of the enthesis organ has never been considered.

Despite its protective role, injuries to the components of the Achilles tendon enthesis organ are prevalent. The Achilles tendon, for example, is the most commonly ruptured of all tendons **[14]**. Caused by the tendons inability to withstand the mechanical loading associated with physical activity, ruptures typically occur in individuals who are normally sedentary but engage in occasional strenuous physical activity **[14]**. The Achilles tendon is also commonly injured through overuse **[15]**, with elite athletes particularly vulnerable **[16, 17]**. Probably caused by repetitive training regimes, many such athletes never regain their pre-injury performance levels **[18]**.

The Achilles tendon enthesis organ is also known to inadvertently injure itself, with Haglund's disease caused by one of the structures being impinged between two of the other structures **[19]**. Conservative treatments are available to relieve pain, although in instances where surgery is necessary success rates range between 69 - 82% **[20-22]**. Injuries to the enthesis, termed enthesopathies, also occur (including well-known

conditions such as tennis elbow and golfer's knee), although it is apparent from the recent review by Benjamin et al.**[7]** that, whilst the consequences of enthesopathies are being investigated biologically, any related biomechanical studies are focussing solely upon the Achilles tendon. Thus, whilst enthesopathies account for up to 50% of injuries for athletes who exercise daily **[23]**, the biomechanical causes and consequences are still unknown. Therefore an improved understanding of the biomechanics of this field may allow for a reduction in such injuries, and an improvement in their management.

The work in this thesis provides the first report on the biomechanics of the enthesis organ. Examining the Achilles tendon enthesis organ in particular, the key biomechanical roles of a number of the components were identified. The interdependency of these structures was also considered, providing information that may ultimately allow for improved methods of treatment.

This work focuses predominantly on the Achilles tendon enthesis organ, previously described as the premiere enthesis **[24]**. The Achilles tendon enthesis organ is examined for evidence of biomechanical functions of which the importance has previously been reported in other areas of the body. The role of soft tissues in load bearing **[25-28]**, in improving joint lubrication **[25, 26]** and stability **[25]** are all factors that are currently overlooked when treating enthesopathies and other enthesis organ injuries and yet, when considered when treating other areas of the body, have been seen to cause significant improvement in results **[29]**.

A number of different methods were utilised to examine the enthesis organ. Magnetic resonance imaging (MRI) and ultrasound (US) were used to provide static and dynamic *in vivo* images, whilst dissecting room cadavers allowed for both micro- and macroscopic analysis. The biomechanical advantage generated by components of the enthesis organ was then determined by the development of a number of protocols, whilst a variety of apparatuses were designed to examine the extent of lubrication and load bearing.

Thus, this thesis provides a thorough and detailed investigation in to the biomechanical functions of the Achilles tendon enthesis organ.

2, The Achilles Tendon Enthesis Organ

2.1 The Achilles Tendon Enthesis Organ

The Achilles tendon originates at the gastrocnemius and soleus muscles of the lower leg and inserts into the calcaneal bone of the foot. The Achilles tendon insertion, or enthesis, consists of a series of 4 tissues **[30]**, acting to dissipate the stress away from the soft-hard tissue interface **[31]**. More recently, the significance of the tissues neighbouring the enthesis have been recognised as providing additional strength and protection to the soft tissue insertion, thus further reducing the risk of failure **[32]**. Due to their similar function, this collection of tissues has been termed the *enthesis organ* **[3]**. Presented in Figure 2.1.1, the components of the Achilles tendon enthesis organ are listed below and shall be discussed in detail within this Chapter:

- The Achilles tendon
- The calcaneus
- The superior tuberosity
- The periosteal fibrocartilage
- The sesamoidal fibrocartilage
- The enthesis fibrocartilage
- Kager's fat pad
- The retrocalcaneal bursa

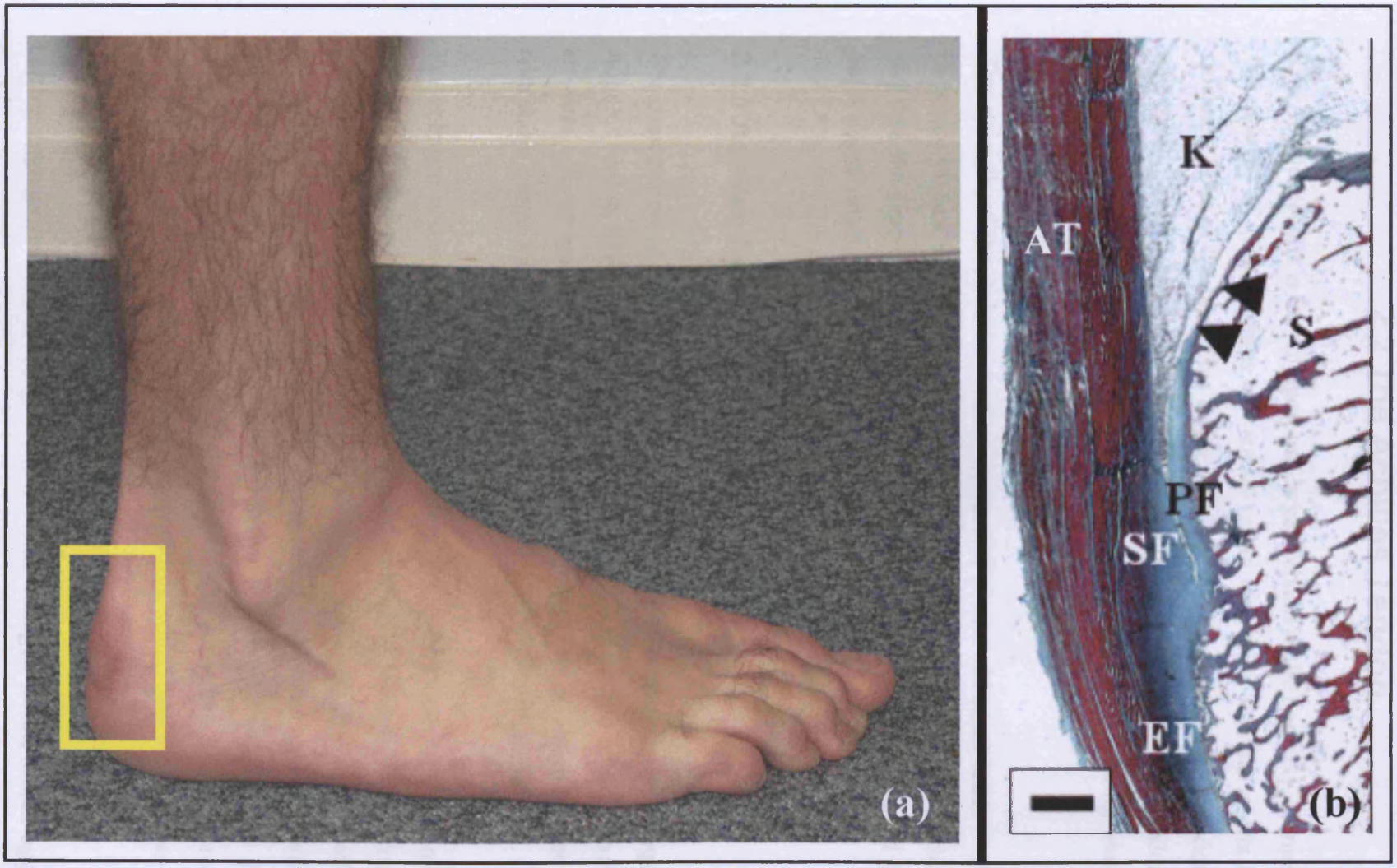

Figure 2.1.1: The Achilles tendon enthesis organ. (a) A macroscopic image of the right foot in the sagittal plane, with the region of the Achilles tendon entheisis organ identified. (b) A low powered histological section of the Achilles tendon enthesis organ in the sagittal plane, stained with Masson's trichrome. AT = Achilles tendon, EF = Enthesis fibrocartilage, K = Kager's fat pad, PF = Periosteal fibrocartilage, S = Superior tuberosity, SF = Sesamoidal fibrocartilage, Arrow heads = retrocalcaneal bursa. Scale bar = 3mm.

2.2 The Achilles Tendon

The Achilles tendon is the strongest and largest tendon in the body **[1]**. It originates at the muscles of gastrocnemius and soleus within the lower leg, and inserts into the calcaneal bone of the foot. This forms a linkage that allows for plantarflexion of the ankle joint, a vital locomotive function. Less obviously, the Achilles tendon - like other tendons - also prevents excessive joint displacement from occurring when under high loading, and thereby preventing joint injury **[33, 34]**.

The strength of the Achilles tendon means that it can withstand loads > 9kN **[2]**. Exposure to such levels of loading is typically associated with sporting participation, and thus the reported 59% of Achilles tendon ruptures being sports-related **[15, 35, 36]** is not surprising. This compares to only 2% of other tendon ruptures **[35]** .

2.2.1 Achilles Tendon Composition:

The composition of the Achilles tendon is significant in influencing its strength. The Achilles tendon, like other tendons, comprises collagen fibres and elastin embedded in an extra cellular matrix (ECM). The ECM is formed from proteoglycan and water, with water comprising 60-80% of the total tendon weight **[35]** (Figure 2.2.1).

The collagen within the Achilles tendon is mainly Type I collagen. This molecule consists of 3 polypeptide chains containing approximately 100 amino acids (coiled in a left-handed helix). The 3 chains are linked in a right-handed triple helix, with intra- and inter-chain bonds ensuring stability. Collagen molecules then aggregate within the extracellular matrix, staggering slightly relative to one another to allow for the alignment of oppositely charged amino acids. These molecules then cross-link between their "heads" and "tails" to form microfibrils, which then further cross-link to form fibrils (Figure 2.2.2).

Further aggregation of the collagen fibrils forms collagen fibres, which aggregate further and are wrapped in endotenon to produce a fascicle. The endotenon contains

both the nervous and vascular supply of the Achilles tendon, whilst also encouraging minimal friction as the fascicles slide past one another on muscular contraction. The fascicles are then enveloped in an epitenon and paratenon, producing the largest - and so the strongest **[37]** tendon in the body, the Achilles tendon.

2.2.2 Achilles Tendon Vascularisation:

Despite the surrounding epitenon and paratenon of the Achilles tendon being highly vascular **[38]**, the blood supply to the Achilles tendon itself is poor. The blood is supplied predominantly from vessels of the anterior paratenon, deriving from the posterior tibial artery **[21, 38-40]**. It is unclear whether the vessels are uniformly distributed throughout the length of the paratenon **[38]**, or if greater blood flow occurs at the enthesis **[21]**, as evident in the foetal Achilles tendon-muscle-bone complex **[41]**. It is also recognised that the blood flow is dependant upon both age **[42]** and exercise **[43]**.

The proximal third of the Achilles tendon receives additional, although not significant, blood supply through vessels of the muscle bellies continuing into the tendon endotenon **[39, 43-47]**. The distal third of the tendon also receives additional vascularisation from small vessels (less than 300μm in diameter **[44]**) of the rete arteriosum calcaneare, fed by the fibular and posterior tibial arteries. These small vessels start at the margin of the insertion and continue proximally for approximately 2cm along the endotenon **[39, 40, 44-47]**.

With both the distal and proximal sections of the tendon receiving additional supply, it could be assumed that the tendon mid-section is relatively avascular. However, whilst avascularity has been identified in the Achilles tendon mid-section **[44, 46, 48]**, it has also been identified in the insertion **[38, 42, 43, 49]**, the insertion and mid-section **[39]**, and the mid-section and origin **[21]**.

Whilst the exact region of avascularity is unclear **[39, 40, 43-48, 50]**, it appears to coincide with an area of concentrated stress 2-5cm proximal to the Achilles tendon enthesis **[51, 52]**. It has been speculated that this stress causes avascularity **[53]**, or

that the twisting of the Achilles tendon as it spans between the muscles and bone act to wring its own vascular supply **[35, 54]**. Its development is also thought to be triggered by **[55]**, or to trigger **[56]**, the development of fibrocartilage.

Avascularity is believed to cause Achilles tendon degeneration **[39, 41, 46]**, thereby decreasing its tensile strength **[44, 45, 57, 58]**. Whilst this may be directly responsible for the increased likelihood of rupture **[21, 38, 39, 42, 44, 46, 59]**, avascularity may also indirectly cause rupture as a consequence of degenerative change **[39, 41, 46]**. Regardless of the method of failure, however, as approximately 80% **[56]** of Achilles tendon ruptures occur at the midsection **[60-62]**, a correlation with avascularity does seem probable. Although this was suggested over 40 years ago **[44]** it is yet to have unanimous support **[21]**.

2.2.3 Achilles Tendon Biomechanical Properties:

Whilst the Achilles tendon is capable of resisting high tensile forces, tendons must also satisfy both kinematic (i.e. flexibility to bend at joints) and damping requirements (i.e. absorption of sudden shock to limit damage to both tendon and muscle) **[16]**. The characteristic strength and flexibility of a tendon is given by the mechanical stability of collagen, allowing it to withstand *in vivo* stresses peaking at approximately 111MPa during running **[63]**, compared to most other tendons which experience peak stresses <30 MPa **[64, 65]**.

The Achilles tendon can also be regarded as a stiff biological spring, as it continually stretches and recoils during the gait cycle **[16]**. The viscoelasticity of the Achilles tendon **[51, 66, 67]** means that at lower strain rates the tendon is less stiff, thus absorbs more energy and hence is less efficient. Conversely, at high rates of loading it has higher strength, thus absorbs less energy and is more efficient **[68]**. This viscoelastic property also affects Achilles tendon failure, with the tensile strength increasing at higher strain rates **[65]**.

The elasticity of the Achilles tendon is due to the wavy nature of the collagen fibres when the tendon is relaxed (Figure 2.2.3). A low axial strain straightens the collagen

fibres **[69-72]**, giving an initial elasticity **[52, 73]** (Figure 2.2.3: zone 1). Once the fibres are straightened, continued loading is resisted by an increased stiffness (the strain rate determines the exact appearance) (Figure 2.2.3: zone 2). At high loading partial failure occurs as the collagen crosslinks fail, thus the collagen fibres - lubricated by proteoglycans **[74, 75]** - slide past one another **[33, 76]** (Figure 2.2.3: zone 3). Whilst complete macroscopic failure typically requires a load of approximately twice that of the associated muscle **[35]** - and as tendons are unlikely to be strained beyond 4% in vivo, failure is usually due to existing degeneration **[35]** (Figure 2.2.3: zone 4). Failure of healthy tendon has, however, previously been reported in an extreme, unfavourable environment **[33, 77]**.

2.2.4 Achilles Tendon Injury:

When the force exerted on the Achilles tendon exceeds its ultimate tensile strength, catastrophic failure may occur, although this risk is minimised by the Achilles tendon remodelling in response to prolonged exercise **[14, 35, 73]**, with the thickness, cross-sectional area and strength all increasing **[78-80]**. The collagen concentration does not increase **[78]**, however, which is a possible reason for the Achilles tendon being the most commonly injured and ruptured tendon in the human body **[35]**.

The Achilles tendon is also the most common site of overuse injury in both men and women **[15]**. This typically occurs as a result of repeated loading that exceeds the elastic limit of the tendon causing microscopic injury **[52, 70, 71, 81]**. Typically, the micro- and macroscopic tendon structure degenerates, causing inflammation, oedema, pain and weakening **[35]**.

The Achilles tendon is most at risk from traumatic injury when loaded at a high strain rate, or following eccentric muscular contraction **[51, 52, 68, 82]**, and thus it is a common cause of complaint in athletes **[54, 83, 84]**. Approximately 7 per 100,000 males experience Achilles tendon rupture **[85, 86]**, typically at ages 30-39 years **[86]**. The decrease in tendon tensile strength with age **[87]**, probably when combined with a change in lifestyle, means that rupture rates peaks in females aged 80 years and over

[86]. In both instances rupture typically occurs at the midsection **[60-62]**, and thus coinciding with avascularity **[21, 38, 39, 44, 46, 88]**.

Whilst the aetiology of rupture in this region remains unclear **[51]**, on healing the collagen fibres of the injured region are replaced by fibrotic scar tissue, meaning a changed structure and organisation. However, despite an improvement over a long period of time **[89]**, the repaired tendon will always have properties inferior to the normal healthy tendon **[90, 91]**.

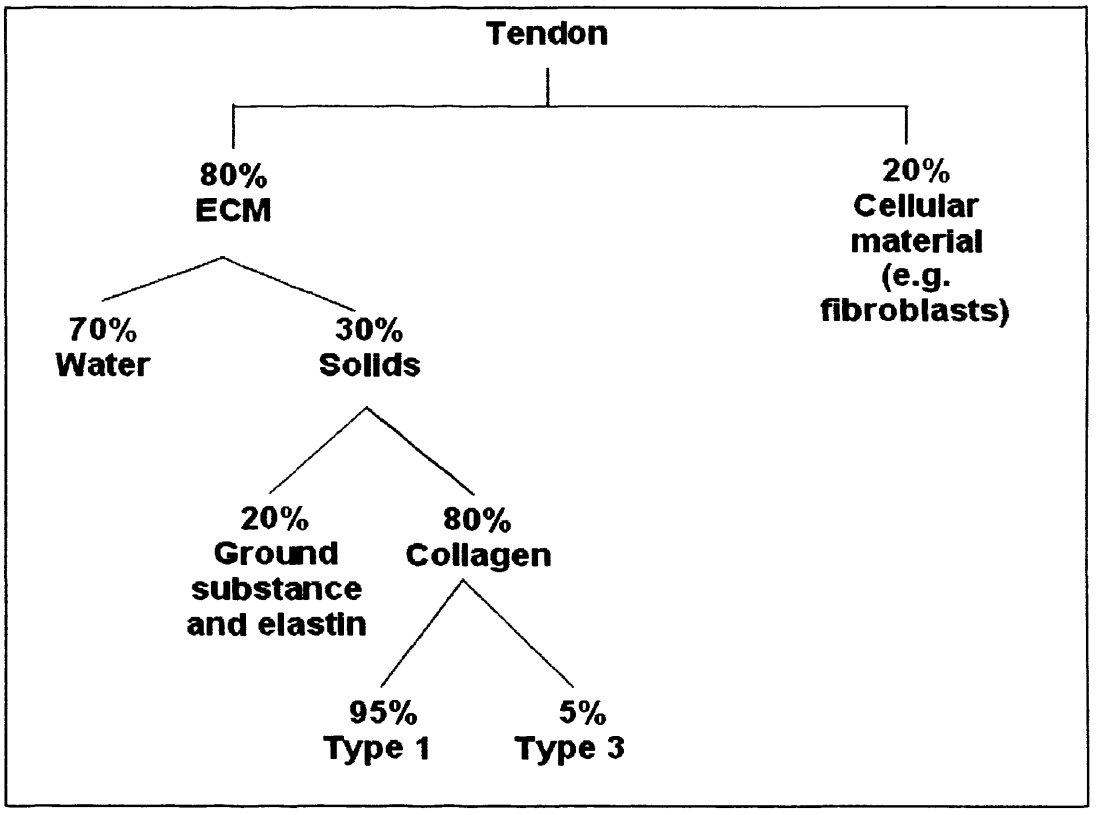

Figure 2.2.1: The composition of human tendons. These values are approximate and vary between sources (Figure adapted from **[65]**).

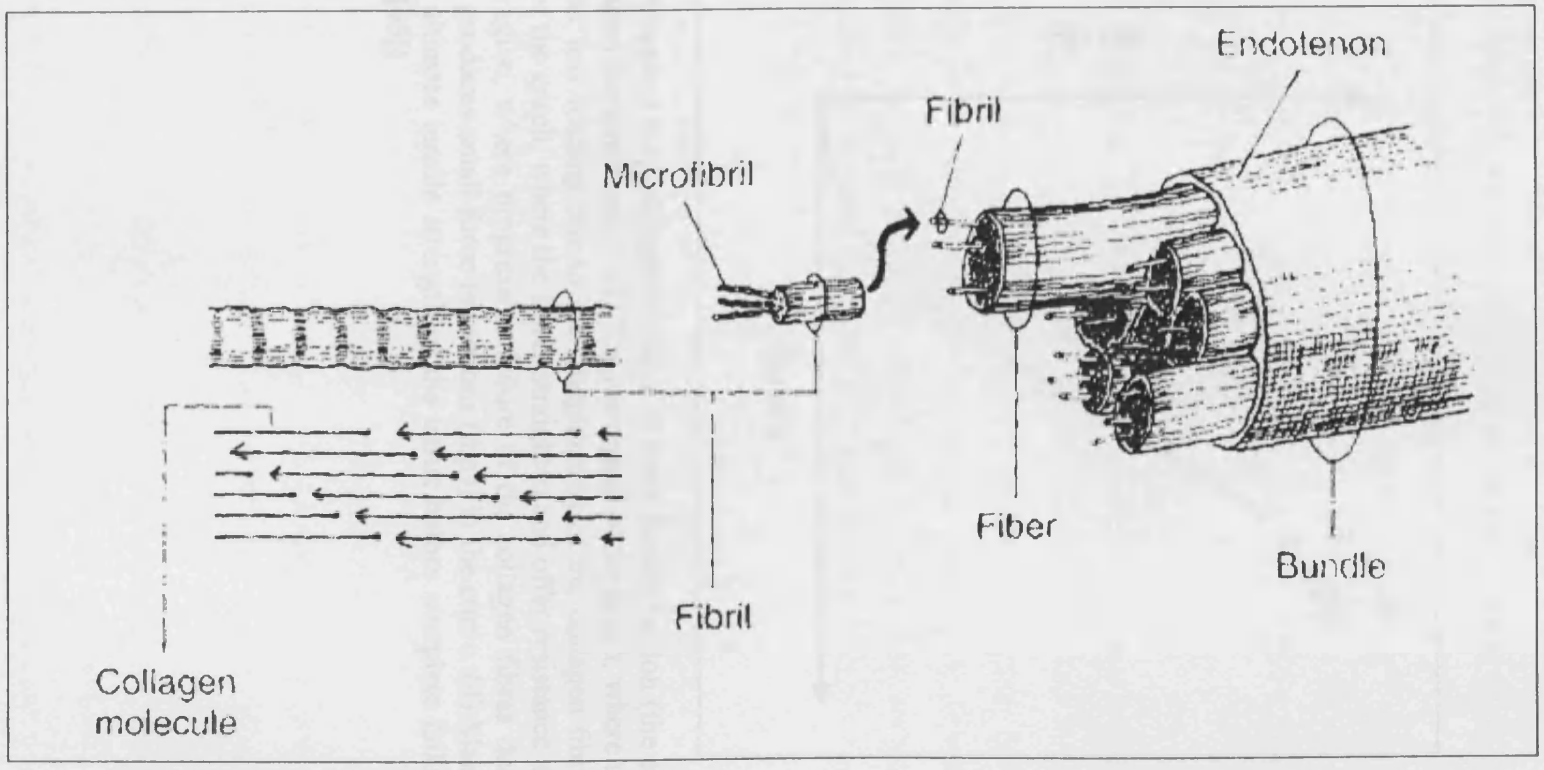

Figure 2.2.2: The structure of human tendons. (Figure adapted from **[65]**)

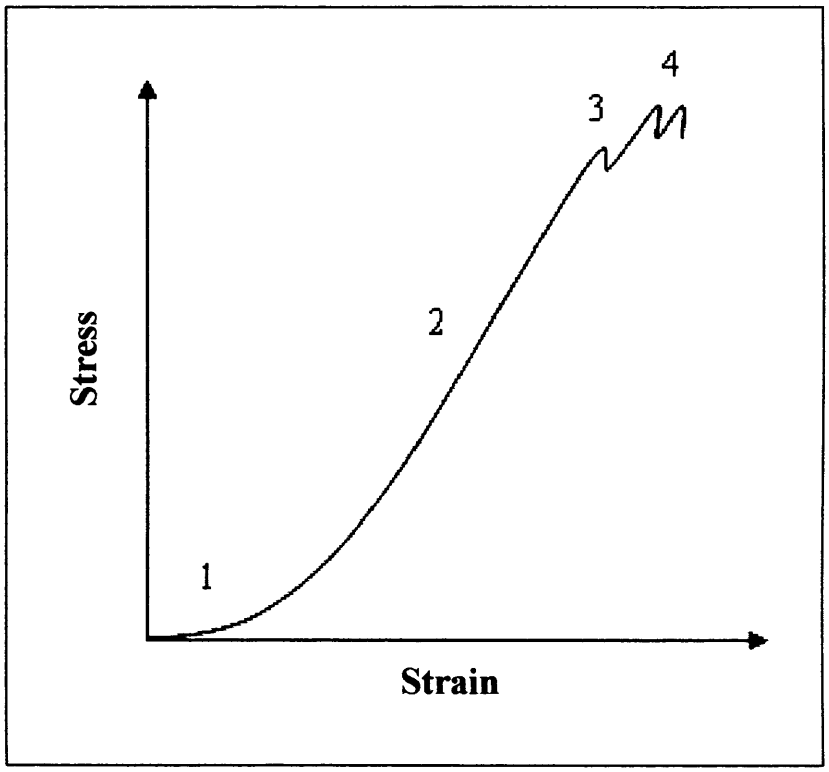

Figure 2.2.3 A typical load-elongation curve of fresh human tendon (the exact nature is dependant upon the strain rate). (1) The toe region of the graph, where the tissue is elongated under low loading due to the straightening of the collagen fibres. (2) The linear region of the graph, where the fibres straighten and offer resistance. (3) The end of the linear region, where progressive failure of the collagen fibres due to partial tensile failure produces small force reductions (dips) in the curve. (4) Maximum load reflecting the ultimate tensile strength of the tissue before complete failure. (Figure adapted from **[65]**)

2.3 The Calcaneus:

Termed a *short bone*, the calcaneus is actually the largest bone in the foot. It has, like every bone, a hard exterior shell that accounts for nearly 80% of the skeletal mass. This cortical bone is responsible for bone strength, providing high resistance to bending and torsion in long bones. Typically, cortical bone has an ultimate tensile strength of 100 – 150 MPa, a Young's modulus of 10 – 15GPa **[92]**, and 1-3% maximum tensile strain **[65]**.

Trabecular bone forms the interior scaffold of the calcaneus. This is less dense than cortical bone, representing the remaining 20% of skeletal mass. Trabecular bone helps maintain bone shape and resist compressive forces, having an ultimate tensile strength of 8 – 50 MPa and can withstand approximately 2-4% strain **[65]**. Despite the large standard deviation in these reported values, the Young's modulus of individual trabeculae has been measured as 10.4 GPa **[92]**, although these values may be higher than those *in vivo* due to dry specimens being tested.

The Achilles tendon attaches to the middle third of the posterior surface of the calcaneus, widening distally into a deltoid shape at the insertion site **[1]**. The shape and surface area of this insertion site is determined by the tensile loads experienced at the time of puberty **[93]**, in a manner similar to the cruiciate ligaments of the knee **[3]**. The Achilles tendon enthesis is further strengthened by the interlocking of the calcified fibrocartilage/subchondral bone fibres, providing protection against shear stress **[21]**. The alignment of the trabeculae in association with an increased bone density **[31, 94-97]** ensures the weak ultimate tensile strength **[98]** of bone is improved, thus meaning it is rarely the site of traumatic failure **[93, 99]**.

Despite the two functionally different materials of bone providing strength to resist bending, torsion and compression, complete - or in less severe instances, incomplete **[15]** - calcaneal fracture can occur. This may be due to bone weakening following a period of overuse, or be caused by trauma due to the application of an excessive external load or through rapid and forced contraction of a muscle causing an avulsion fracture **[15]**.

2.4 The Superior Tuberosity:

The posterosuperior prominence of the calcaneus, termed the superior tuberosity, has been observed to vary in size **[100]**. The Achilles tendon runs over the superior tuberosity prior to insertion into the calcaneus. In doing so, it has been hypothesised that the superior tuberosity acts as a pulley upon the Achilles tendon **[31]**, and thus it may be an important biomechanical component in the Achilles tendon enthesis organ.

The superior tuberosity is clinically infamous for being the cause of Haglund's disease **[19]**, whereby the neighbouring retrocalcaneal bursa is inflamed due to impingement against the adjacent Achilles tendon **[101-103]**. This scenario is particularly likely on dorsiflexion (Appendix A1), where the superior tuberosity rotates in a posterior and inferior direction and thus moves towards the Achilles tendon (Figure 2.4.1).

2.4.1 Haglund's Disease Diagnosis:

Care is required on diagnosis of Haglund's disease, as it is one of a number of hindfoot disorders with similar symptoms. Thus, it is typical for lateral radiographs to be examined for confirmation of the presence of the condition, as they allow the sagittal profile of the superior tuberosity to be assessed. A number of techniques have been designed to quantify the sagittal prominence of the superior tuberosity **[104-113]**. All of these have, however, had problems identified by Chauveaux et al. **[111]** that are likely to cause inconsistent measuring. It is likely that inconsistent diagnoses influences the success rates of surgical treatment.

The first method of quantifying the prominence of the superior tuberosity was published in 1945 by Fowler & Philip **[104]**. This technique proposed quantification of the superior tuberosity prominence by measuring the angle between the tangent of the posterosuperior prominence at the insertion of the Achilles tendon, with the line inclined to the anterior tubercle and the medial process of the plantar tuberosity. Described schematically in Figure 2.4.2(a), this technique defines superior

tuberosities at risk of developing Haglund's disease where the angle subtended is >75°. Inconsistencies with this technique were reported, however, due to the ambiguous definition of the angle, especially on the dorsal surface **[105, 106]**. As changing the critical angular threshold in an attempt to improve accuracy proved unsuccessful **[105, 107]**, modification of the original technique was attempted. The Angle of Steffensen and Evensen **[108]** uses the long axis of the calcaneus as reference, rather than the line inclined to the anterior tubercle and plantar tuberosity. This technique describes superior tuberosities measuring an angle > 60° of being at risk of causing Haglund's disease (Figure 2.4.2(b)).

The Fowler & Philip angle has even been summated with another technique in an attempt to achieve a more robust method of tuberosity prominence quantification. The Total Angle **[109]** (Figure 2.4.2(c)) combines the Fowler & Philip angle with the Calcaneal Inclination Angle to account for the angle of the calcaneus in relation to the ground. Where the Total Angle >90°, Haglund's disease is predicted.

The Chauveaux-Liet (CL) Angle **[111]** is very similar to the Total Angle, calculating the superior tuberosity prominence using 2 angles. Angle α, termed the *angle of verticalization*, is the angle formed between the plantar surface of the calcaneus and the horizontal surface of the ground. Angle ß, termed the *posterior angle of the calcaneus*, is measured between a vertical line perpendicular to the ground and tangential to the most posterior part of the superior tuberosity, with a line passing through the apex of the posterosuperior crest and the most posterior point of the tuberosity (Figure 2.4.2 (d)). The CL angle is defined as the difference between Angle α and Angle ß, with non-Haglund superior tuberosities having a CL < 10°.

The Parallel Lines of Heneghan & Pavlov **[112]** technique (Figure 2.4.3) requires a line be drawn along the inferior calcaneal border, with a second line drawn parallel along the upper border of the calcaneus, through the posterior facet margin. If the superior tuberosity extends above this second line, it is deemed likely to cause Haglund's disease. No further precision is possible **[112]**, however, nor does the technique account for the angle of the posterior surface of the superior tuberosity **[111]**.

Whilst the relative success of the Total Angle, CL Angle and the Parallel Lines of Heneghan & Pavlov has been noted **[110]**, poor correlation was reported when attempting anatomo-radio-clinical validation **[111]**. The reliability of the most recently suggested technique, xeroradiography, has yet to be proven **[113]**.

Whilst the poor consistency and reliability of these techniques is likely to limit success rates, the biomechanical consequences of such a surgical procedure may equally hinder success.

2.4.2 Haglund's Disease Treatment:

Whilst the exact management of Haglund's disease depends upon the severity of the symptoms, the first stage typically attempts to anteriorly rotate the superior tuberosity and thus effectively reduce its prominence. Achieved by incorporating an additional heel wedge within the shoe, poor results have been reported **[114]**. In more advanced cases anti-inflammatory medication may be prescribed, and failing this local cortisone steroids administered. Caution should, however, be exercised as cortisone steroids have been reported to alter the biomechanical properties of tendon **[115-117]**, leading to an increased likelihood of tendon rupture **[118, 119]**. Hence, in instances where anti-inflammatory medication is yielding unsatisfactory results, a mechanical, rather than medicinal solution, is typically sought.

By resecting the superior tuberosity, the structure responsible for causing the pain is removed **[19, 120]**. A small incision is made through the skin at the level of the superior tuberosity to allow for the introduction of the arthroscope and instruments. Kager's fat pad is routinely excised to create an unobstructed view of the superior tuberosity, before the area of impingement is identified and the prominence resected using a synovial resector, as the bone is very soft. Bone resection continues until no further impingement will occur, before the loose debris is removed and the rough edges smoothed **[121]**. Typically, the inflamed areas of the retrocalcaneal bursa and Achilles tendon are also excised **[122, 123]**. However, despite these efforts to remove the cause of pain, success rates range between only 69 - 81% **[20-22]**, with even a

worsening of symptoms reported in some instances **[21]**. It has been reported that the likelihood of success can be improved, however, when surgery is performed within a year of the onset of problems **[124]**. This avoids an extended period of tendon degeneration **[125]**.

Another surgical method by which to resect the superior tuberosity has previously been reported. In 1939 Zadek **[120]**, and later in 1965 Keck & Kelly **[106]**, proposed techniques whereby the superior tuberosity prominence is reduced by removing a wedge from the mid-portion of the calcaneus, with the consequent anterior rotation of the superior tuberosity alleviating impingement of the retrocalcaneal bursa. Clearly, however, the technique is highly invasive, requiring pins and staples to secure the calcaneus into its new shape **[28, 126]**, followed by a significant period of time with the entire lower leg in a plaster cast **[120, 124]**. Surprisingly, however, the Zadek wedge osteotomy was reported to give results comparable with the less invasive technique, with at least good results in 22 out of 29 patients (i.e. 75%) **[110]**.

2.4.3 The Biomechanical Importance of the Superior Tuberosity:

Whilst it has previously been hypothesised that the superior tuberosity acts as a pulley on the Achilles tendon **[31]**, neither the biomechanical advantage nor the consequence of surgical resection have been considered. In addition, the superior tuberosity may have biomechanical functions similar to other soft tissues, which include providing lubrication **[25, 26]**, load bearing **[25-28]**, and stability**[25]** to a synovial joint. Thus removal of the superior tuberosity – and the subsequent success rate – may be dependant on a number of factors other than simply removing the source of pain.

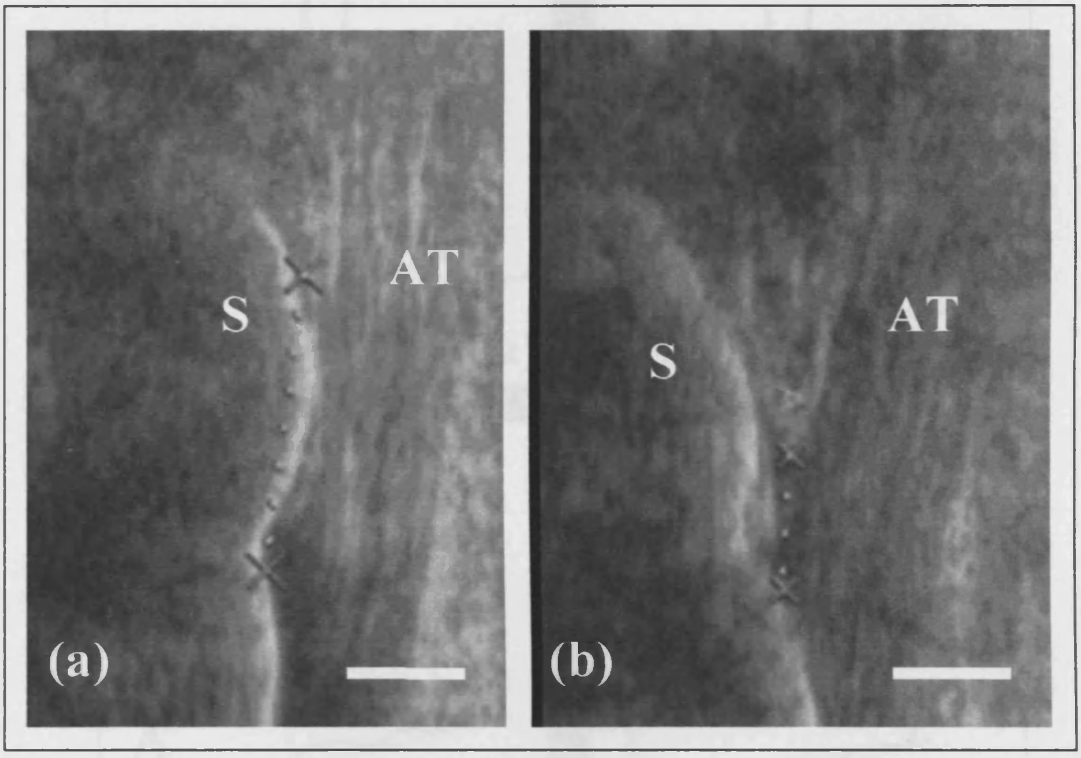

Figure 2.4.1: A sagittal ultrasound of the Achilles tendon insertional region. The superior tuberosity moves nearer to the Achilles tendon on dorsiflexion as a consequence of the posteroinferior rotation of the calcaneus. (a) The foot in dorsiflexion causes the superior tuberosity to move towards the Achilles tendon. (b) The foot in plantarflexion moves the superior tuberosity away from the Achilles tendon. AT= Achilles tendon, S = Superior tuberosity, Scale bar = 4mm.

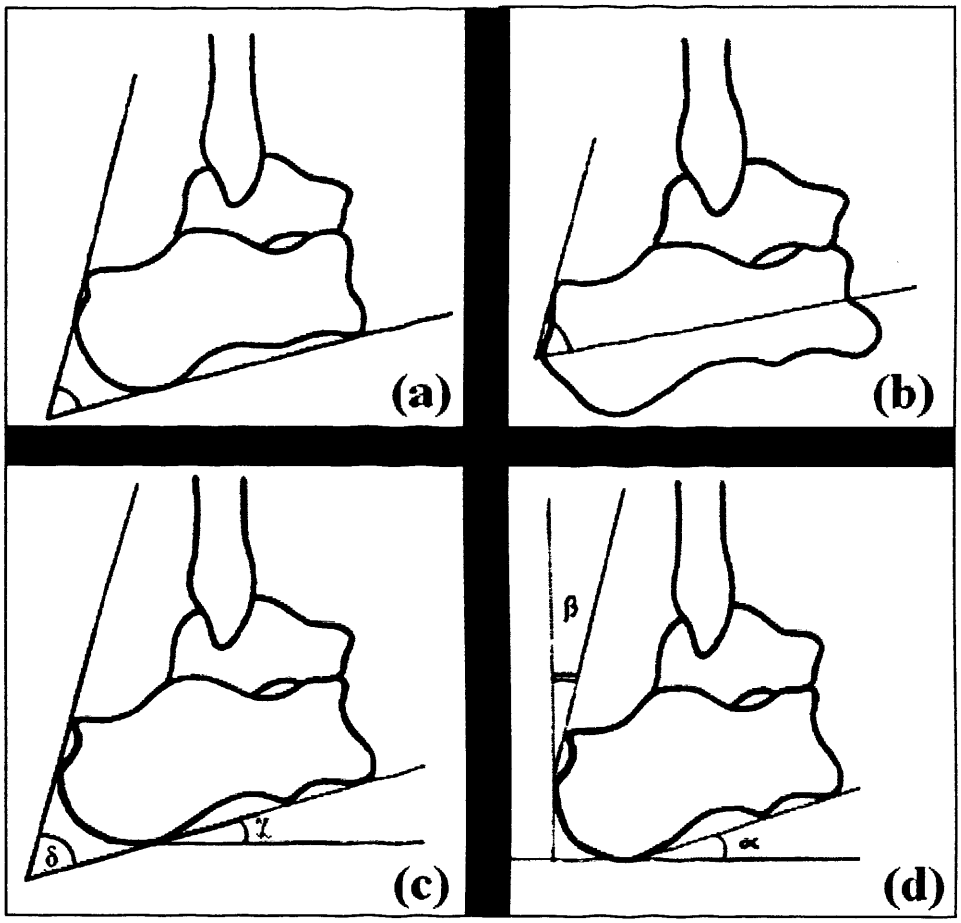

Figure 2.4.2: Schematic representations **[111]** of the techniques used to measure the superior tuberosity prominence. (a) The Angle of Fowler & Philip. An angle > 75° signifies probable Haglund's disease. (b) The Angle of Steffenson & Evensen. An angle > 60° signifies probable Haglund's disease. (c) The Total Angle of Ruch. An angle >90° signifies probable Haglund's disease. (d) The CL Angle. An angle >10° signifies probable Haglund's disease.

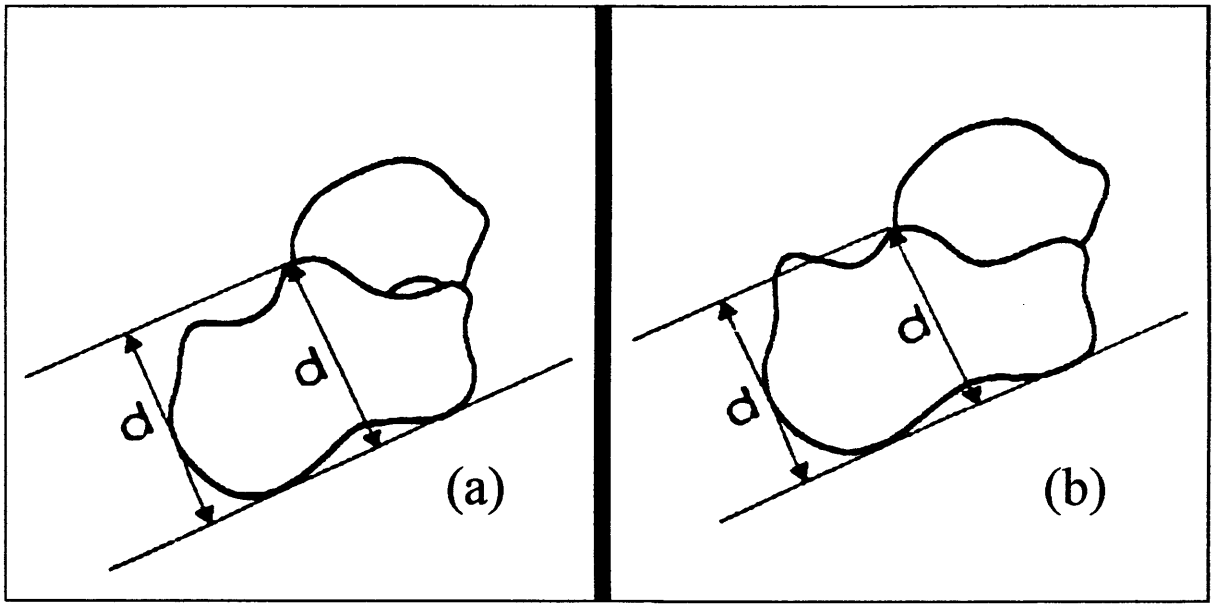

Figure 2.4.3: Schematic representation **[111]** of the Parallel lines of Heneghan and Pavlov technique used to measure the superior tuberosity prominence (a) The superior tuberosity is below the upper line, thus is not likely to induce Haglund's disease. (b) The superior tuberosity is above the upper line, thus is deemed at risk of inducing Haglund's disease.

2.5 Enthesis Fibrocartilage

It is typically suggested that the enthesis serves to balance the differing elastic moduli of the tendon and bone **[127]**, thereby ensuring the strongest possible union. In attaching to the calcaneus, the Achilles tendon enthesis is classified as a fibrocartilaginous enthesis **[128]** (otherwise known as chondral **[129]** or direct **[73]** entheses). A fibrocartilaginous enthesis is typical of the epiphysis **[130]**. This is opposed to a fibrous enthesis **[128]** (otherwise known as periosteal **[129]** or indirect **[73]** entheses), which is found at the diaphysis **[130]**.

The fibrocartilaginous enthesis was first described in 1929 **[30]** as comprising of 4 different tissues (Figure 2.5.1):

1. Achilles tendon
2. Uncalcified fibrocartilage
3. Calcified fibrocartilage
4. Subchondral bone

Thus, fibrocartilaginous entheses consists of 2 fibrocartilages, sandwiched between the two mating tissues. These fibrocartilages are collectively termed the enthesis fibrocartilage.

2.5.1 Uncalcified Fibrocartilage:

Uncalcified fibrocartilage is composed mainly of collagen fibres, embedded into a cartilage matrix. This retains the fibres in their longitudinal arrangement, resulting in anisotropic material properties **[130]**. The main role of the uncalcified fibrocartilage is to gradually bend the collagen fibres of the tendon away from the hard tissue interface when under loading, thereby dissipating stress **[73, 130]**. This role is commonly compared to that of the rubber grommet protecting the flex inserting into an electrical plug **[21]**. It has been suggested that this curving of the fibres could be regarded as creating a pulley, an effect further emphasised by the wedge shape of the uncalcified fibrocartilage **[31]**. This concept will be developed later.

The quantity of uncalcified fibrocartilage at the enthesis varies and is thought to be proportional to the loading experienced. A significant region of uncalcified fibrocartilage is found in the patellar tendon of a jumper's knee, whereas joints of less than average loading - such as those of patients affected by rheumatoid arthritis - have less uncalcified fibrocartilage **[131]**. In accordance with the same principle, the deepest part of the enthesis is likely to contain the greatest amount of fibrocartilage, due to being compressed by the superficial fibres when the tendon is under tension **[130, 132]**.

2.5.2 Calcified Fibrocartilage:

The uncalcified and calcified fibrocartilages are separated by a front of calcification known as the tidemark (t, Figure 2.5.1). Typically appearing during adolescence, the exact function of the tidemark is unclear, although it is often the location where the soft tissues fall away from the bone after maceration **[130]**. The other interface of calcified fibrocartilage - with subchondral bone, is the critical site in determining the strength of the Achilles tendon anchorage. This interface is of a highly irregular appearance **[128]**, with numerous regions of overlap **[3]** and interlocking **[31]** that are likely to increase the area of contact, and thereby increasing the ultimate tensile strength. Interfascicular tissues, termed the *Fibres of Sharpey*, also strengthen the enthesis, blending with the periosteum collagen fibres before passing through the cortical bone of the calcaneus **[1]**.

The enthesis is further strengthened and protected by the stiffness of the calcified fibrocartilage, giving rise to the 'stretching brake' theory **[133]**. Appearing to be based on Poisson's ratio **[134]**, this theory states that if a tendon is so stiff that it resists compression, then neither can it be stretched **[135]**. With a tendon's ability to stretch and recoil, this prevents the inevitable narrowing from occurring abruptly at the tissues interface, thereby maximising its strength **[133]**.

Thus, in promoting a gradual bending of the collagen fibres in addition to preventing deformation at the interface, the enthesial fibrocartilage is said to offer a two-tiered protection against stress **[21]**.

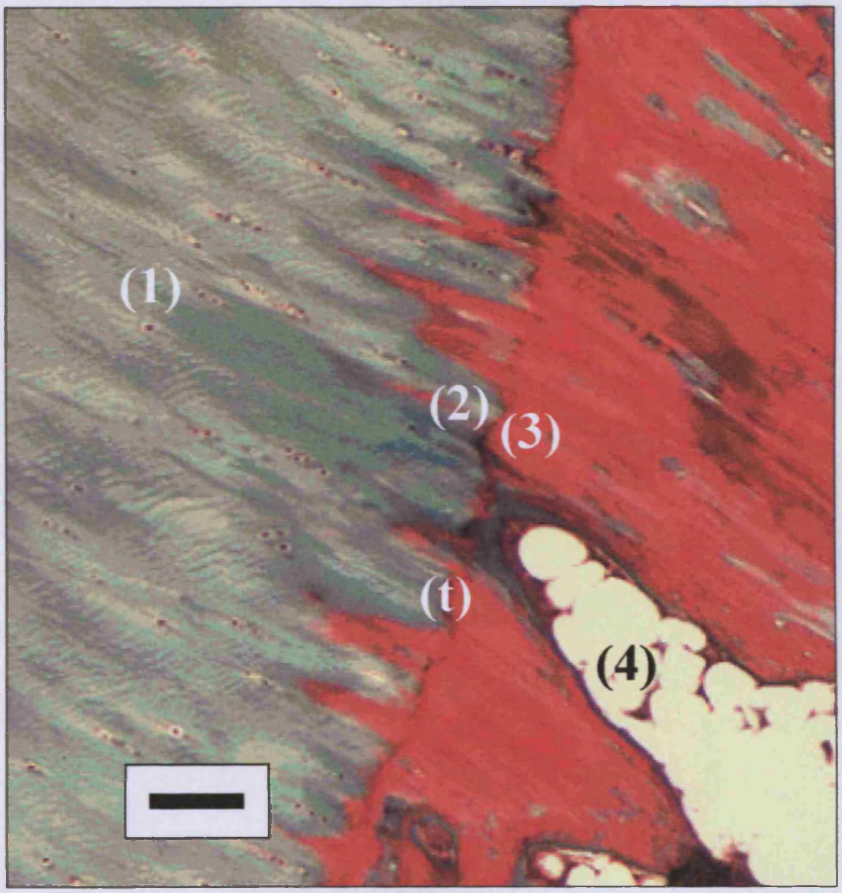

Figure 2.5.1: Sagittal histological section of the Achilles tendon enthesis (viewed under x5 objective lens). (1) Achilles tendon, (2) Uncalcified fibrocartilage, (3) Calcified fibrocartilage, (4) Bone, (t) Tidemark. Scale bar = 100μm.

2.6 The Periosteal & Sesamoidal Fibrocartilages

The periosteal fibrocartilage typically replaces the periosteum covering of the superior tuberosity. The periosteal fibrocartilage develops following, and protects against, compression by the Achilles tendon **[31, 136, 137]**. As the Achilles tendon undergoes strain when under load, it can be imagined how the tendon may effectively rub against the surface of the tuberosity. Thus, it is also possible that the periosteal fibrocartilage protects the superior tuberosity from this microscopic sawing.

Located on the deep surface of the Achilles tendon, the exact position of the sesamoidal fibrocartilage is dependant upon that of the periosteal fibrocartilage **[138]**. Like the periosteal fibrocartilage, the sesamoidal fibrocartilage forms in response to compression against the superior tuberosity **[31, 136, 137]** protecting the conjoining surface of the Achilles tendon. It may also protect against fretting of the tendon should the microscopic sawing hypothesised above occur.

2.6.1 Fibrocartilage Properties:

The glycosaminoglycan (GAG) content of fibrocartilage ensures it is an effective tissue at resisting load. GAG's are long, unbranched polysaccharides that attach to the proteoglycan Aggrecan. They successfully resist compression by utilising the incompressibility of water **[128]** as, due to having a negative charge density (the reasons of which are beyond the scope of this thesis), they create areas of high osmotic pressure **[139]**. The consequential osmosis thus resists compression and hence transfers stress **[128]**.

The orientation of the sesamoidal fibrocartilage collagen fibres is such that they are of a basket-weave appearance, and differs significantly from the longitudinally aligned fibres of the Achilles tendon. The criss-crossing of the sesamoidal fibrocartilage collagen fibres is secured by the extracellular matrix (ECM) **[1, 125]**. It has been hypothesised that this region of speciality prevents the collagen fibres from splaying

on compression **[130]** against the superior tuberosity, and thus this is likely to minimise the induced stress.

2.7 The Retrocalcaneal Bursa:

The retrocalcaneal bursa is a c-shaped, concave **[140]** sac that is located immediately anterior to the Achilles tendon, fitting over the superior tuberosity **[140-143]**. This location means the bursa increases the lever arm potential of the Achilles tendon **[144]**. The retrocalcaneal bursa is lined with synovial membrane, which extends over the distal limit of Kager's fat pad **[103]**. The presence of synovium means that the small amount of highly viscous, hyaluronate-rich fluid within the bursa is likely to be synovial fluid **[145]**.

Functionally, the retrocalcaneal bursa decreases the friction as the Achilles tendon slides over the superior tuberosity **[144]**. Clinically, the retrocalcaneal bursa is frequently recognised as a site of inflammation. Inflammation of the synovial membrane of the retrocalcaneal bursa – termed retrocalcaneal bursitis **[101-103]** - is typically caused due to impingement by a prominent superior tuberosity. In patients with Haglund's disease, magnetic resonance images (MRI's) reveal excessive fluid in the retrocalcaneal bursa **[146]**. Unfortunately, should retrocalcaneal bursitis occur, the superior tuberosity may become enlarged in response **[104]**. This may further irritate the bursa and the Achilles tendon, which in turn may cause further enlargement of the superior tuberosity, and a cycle of injury, response to injury, and reinjury is established **[147]**. In such instances, surgical intervention is typically the only solution.

2.8 Kager's Fat Pad

Kager's fat pad is a mass of adipose tissue that occupies the space within Kager's triangle **[148-150]** (of which only the distal part is visible in Figure 2.1.1(b)). Kager's fat pad is a commonly used radiographic landmark, appearing distinctly on lateral radiographs as a sharply marginated, radiolucent triangle **[148]**. Kager's triangle, and thus Kager's fat pad, typically extends from the retrocalcaneal bursa and the calcaneus inferiorly, to the Achilles tendon posteriorly, and the flexor hallucis longus (FHL) muscle anteriorly **[103, 148, 149, 151]**. It has previously been hypothesised that Kager's fat pad may act as a variable space filler by moving into the retrocalcaneal bursa **[152]**. This movement may allow it to convey a mechanical advantage to the Achilles tendon and associated muscles **[109, 144, 152]**, by increasing their respective lever arms. It has also been suggested that, through proprioception, Kager's fat pad may also control the angle at which the Achilles tendon inserts into the calcaneus **[153]**. These hypotheses have, however, yet to be investigated, and thus a lack of firm physiological or biomechanical knowledge means that the fat pad is routinely excised when performing arthroscopic surgery, with apparently little consideration to the consequences.

2.9 Conclusion

The collection of tissues that form the Achilles tendon enthesis organ is clearly highly specialised. They act together to protect and strengthen the insertion of the Achilles tendon where, as the Achilles tendon is the strongest tendon in the human body, stresses >100 MPa have previously been reported **[63]**. The Achilles tendon enthesis attaches to the calcaneus in a manner designed to maximise strength against both tensile and shear forces, whilst the fibrocartilages of the Achilles tendon enthesis organ protect the zones of the soft tissues that compress against one another. Thus, the Achilles tendon enthesis organ acts to strengthen and protect itself.

Afflicting solely the Achilles tendon, Haglund's disease is a condition that it appears the Achilles tendon enthesis organ cannot protect itself against sufficiently. The treatment of Haglund's disease appears poorly managed, with the multitude of diagnostic techniques causing confusion when attempting to identify a superior tuberosity that is likely to impinge the retrocalcaneal bursa. Should surgery be required, no formal guidelines determine the extent to which resection should occur, and thus both Kager's fat pad and the superior tuberosity are resected until impingement is impossible **[121]**. Whilst <82% of patients treated surgically report a reduction in pain immediately post-operatively, no studies have previously considered the biomechanical consequences of surgery, nor evaluated the long-term welfare of the patients.

Thus, this thesis examines the Achilles tendon enthesis organ biomechanics with particular reference to the superior tuberosity and Kager's fat pad. This information shall be useful in the treatment of hindfoot disorders, with particular implications for the improvement of Haglund's disease management.

3, The Biomechanical Influence of the Superior Tuberosity

3.1 Haglund's Disease

Whilst the biomechanical influence of the superior tuberosity has never been investigated, it has previously been hypothesised that it acts as a pulley upon the Achilles tendon **[31]**. It would appear, however, that the significance of this role is likely to differ from person to person, as the size of the superior tuberosity varies **[100]**.

The superior tuberosity has been hypothesised as acting as a pulley when the superior tuberosity and the deep surface of the Achilles tendon oppose each other during ankle flexion **[31]**. This is likely to be a particularly frequent occurrence on dorsiflexion, where the superior tuberosity is subsequently rotated in a posteroinferior direction, towards the Achilles tendon. It is also apparent, however, that the contact between the Achilles tendon and the superior tuberosity may impinge the retrocalcaneal bursa (situated between the two surfaces), causing inflammation. This inflammation was first reported by Haglund **[19]**, and hence has since been termed Haglund's disease.

Care is required when diagnosing Haglund's disease, as its symptoms are similar to other hindfoot disorders. It is typical for lateral radiographs to be examined for confirmation of the diagnosis of the condition, as these images allow the sagittal two dimensional profile of the superior tuberosity to be assessed. However, the published techniques designed to identify likely cases of Haglund's disease from these images**[104-113]** have all been reported as being inconsistent **[111]**, and thus a 'gold standard' has yet to be developed.

Haglund's disease is initially treated conservatively through the use of orthotics and then, if necessary, corticosteroids. In cases where insufficient pain relief is reported, surgery is performed to resect the superior tuberosity. Follow-up studies have determined that a reduction in pain is present in <82% of cases **[20-22]**. No studies have, however, reported the biomechanical consequences of removing a prominent pulley from this mechanical system. It is possible, for example, that this may affect the distribution of load throughout the Achilles tendon enthesis organ, thus potentially causing additional hindfoot injuries post-operative.

Thus, the work in this chapter aimed to provide an assessment of the superior tuberosity's biomechanical role in the Achilles tendon enthesis organ. The superior tuberosity was examined histologically in an attempt to devise a method by which to quantify its size microscopically. The role of the superior tuberosity in providing the Achilles tendon with a biomechanical advantage was examined using both magnetic resonance imaging (MRI) and theoretically, and the effect of resection discussed. Finally, a physiological and mechanical assessment of the loading upon the superior tuberosity was performed.

3.2 Materials & Methods:

A number of techniques were used to thoroughly examine the superior tuberosity. Dissecting room cadavers were used to micro- and macroscopically examine the structure, whilst the biomechanical influence of the superior tuberosity on the Achilles tendon enthesis organ was examined using ultrasound and by the fabrication of a specially designed apparatus.

3.2.1 Microscopic Quantification:

Histological processing of cadaveric specimens allowed for microscopic examination of the superior tuberosity. Prior to histological sectioning, however, it was necessary to follow a series of steps to collect and suitably prepare the specimens.

3.2.1.1 Specimen Preparation

Seven specimens were collected from elderly dissecting room cadavers (4 male, 3 female; aged 63-87 years), donated to Cardiff School of Biosciences (Cardiff University, UK) for anatomical investigation under the provision of the 1984 Anatomy Act and the 1961 Human Tissue Act. The cadavers had been perfusion-fixed in 4% formaldehyde, 25% alcohol for a minimum of 72 hours, thus reducing degradation and the risk of infection. Using a fine-bladed saw, 2 parallel vertical cuts were made into the posterior surface of the calcaneus, a distance of 8mm apart about the midline. The Achilles tendon and Kager's fat pad were also cut in the same plane using both the fine saw and a scalpel, whilst a transverse cut was made through the tendon approximately 50 mm proximal to the enthesis. The specimen was then removed using a hammer and an 8mm chisel on the plantar surface of the calcaneus (Figure 3.2.1).

Once removed, the specimens were further fixed by soaking in 10% neutral buffered formal saline for 1 week. The specimens were then decalcified (i.e. softened) by soaking in 2% dilute nitric acid for an additional 3 days, to ease cutting. At this stage the specimens were then trimmed to a maximum dimension of 50mm (height) x

30mm (width). The specimens were dehydrated using a series of alcohol solutions of gradually increasing strength (70%, 90%, 100%), cleared in xylene (to ensure that the tissue was miscible with melted paraffin), and finally embedded in 58°C molten paraffin wax.

3.2.1.2 Histological Sectioning:

The blocks of paraffin wax (containing the tissue) were then trimmed to minimal dimensions, before being mounted on the chuck of a rotary microtome (Appendix A2). Nine, 8μm thick sections were then cut at 500μm intervals (termed 'sample points') throughout the tissue specimen (Figure 3.2.2), floated on water within a bath heated to 40°C, and then collected onto a glass microscope slide. The sections were dried, initially on a slide heater for 30 minutes, before being moved into an oven at 45°C for 5 days.

3.2.1.3 Histological Staining:

A series of stains and counter-stains are commonly used to aid tissue identification. Miscibility with these water-based stains was ensured by using xylene to remove all traces of wax. Gradual rehydration of the slides was achieved by passing them through a series of alcohol solutions with decreasing concentrations (100%, 90%, 70%), before being submerged in water. Once the tissue was rehydrated, the sections were stained with Masson's trichrome. This stain was used to identify the collagen fibres that had experienced tension **[154]**. In these regions, the alignment of the charged groups associated with the collagen molecules resulted in strong binding of, and thus staining by, the red dye. In regions of the specimen where the matrix was subject to compression, the red dye was washed away and hence did not stain, leaving a green counterstain.

3.2.1.4 Superior Tuberosity Measurements:

The current methods for measuring the size of a superior tuberosity are based on radiographs. These images are, however, low-powered and generally of poor resolution, and thus the accuracy of any measurements is likely to be reduced. A histological image is of far higher resolution and thus is likely to improve the

accuracy of any measurements. However, in processing the specimens for histological examination, the anatomical landmarks used by the published methods were resected. Thus a new method to microscopically quantify the superior tuberosity needed to be devised.

In developing a new method, the structures of the Achilles tendon enthesis organ that could be used as a reference frame for measuring were identified. Such a point had to maintain a consistent position through all the sections of that specimen, and ideally be independent of any other structure. Thus, a number of reference landmarks were identified (Figure 3.2.3):

- The Apparent Achilles Tendon Axis:

This was defined by the general long axis of the deep surface of the Achilles tendon.

- The Approximated Achilles Tendon Axis:

This was defined by the general orientation of the superficial Achilles tendon collagen fibres at the enthesis. Whilst the Achilles tendon position may have been affected by the processing of the specimen, the collagen fibres are likely to reflect their *in vivo* orientation. They are also likely to be of consistent orientation across the specimen.

- The Enthesis Proximal Point:

This point, the most proximal point of the tendon-bone interface, was easily identifiable across all specimens.

- The Superior Tuberosity Asymptote

This reference point had to be defined with respect to a reference plane. Some of the specimens did not have an asymptotic point as it had been resected during processing.

These landmarks were then used to devise a number of different methods by which to quantify the superior tuberosity. Each method measured the prominence of the 7

specimens at 6 sample points (i.e. every 500μm). Thus the tuberosity was examined across a distance of approximately 2mm either side of its midline. In some instances, however, it was not possible to obtain a measurement within a sample point due to insufficient quality.

The histological specimens were scanned on a conventional flatbed scanner (1200 DPI), and the images stored as high quality JPEG files. These images were then magnified to fit an A4 page, before a scaled grid was electronically positioned over the image. The images were then printed and measured. An example of each calculation can be found in Appendix A3.

- Technique 1:

Using the Apparent Achilles tendon axis as a reference frame, the superior tuberosity prominence was quantified by measuring the area between this axis and the superior tuberosity. As there was not an obvious proximal boundary, this measurement was made within a 9mm radius of the Enthesis Proximal Point, the maximum dimension that would provide measurements for all specimens (Figure 3.2.4).

As the superior tuberosity size increased, the area between the two structures decreased. Thus, the reciprocal of this area was calculated to ensure that a lower value quantified a smaller superior tuberosity.

The success of this technique was limited however, as it did not describe the superior tuberosity prominence - merely the area, and thus two profiles of very different shape may have been identically quantified. Hence a more sophisticated method of superior tuberosity quantification was required, allowing measurement of its two-dimensional profile.

- Technique 2:

Technique 2 was developed to measure the gradient of the superior tuberosity profile, ensuring a result more representative of its shape was achieved. The gradient of the

superior tuberosity was measured relative to the Approximated Achilles Tendon Axis, thought to be the more consistent reference axis as it was unlikely to have been affected during histological processing. Whilst this axis was not necessarily the most accurate due it being an approximation, the method of measurement was likely to be sensitive to reference axis orientation and thus it was decided that using this axis would achieve more consistent results across the different specimens.

A coordinate system was established about the Enthesis Proximal Point, with the y-axis defined along the Approximated Achilles Tendon Axis. In order to closely approximate the curve of the superior tuberosity, the gradient of the tuberosity profile was taken at 1mm increments along the x-axis, along a total length of 5mm (Figure 3.2.5). The 5 gradients were then summated to allow the superior tuberosity to be quantified by a single value.

Whilst this technique appeared consistent, it was flawed in instances where the superior tuberosity extended across the reference axis. This lack of robustness meant that the technique was unable to quantify all shapes of superior tuberosity and thus was insufficiently reliable. Modifications to offset the y-axis and thereby encompass all shapes of superior tuberosity also proved unsuccessful, and thus a third technique was developed.

- Technique 3:

The other two techniques had identified the need for a robust method of quantification that differentiated between superior tuberosity shapes. Technique 3 achieved this by utilising the radius of the tuberosity profile as an indication of its shape and size. The asymptote of the superior tuberosity (defined against the Approximated Achilles Tendon Axis) was measured against the Approximated Achilles Tendon Axis, with the measurement centred on the Enthesis Proximal Point (Figure 3.2.6). The reciprocal of this value was calculated to obtain a proportional relationship (i.e. a larger superior tuberosity is represented by a larger value).

The consistency achieved using this method to quantify the prominence of superior tuberosity of the 7 specimens was deemed acceptable, and thus no further techniques were developed.

3.2.2 Mechanical Advantage:

The potential for the superior tuberosity to mechanically advantage the Achilles tendon by increasing its lever arm was assessed both theoretically and by using magnetic resonance imaging (MRI). Initially, the *in vivo* variation of the Achilles tendon lever arm length due to both the superior tuberosity size and angle of ankle flexion was assessed.

3.2.2.1 Achilles Tendon Lever Arm Assessment:

The protocol used to measure this effect is detailed below, whilst a brief account of the theory underpinning MRI is given in Appendix A4.

MRI provides high resolution *in vivo* images that allows for unprecedented examination and analysis in 3 orthogonal planes, although in this instance only a sagittal view is of interest. As there were no research-based MRI facilities in the local area, collaboration was formed with Professor Graeme Bydder at the University of California (San Diego, USA). Whilst it was not possible to personally use the imaging equipment due to the obvious geographical problems, constant communication with Prof Bydder ensured that the devised protocol was followed, thus giving a series of informative images

The right foot of 3 healthy male volunteers (age 31, 51 & 60 years) was imaged using a 1.5 T Siemens MR scanner (Erlangen, Germany). None of the volunteers had a history of significant injury to the Achilles tendon or ankle, and all 3 were asymptomatic. The versatility of MRI in identifying different tissues at different intensities meant that there were a number of parameters to be set. In order to ensure that the fat pad was the focus of the image, T1 weighted non-fat saturated

conventional spin echo scans, with a matrix size 512 x 384, the field of view 18cm, repetition time 480ms and echo time 12ms were used. On completion of imaging, the files were transferred either onto a compact disc and posted, or sent electronically from the USA.

The images were then analysed in Cardiff on a personal computer using the DicomWorks freeware package, software that allows for measurements to be made directly from the MRI. The affect of the superior tuberosity on the Achilles tendon lever arm length was examined by calculating the difference in perpendicular distance between the ankle axis (defined as the midpoint of the articulating surface of the tibia) and the enthesis proximal point, and the ankle axis and most posterior aspect of the superior tuberosity (Figure 3.2.7). This procedure was repeated at maximum plantarflexion, the anatomical (neutral) position, and maximum dorsiflexion.

The superior tuberosity size was then measured using the most reliable of the techniques described above to determine the influence of the superior tuberosity size on the lever arm.

- Validation:

The reliability of each technique was determined through validation, to allow identification of the most successful method of superior tuberosity quantification. Ideally, each technique would have been used to measure a number of different superior tuberosities, and then these results compared to an existing 'gold standard' technique. Unfortunately, however, no 'gold standard' currently exists. Equally, the resection of prominent landmarks meant that the current techniques could not be used. Thus, it was necessary to devise a method of validation.

3.2.2.2 Achilles Tendon Advantage:

The affect on the mechanical advantage of the Achilles tendon as a result of variation in the lever arm length was assessed theoretically. The model developed by Trew & Everett **[155]** was utilised to achieve this aim. By resolving the ground reaction force

recorded and by considering the centre of mass of the foot, the authors created a free body diagram that allowed for moments to be taken, ultimately allowing for calculation of the Achilles tendon tensile load. Having recorded a ground reaction force of 1026N at late stance phase during the gait cycle, and by taking moments about the centre of mass, the authors calculated the force of the Achilles tendon (AT_F) (Equation 3.2.1). This was dependant on the distance between the ankle axis and the line of action of the muscle (i.e. the lever arm length as defined earlier) (Figure 3.2.8). Thus, by varying this distance, the affect on the mechanical advantage of the Achilles tendon could be examined:

$$AT_F = M_{ankle} / AT_D$$

Equation 3.2.1: The Achilles tendon tensile force (AT_F) defined as the ratio of the ankle moment (M_{ankle}) and the Achilles tendon lever arm length AT_D **[155]**.

3.2.3 Enthesis Shear Stress:

The effect of the superior tuberosity size and angle of ankle flexion on the enthesis shear stress was examined theoretically to determine the biomechanical consequences of calcaneal resection. This was achieved using Equation 3.2.2:

$$\tau = \frac{AT_F}{A}$$

Equation 3.2.2: The shear stress (τ) is defined as the ratio of the tensile force (AT_F) and cross sectional area (A)

The area of the Achilles tendon-calcaneus insertion site was measured from the posterior surface of calcanei specimens. The posterior surface of 4 dried calcanei specimens was photographed – including a ruler to provide a scale for the images (Figure 3.2.9). A scaled grid was then positioned over the image and the area calculated by summating the squares. The shear stress was then calculated using Equation 3.2.2, relying upon the Achilles tendon tensile force calculated above. This value was then compared to the ultimate tensile strength of the union, and the implications of the superior tuberosity size on the enthesis biomechanics discussed.

3.2.4 Superior Tuberosity Loading:

The loading on the superior tuberosity was examined to investigate whether a correlation existed with its size. This information may be useful in determining the cause of Haglund's disease.

3.2.4.1 Apparatus 1:

The first mechanical model was fabricated consisting of a Perspex calcaneus to which fresh bovine tendon was attached. The model was designed to allow for the affect of the superior tuberosity prominence and the angle of ankle flexion to be investigated. The geometry of the model was based upon that observed in dissection room cadavers although, to ensure a high resolution of results, was fabricated 3-fold larger. The variation in superior tuberosity size observed histologically was represented by 4 different profiles (Figure 3.2.10). The range of ankle flexion was broadly represented by 5 different positions of model angle (30° dorsiflexion (DRF), 15° DRF, 0°, 15° plantarflexion (PLF), 30° PLF). These increments were chosen to ensure an achievable number of experiments were planned, yet for the affect of the 2 parameters to still be observed.

Two fresh flexor bovine tendons were harvested from skinned, 18 month old legs, to represent the Achilles tendon. This donor was chosen due to having similar dimensions and properties to the Achilles tendon **[156]**, whilst also being obtainable. The distal end of the tendon was clamped between a knurled region of the Perspex model and a cylinder with a knurled wall. The cylinder was pivoted off-centre along its long axis, allowing it to self-tighten as water was squeezed out of the tendon as it compressed during loading and thus avoiding slippage.

A number of methods were explored for measuring the load on the surface of the superior tuberosity. Initially, a series of springs positioned in the posterior surface of the calcaneus were considered from which, using Hooke's law, the force upon them could be calculated. This idea was rejected, however, due to the distance required between the centres of the springs being such that the resolution of the system would be insufficient. The use of photoelastic film was then briefly considered, before being discounted due to a lack of equipment.

Pressure sensitive film was eventually decided upon to allow derivation of the contact load, due to its ease of application and as it was stand-alone (i.e. did not rely on having any other components). Pressurex pressure sensitive film (Sensor Products LLC, New Jersey, USA) was fixed onto the superior tuberosity surface using double-sided sticking tape. Two different sensitivities of film were available (28-85 PSI, 70-350 PSI), to allow measurement of a wide range of pressure. The pressure of the tendon compressing against the superior tuberosity was measured by the bursting of capillaries within the pressure sensitive film releasing a substrate onto an adjoining developer sheet. This caused the developer sheet to become red in colour. The exact shade of colour was dependant upon the number of capillaries burst, which ultimately depended upon the magnitude of the pressure. The comparison of the colour of the developer sheet with a calibrated scale allowed the pressure to be determined (Appendix A5). This measurement considered both the temperature and humidity of the laboratory conditions, and was reported by the manufacturers to have an accuracy of ±15%. A known load was applied to both films and, on measuring the cross sectional area, the film was validated.

Once the pressure sensitive film was positioned, the apparatus was secured to a Losenhausen tensometric testing machine (Düsseldorf, Germany). In a position mimicking the neutral position, the apparatus was then fitted with 1 of the 4 superior tuberosity profiles. The proximal end of the tendon was then attached to the crosshead of the machine using a wedge grip, and a preload of 0.01kN applied. The tendon was then strained at $5\%s^{-1}$ (within the range previously reported **[14, 157]**). Unfortunately, however, slippage of the tendon at the distal clamp repeatedly occurred at approximately 0.2kN, a load that is below the desired *in vivo* condition. Thus, the clamp design was modified.

3.2.4.2 Apparatus 2:

Due to the success of the proximal clamp at securing the tendon, a wedge grip was fabricated to attach the tendon to the Perspex model (Figure 3.2.11). The clamp was continually tightened as the water was squeezed from the tendon as it was loaded. The tendon was again loaded at $5\%s^{-1}$ (within the range previously reported **[14, 157]**) to

0.4kN, a realistic *in vivo* condition **[2]**. For statistical significance a number of repetitions of each experiment would have been performed, however only 2 repetitions were possible per experiment due to the specimen drying out and degrading.

On completion of the test, the pressure sensitive paper was analysed. The distributed pressure on the superior tuberosity surface was determined by reading from the calibrated scale. The identification of different regions of pressure along the superior tuberosity surface was not possible, due to the difficultly in differentiating between the shades of red on the developer sheet. The contact area was also measured. This was only an approximation, however, as any pressure < 70PSI would not have made an impression on the developed sheet. As the system has a reported accuracy of ±15%, this error was deemed relatively insignificant.

3.2.4.3 Periosteal Fibrocartilage Thickness:

The periosteal fibrocartilage (PF) thickness was examined histologically to determine the region of maximum loading of the superior tuberosity. The PF of the 7 histologically processed cadaveric specimens (4 males, 3 female; aged 63-87 years) was measured under magnification (using x5 objective lens). The magnified image was displayed on a television screen which, through using a calibrated scale, allowed for measurement of both the PF thickness and position relative to the Enthesis Proximal Point. The periosteal fibrocartilage thickness of 3 sections of each sample point was measured at 500μm intervals along the edge of the superior tuberosity perpendicular to the underlying subchondral bone, until no fibrocartilage was present.

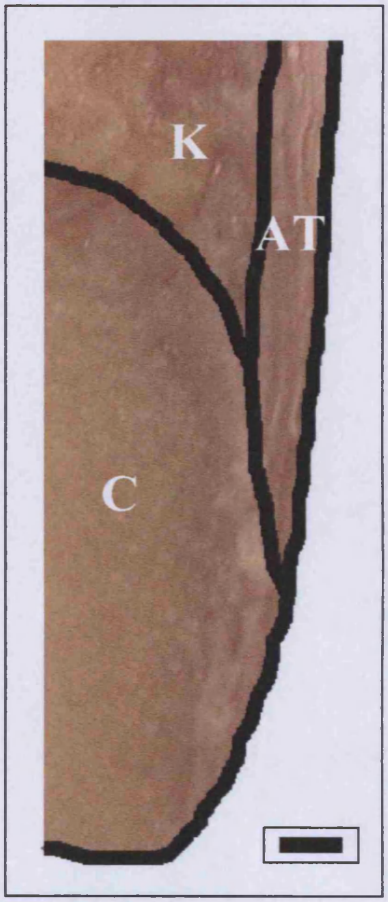

Figure 3.2.1: A low powered sagittal section through the Achilles tendon enthesis organ. AT = Achilles tendon; C = Calcaneus; K = Kager's fat pad; Scale bar = 4mm.

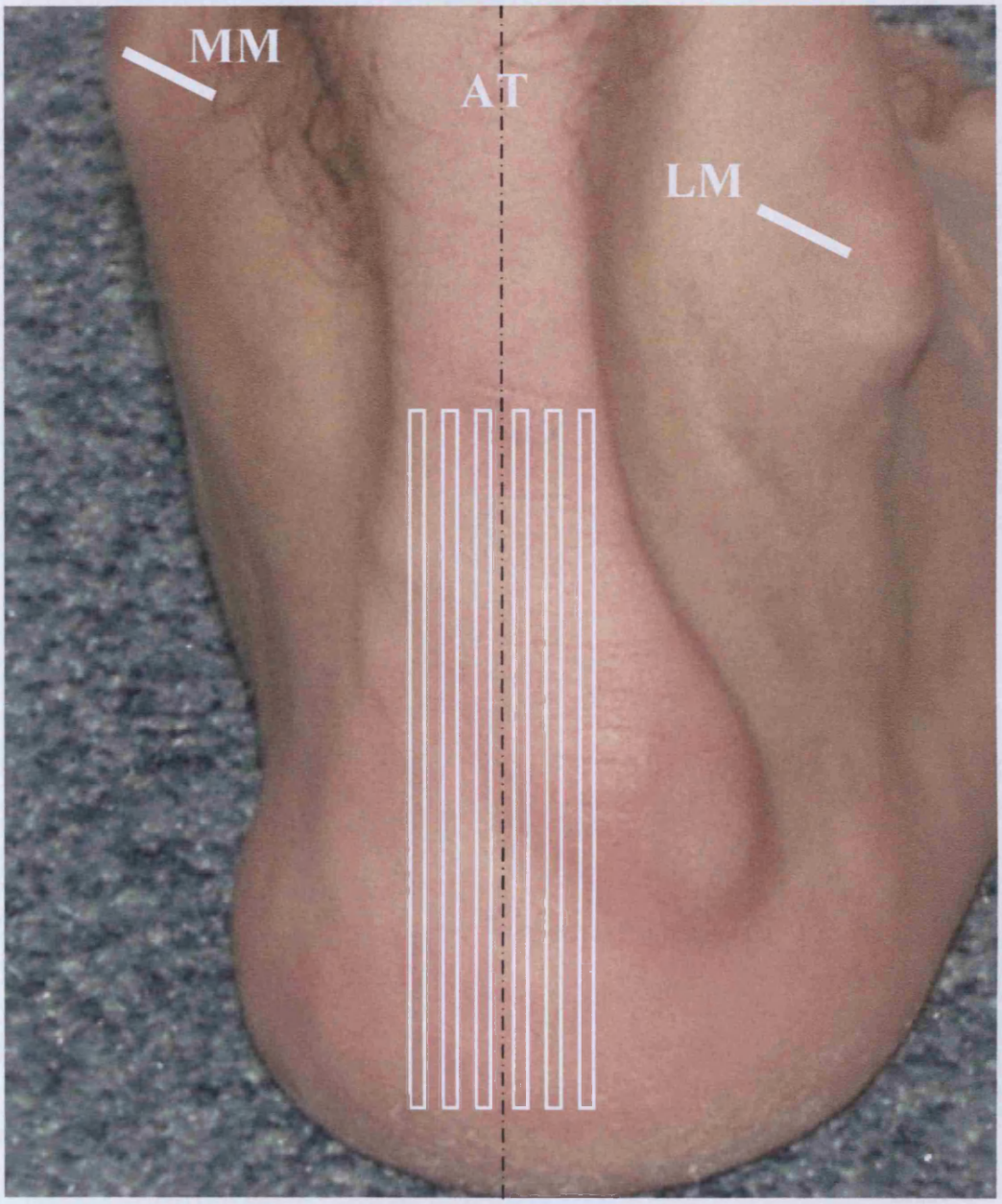

Figure 3.2.2: A view of the posterior surface of the heel, schematically demonstration the 6 sample points about the Achilles tendon midline, separated by a distance of 500μm. Within each sample point, 9, 8μm thick sections were taken. AT = Achilles tendon; MM = Medial malleolus, LM = Lateral malleolus.

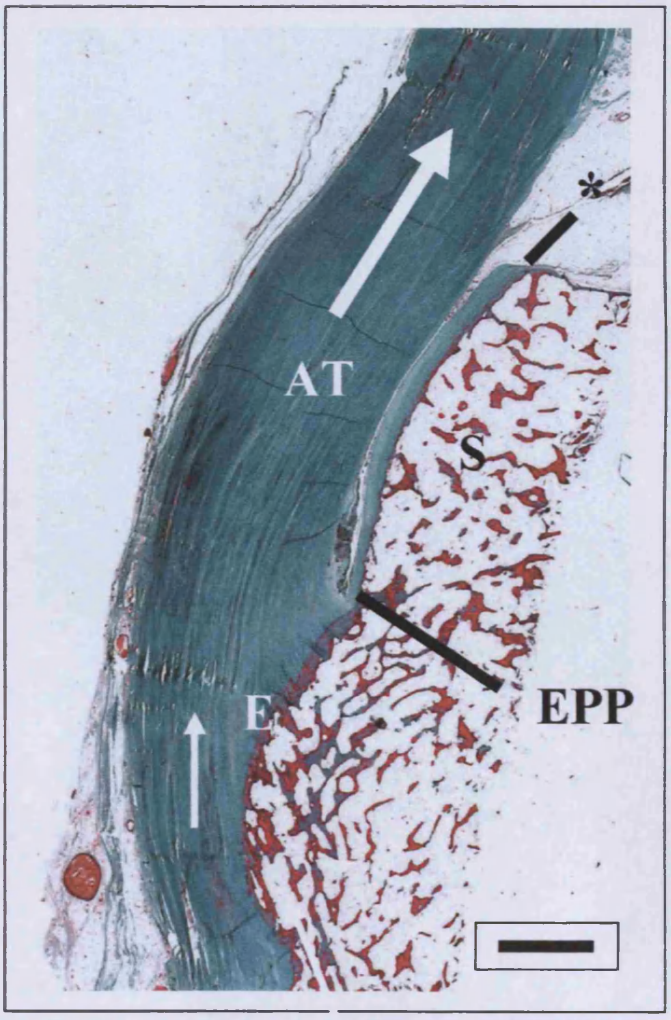

Figure 3.2.3: The anatomical landmarks identified to be used as reference frames within the Achilles tendon enthesis organ. AT = Achilles tendon; E = Enthesis; EPP = Enthesis proximal point; Small arrow = Approximated Achilles tendon axis; Large arrow = Apparent Achilles tendon axis; * = Superior tuberosity asymptote Scale bar = 3mm

Figure 3.2.4: Technique 1: Quantifying the superior tuberosity size by calculating the area between the Apparent Achilles tendon axis and superior tuberosity. Measurement acquired using a low powered histological section in the sagittal plane of the Achilles tendon enthesis organ. AT= Achilles tendon; C = Calcaneus; S= Superior tuberosity; Arrowhead = Enthesis proximal point; Highlighted area = Area between tendon and bone with 9mm radius of enthesis; Scale bar = 2mm.

Figure 3.2.5: Technique 2: Quantifying the superior tuberosity size by measuring the gradient over 5mm. The axes are defined by the Approximated Achilles tendon axis. Measurement acquired using a low powered histological section in the sagittal plane of the Achilles tendon enthesis organ. AT = Achilles tendon; C = Calcaneus, S= Superior tuberosity, Scale bar = 2mm

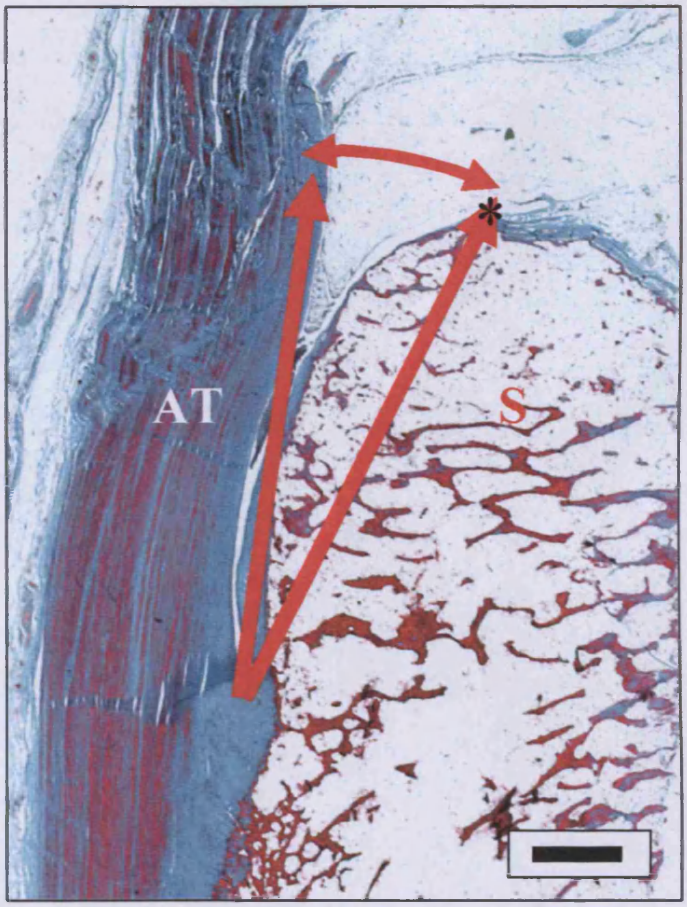

Figure 3.2.6: Technique 3: The superior tuberosity is quantified between the Apparent Achilles tendon axis and the asymptotic point of the superior tuberosity relative to this axis. AT = Achilles tendon, S = Superior tuberosity, * = Asymptotic point, Scale bar = 3mm.

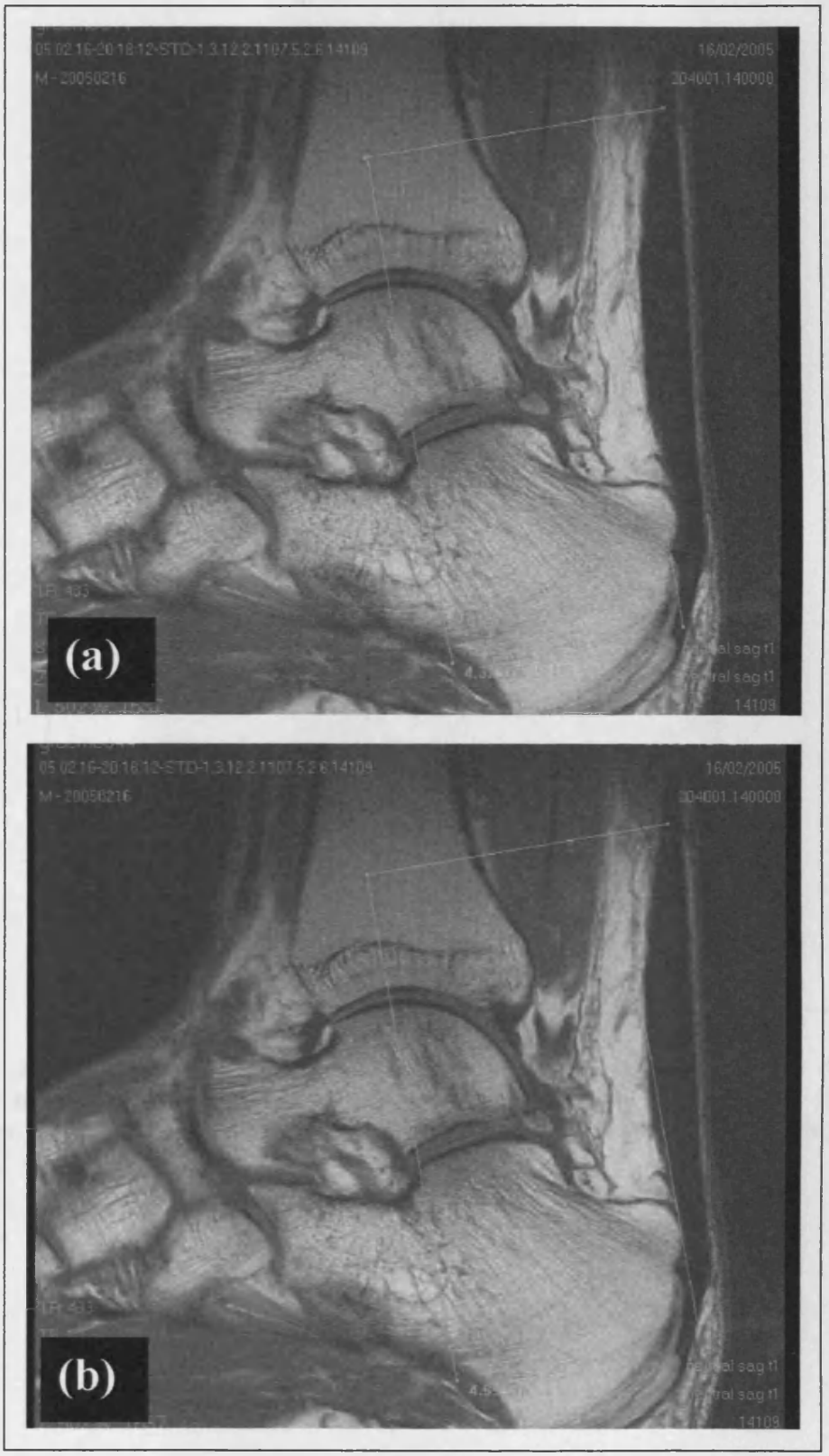

Figure 3.2.7: The Achilles tendon lever arm was measured from sagittal MRI's using Dicomworks. (a) The lever arm was measured from the ankle axis to the enthesis proximal point (b) The lever arm was measured from the ankle axis to the posterior point of the superior tuberosity.

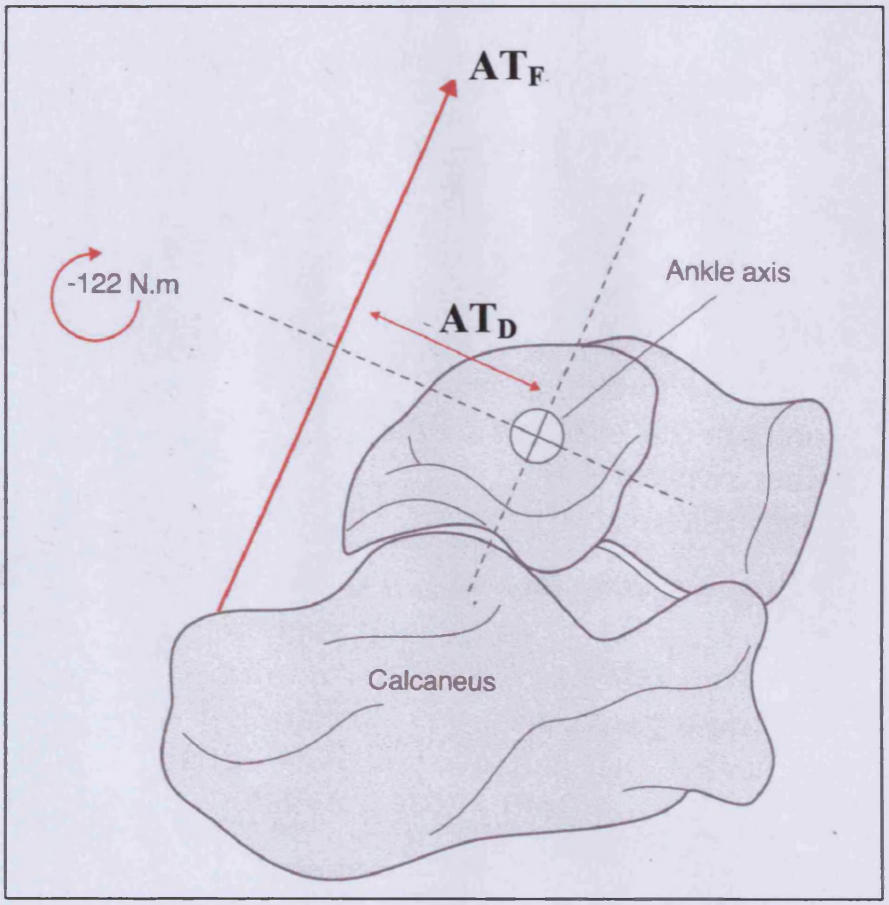

Figure 3.2.8: A schematic diagram demonstrating the calculation of the Achilles tendon tensile force (AT_F) about the ankle axis. AT_D = Perpendicular distance between the axis of load application and the pivot (Adapted from Trew & Everett **[155]**).

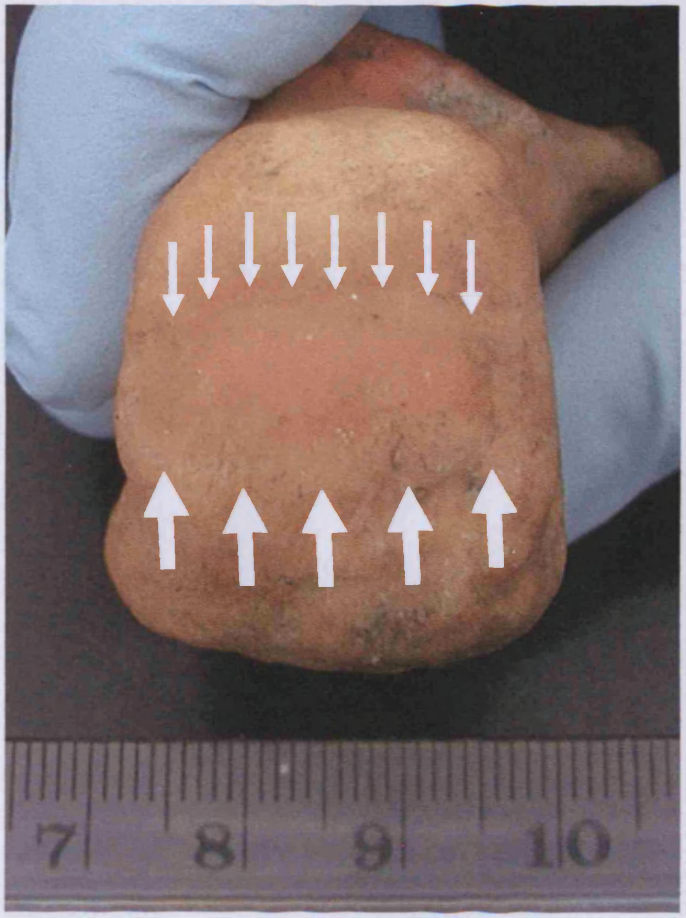

Figure 3.2.9: The posterior surface of the calcaneus. The zone of Achilles tendon attachment, in the middle third of the surface, can be identified and measured to allow the stress at the enthesis to be calculated. Large arrows = distal border of insertion zone, Small arrows = proximal border of insertion zone.

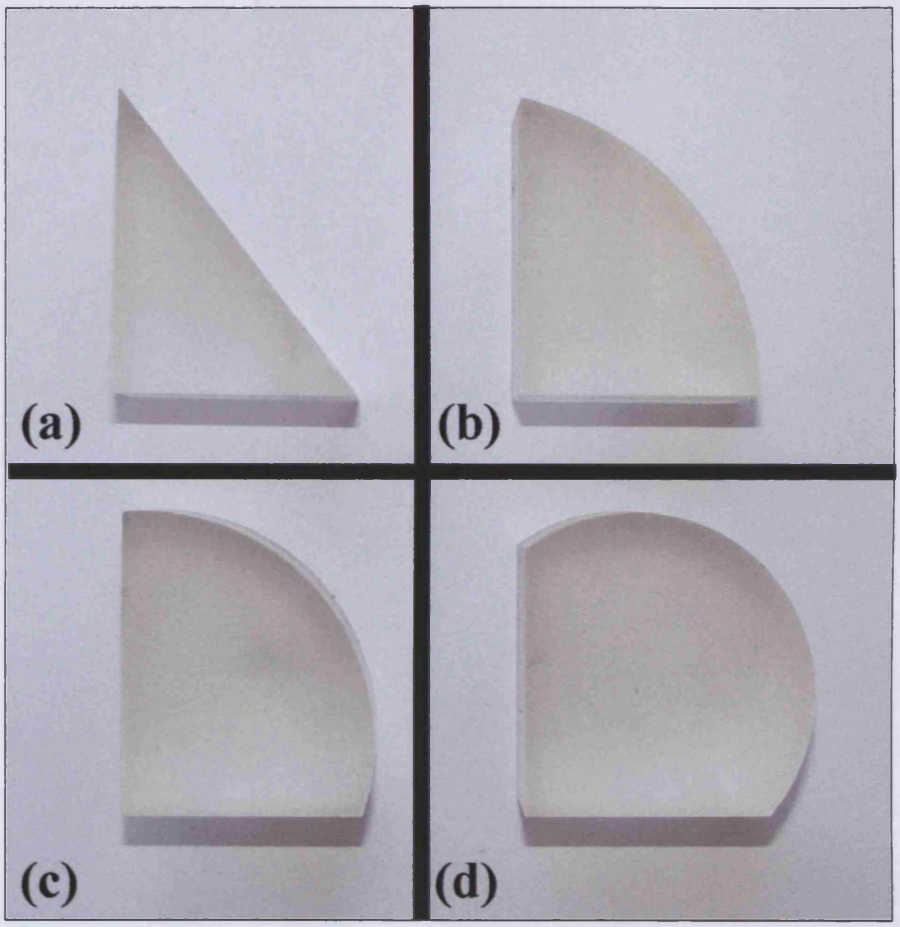

Figure 3.2.10: The superior tuberosity profiles fabricated to reflect the range of sizes observed in dissecting room cadavers (a) Profile 1, (b) Profile 2, (c) Profile 3, (d) Profile 4.

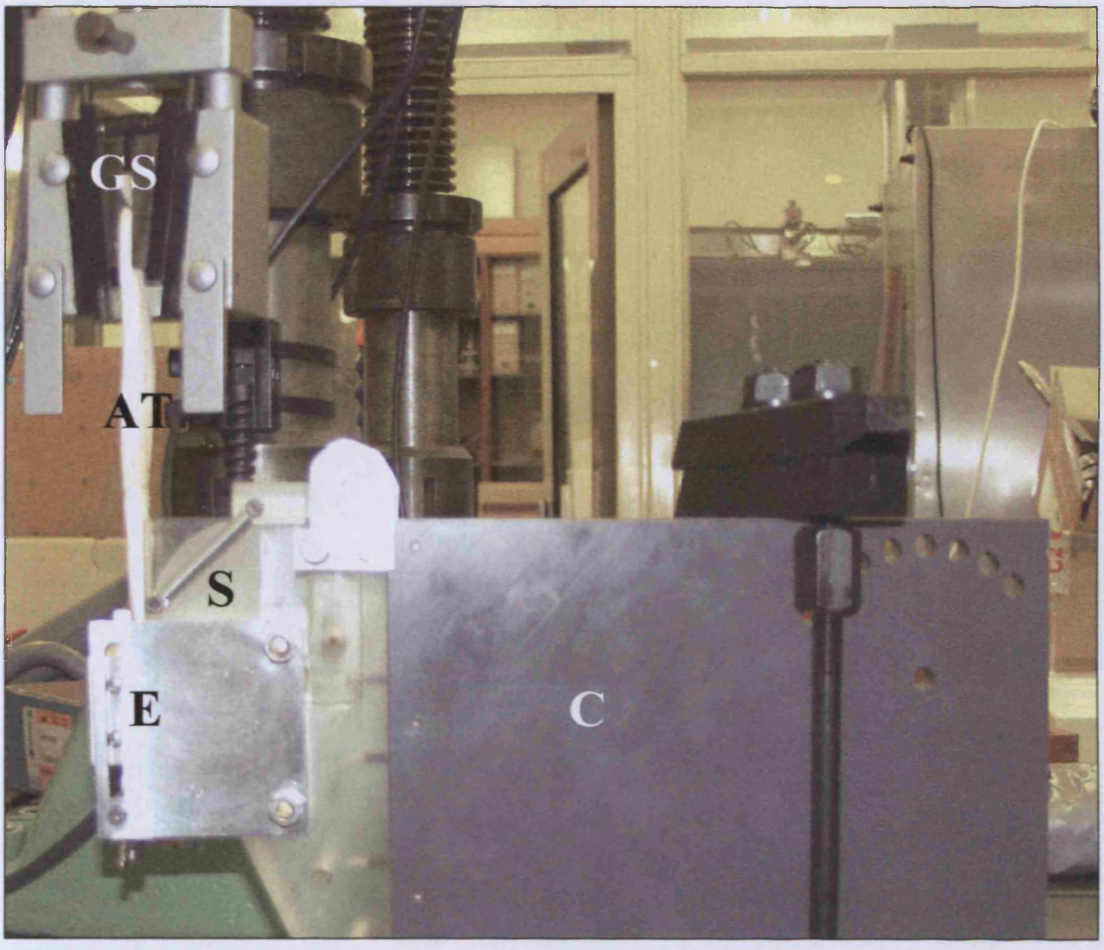

Figure 3.2.11: The mechanical model used to investigate the loading imparted on the superior tuberosity from the Achilles tendon. AT = Achilles tendon (represented by bovine flexor tendon), C = Calcaneus (represented by Perspex model), E = Achilles tendon enthesis (represented by a wedge clamp), GS = Gastrocnemius and soleus (load generated by crosshead displacement), S = Superior tuberosity (represented by Perspex profile).

3.3 Results

3.3.1 Superior Tuberosity Prominence:

The histologically processed specimens were examined to determine a more reliable method of measuring the superior tuberosity size. Where the quality of the specimen was insufficient, a '-' is recorded.

3.3.1.1 Superior Tuberosity Measuring Techniques:

- Technique 1:

Using the Apparent Achilles tendon Axis as a reference axis, the superior tuberosity prominence was quantified by measuring the area between this axis and the tuberosity that was within a 9mm radius of the Enthesis proximal point. The reciprocal of this area was calculated to ensure that a higher value quantified a larger superior tuberosity (Table 3.3.1).

Table 3.3.1: The superior tuberosity prominence measured using Technique 1.

	Superior Tuberosity Size, $x10^4$ (m^{-2})					
	Sample Point 1	**Sample Point 2**	**Sample Point 3**	**Sample Point 4**	**Sample Point 5**	**Sample Point 6**
Spec 1	-	3.2	3.1	2.8	2.6	4.0
Spec 2	100	100	66	50	33	33
Spec 3	33	22	29	33	-	-
Spec 4	12	8	9	7	-	12
Spec 5	20	-	20	-	-	-
Spec 6	-	50	33	33	7	-
Spec 7	-	40	50	67	50	50

- Technique 2:

The superior tuberosity size was defined by summation of the gradient measured relative to the Approximated Achilles tendon Axis of 5, 1mm intervals from the Enthesis proximal point (Table 3.3.2):

Table 3.3.2: The superior tuberosity prominence measured using Technique 2.

	Superior Tuberosity Size					
	Sample Point 1	**Sample Point 2**	**Sample Point 3**	**Sample Point 4**	**Sample Point 5**	**Sample Point 6**
Spec 1	-	22	20	21	26	27
Spec 2	67	57	67	55	54	42
Spec 3	61	64	68	67	-	-
Spec 4	32	28	29	18	-	29
Spec 5	32	-	24	-	-	-
Spec 6	-	41	36	43	24	-
Spec 7	-	35	39	39	44	27

- Technique 3:

The superior tuberosity size was defined by the angle between the Approximated Achilles tendon Axis and the asymptotic point of the superior tuberosity. The reciprocal was calculated to ensure that a smaller angle represented a smaller superior tuberosity (Table 3.3.3).

Table 3.3.3: The superior tuberosity prominence measured using Technique 3.

	Superior Tuberosity Size, $x10^{-3}$ (degrees^{-1})					
	Sample Point 1	**Sample Point 2**	**Sample Point 3**	**Sample Point 4**	**Sample Point 5**	**Sample Point 6**
Spec 1	-	22	22	22	21	29
Spec 2	100	67	100	50	40	40
Spec 3	67	50	56	40	-	-
Spec 4	33	26	33	25	-	29
Spec 5	29	-	25	-	-	-
Spec 6	-	40	67	40	50	-
Spec 7	-	67	67	67	83	67

The reliability of each technique was determined through validation, to allow identification of the most reliable method by which to quantify the superior tuberosity prominence. Ideally, each technique would have been used to measure a number of different superior tuberosities, and then these results compared to an existing 'gold standard' technique. Unfortunately, however, no 'gold standard' currently exists.

Equally, the resection of prominent landmarks meant that the current techniques could not be used. Thus, it was necessary to devise a method of validation.

Validation of the techniques was performed against each of the 7 specimens in order to determine the most reproducible method. Each of the 3 techniques was used to measure the 6 sample points of each specimen. The tuberosity size of each sample point within each specimen was then ranked from highest to lowest (Table 3.3.4(a)). For example, on reading from Table 3.3.4(a) it can be determined that Technique 1 defined the superior tuberosity of Sample Point 6 of Specimen 1 as the largest of the 6 Sample Points. Sample Point 5 of Specimen 1 was identified as the smallest superior tuberosity

A reliable technique was identified when 2 methods identically ranked the sample points of a specimen (Table 3.3.4 (b)). For example, Techniques 1 & 3 were reliable methods for quantifying Specimen 1.

The most reliable of the 3 techniques was identified as that most frequently correlating with the other methods. Technique 3 was seen to correlate with other methods in 5 out of the 7 specimens, and thus was identified as the most reliable.

Table 3.3.4 (a): The most reproducible technique was determined by comparing the order, from largest to smallest, that the sample points of each specimen were quantified.

	Tech 1	Tech 2	Tech 3	Correlation
Spec 1	**6,2,3,4,5**	6,5,2,4,3	**6,2,3,4,5**	1,3
Spec 2	1,2,3,4,5,6	**1,3,2,4,5,6**	**1,3,2,4,5,6**	2,3
Spec 3	1,4,3,2	**1,3,2,4**	**1,3,2,4**	2,3
Spec 4	1,6,3,2,4	**1,3,6,2,4**	**1,3,6,2,4**	2,3
Spec 5	**1,3**	**1,3**	**1,3**	1,2,3
Spec 6	2,3,4,5	4,2,3,5	3,5,2,4	-
Spec 7	4,3,5,6,2	5,3,4,2,6	5,2,3,4,6	-

Table 3.3.4(b): By determining the frequency of correlation with the other techniques, the most reliable method was identified.

Technique	Cumulative correlation
1	1
2	4
3	5

3.3.2 The Mechanical Advantage of the Superior Tuberosity:

3.3.2.1 The Lever Arm Length of the Achilles tendon

The insertional region of the Achilles tendon was examined using MRI in 3 subjects to determine the extent to which the Achilles tendon is posteriorly displaced by the superior tuberosity prominence (Table 3.3.5(a)). The relative increase in Achilles tendon lever arm as a consequence of this displacement was then calculated (Table 3.3.5(b)). The superior tuberosity size was then measured (Table 3.3.5(c)) to allow for it's affect on the lever arm length to be determined (Figure 3.3.1).

Table 3.3.5(a): The posterior displacement (mm) of the Achilles tendon caused by the superior tuberosity and angle of ankle flexion

Posterior displacement of the Achilles tendon (mm)									
Subject	Dorsiflexion			Neutral			Plantarflexion		
	Image 1	Image 2	Image 3	Image 1	Image 2	Image 3	Image 1	Image 2	Image 3
1	1.2	1.2	1	0	0	0	0	0	0
2	3.2	3	2.5	2.7	2.7	2.5	2.5	2.2	2.1
3	1	0.8	0.5	0	0	0	0	0	0

Table 3.3.5(b): The increase in Achilles tendon lever arm due to both the superior tuberosity and angle of ankle flexion (%)

Increase in Achilles tendon lever arm due to the superior tuberosity (%)									
Subject	Dorsiflexion			Neutral			Plantarflexion		
	Image 1	Image 2	Image 3	Image 1	Image 2	Image 3	Image 1	Image 2	Image 3
1	3.0	2.8	2.4	0	0	0	0	0	0
2	5.2	5.2	5.0	5.4	5.0	5.0	6.5	6.2	6.0
3	2.8	2.6	2.5	0	0	0	0	0	0

Table 3.3.5(c): The superior tuberosity size, $x10^{-3}(degrees^{-1})$

Subject	Superior tuberosity size, $x10^{-3}$ ($degrees^{-1}$)		
	Image 1	Image 2	Image 3
1	39	37	36
2	52	50	48
3	41	40	40

3.3.2.2 Achilles Tendon Mechanical Advantage

Equation 3.2.1 was used to determine the effect of the superior tuberosity size and the angle of ankle flexion on the variation of the Achilles tendon tensile force and thus the Achilles tendon mechanical advantage. These results are graphically displayed in Figure 3.3.2

3.3.3 Enthesis Shear Stress:

3.3.3.1 Enthesis Cross-sectional Area

The approximate area of attachment was measured from 4 dry, cadaveric specimens, to allow for the calculation of the shear stress at the enthesis.

Table 3.3.6: The area of the Achilles tendon enthesis

Specimen	Area, $x10^{-6}$ (m^2)
1	180
2	250
3	215
4	133
Mean	**194**

3.3.3.2 Enthesis Shear Stress:

The shear stress at the enthesis was calculated by using the data calculated in 3.3.2.2 and in Table 3.3.6. These results are displayed graphically in Figure 3.3.3.

3.3.4 Superior Tuberosity Loading:

3.3.4.1 Mechanical Assessment:

The influence of superior tuberosity size and ankle angle on the load borne from the Achilles tendon by the superior tuberosity was examined. This was achieved by fabricating a mechanical model to measure the pressure on the superior tuberosity

surface. Four different superior tuberosity sizes were produced (Figure 3.2.10), and the angle of the apparatus changed to represent 5 different ankle angles (30° & 15° dorsiflexion, neutral, 15° & 30° plantarflexion). This pressure was measured using pressure sensitive paper (PSI, Table 3.3.7(a)) and converted into SI units (kPa) (Table 3.3.7(b), Figure 3.3.5). The resolution of this method was, however, insufficient to allow for differentiation of the pressure along the surface. Thus, the recorded pressure was assumed uniform across the contact area. By measuring this contact area (Table 3.3.8(a)), the contact force could be derived (i.e. P=F/A) (Table 3.3.8(b)). This force was then calculated as a percentage relative to the tensile load applied (0.4kN) to the tendon (Table 3.3.8, Figure 3.3.6). Only 2 tests were performed for each experiment to preserve the very limited supply of fresh tissue.

Table 3.3.7(a): The pressure (PSI) recorded on the surface of the superior tuberosity when in contact with bovine flexor tendon

	Pressure (PSI)				
	30° DRF	**15° DRF**	**Neutral**	**15° PLF**	**30° PLF**
Profile 1					
Test 1	0	0	0	0	0
Test 2	0	0	0	0	0
Mean	**0**	**0**	**0**	**0**	**0**
Profile 2					
Test 1	83.00	83.00	85.00	0	0
Test 2	83.00	83.00	85.00	0	0
Mean	**83.00**	**83.00**	**85.00**	**0**	**0**
Profile 3					
Test 1	114.00	83.00	85.00	78.00	0
Test 2	114.00	83.00	85.00	69.00	0
Mean	**114.00**	**83.00**	**85.00**	**73.50**	0
Profile 4					
Test 1	142.00	114.00	95.00	85.00	78.00
Test 2	142.00	114.00	83.00	85.00	83.00
Mean	**142.00**	**114.00**	**89.00**	**85.00**	**80.50**

Table 3.3.7(b): The pressure (kPa) recorded on the surface of the superior tuberosity when in contact with bovine flexor tendon

	Pressure (kPa)				
	30° DRF	**15° DRF**	**Neutral**	**15° PLF**	**30° PLF**
Profile 1					
Test 1	0	0	0	0	0
Test 2	0	0	0	0	0
Mean	**0**	**0**	**0**	**0**	**0**
Profile 2					
Test 1	570	570	590	0	0
Test 2	570	570	590	0	0
Mean	**570**	**570**	**590**	**0**	**0**
Profile 3					
Test 1	790	570	590	540	0
Test 2	790	570	590	480	0
Mean	**790**	**570**	**590**	**510**	**0**
Profile 4					
Test 1	980	790	660	590	540
Test 2	980	790	570	590	570
Mean	**980**	**790**	**615**	**590**	**555**

Table 3.3.8(a): The area of contact on the superior tuberosity (m^2)

	Contact area, $x10^{-4}$ (m^2)				
	30° DRF	**15° DRF**	**Neutral**	**15° PLF**	**30° PLF**
Profile 1					
Test 1	0	0	0	0	0
Test 2	0	0	0	0	0
Mean	**0**	**0**	**0**	**0**	**0**
Profile 2					
Test 1	1.44	1.44	0.75	0	0
Test 2	1.69	1.54	0.75	0	0
Mean	**1.57**	**1.49**	**0.75**	**0**	**0**
Profile 3					
Test 1	4.00	2.70	1.65	0.65	0
Test 2	4.18	2.70	1.70	0.55	0
Mean	**4.09**	**2.70**	**1.68**	**0.60**	**0**
Profile 4					
Test 1	6.50	4.00	2.04	1.82	0.54
Test 2	7.20	4.00	2.04	2.04	0.57
Mean	**6.85**	**4.00**	**2.04**	**1.93**	**0.56**

Table 3.3.8(b): The contact force on the superior tuberosity (N)

	Contact force (N)				
	30° DRF	**15° DRF**	**Neutral**	**15° PLF**	**30° PLF**
Profile 1					
Test 1	0	0	0	0	0
Test 2	0	0	0	0	0
Mean	**0**	**0**	**0**	**0**	**0**
Profile 2					
Test 1	82.4	82.4	44.0	0	0
Test 2	96.7	88.1	44.0	0	0
Mean	**89.6**	**85.3**	**44.0**	**0**	**0**
Profile 3					
Test 1	314	155	96.7	35.0	0
Test 2	329	155	99.6	26.2	0
Mean	**321**	**155**	**98.2**	**30.4**	**0**
Profile 4					
Test 1	636	314	134	107	56.5
Test 2	705	314	117	110	60.1
Mean	**671**	**314**	**126**	**113**	**58.3**

Table 3.3.9: The mean percentage of the 0.4kN Achilles tendon tensile load borne by the superior tuberosity

	Mean percentage of loading on ST (%)				
	30° DRF	**15° DRF**	**Neutral**	**15° PLF**	**30° PLF**
Profile 1	0	0	0	0	0
Profile 2	22.4	21.3	11.0	0	0
Profile 3	80.3	38.8	24.5	7.6	0
Profile 4	168	78.5	31.5	28.3	14.6

Whilst the mechanical model provided useful data detailing the load borne by the superior tuberosity, the resolution of the measuring system was limited. Thus, any difference in load borne along the length of the superior tuberosity was unlikely to be identified.

3.3.4.2 Physiological Assessment:

As fibrocartilage is believed to develop in response to loading **[31, 136, 137, 158]**, the thickness of the periosteal fibrocartilage (PF) was used to provide additional data. The absolute thickness of the PF could not be related to the *in vivo* loading environment experienced, as cadaveric case history was not available. By identifying the position of maximum thickness and thus indicating the position of maximum loading, however, this data was normalised. Thus, measuring was performed in 2 stages.

First, the PFC thickness of 3 sections from each sample point of each cadaveric specimen was measured at 500μm intervals perpendicular to the underlying subchondral bone. The maximum thickness of each sample point was then identified (Table 3.3.10). Where the quality of the section was insufficient to measure the periosteal fibrocartilage, no result was recorded (signified by a '-').

Table 3.3.10: The maximum periosteal fibrocartilage thickness (μm) per sample point of each specimen.

Maximum PF Thickness (μm)						
Spec	**Sample Point**					
	1	**2**	**3**	**4**	**5**	**6**
1	-	330	330	450	520	530
2	400	350	800	400	550	550
3	850	700	700	700	700	-
4	1200	700	750	500	1400	-
5	1200	1400	1100	1100	2200	-
6	-	800	700	800	-	-
7	600	650	650	650	620	600

The position of maximum PF thickness along the length of the superior tuberosity size was then identified. Due to the length of the superior tuberosity being dependant on the size of the tuberosity, the position of the maximum thickness had to be normalised. This was achieved by calculating the position of maximum thickness relative to the superior tuberosity length (where the superior tuberosity is defined between the most proximal point of the enthesis and the asymptotic point) (Table 3.3.11). Where the asymptotic point of the superior tuberosity could not be identified, a calculation could not be performed ('N/A' was recorded). No result was recorded where the histological section quality was insufficient (signified by a ' - ').

Table 3.3.11: The relative position (%) along the length of superior tuberosity of the maximum periosteal fibrocartilage thickness

Relative Position of Maximum PF Thickness (%)						
Spec	**Sample Point**					
	1	**2**	**3**	**4**	**5**	**6**
1	-	33	33	25	N/A	36
2	90	94	N/A	N/A	33	35
3	66	85	77	60	N/A	-
4	70	85	77	60	N/A	-
5	20	-	N/A	-	-	-
6	-	33	94	38	-	-
7	N/A	77	75	75	75	60

These results are displayed graphically in Figure 3.3.6.

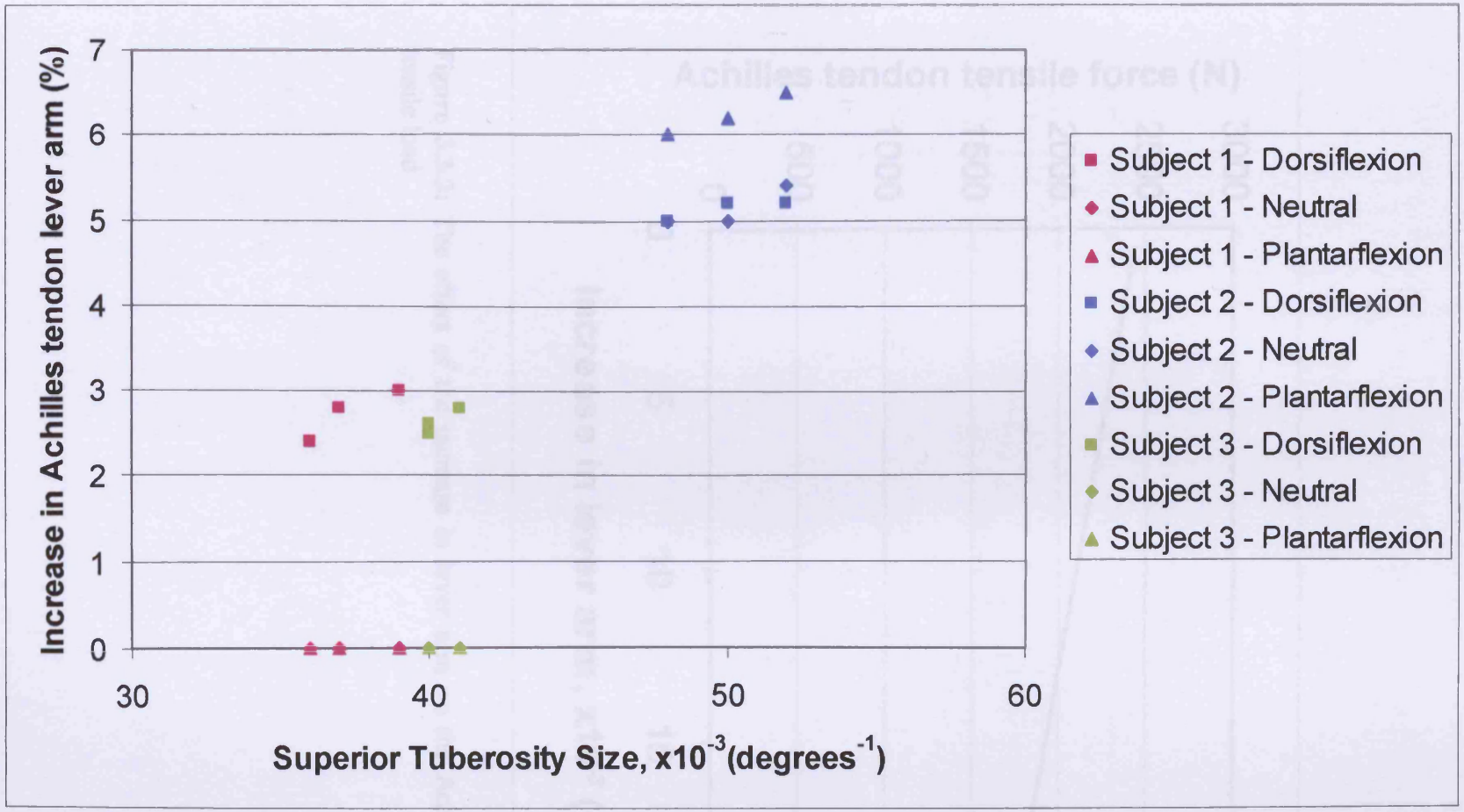

Figure 3.3.1: The superior tuberosity size influences the Achilles tendon lever arm length.

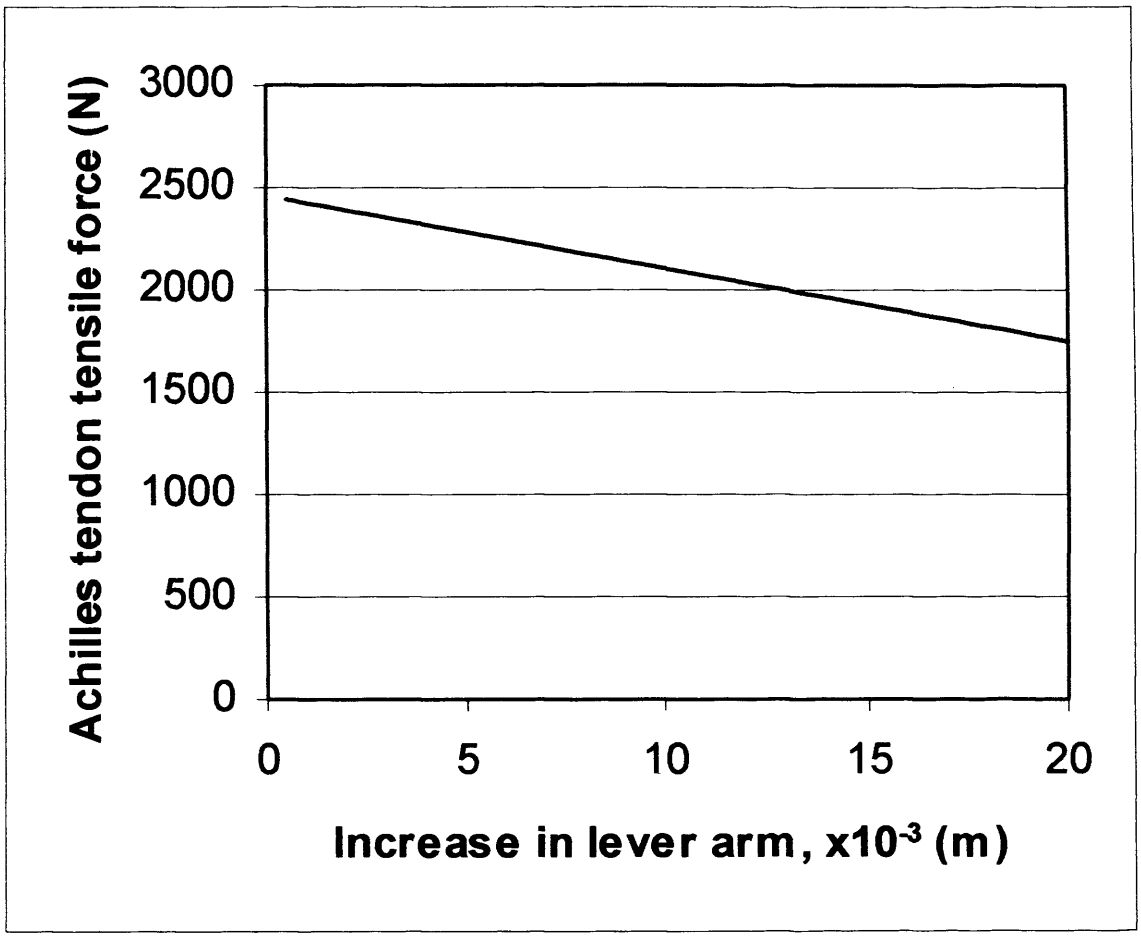

Figure 3.3.2: The effect of the increase in lever arm on the Achilles tendon tensile load

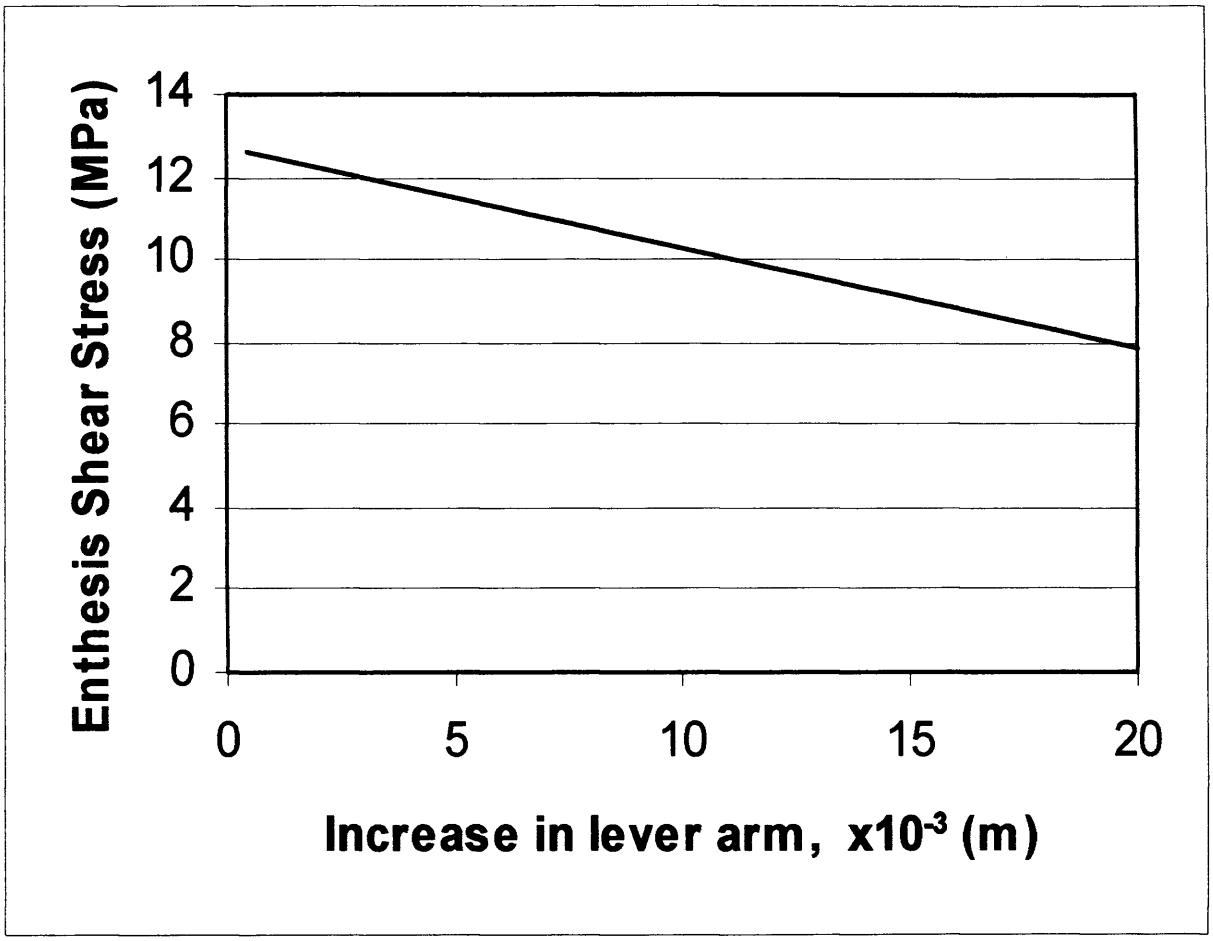

Figure 3.3.3: The effect of the increase in lever arm on the Achilles tendon enthesis shear stress

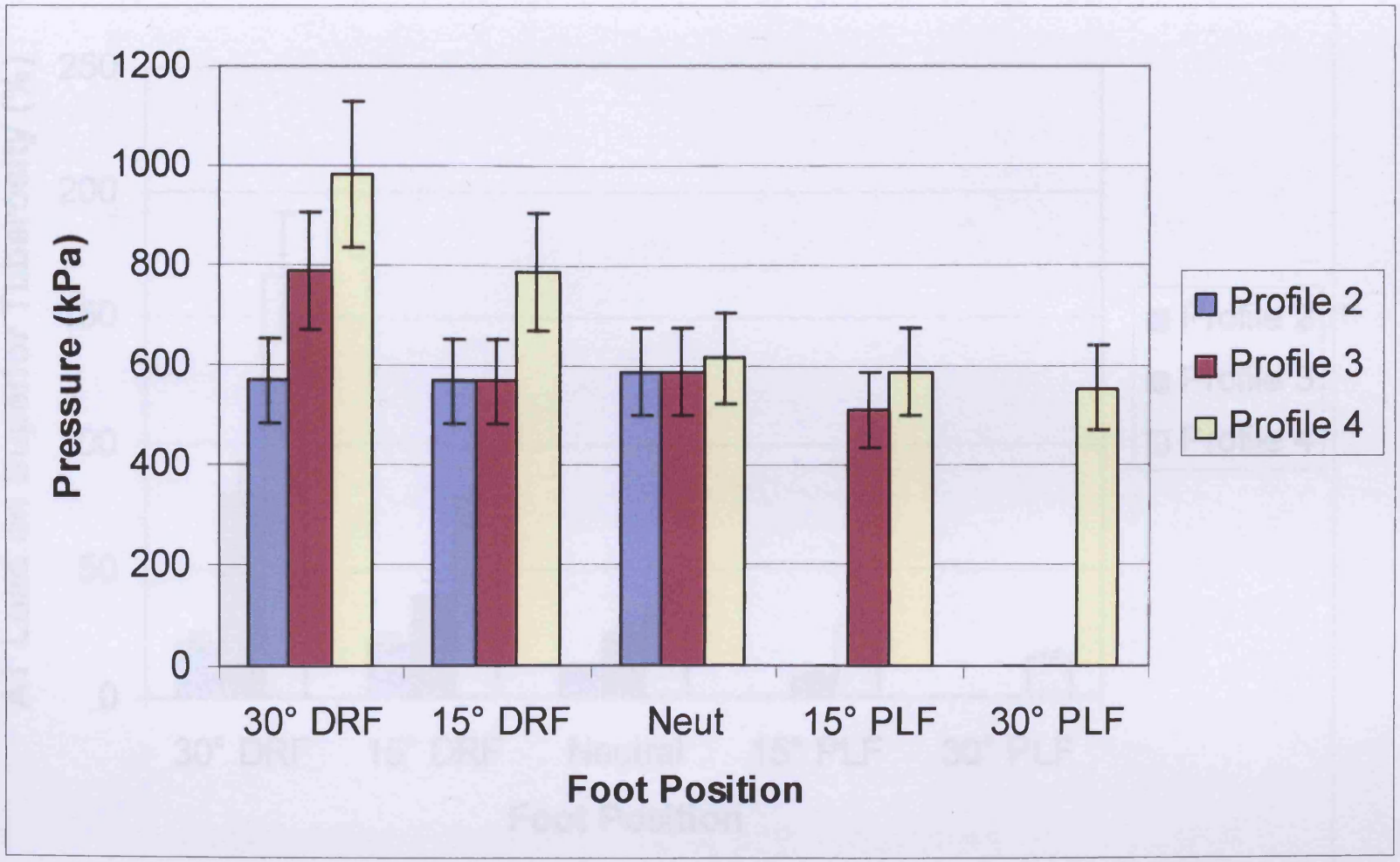

Figure 3.3.4: The pressure recorded on the superior tuberosity. ±15% error bars reflect the published accuracy of the pressure sensitive paper.

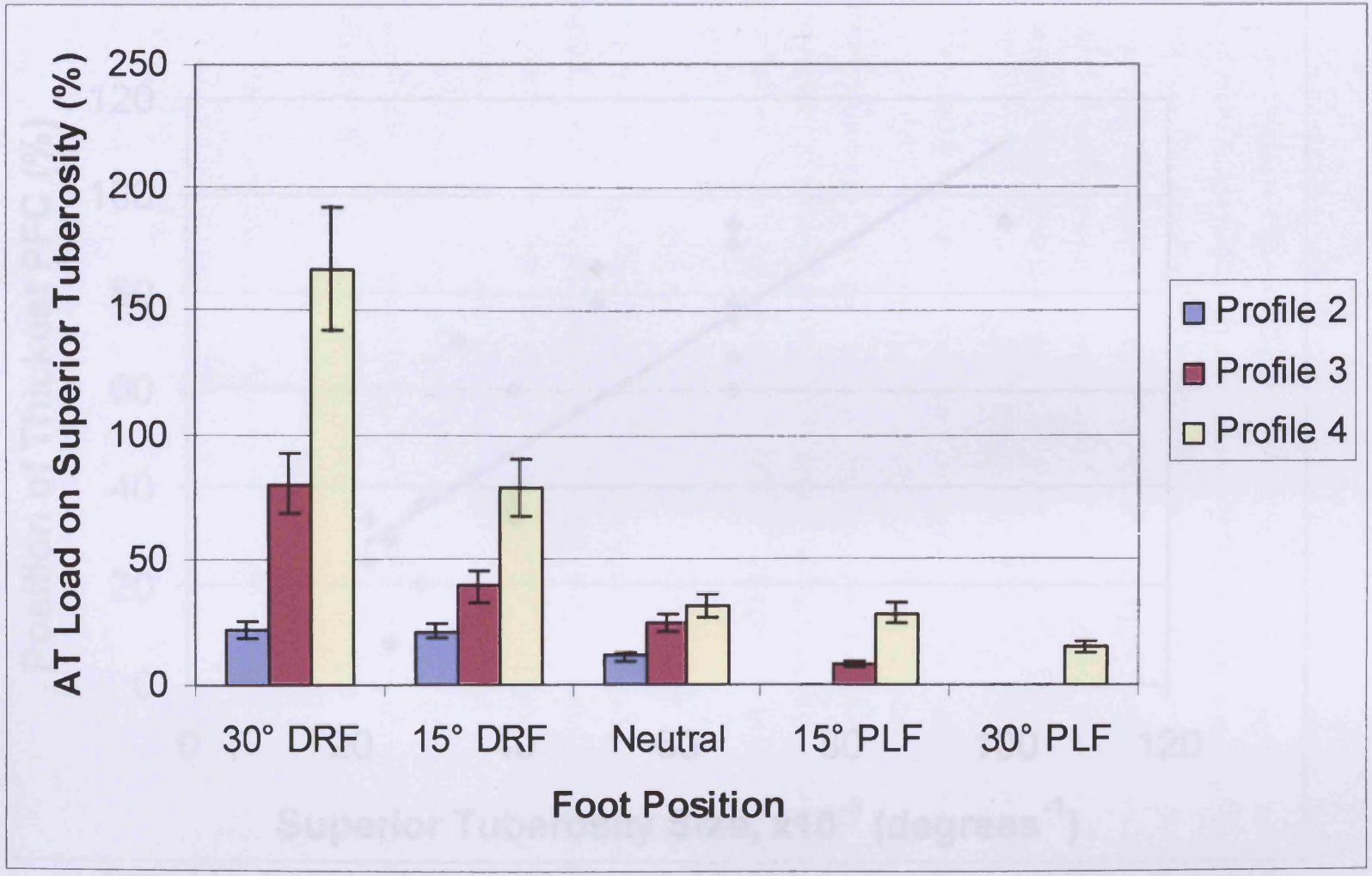

Figure 3.3.5: The load recorded on the superior tuberosity, relative to the 0.4kN tendon tensile load. ±15% error bars reflect the published accuracy of the pressure sensitive paper.

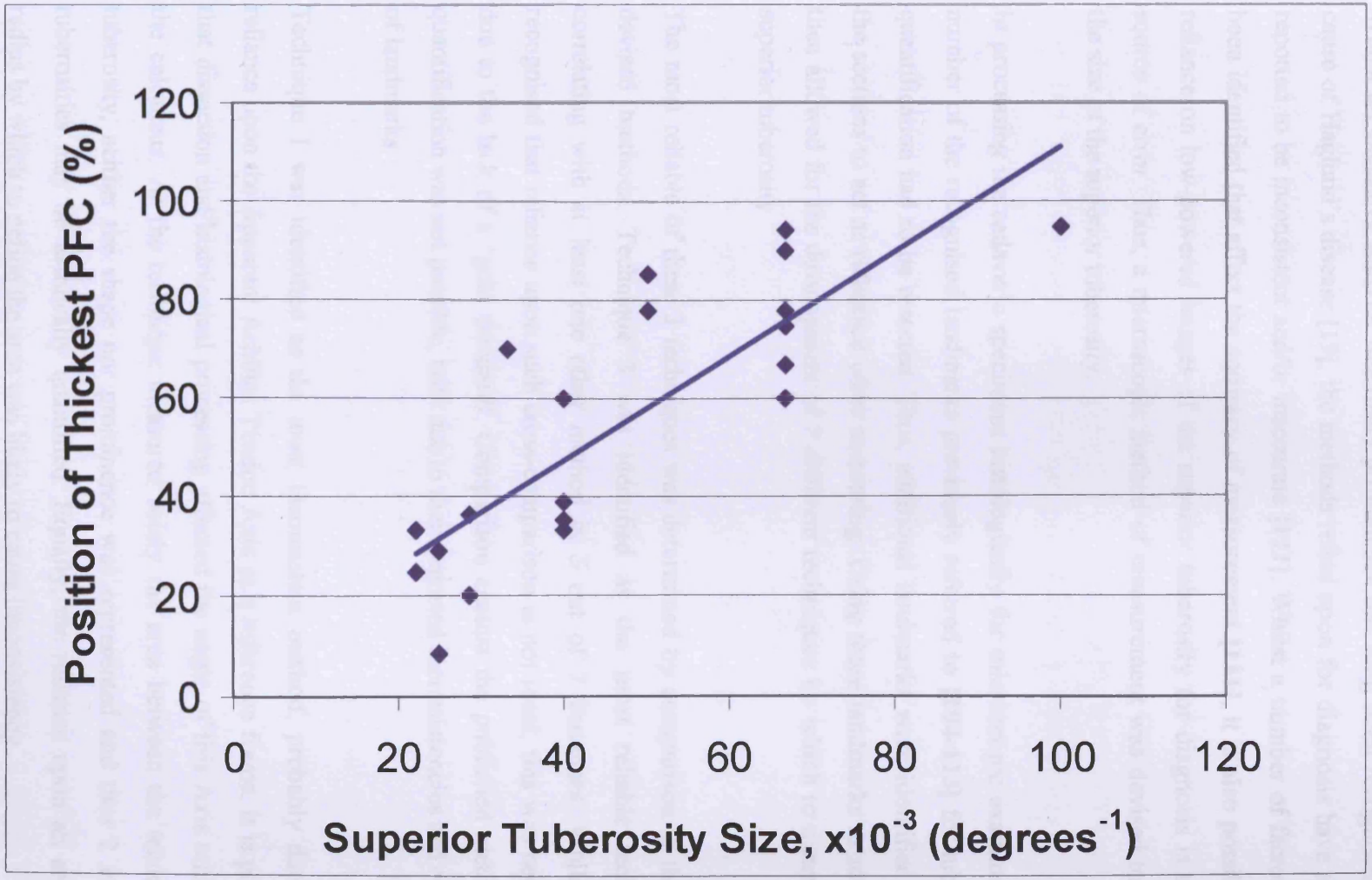

Figure 3.3.6: The relationship between the position of the thickest region of periosteal fibrocartilage and the superior tuberosity size. $R^2 = 0.70$.

3.4 Discussion

Whilst an excessive superior tuberosity prominence has long been recognised as the cause of Haglund's disease **[19]**, the methods relied upon for diagnosis have all been reported to be inconsistent and/or inaccurate **[111]**. Whilst a number of factors have been identified that affect the accuracy of measurement **[111]**, it is also possible that reliance on low-powered images of the superior tuberosity for diagnosis is a likely source of error. Thus, a microscopic method of measurement was devised to assess the size of the superior tuberosity.

In processing the cadaveric specimens histologically for microscopic examination, a number of the recognised landmarks previously referred to **[104-113]** for tuberosity quantification had to be resected. Thus, additional landmarks were identified within the sections to act as reference when measuring. Using these landmarks as reference then allowed for the development of 3 different techniques by which to quantify the superior tuberosity.

The most reliable of these 3 techniques was determined by comparison to the other devised methods. Technique 3 was identified as the most reliable technique, correlating with at least one other method in 5 out of 7 instances. Whilst it is recognised that reliance upon such cross-comparison is not ideal, this was necessary due to the lack of a 'gold standard'. Comparison against the published methods of quantification was not possible, both due to their reported inconsistencies and removal of landmarks.

Technique 1 was identified as the most inconsistent method, probably due to its reliance upon the Apparent Achilles Tendon Axis as a reference frame. It is probable that dissection and histological processing affected the angle of this Axis relative to the calcaneus. As the technique measured solely the area between the tendon and tuberosity, neither the shape nor prominence was represented and thus 2 superior tuberosities may be identically quantified. Equally, the reliance upon an arbitrary radius by which to define the area was likely to cause inconsistency.

Whilst Technique 2 appeared to reliably quantify the superior tuberosity shape and profile, it could not quantify any superior tuberosities that extended across the reference y-axis. This lack of robustness meant that the technique was unable to quantify all shapes of superior tuberosity and thus was insufficiently reliable.

Technique 3 was identified as the most reliable method of superior tuberosity quantification. This was surprising as it did not directly measure the size of the prominence, as in earlier methods. Instead, it relied upon the arc of the superior tuberosity. Thus, in instances where the curve was discontinuous and thus inconsistent - as in Specimen 7, the method failed.

As only 7 specimens were available for examination, the accuracy of the assessment protocol was not statistically significant. A greater number of specimens are required to be examined for the statistical confidence in the technique to be assessed. This is particularly important given the method of self-validation that was employed, due to no 'gold standard' existing. A number of superior tuberosities were not quantified, due to the asymptotic point having been resected to allow for histological processing. Should this technique be translated to a clinical environment, however, macroscopic radiographic images would not present such a problem.

The posterior displacement and subsequent lengthening of the Achilles tendon lever arm as a result of both a prominent superior tuberosity and dorsiflexion of the foot was examined in relation to the shear stress at the enthesis. This is significant as it has implications in the treatment of Haglund's disease and the removal of the superior tuberosity. In such cases, a large superior tuberosity – and thereby a long Achilles tendon lever arm, is resected and thus the Achilles tendon lever arm is shortened. With a reduction in lever arm length occurring – perhaps to the extent of 15-20mm – an increase in Achilles tensile force (Figure 3.3.2), and thus the shear stress at the enthesis (Figure 3.3.3), would be expected. However, as a fresh human Achilles tendon enthesis withstood a stress of greater than 71MPa when a human Achilles tendon-bone complex was tested *in viva* **[14]**, such an increase in shear stress to approximately 13MPa post-operatively appears inconsequential. Whilst this figure is

influenced by additional factors such as body weight and activity, as the ultimate tensile loading of the Achilles tendon has been estimated at 9kN, it is this that is likely to fail first **[2]**.

When examined mechanically, the pressure borne by the superior tuberosity from the Achilles tendon varied considerably, and was again dependent on both the foot position and the size of the superior tuberosity. As expected, at all flexion angles Profile 4 recorded the maximum pressure (Figure 3.3.4). Interestingly, however, the pressure on the surface of Profiles 2 & 3 was identical in two out of three foot positions (Figure 3.3.4), with the pressure unexpectedly increasing slightly between dorsiflexion and the neutral position. It is likely, however, that this increase is due to a measurement error, as indicated by the magnitude of the error bars.

Whilst the pressure borne by the superior tuberosity is probably a more likely criterion against which potential damage to the contacting surfaces can be assessed, the load borne is useful to examine as it can be compared directly to the Achilles tendon tensile load. It was observed that a large superior tuberosity may be compressed by a load equivalent to approximately 160% of the Achilles tendon tensile load (Figure 3.3.5). Where a superior tuberosity is significantly smaller, one-eighth of this compressive load may be experienced. As the ultimate tensile loading of the Achilles tendon has previously been estimated at 9kN **[2]**, this potentially translates to an 8kN difference in the compressive load experienced on the different superior tuberosities, depending on their shape.

In experiencing an equal and opposite reaction force from the surface of the superior tuberosity, the Achilles tendon strain is likely to increase. As the loading upon the tendon changes during ankle flexion it will, whilst in contact with the superior tuberosity, be extending and recoiling during the gait cycle. Effectively sliding over the superior tuberosity, this movement is likely to cause wearing of the conjoining surfaces, as has been previously reported in the knee and hip joints **[159]**.

Whilst these results have clinical implications, caution should be exercised when interpreting due to the simplifications of the apparatus. Whilst the geometry of both the attachment of and contact between the calcaneus and Achilles tendon *in vivo* is

non-uniform, the geometry of the model in the z-direction was uniform for simplicity. Thus, the uneven distribution of load and pressure expected *in vivo* was not produced, and hence its effects not considered. Equally, whilst the rigid Perspex surface was likely to provide an accurate representation of the bony superior tuberosity surface, the affect of the periosteal and sesamoidal fibrocartilages on the contact was not considered. Also, whilst the material properties of the bovine flexor tendon was similar to the human Achilles tendon **[156]**, the use of fresh human tissue should be considered to further improve the accuracy of the results. Ethical restrictions meant that this was not possible in this study.

It appeared from the mechanical model that the superior tuberosity controls the insertional angle of the Achilles tendon. A prominent superior tuberosity is likely to promote a more gentle curving of the Achilles tendon *in vivo*, and thus probably dissipate the bending of the collagen fibres. This has previously been identified as a vital protective role of the enthesis fibrocartilage **[73, 130]**. Where a smaller tuberosity is present, the increased bending of the collagen fibres at the interface would intuitively weaken the insertion. However, such stress concentrations could not be modelled using this apparatus. Ideally, this effect of the superior tuberosity would be modelled computationally as consideration of the individual tissues within the Achilles tendon enthesis organ could be accurately represented. Indeed, a finite element model to perform such an analysis was developed for this study. It became apparent, however, that material property data for the tissues within the enthesis organ was extremely limited, as well as the contact within the Achilles tendon enthesis organ being challenging to model. Whilst these problems significantly limited the development of this model, a geometrically-accurate two dimensional model of the mechanical apparatus described above was developed. This is discussed in Appendix A6, and will hopefully prove a useful position from which to continue to evaluate the Achilles tendon enthesis organ computationally when a more thorough knowledge of the material properties within it have been obtained.

The periosteal and sesamoidal fibrocartilages of the Achilles tendon enthesis organ have been identified as protecting these conjoining surfaces from such wear. Whilst the variation in the thickness of these fibrocartilages could indicate the load borne physiologically, the thickness is also likely to be affected by parameters including

gender and body weight. The data could not be normalised, however, as there was not any case history available for the dissecting room cadavers. Thus, the position of maximum periosteal fibrocartilage thickness was examined, which was probably indicative of the position of maximum load. This was seen to correlate with superior tuberosity size, and thus could prove useful in predicting the area of the Achilles tendon and superior tuberosity where degeneration would first be anticipated in cases of Haglund's disease.

3.5 Conclusions

The major conclusions of the work presented in this chapter are:

1. A method of microscopic superior tuberosity quantification was devised in recognition of the poor results currently reported using techniques based upon macroscopic radiographs.

2. The superior tuberosity size and angle of ankle flexion both affect the shear stress at the Achilles tendon enthesis.

3. Superior tuberosity resection to surgically cure Haglund's disease appears unlikely to increase the risk of exceeding the ultimate tensile load of the enthesis.

4. The role of the superior tuberosity in controlling the Achilles tendon insertional angle was identified and the consequences of this angle changing following resection discussed.

5. The pressure upon the superior tuberosity as a consequence of contacting the Achilles tendon was found normally to be dependant on both superior tuberosity shape and angle of ankle flexion.

6. The load on the superior tuberosity was found to vary depending on both foot position and tuberosity size. An 8-fold difference in compressive load was observed between the largest and smallest tuberosity when under the same loading conditions and in the same foot position.

4, The Biomechanical Anatomy of Kager's Fat Pad

4.1 Introduction

Kager's fat pad is recognised as a structure within the Achilles tendon enthesis organ, although neither its biomechanical nor physiological function is understood. Kager's fat pad is frequently referred to by clinicians as it is a commonly used radiographic landmark. This is due to its distinct appearance on lateral radiographs as a sharply marginated, radiolucent triangle **[148]** (Figure 4.1.1). The fat pad is situated within Kager's triangle, and thus it is bordered anteriorly by flexor hallucis longus (FHL), posteriorly by the Achilles tendon and inferiorly by the calcaneus **[103, 148, 149, 151]**.

It has previously been hypothesised that Kager's fat pad may act as a "variable space filler" within the Achilles tendon enthesis organ **[152]**, presumably moving into the retrocalcaneal bursa on ankle flexion. Such movement has been predicted to convey a mechanical advantage to the Achilles tendon **[144, 152]** and the triceps surae **[109]** by increasing their respective lever arms. A lack of detailed biomechanical knowledge, however, means that the significance of Kager's fat pad remains unclear. As a consequence, the fat pad is commonly removed when performing arthroscopic ankle surgery to allow for an unobstructed view of the site of interest. Here, comparison can be drawn to the knee meniscus that too was excised before its biomechanical functions were fully established **[29]**. As the physiological and biomechanical significance of menisci have since been identified, their preservation is now strongly favoured.

The purpose of the work in this chapter was to describe the anatomical structure of Kager's fat pad and thereby improve the biomechanical understanding of the fat pad within the Achilles tendon enthesis organ. By using a number of different analytical techniques, a thorough micro- and macroscopic examination of the structure was performed *in vivo* and cadaverically.

Histologically processing cadaveric specimens allowed a microscopic examination of the structure of Kager's fat pad, thereby enabling specialised regions of the tissue to be identified and the biomechanical significance hypothesised. Macroscopic

examination of the fat pad was also performed using the dissecting cadavers to assess Kager's fat pad macroscopically. Kager's fat pad was also investigated using MRI to examine the tissue in 3 orthogonal planes, thus identifying any divisions within the tissue. Doppler ultrasound was also used to examine the blood supply both to and through the fat pad.

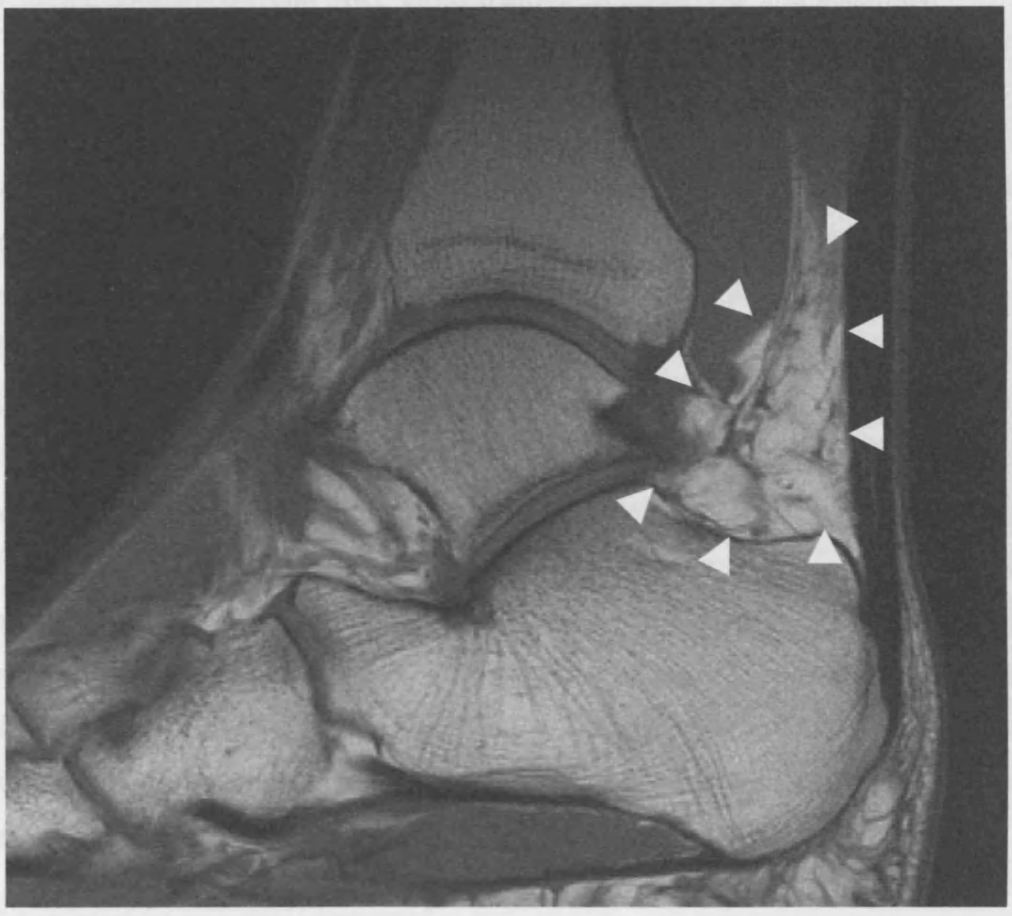

Figure 4.1.1: A sagittal MRI of the ankle joint, highlighting Kager's triangle in which Kager's fat pad is situated. Kager's triangle is commonly used as a reference frame when evaluating disorders of the ankle joint, due to its distinct radiographic appearance. Arrowheads = The borders of Kager's fat pad.

4.2 Materials and Methods

The work in this Chapter provided a thorough micro- and macroscopic examination of Kager's fat pad and therefore allowed its biomechanical functions to be assessed. Examination was achieved by utilising a number of imaging and analytical techniques including sonographic and MRI, gross anatomical dissection, and histology.

4.2.1 Gross Anatomical Dissection:

Six perfusion-fixed, elderly dissecting room cadavers (3 males, 3 females, 71-101 years) donated to Cardiff School of Biosciences (Cardiff University, UK) for anatomical investigation under the provision of the 1984 Anatomy Act and the 1961 Human Tissue Act, were dissected to examine the gross anatomy of Kager's fat pad. A hemisection of the posterior aspect of the calcaneus of 2 cadaveric right feet allowed for appreciation of the relationship between Kager's fat pad and the neighbouring structures. The hemisections were achieved by using a fine saw to cut along the midsection of the posterior surface of the calcaneus. A second saw cut was made into the medial surface of the calcaneus. Beginning at approximately the midsection of the calcaneus, the cut was made at an angle of approximately 45° to the plantar surface, towards the Achilles tendon. This cut was continued to a depth until it met with the first saw cut. A scalpel was used to dissect the Achilles tendon and the fat pad where necessary, to allow for completion of the hemisection.

A second dissection removed the skin from the posterior surface of the calcaneus, exposing the deep fascia. A long incision was made along the midline of the posterior surface of 2 right feet. Careful manipulation of the scalpel allowed for exposure of the deep fascia. Using tweezers to ensure the skin remained taut, the dissection continued until the deep fascia and paratenon were fully exposed. The relationship between the deep fascia and Kager's fat pad was then qualitatively investigated.

The third dissection investigated the blood supply to Kager's fat pad. A hemisection on 2 right feet was again performed following the protocol of the first dissection. By careful dissection of Kager's fat pad, blood vessels were identified and traced back to

determine the origin of their supply. This procedure was repeated on both the medial and lateral aspect of the fat pad.

4.2.2 Histological Analysis:

The cadaveric histological sections produced in Chapter 3 (4 male, 3 female; aged 64-87 years) were analysed with reference to the biomechanical anatomy of Kager's fat pad. Initially, examination of the fat pad geometry under low powered magnification (using a x1.6 objective lens) allowed for a qualitative assessment of the fat pad geometry. A general examination of the fat pad was then performed under a variety of magnifications (using x1.6, x2.5, x5, and x10 objective lenses) to thoroughly investigate the components of the structure. The microscope was calibrated by taking a series of photographs of a 1mm (100 x 10 μm) calibration slide with the same range of objective lenses.

Specific regions of Kager's fat pad were then focussed upon and examined following identification during gross investigation. Again, a range of magnifications (using x1.6, x2.5, x5, x10 objectives) ensured a thorough analysis.

4.2.3 MRI Protocol:

MRI imaging allowed for high resolution images of Kager's fat pad *in vivo*. In all instances the right foot of 3 healthy male volunteers (age 31, 51 & 60 years) was imaged using a 1.5 T Siemens MR scanner (Erlangen, Germany). None of the volunteers had a history of significant injury to the Achilles tendon or ankle, and all 3 were asymptomatic. The versatility of MRI in identifying different tissues at different intensities meant that there were a number of parameters to be set. In order to ensure that the fat pad was the focus of the image, T1 weighted non-fat saturated conventional spin echo scans, with a matrix size 512 x 384, the field of view 18cm, repetition time 480ms and echo time 12ms were used. On completion of imaging, the files were transferred either onto a compact disc and posted, or sent electronically from the USA. The images were then analysed on a personal computer using the

DicomWorks freeware package in Cardiff. This software allows for measurements to be made directly from the MRI.

The first series of MRI's was designed to provide a general analysis of Kager's fat pad although, due to its size, only the distal aspect was included in this image. With the subject in the supine position, MRI's were acquired of the subject's foot in 3 different positions. The subject was imaged with the foot in a position of maximum dorsiflexion, the anatomical (neutral) position, and in maximum plantarflexion. Images were acquired in 3 orthogonal planes, with a slice thickness of 3mm, and with zero gap. On viewing the images in DicomWorks, the movement of Kager's fat pad was examined qualitatively rather than quantitatively, as the low power reduced the measuring accuracy.

A second MRI study was designed to examine whether, when contracting to flex the big toe, the increase in FHL girth influences the position of Kager's fat pad. The same 3 subjects were imaged flexing and then extending their big toe whilst in the supine position. Imaging was focussed upon the anterior wall of Kager's triangle, with the ankle remaining in the neutral position to ensure only one variable. Qualitative analysis was again performed using DicomWorks.

4.2.4 Doppler Ultrasound Examination:

Doppler ultrasound was used to assess the blood flow through Kager's fat pad in order to identify whether the tissue was influential in the vascularisation of the neighbouring Achilles tendon. Whilst the protocol is detailed below, a brief account of the theory underpinning the technique is given in Appendix A7.

The study was performed at the University Hospital of Wales (Medical Physics and Clinical Engineering Directorate, UHW, Cardiff, UK). Doppler ultrasound was used to measure the rate of blood flow both through Kager's fat pad and across the fat pad-Achilles tendon boundary. The technique is based upon the Doppler Effect - where the frequency of the sound waves emitted by a moving object change, and is typically observed when listening to a moving siren or train. As the change in frequency is dependant upon the rate at which the object is moving, this system can be used to

measure speed. Thus when applied to ultrasound, Doppler ultrasound can be utilised to measure the speed of blood flow within the body.

Doppler ultrasound was performed on 4 healthy volunteers (male, 24-57 years), and one patient presenting with Achilles tendonitis (female, age unknown). The subjects were examined prone, with the foot in the neutral position. Attention was focussed in particular on the posterior border of Kager's triangle, examining for evidence of blood flow passing across this border and into the Achilles tendon. A qualitative assessment was made based on the approximate number of blood vessels evident.

4.3 Results:

4.3.1 Gross Anatomical Examination:

Gross anatomical examination of Kager's fat pad was undertaken following hemisection of the posterior hindfoot. The boundaries forming Kager's triangle were identified, and it was evident that these structures caused the triangle to converge proximally. At its most distal extremity, Kager's fat pad could be seen to form a wedge, apparently projecting into the retrocalcaneal bursa. The most distal tip of this wedge was noticeably more rigid on palpation, indicative of fibrosis.

The distal wedge of Kager's fat pad was positioned between the superior tuberosity and the Achilles tendon, appearing to be securely attached to these neighbouring structures by fibrous anchors. Anteriorly, the fat pad blended with the periosteum of the calcaneus, whereas posteriorly the fatty wedge was attached to the Achilles tendon. These anchors also form the superior wall of the retrocalcaneal bursa (Figure 4.3.1).

Kager's fat pad appeared to be divided in the coronal plane by a fibrous sheath. Further dissection revealed that this sheath was an extension of the Achilles tendon paratenon. The paratenon isolated the posterior portion of the fat pad, separating it from that situated anteriorly. The paratenon also bordered the medial and lateral sides of the distal wedge, as it spanned between the Achilles tendon and the superior tuberosity.

Small blood vessels were identified within Kager's fat pad. These vessels were tortuous and were found predominantly in the posterior aspect of the fat pad. Vessels lying superficially, identified as branching from the posterior tibial artery, supplied the inferior and medial aspects of Kager's fat pad. The superior and lateral regions of the fat pad were served by deeper blood vessels, supplied from the peroneal arteries.

4.3.2 Histological Examination:

Kager's fat pad varied significantly in size. In particular, where a large superior tuberosity was present, the distal extremity of the fat pad was long and thin. Conversely, where a small superior tuberosity was present, the fat pad was obviously larger (Figure 4.3.2). A synovial membrane lining the distal wedge of the fat pad was also evident.

A synovial invagination was also evident within Kager's fat pad, in particular in those specimens where there was a large superior tuberosity (Figure 4.3.3). The synovial invagination separated the distal wedge of the fat pad from the larger, proximal section. The most distal tip of the wedge was typically of fibrous appearance (Figure 4.3.4). The wedge was attached to the neighbouring Achilles tendon posteriorly by fibrous strands, and with the calcaneus anteriorly by blending with the periosteum (Figure 4.3.3). The anchoring of the distal wedge of the fat pad to the neighbouring structures is also evident in Figure 4.3.3. Anteriorly, Kager's fat pad blends with the calcaneus, whereas posteriorly it is attached to the Achilles tendon.

In a minority of specimens there was a meniscus extending into the retrocalcaneal bursa from the most proximal point of the enthesis. Whilst this was predominantly found on specimens with large superior tuberosities, it was not apparent in all such specimens, as evident in Figure 4.3.5.

4.3.3 Magnetic Resonance Imaging:

On observing the sagittal MRI's, it was again noted that the posterior fat pad was bound within the paratenon of the Achilles tendon, as evident in Figure 4.3.6(a). The area of fat pad situated anteriorly was bound within the FHL tendon sheath, and the boundary between the two tissues can be identified in Figure 4.3.6(b) as an inverted-J shape. On plantarflexion this shape changed to that of an 'L', as in Figure 4.3.6(c), with the shape of Kager's triangle also changing significantly. Despite being static images, it was possible to discern movement of Kager's fat pad. The position of the fat pad was noticeably different when the ankle was in different positions of flexion.

When the foot was plantarflexed, the distal wedge of Kager's fat pad was significantly nearer to the enthesis than when the foot was dorsiflexed.

4.3.4 Doppler Ultrasound:

Doppler ultrasound was used to examine the blood flow within Kager's fat pad, in particular across the fat pad-tendon interface. Both healthy subjects (4 males, 24-57 years) and a subject presenting with Achilles tendonitis were examined (female, age unknown). Blood vessels were evident only in the Achilles tendon paratenon in the healthy subjects. In contrast, a florid image was observed when examining the subject presenting with Achilles tendonitis. Here, there was evidence of blood vessels passing through Kager's fat pad, across the posterior boundary and into the Achilles tendon. The healthy, contralateral Achilles tendon of the patient was also imaged, showing little vascularisation. The image of the inflamed tendon can be viewed in Figure 4.3.7(a), whilst the healthy, contralateral limb can be seen in Figure 4.3.7(b).

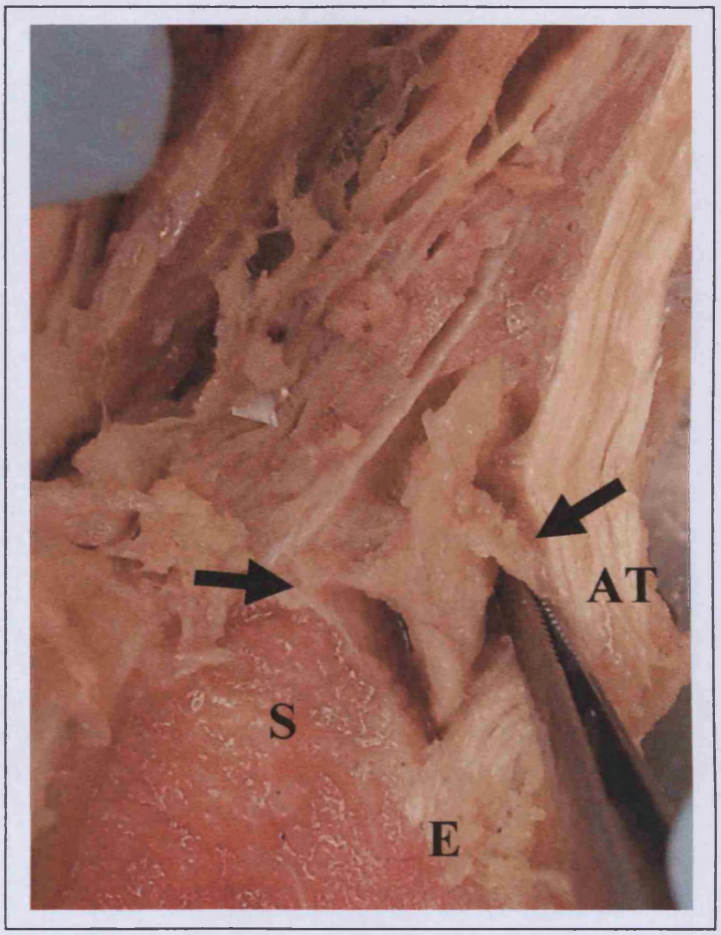

Figure 4.3.1: A sagittal hemisection of the Achilles tendon enthesis showing the fibrous anchors that attach the wedge of Kager's fat pad to the surrounding structures. The distal wedge of Kager's fat pad is secured to the periosteum anteriorly, and to the Achilles tendon posteriorly. These anchors also form the superior boundary of the retrocalcaneal bursa. AT =Achilles tendon, E = Enthesis, S = Superior tuberosity, Arrows = Fibrous anchors.

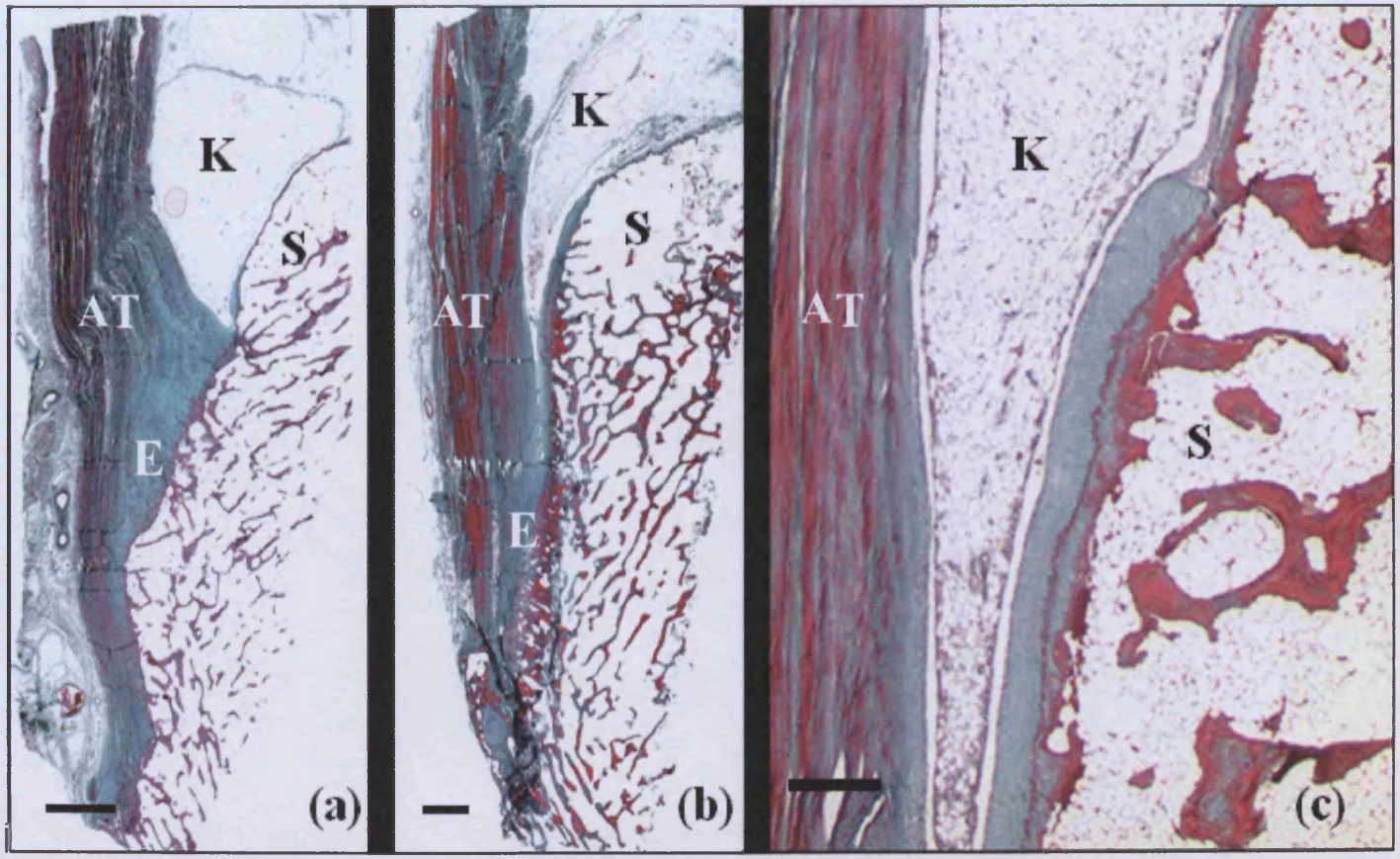

Figure 4.3.2: Low powered sagittal histological sections showing the different size of Kager's fat pad with respect to the superior tuberosity. (a) Kager's fat pad is relatively large where there is a small superior tuberosity. Scale bar = 2mm. (b) Kager's fat pad is long and thin where there is a prominent superior tuberosity. Scale bar = 2mm. (c) Kager's fat pad extends as far as possible between the Achilles tendon and the superior tuberosity (using x 1.6 objective lens). Scale bar = 500μm. AT = Achilles tendon; E = Enthesis, K = Kager's fat pad; S = Superior tuberosity.

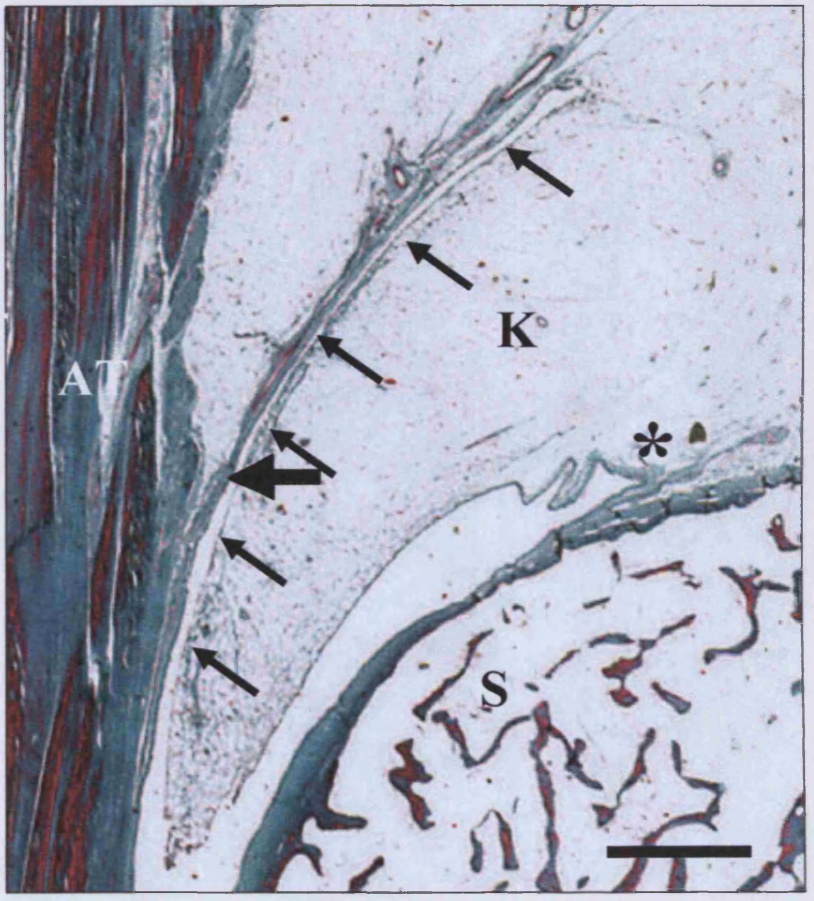

Figure 4.3.3: A sagittal histological section of the distal aspect of Kager's fat pad, identifying the synovial invagination. Superficial fibrous strands anchor Kager's fat pad posteriorly to the Achilles tendon, whilst the fat pad blends anteriorly with the calcaneal periosteum. AT = Achilles tendon; K = Kager's fat pad; S = Superior tuberosity; Small arrows = Synovial invagination; Large arrow = Fibrous tether; * = Periosteal blending. Scale bar = 1mm.

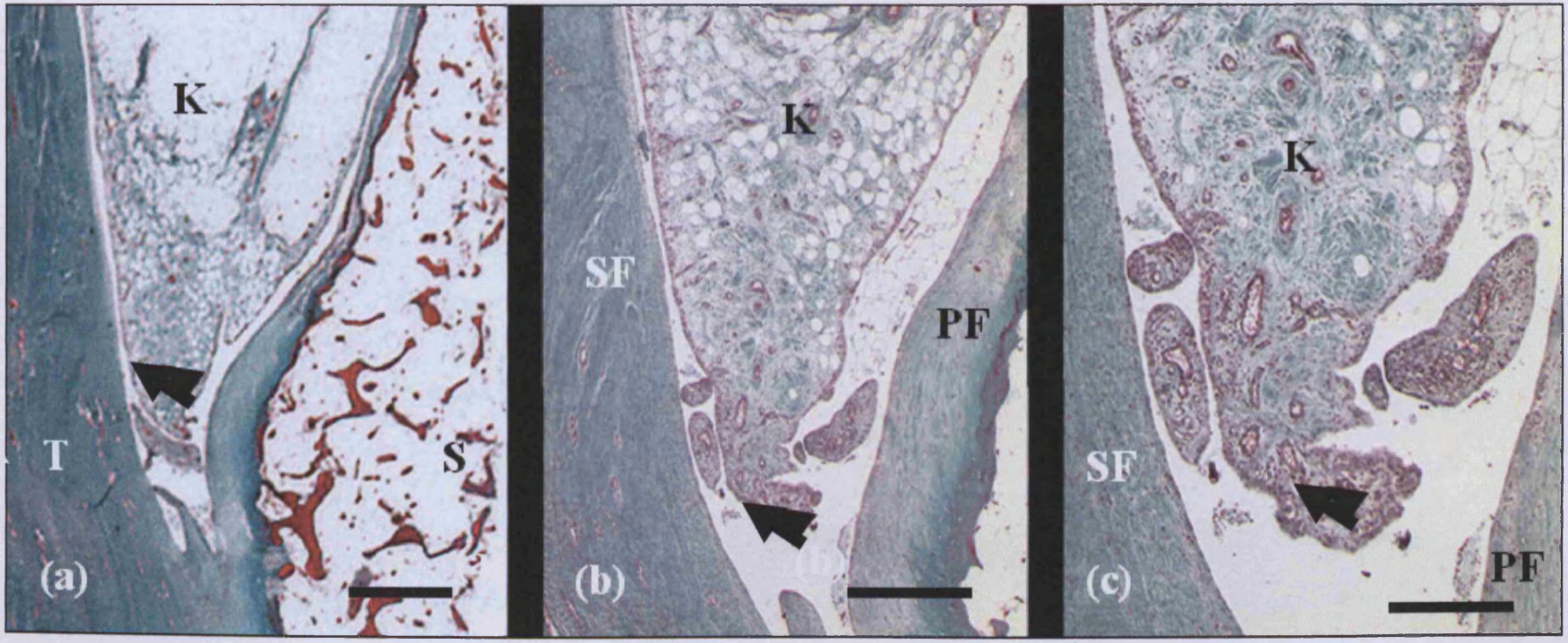

Figure 4.3.4: Sagittal histological sections identifying the fibrous tip of Kager's fat pad. (a) Magnified using x 1.6 objective lens. Scale bar = 500μm. (b) Magnified using x 2.5 objective lens. Scale bar = 300μm. (c) Magnified using x 5 objective lens. Scale bar = 150 μm. AT= Achilles tendon, K = Kager's fat pad, PF = Periosteal fibrocartilage S = Superior Tuberosity, SF = Sesamoidal fibrocartilage, Arrows = Fibrous tissue.

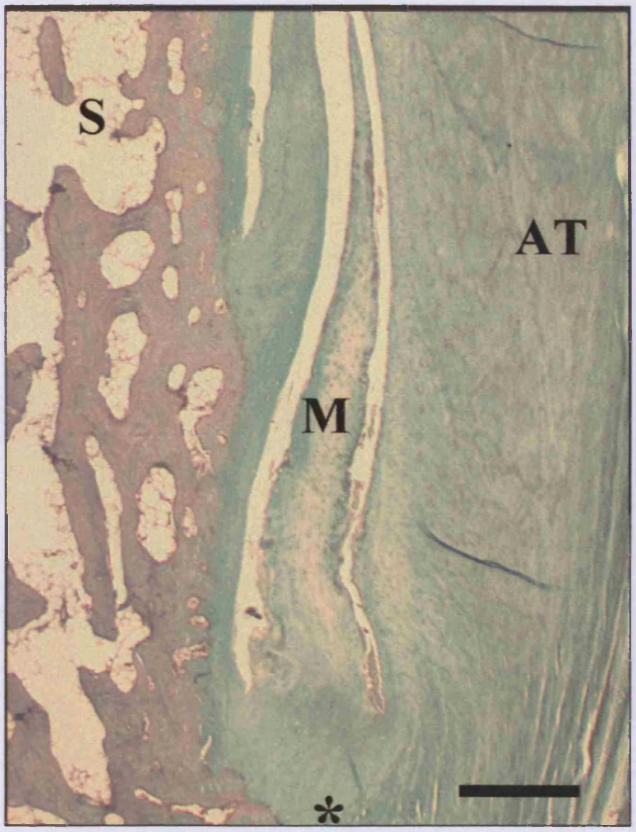

Figure 4.3.5: Sagittal histological section of a meniscal fold, evident in a number of specimens protruding into the retrocalcaneal bursa from the most proximal point of the enthesis (magnified using x1.6 objective lens). AT = Achilles tendon; M = Meniscus; S = Superior tuberosity; * = Enthesis proximal point; Scale bar = 500μm.

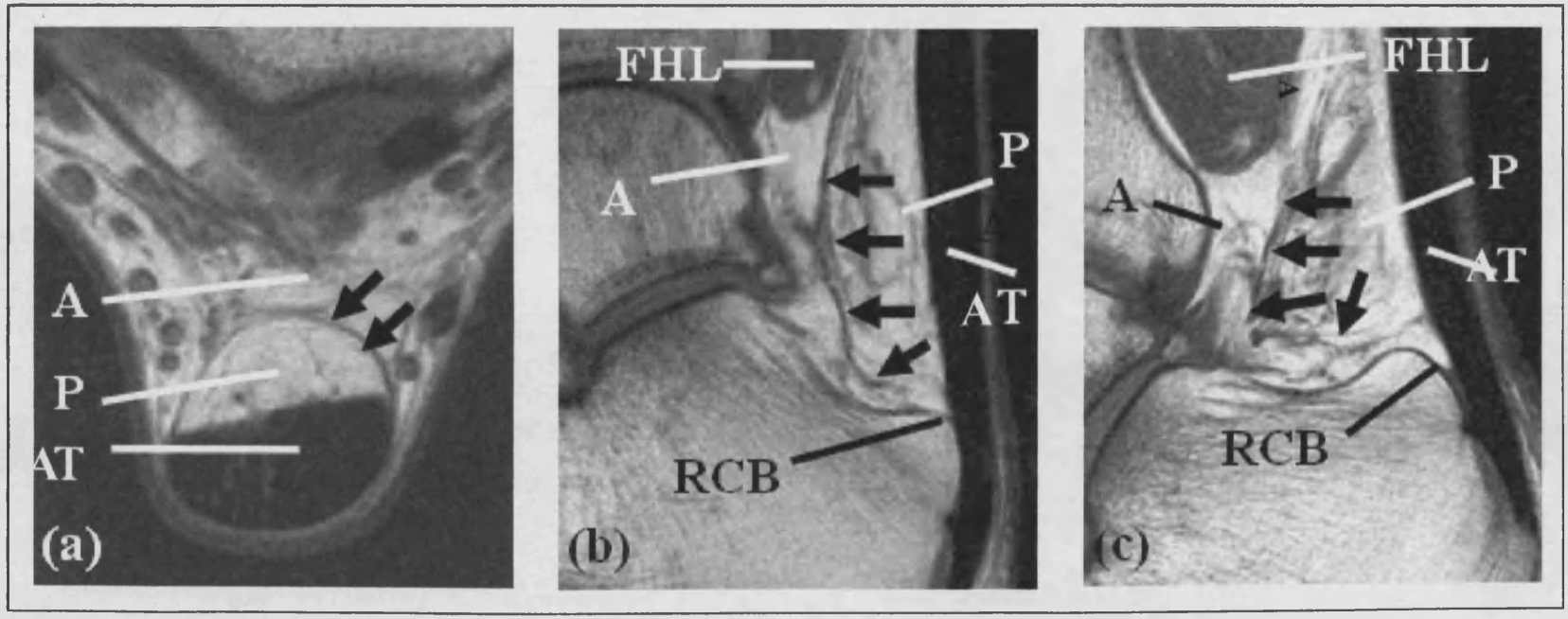

Figure 4.3.6: Macroscopic examination of the anterior-posterior divide within Kager's fat pad. (a) A transverse MRI demonstrating the enveloping of the posterior aspect of Kager's fat pad within the Achilles tendon paratenon. (b) A sagittal MRI demonstrating the inverted J-shape of the anterior-posterior border when the foot is in maximum dorsiflexion. (c) A sagittal MRI showing how the inverted J-shape transforms to an L-shape when the foot is moved to maximum plantarflexion. Note how the FHL has thickened, and the fatty wedge now protrudes into the retrocalcaneal bursa. A = Anterior aspect of Kager's fat pad, AT = Achilles tendon, FHL = Flexor hallucis longus muscle belly, P = Posterior aspect of Kager's fat pad, RCB = Retrocalcaneal bursa, Arrows = Paratenon.

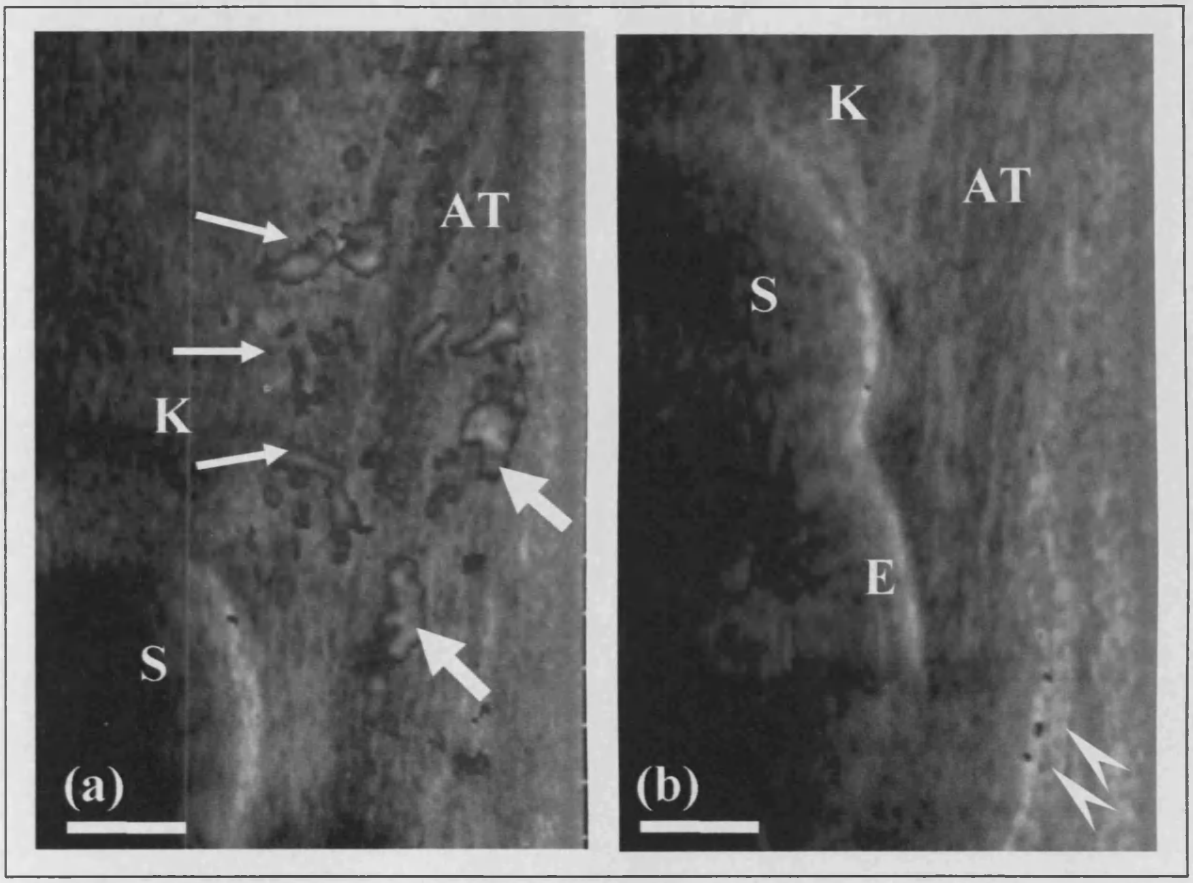

Figure 4.3.7: Sagittal US images of Kager's fat pad demonstrating the increased blood flow during Achilles tendonitis. (a) The Achilles tendon of a subject presenting with Achilles tendonitis. Significant blood supply is evident with blood vessels apparently coursing through Kager's fat pad, crossing the posterior border and into the Achilles tendon. (b) The healthy, contralateral limb. As is typical, a limited blood supply is evident in the Achilles tendon paratenon. AT = Achilles tendon E = Enthesis, K = Kager's fat pad, S = Superior tuberosity, Small arrow = Region of blood vessels evident within Kager's fat pad, Large arrow = Region of blood vessels evident within the Achilles tendon, Arrow head = Region of blood vessels within the paratenon. Scale bar = 4mm

4.4 Discussion

Following a combined histological, gross anatomical and imaging study, it has been possible to discern 3 different regions of Kager's fat pad. Each of these regions appeared to have adaptations that allow for the efficient performance of specific functions.

Clearly visible in both MRI and dissection, the Achilles tendon paratenon divided the main bulk of Kager's fat pad into an anterior and a posterior region. The posterior region was closely associated with the Achilles tendon and thus termed the *Achilles-associated fat pad.* The anterior part of Kager's fat pad was associated with the FHL, and thus was termed the *FHL-associated fat pad.* This separation appeared particularly significant on ankle flexion, where the deformation of Kager's triangle caused the shape of the division to change from an inverted J to an L-shape.

During ankle flexion the Achilles-associated fat pad remained still relative to the remaining bulk of the fat pad. It is hypothesised that this is to prevent the shearing of the blood vessels that are evident coursing through the Achilles-associated fat pad-Achilles tendon interface. The blood vessels were identified as being of tortuous nature, and thus a degree of movement between the Achilles-associated fat pad and the Achilles tendon would appear permissible without causing vascular damage. The blood flow through these vessels was examined by Doppler ultrasound, and appeared to vary depending on the health of the Achilles tendon - with a marked increase during Achilles tendonitis. Whilst apparently linked to Achilles tendon inflammation, the coursing of these vessels across the Achilles-associated fat pad-Achilles tendon interface indicates a possible rehabilitative role for Kager's fat pad. Whilst this result was validated against the contralateral limb, only one patient was examined. Thus, additional subjects are necessary for this result to be both statistically and clinically significant.

On MRI's the FHL-associated fat pad is clearly identifiable as a column of fat extending distally from FHL, enclosed within an extension of the FHL tendon sheath.

Whilst this movement coincided with the paratenon changing shape (as discussed above), the consequence it is currently unclear.

The third region of Kager's fat pad to be identified was that of the distal fatty wedge. This wedge has been termed the *bursal-protruding wedge* (BPW), as it protrudes into the retrocalcaneal bursa. The size of the BPW was seen to depend on that of the superior tuberosity. Where a large superior tuberosity was present the BPW was thin, ensuring it reached into the retrocalcaneal bursa. In such instances, the movement of the wedge appeared more significant and the BPW appeared to be separated from the main body of the fat pad by a synovial membrane invagination, as identified histologically. As synovial fluid is recognised as an efficient lubricant **[160, 161]**, it is likely that any movement between these two surfaces would be aided by a low coefficient of friction.

On moving the foot from the neutral position to plantarflexion, the angle between the superior tuberosity and the Achilles tendon increased, as expected. The BPW entered the retrocalcaneal bursa progressively on the increasing of this angle as a direct benefit of its wedge-shape, appearing to maintain contact with the opposing surfaces throughout. BPW movement in the medial-lateral plane appeared through transverse MRI to be restricted by the paratenon spanning between the Achilles tendon and the superior tuberosity. The decreasing of the insertional angle as the foot returned to the neutral position from plantarflexion was likely to have been at least partly responsible for the expulsion of the BPW from the retrocalcaneal bursa.

The fibrosis evident on the leading edge of the BPW may be as a direct consequence of this movement into the retrocalcaneal bursa. Whilst it is unclear whether fibrosis development is related to age **[28]**, the lack of fibrosis in the specimens with smaller superior tuberosities suggests that it develops due to a local biomechanical stimuli. Similar fibrous tissue has previously been observed in the calcaneal fat pad (which protects the underside of the heel) **[162-164]**, and is believed to aid in maintaining shape, whilst resisting and reinforcing against external forces **[28, 165]**. Thereby acting as a shock absorber **[166-168]**, it also protects the neighbouring structures from excessive local stress **[169]** and reduces plantar pressure **[163, 170, 171]**. Thus, in

exhibiting fibrosis, the leading wedge of Kager's fat pad may mimic some, if not all, of these functions.

Kager's fat pad, and in particular the BPW, can also be compared to the knee meniscus. Geometrical comparisons can be made when considering the meniscus extending from the proximal aspect of the enthesis in some of the Achilles tendon enthesis organ specimens. The meniscus is seen extending into the retrocalcaneal bursa from the opposite side of the fat pad, particularly in instances where there is a large superior tuberosity prominence. Thus the Achilles tendon enthesis organ has two wedges of tissue sandwiched between two conjoining surfaces. This configuration bears a striking resemblance to the knee meniscus as, when viewed in the sagittal plane, the two wedges of the knee meniscus are sandwiched between the conjoining femoral condyles and tibial plateau (Figure 4.4.1(a) & (b)). The knee meniscus also exhibits similar movement to Kager's fat pad. Due to its wedged-shape, a net resultant force generated in response to the applied load tends to extrude the menisci from the joint. This is resisted by the circumferentially oriented collagen fibres and their attachments to the meniscal horns, creating circumferential hoop stresses **[172, 173]**. Attachments that presumably act to restrict movement were also evident on Kager's fat pad - the fatty wedge was attached to the calcaneal periosteum anteriorly and the Achilles tendon posteriorly, approximately 10mm from its leading edge. These attachments were neither as fibrous nor robust, however, as those anchoring the meniscus. It has been proposed that the anchors of the knee meniscus also help the meniscus recover its original dimensions after a load is removed **[172, 174]**. If this can be extrapolated to Kager's fat pad, the extent to which its movement out of the retrocalcaneal bursa is restricted by the anchors will assist in determining its biomechanical function. Taut anchors would restrict the proximal movement of the BPW during dorsiflexion, and thus potentially cause the fat pad to bear load. Conversely, slack anchors would allow the fat pad to be fully expelled, thus avoiding impingement between the Achilles tendon and the superior tuberosity.

The fibrous anchors of Kager's fat pad also formed the superior border of the retrocalcaneal bursa, presumably ensuring the synovial fluid remains within the bursa. As the remaining part of the wedge is lined with synovial membrane and protrudes into the synovial fluid-filled retrocalcaneal bursa, the lubrication properties of

synovial fluid **[160, 161]** suggests a highly specialised environment that allows the conjoining surfaces to slide past one another with a low coefficient of friction. The importance of the knee meniscus in minimising friction has previously been reported, with the friction within the knee joint increasing following meniscectomy **[29]**. The role of the knee meniscus in spreading the synovial fluid within the joint capsule **[29]** means its preservation during surgery is now desirable, advice opposite to that given thirty years ago **[29]**. Whether a similar function – and thus similar advice, is applicable to Kager's fat pad, remains to be determined.

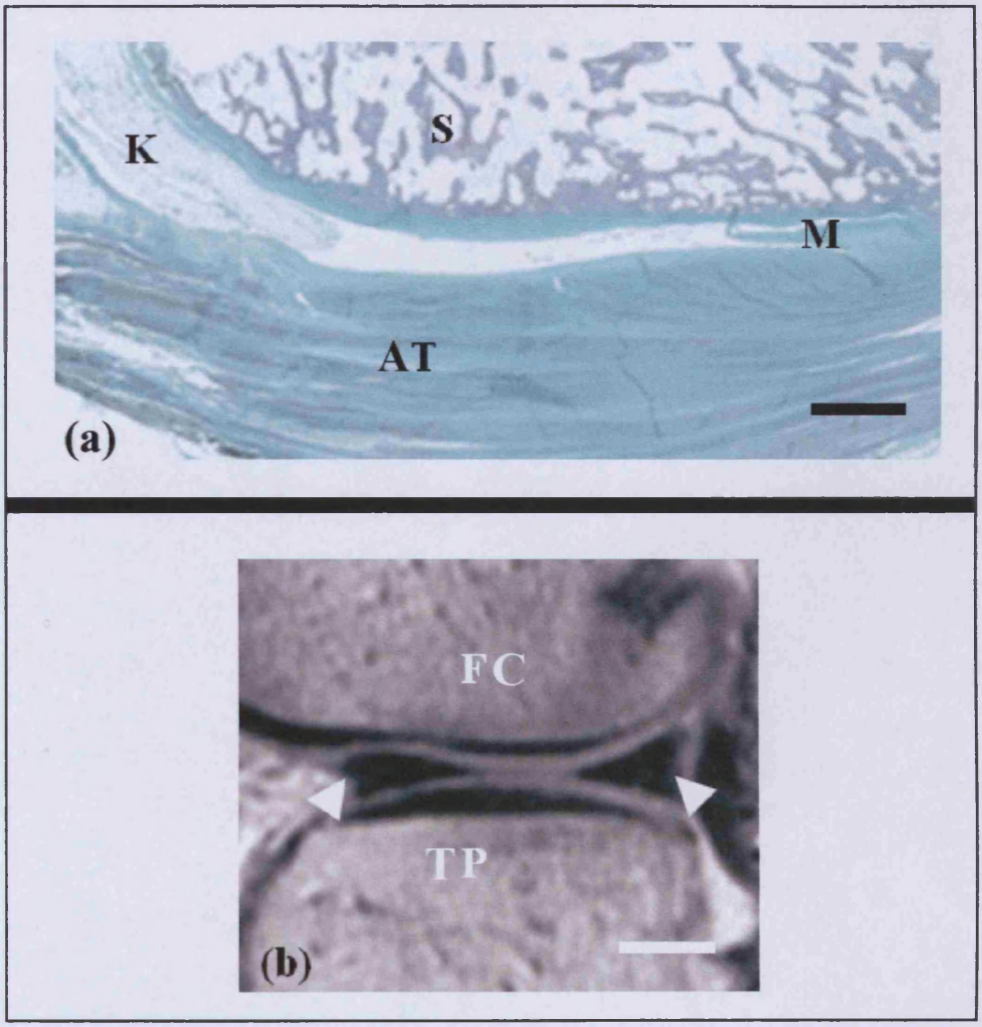

Figure 4.4.1: Comparison between the geometry of the Achilles tendon enthesis organ and the knee joint. (a) A histological section in the sagittal plane of the Achilles tendon enthesis organ (rotated 90 degrees counter-clockwise). Kager's fat pad and the meniscus form a wedge at either end of the conjuncture. Scale bar = 2mm. (b) A sagittal MRI of the knee joint. The meniscus forms a wedge at either side of the conjuncture. Scale bar = 20mm. AT = Achilles tendon, FC = Femoral condyle, K = Kager's fat pad, M = Meniscus, S = Superior tuberosity, TP = Tibial plateau, Arrows = Knee meniscus.

4.5 Conclusions

The work in this chapter led to the following conclusion being drawn:

1. Kager's fat pad was identified as comprising 3 separate parts and was hypothesised to play both a biomechanical and rehabilitative role in the Achilles tendon enthesis organ.

2. The bursal protruding wedge of Kager's fat pad moved into the retrocalcaneal bursa and may bear load within the Achilles tendon enthesis organ, due to the evidence of fibrosis. Its synovial lining is also indicative of the fat pad influencing the lubrication of the Achilles tendon enthesis organ.

3. The FHL-associated part of Kager's fat pad moved inferiorly on plantarflexion, coinciding with the protrusion of the BPW. A relationship between the movements of these 2 structures was not, however, established.

4. The Achilles-associated part of Kager's fat pad remained still relative to the Achilles tendon and was hypothesised to protect the blood vessels that traversed the interface of these structures.

5, The Biomechanical Influence of Kager's Fat Pad

5.1 The Biomechanics of Kager's fat pad

It has previously been hypothesised that Kager's fat pad acts as a 'variable space filler', plunging into the retrocalcaneal bursa **[152]**. Whilst no studies had confirmed this, the previous chapter has qualified the fat pad movement. This movement is predicted to improve the mechanical efficiency of the Achilles tendon **[144, 152]** and the triceps surae **[109]** by increasing the lever arm. The previous Chapter also hypothesised that the fat pad may bear load within the Achilles tendon enthesis organ, due to the fibrosis evident histologically on the leading edge. This is akin to the calcaneal fat pad, that is known to bear approximately 70% of the body weight **[175]** on heel strike, absorbing 90% of the energy generated **[176]**.

Kager's fat pad is also of similar shape to the knee meniscus. Whilst known to load bear **[177-180]**, menisci are also responsible for lubricating the synovial joint **[29]**. As the distal wedge of Kager's fat has a synovial membrane and protrudes into the synovial fluid-filled retrocalcaneal bursa, it appears that the fat pad may be important in lubricating the Achilles tendon enthesis organ. Whilst the importance of lubrication in minimising friction between biological tissues has been reported (synovial joints **[29, 181-184]**; skin **[185-188]**; inter-tissue friction **[183, 189]**), no studies have previously considered the lubrication role of fat pads **[1]**.

Thus, in examining the biomechanical role of Kager's fat pad within the Achilles tendon enthesis organ, this chapter investigated the tribological (i.e. lubrication) function of the fat pad. The work in this chapter also aimed to assess the role of the fat pad in mechanically advantaging the Achilles tendon enthesis organ, and to determine the extent to which the fat pad influences the load exerted on to the superior tuberosity by the Achilles tendon.

The role of Kager's fat pad was comprehensively analysed using a number of different techniques. Dynamic ultrasound was used to assess the movement of the fat pad in vivo during ankle flexion. An apparatus was then fabricated to determine the lubrication regime between Kager's fat pad and the superior tuberosity. Finally, the

load-bearing of Kager's fat pad within the Achilles tendon enthesis organ was examined using the mechanical model described in Chapter 3.

5.2 Materials and Methods

The work described in this Chapter aimed to determine the biomechanical role of Kager's fat pad within the Achilles tendon enthesis organ. In doing so, the mechanical advantage, lubrication, and load bearing roles of Kager's fat pad were assessed. These are functions that have been identified to be important in the similar tissues **[28, 29, 168, 177-180, 190-195]**.

5.2.1 Sonographic Examination:

A series of studies were devised to quantify the movements of Kager's fat pad. The first protocol dynamically examined the affect of ankle flexion on the Achilles tendon enthesis organ. Five volunteers (4 males, 1 female; age ranges 24-57 years) were scanned in the prone position. None of the volunteers had a history of significant injury to the Achilles tendon or ankle, and all 5 were asymptomatic.

The US transducer was positioned on the posterior surface of the Achilles tendon, aligned with the superior tuberosity. Thus an image of the Achilles tendon enthesis organ in the sagittal plane was produced. The volunteers were then asked to continually flex their right ankle through its entire range. The position of the transducer was refined until the image included at all times the distal aspect of the fat pad and the Achilles tendon enthesis. Excess ultrasonic gel was used to ensure the transducer remained in continual contact with the skin. Movie files were recorded of each patient to allow for the influence of the adjacent structures to be qualitatively analysed. Still images of extreme plantarflexion, the neutral position, and extreme dorsiflexion were also recorded to allow for quantitative measurement. The straight-line distance between the most proximal point of the enthesis and the distal tip of Kager's fat pad was measured directly from the US image using software built in to the US machine, and the angle of ankle flexion recorded.

The second study, which was a development of the first study, aimed to dynamically examine the entirety of Kager's fat pad during ankle flexion, determining how it deforms when the shape of Kager's triangle changes on ankle flexion. The transducer

was held in a more proximal position than in the previous study, and the imaging depth increased. Five normal volunteers (5 males; age ranges 24-57 years) in the prone position continually flexed their ankle through its entire range. Excess ultrasonic gel again ensured a constant contact between the transducer and the skin. Movie images were recorded, allowing the shape of Kager's fat pad to be qualitatively analysed against the angle of ankle flexion.

The third study examined how the distal aspect of Kager's fat pad was affected by the surrounding structures, and in particular FHL. This muscle is a weak plantarflexion muscle, whilst it is also responsible for flexing of the big toe. In order to dynamically analyse the affect of this muscle alone on Kager's fat pad, the ankle position was fixed. The subject was then imaged in the prone position whilst flexing and extending their big toe, thus causing isolated contraction and relaxation of FHL. Movie images were again recorded to allow for qualitative analysis.

The effect of Achilles tendon loading was also examined. The same 5 participants were first imaged in an unloaded environment, lying prone. The ankle was then positioned at 3 different angles (maximum dorsiflexion; maximum plantarflexion and in the anatomical neutral position (i.e. 90 degrees)) to ensure higher quality still images could be obtained. The exact angle of flexion was measured using a goniometer. A movie of complete ankle flexion was also recorded for reference. Loading of the Achilles tendon was then performed, with subjects being asked to stand on tip-toe, thus loading the Achilles tendon in plantarflexion. Standing up-right ensured the Achilles tendon was loaded in the neutral position, whilst loaded dorsiflexion was performed leaning against a wall whilst retaining their heel on the floor. A number of still US images were taken of each position. The distance between the distal aspect of Kager's fat pad and the enthesis was measured using inbuilt software following the earlier described protocol. Thus, a comparison could be drawn between the positions of the fat pad when the Achilles tendon was loaded, to when it was unloaded.

5.2.1.1 The Insertional Angle:

The angle between the Achilles tendon and the superior tuberosity was examined using MRI to determine whether this influenced the movement, and thus possibly the biomechanics, of Kager's fat pad (Figure 5.2.1). Three normal male volunteers (age 31, 51 & 60 years) were imaged in the prone position with their foot in maximum dorsiflexion. The angle of ankle flexion was measured manually using a goniometer, and this was compared to the insertional angle measured from the MRI. The angle of ankle flexion was then increased at 10 degree increments, moving to plantarflexion. The corresponding insertional angle was then measured.

5.2.2 Increasing the Achilles Tendon Mechanical Advantage :

By using a technique identical to that described in Chapter 3, the effect of Kager's fat pad in increasing the Achilles tendon lever arm was examined from MRI's **[109, 144, 152]**. The perpendicular distance between the ankle axis and the most posterior aspect of the superior tuberosity was measured, and then the ankle axis and the most posterior aspect of the BPW. The effect of the fat pad on the lever arm was then calculated using Equation 3.2.1.

5.2.3 The Lubrication Regime at the Fat Pad-Bone Conjuncture:

The lubrication regime present at the fat pad-superior tuberosity conjuncture was investigated to determine whether Kager's fat pad was important in minimising friction between the two surfaces. This has potential consequences for the health of the conjoining surfaces.

5.2.3.1 Apparatus 1 – Bovine Synovial Membrane:

An apparatus was fabricated based upon previously published systems **[183, 189]**. The apparatus (Figure 5.2.2) consisted of a $10mm^2$ mild-steel arm to which the specimen holder was attached. Synovial membrane was harvested from the metacarpophalangeal (MCP) joint of skinned bovine legs, 18 months old and obtained fresh from an abattoir (Figure 5.2.3). This was attached to the specimen holder - a small PMMA cylinder - using Dermabond tissue adhesive (Ethicon Inc., US). The vertical position of the specimen holder was adjusted to ensure the arm was

horizontal. A counter-balance on the other end of the arm ensured zero net loading. A vertical load, N_H, was applied to the specimen. The maximum load that could be applied was 4.5N, as any greater load caused deflection of the arm to an extent that the apparatus failed. Loading at 0.5N increments (0.5, 1, 1.5, 2, 2.5, 3, 3.5, 4, 4.5N) ensured a range of test conditions were examined. The pillar itself rotated within a ball bearing set into the base of the apparatus. Fresh synovial fluid was aspirated from the medial and lateral sides of the metacarpophalangeal (MCP) joint cavities of fresh, skinned bovine legs, using a 20ml gauge needle and syringe. Excess fluid was then used to lubricate the conjunction with the rotating disc, spread with a brush to ensure uniform distribution.

In order for the sliding speed of the apparatus to replicate the speeds of Kager's fat pad *in vivo*, the fat pad speed was determined from the stored dynamic ultrasound movies taken earlier. Kager's fat pad was seen to reach speeds of approximately 15mm/s during gentle cadence, and approximately two and a half times greater during running. A variety of sliding speeds at the conjunction were achieved experimentally (50, 54, 69, 83, 98, 115mm/s) both by altering the supply voltage to the electric motor driving the disc, and changing the position of the specimen from the centre of the disc. This was necessary to allow for a change in the Sommerfeld number and thereby identification of the lubrication regime from the Stribeck curve (Figure 5.2.4).

In the original studies **[183, 189]**, arm deflection was measured using a linear variable displacement transducer (LVDT). This method of measurement could not be replicated here, however, as after a thorough search of all known transducer suppliers it was not possible to obtain a suitable device. The available LVDT's were too stiff, and thus would not have been displaced by the very low frictional forces expected. Whilst the force on the LVDT could have been increased by moving it nearer to the arm pivot, the limited displacement would have resulted in the system having poor resolution.

This problem was overcome by using an extension spring to resist arm rotation. In the knowledge of the spring stiffness and the extension, the force could be measured using Hooke's law, as in Equation 5.2.1.

$$F_S = kx$$

Equation 5.2.1: Hooke's law governs the force resisted by a spring. F_S = Spring force; k = Spring stiffness; x = Spring extension.

Whilst the spring constant was detailed by the manufacturer, this was verified by loading the spring and measuring its extension. Once verified, the spring was positioned horizontally between the arm and a fixed point. The exact position at which the spring attached to the arm could be varied, effectively varying the stiffness of the spring. A greater arm deflection was encouraged as this would be expected to decrease the relative error, thus improving the resolution and accuracy of the system.

The spring extension was derived by measuring the rotation of the pillar, and hence the arm. This was measured by mounting a potentiometer on the underside of the pillar. A supply voltage was connected to the input of the potentiometer, whilst the output was connected to a PC via a datalogger (Pico Technology Ltd, UK), to allow the voltage change to be logged. Once the disc had been ramped up to the desired speed thus avoiding hyper-rotation and the arm allowed to settle, logging occurred at 0.1Hz for 10 seconds. Following calibration of the apparatus to determine that an angle change of 1 degree was equal to a 0.03V change, the loading of the spring was calculated (as detailed in Equation 5.2.2 (a)-(c)).

$$\theta = \frac{\Delta V}{0.03}$$

Equation 5.2.2(a): The angle of arm rotation (θ, degrees) was calculated by dividing the total voltage change (ΔV) by 0.03V

Knowing the distance between the spring mounting position and the pivot (D_S), the spring extension could be approximated by equating it to the arc subtended by the arm following rotation through angle θ (Equation 5.2.2(b)). This geometry is schematically explained in Figure 5.2.5(a).

$$x = \frac{2\pi D_s \theta}{360}$$

Equation 5.2.2(b): The spring extension (x, mm) was approximated to the arc length created following arm rotation length.

In the knowledge of the spring stiffness (k=0.07N/mm), Hooke's law was used to calculate the force resisted by the spring (F_S):

$$F_s = 0.07x$$

Equation 5.2.2(c): Hooke's law is used to calculate the force resisted.

Having determined the force on the spring, it was then necessary to calculate the frictional force experienced at the specimen holder (F_H). This was achieved by resolving the moments about the pivot of the arm (Equation 5.2.3(a) & (b)), as is diagrammatically explained in Figure 5.2.5(b).

$$F_S.D_S - F_H.D_H = 0$$
$$\therefore F_H = \frac{F_S D_S}{D_H}$$

Equation 5.2.3(a): The calculation of the frictional force experienced at the specimen holder (F_H), following the resolution of the moments about the pivot of the suspended arm.

Knowing the frictional force (F_H) and the reactant force (N_H) at the specimen holder, the coefficient of friction (μ) between the specimen and the counterface was calculated (Equation 5.2.3(b)).

$$F_H = \mu.N_H$$
$$\therefore \mu = \frac{F_H}{N_H}$$

Equation 5.2.3(b): The relationship between the frictional force and normal load.

The lubrication regime present at the conjuncture was determined by reference to the Stribeck curve (Figure 5.2.4), where the ratio between the coefficient of friction and the Sommerfeld number (Equation 5.1.3) is plotted. As little is known about the variation of the viscosity of the lubricant - synovial fluid – at the high shear rates expected in these experiments **[161]**, the reduced Sommerfeld number was calculated (Equation 5.2.4). This is identical to the approach adopted by Cooke et al. **[183, 189]**.

$$S = \frac{V}{L}$$

Equation 5.2.4: The reduced Sommerfeld number

An example is included in Appendix A8 to clarify the above calculation.

As with any new apparatus, validation was necessary to ensure that accurate results were being obtained. Validation was undertaken by comparing the coefficient of friction and determining the lubrication regime of synovial membrane using the apparatus, and then comparing these results to those previously published **[183, 189, 196]**.

5.2.3.2 Apparatus 2 – Bovine Synovial Membrane:

Modifications were made to Apparatus 1 in an attempt to reduce the inherent friction and inaccuracies and thus achieve successful validation. Possible improvements were identified – as listed below – giving rise to Apparatus 2 (Figure 5.2.6).

- The Ball Bearing:

The ball bearing in which the pillar rotated was identified as an area of unnecessarily high friction. Thus, the protective plastic grommet was removed to avoid friction with the conjoining surfaces, and the lubricant cleaned from the bearing and replaced. These modifications resulted in the pillar rotating significantly more freely.

- The Ball Bearing – Pillar Interface:

The pillar was identified as being of an insufficiently tight fit, thus deflecting when the suspended arm rotated. This was corrected by a second ball bearing being positioned directly underneath the first, and the pillar being extended to fit through both of these. This ensured the pillar remained stable within the bearing.

- The Pillar – Arm Pivot:

The channel in which the arm was pivoted by the pin had to be slack to ensure unhindered movement in the desired plane. However, as a consequence the arm was able to move in planes other than that desired when the arm was deflected. This was improved by changing the design to a yoke mechanism, thereby minimising the undesired rocking of the arm. The arm was fitted through a sleeve that was tightened using two grub screws to avoid it rotating when the arm was deflected.

- The Suspension Arm:

The possibility of the suspension arm bending was identified. Thus, an over-engineered arm was fabricated to ensure that there was no possibility of it bending during testing. Using an aluminium tube (wall thickness 5mm, outer diameter 25mm, length 300mm) increased the strength of the arm, whilst using a hollowed cross-section reduced the arm's second moment of area and thus minimised 'throwing'.

- Spring Position:

The spring position was identified as imparting a torsional force on the arm, as it was not resisting the movement of the arm in direct alignment to the frictional force (Figure 5.2.7). In order to achieve the ideal set-up, the spring needed to be anchored directly opposed to the frictional force of the specimen holder. To ensure suitable deflection of the arm, a spring of stiffness 0.01N/mm was required. However, despite an extensive search, such spring stiffness proved unavailable. The lowest spring stiffness that could be obtained (0.02N/mm) was used instead, thus reducing – but not totally alleviating - the effect of torsion upon the arm.

- Apparatus Orientation:

Two surface spirit levels were used to ensure that the disc was horizontal when the apparatus was positioned for experimental use, with feet fitted to each leg to allow for adjustment where necessary. These spirit levels were also used to check the orientation of the specimen, to ensure that the major axis was parallel to the disc surface.

- The Sommerfeld Number:

The range of speeds and loads used was increased to broaden the test conditions and thus the Sommerfeld number. The speed was varied both by changing the supply voltage to the disc and the position of the specimen (16, 21, 33, 52, 75, 95, 117, 142mm/s), allowing a more realistic *in vivo* speed to be used. The range of loads used was increased to generate a wider range of Sommerfeld number (0.5, 1, 1.5, 2, 4, 7, 10N), and hence examine the lubrication regime more thoroughly.

- The Lubricating Fluid

It was found that the lubricating fluid kept seeping through the gap between the glass/plastic disc and the metal plate to which it was mounted. This was problematic as the supply of synovial fluid was limited. Bluetak was used around the perimeter of the disc in an attempt to correct this problem.

Following these modifications, validation against Cooke **[183, 189]** was successful. Thus, the lubrication regime of the fat pad-bone interface could be examined.

5.2.3.3 Apparatus 2 - Bovine Fat Pad:

Ethical restrictions meant that it was not possible to examine the lubrication regime of fresh human tissue, and thus a bovine fat pad was used instead. The interphalangeal fat pad was harvested from skinned bovine legs, 18 months old and obtained fresh from an abattoir (Figure 5.2.8). By observation, the material properties of this appeared to closely resemble those of Kager's fat pad, although due to a lack of data a quantitative comparison was not possible.

Fresh synovial fluid was aspirated from the medial and lateral sides of the metacarpophalangeal (MCP) joint cavities, using a 20ml gauge needle and syringe. The specimen of bovine fat pad was attached to the arm in a manner identical to that reported earlier.

Due to a very limited supply of this tissue, the fat pad was replaced only when changing the conjoining surface material. Excess synovial fluid was applied at the start of each new surface, and was evenly distributed using a brush throughout each test. The supply of fluid was replenished to ensure the surfaces were always covered, although supply was limited. In order to minimise the effect of any wearing or aging of the specimens, the tests were performed in a sequence that ensured alternation between a low and a high Sommerfeld number.

5.2.3.4 Surface Roughness

Whilst not directly used to calculate the lubrication regime, the surface roughness affected the frictional force. In measuring the surface roughness of both the PMMA and glass discs, a better understanding and interpretation of the results was achieved. The roughness of a surface (not to be confused with surface waviness, Appendix A9) may be defined by a number of parameters. The most commonly used method calculates the arithmetic mean (Ra) of the surface roughness, as in Equation 5.2.5.

$$Ra = \frac{1}{n}\sum_{i=1}^{n} |z_i|$$

Equation 5.2.5: The arithmetic mean deviation, Ra, used to quantify the surface roughness.

The average roughness, Ra, of the PMMA and glass discs was measured using a Talysurf machine (Form Talysurf Series 2, Taylor-Hobson Ltd., UK). A stylus under a very small load was moved over the surface, following the surface profile of the asperities. The displacement of the stylus was recorded and a trace of the surface roughness produced. Four, 10mm measurements were taken of both bearing surfaces, and the Ra value calculated using Equation 5.2.5. The mean Ra value of the 4 measurements was then calculated.

5.2.4 Superior Tuberosity Loading:

The change in *in vivo* pressure- and load-bearing on the superior tuberosity as a consequence of Kager's fat pad was examined using the mechanical model described

in detail in Chapter 3. Fresh bovine flexor tendon was, due to its similar properties and dimensions **[156]** used to replicate the human Achilles tendon. The bovine tendon was secured to the apparatus using a wedge-grip. The other end of the tendon was attached using a wedge grip to a Losenhausen tensometric testing machine (Düsseldorf, Germany). The apparatus was then fitted with 1 of 4 pieces of Perspex fabricated to replicate the superior tuberosity. These 4 different shapes were based broadly upon the range of cadaveric superior tuberosity sizes evident (Figure 3.2.10).

The apparatus could also be adjusted to replicate ankle flexion. A fresh bovine fat pad, dissected from the interphalangeal joint, was positioned in between the tendon and the 'bone'. The surfaces of the adjacent tissues were lubricated with fresh bovine synovial fluid (collected as detailed in 5.2.3) in order to mimic the *in vivo* lubrication. This was again aspirated from the medial and lateral sides of the metacarpophalangeal (MCP) joint cavities, using a 20ml gauge needle and syringe.

The medial and lateral movements of the fat pad were restricted to mimic the Achilles tendon paratenon *in vivo*. The position of the fat pad was cross-referenced against ultrasound images for accuracy. As in Chapter 3, the Achilles tendon was loaded to 0.4kN at 5mm/s strain rate, realistic *in vivo* conditions. A layer of pressure sensitive paper (Sensor Products LLC, New Jersey, USA) adhered to the surface of the superior tuberosity allowed measurement of the pressure exerted upon it. Two different sensitivities of film were used (28-85 PSI, 70-350 PSI) to allow for a wide range of pressure to be measured. Whilst 3 tests were planned for each combination of ankle flexion and superior tuberosity shape, only two such tests were performed in each experiment in order to preserve the fresh tissue.

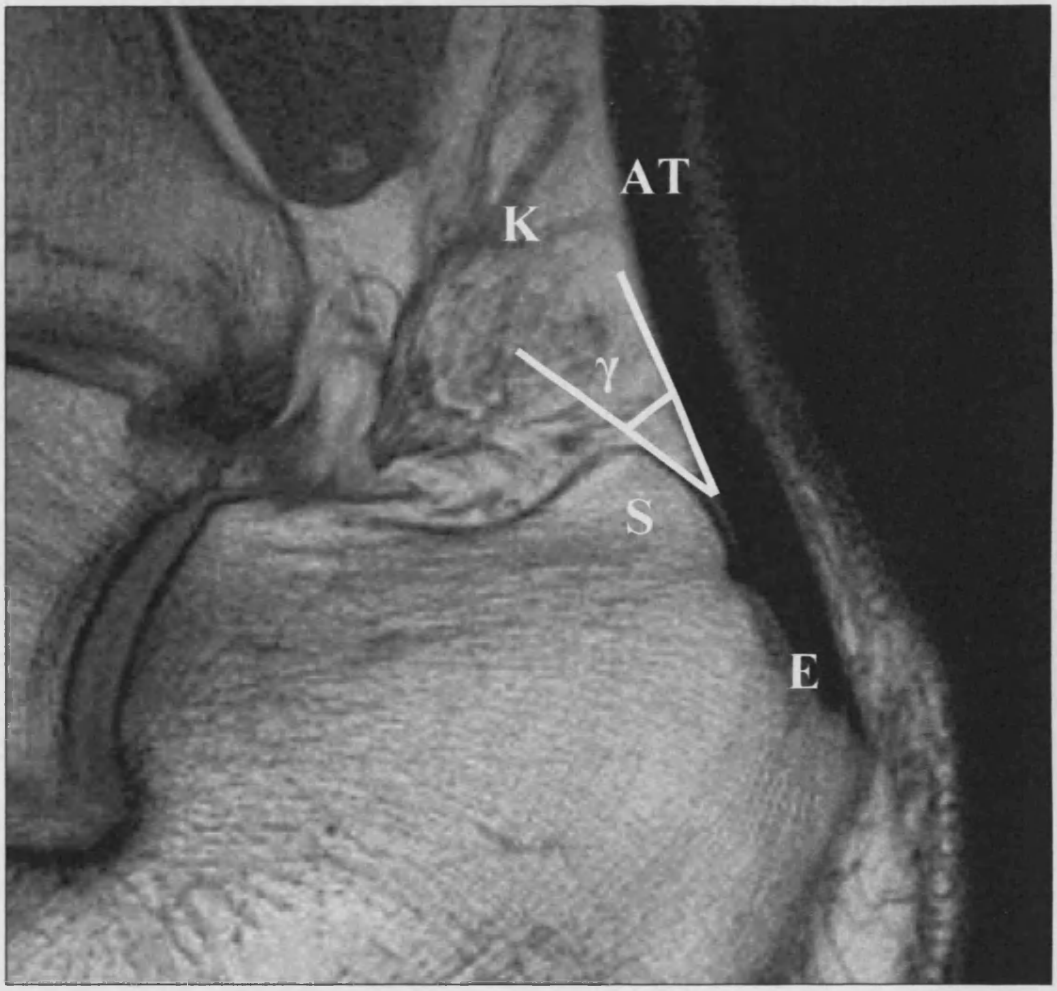

Figure 5.2.1: A sagittal MRI of the hindfoot, with the foot in maximum plantarflexion. The insertional angle (γ) is defined as the angle between the deep surface of the Achilles tendon (AT) and the superior tuberosity (S). E = Enthesis, K = Kager's fat pad.

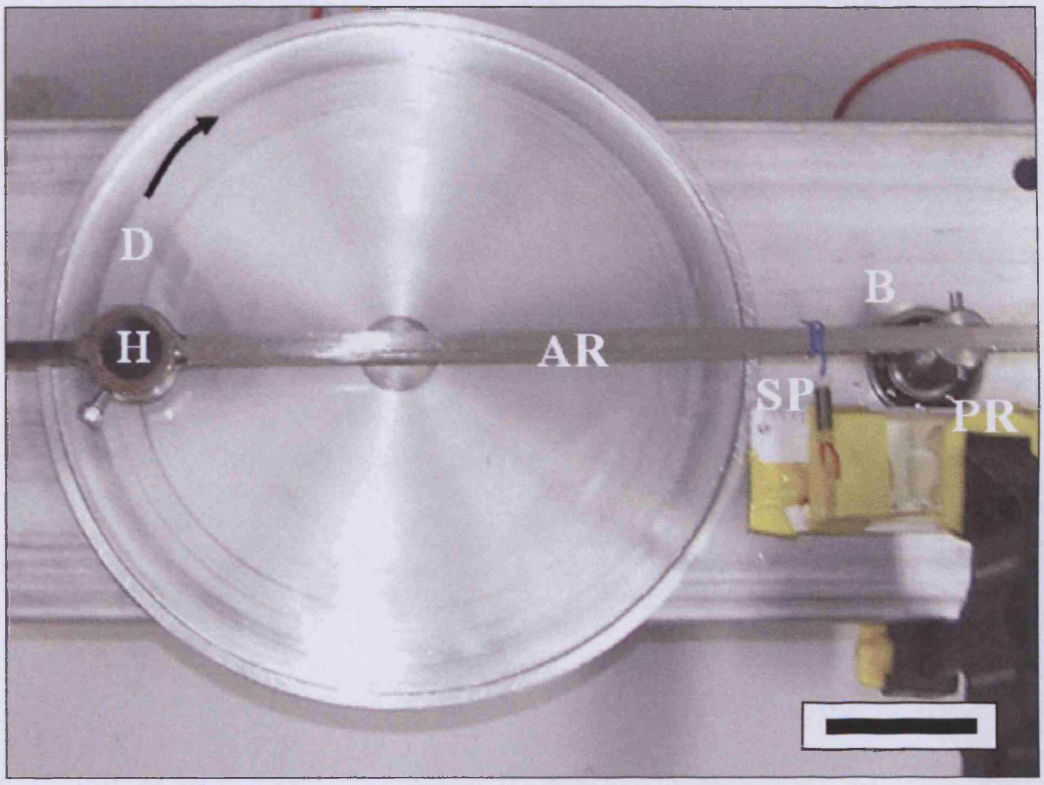

Figure 5.2.2: The first apparatus used to investigate the lubrication regime between Kager's fat pad and the calcaneus. AR= Arm; B= Ball bearing; D= Rotating disc; H= Specimen holder; PR= Pillar; SP= Spring; Arrow = Direction of rotation, Scale bar = 60mm.

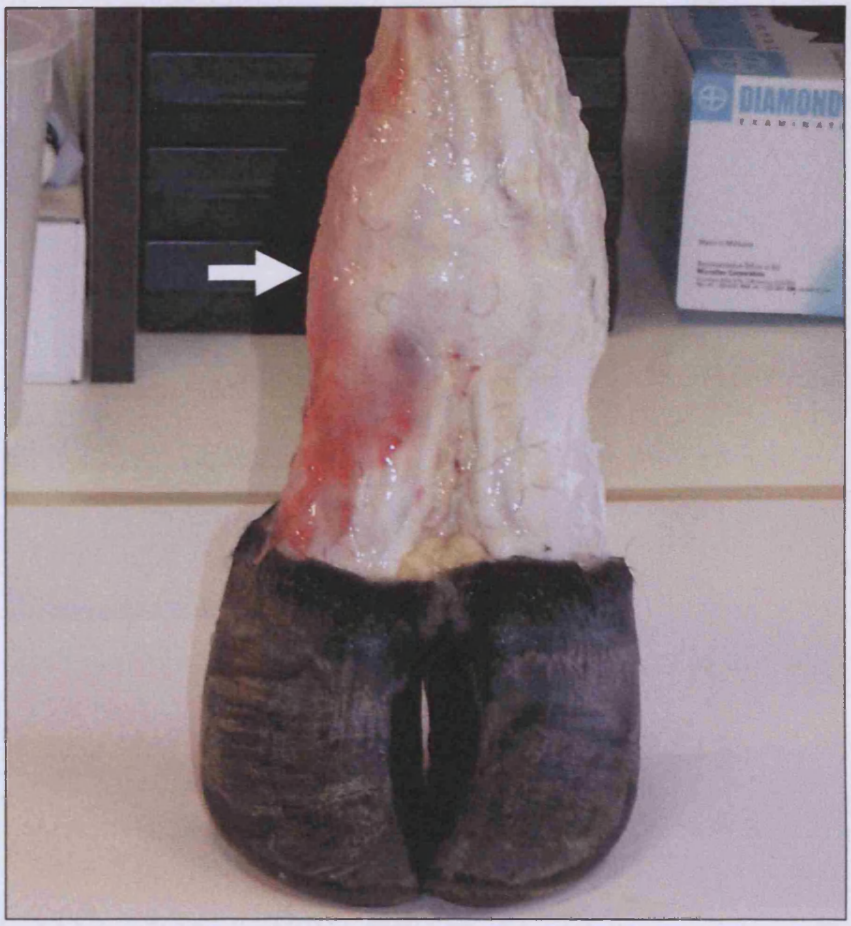

Figure 5.2.3: Anterior view of a skinned, 18 month old bovine leg, identifying the metacarpophalangeal (MCP) joint. From here, both the synovial membrane specimen and the synovial fluid were harvested. Arrow = MCP joint.

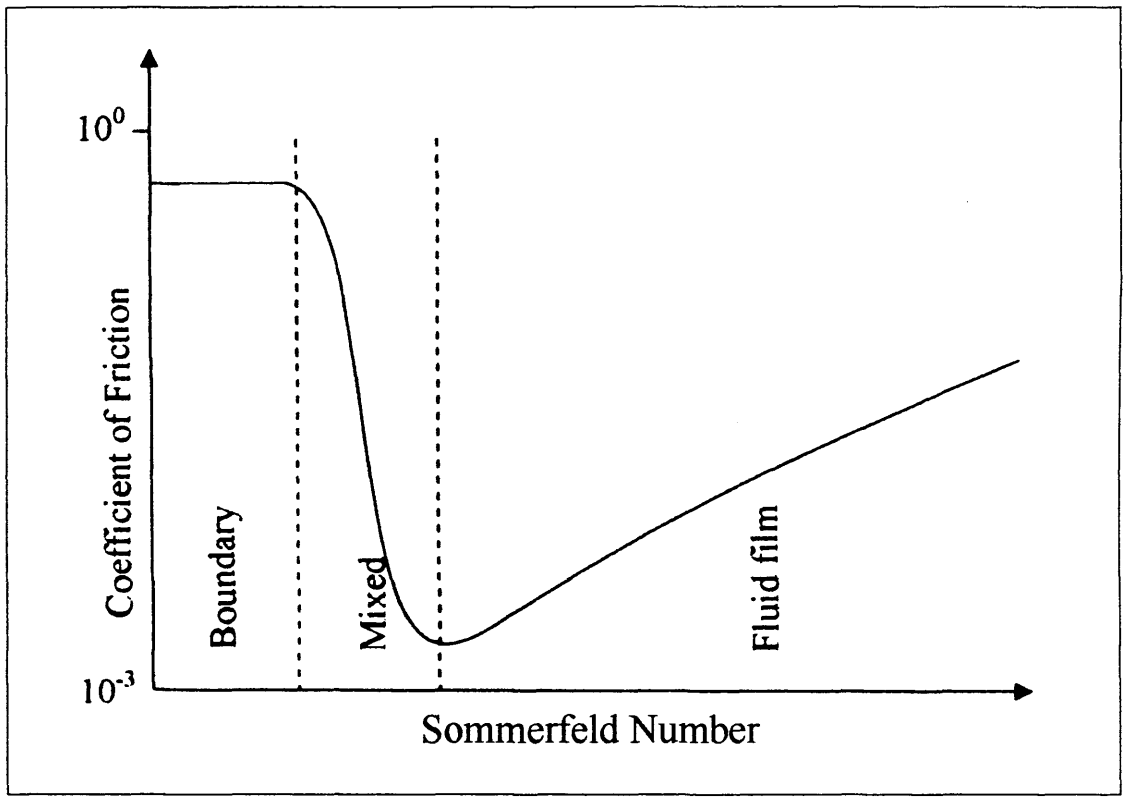

Figure 5.2.4: The Stribeck curve. The trace of the coefficient of friction against the Sommerfeld number allows for the identification of 3 different lubrication regimes.

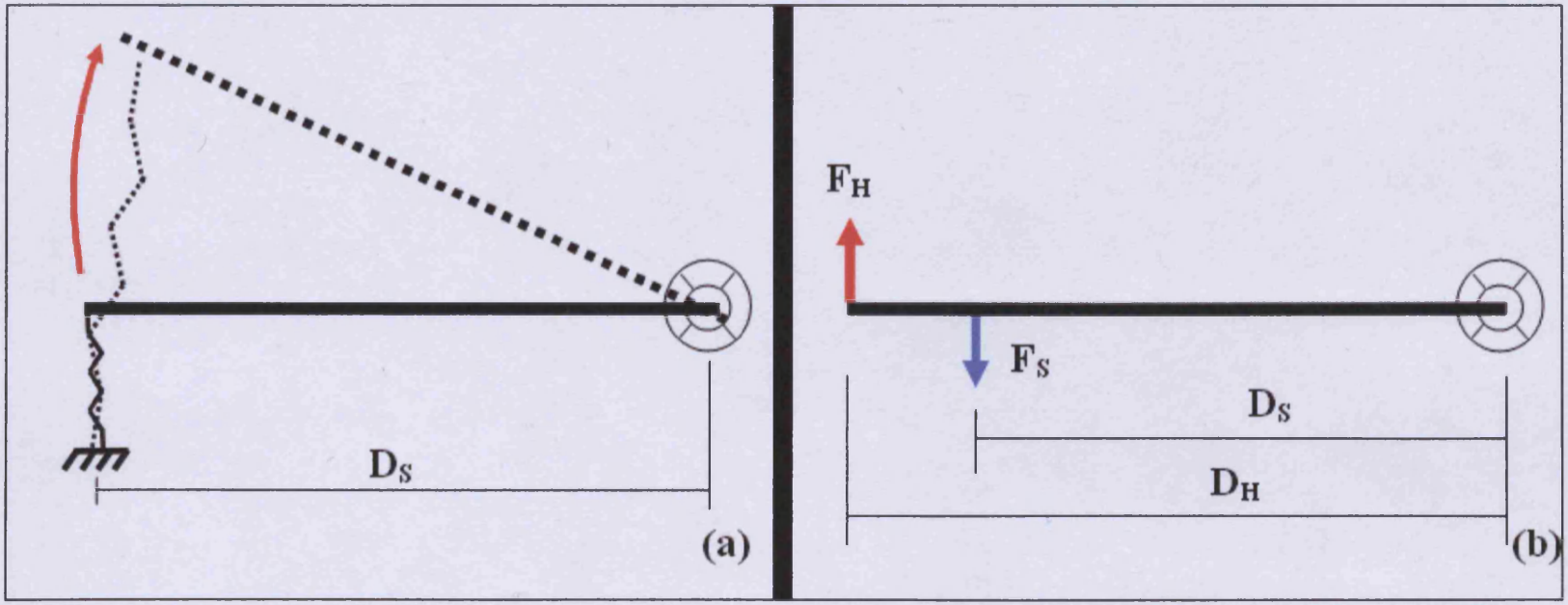

Figure 5.2.5: Schematic representations detailing the suspended arm movements. (a) The extension of the spring is approximated to the arc subtended by the arm on rotation. (b) The moments of the suspended arm resolved about the pivot in order to determine the frictional force at the specimen holder, F_H.

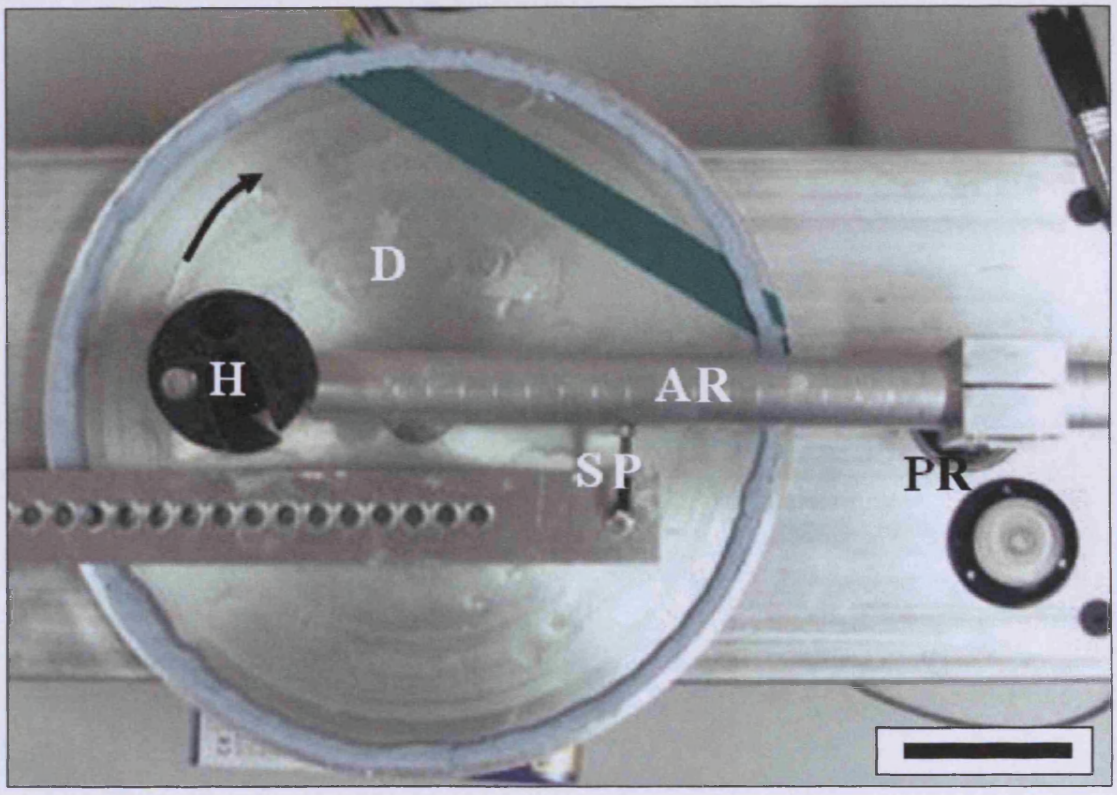

Figure 5.2.6: The second apparatus used to investigate the lubrication regime between Kager's fat pad and the calcaneus. AR= Arm; D= Rotating disc; H= Specimen holder; PR= Pillar; SP= Spring; Arrow = Direction of rotation. Scale bar = 60mm.

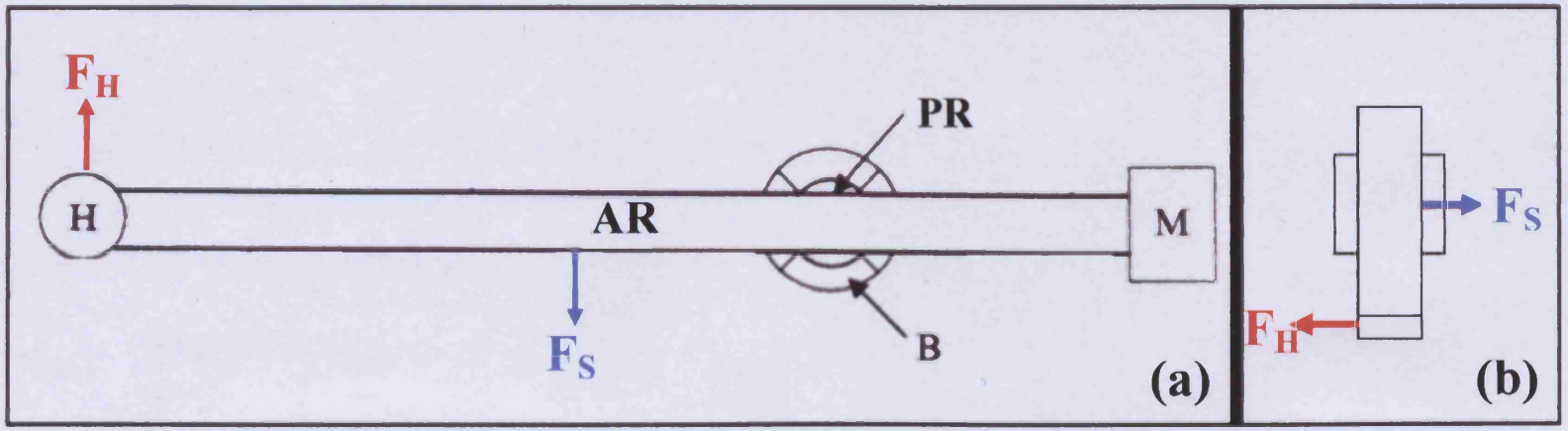

Figure 5.2.7: The coupling effect caused by the skewed alignment of the frictional (F_H) and resistive (F_S) forces in the Apparatus 1. (a) Viewed from above, flexion of the suspension arm may be caused by the unaligned forces creating a couple (b) How the vertical couple may cause undesirable rotation of the arm AR= Arm; B= Bearing; H= Specimen holder; M= Counterbalance mass; PR = Pillar.

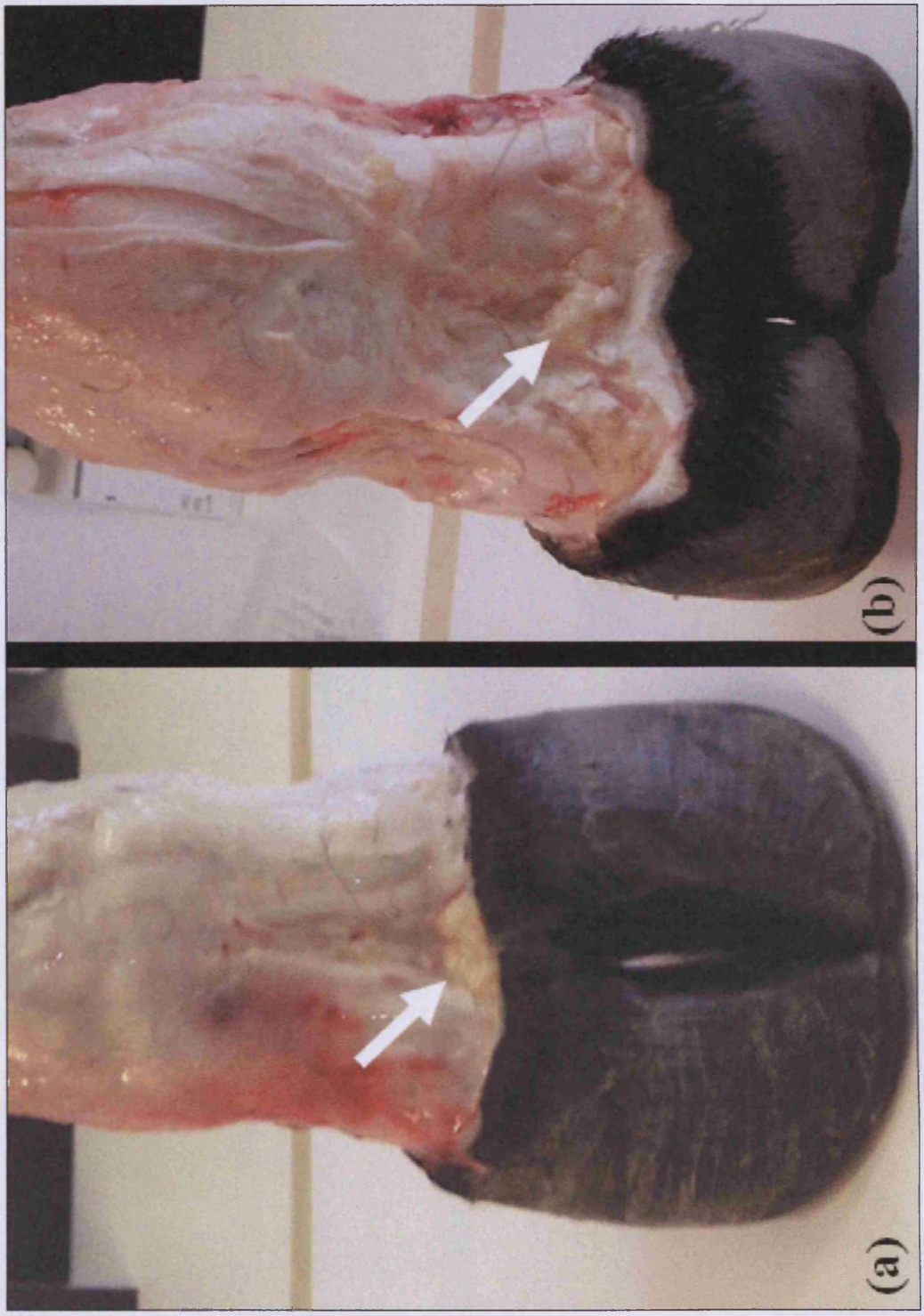

Figure 5.2.8: The interphalangeal fat pad of a fresh, skinned, 18 month old bovine leg. (a) Anterior view. (b) Posterior view. Arrow = Fat pad.

5.3 Results:

5.3.1 Movements of Kager's Fat Pad:

Kager's fat pad was dynamically observed moving into and out of the retrocalcaneal bursa on ankle flexion. With the foot in maximum dorsiflexion, the bursal protruding wedge (BPW, the distal wedged-shape extension) of Kager's fat pad was fully expelled from the retrocalcaneal bursa. As the foot was moved to a position of maximum plantarflexion, the distal wedge was observed moving into the retrocalcaneal bursa. This is evident in Figure 5.3.1. The Achilles-associated fat pad (situated posteriorly and associated with the Achilles tendon) was, however, relatively still during ankle flexion, with little movement discernable relative to the Achilles tendon. In contrast, the FHL-associated fat pad (situated anteriorly and associated with the FHL) exhibited significant motion between the periods when the foot was in the neutral position and when in plantarflexion. The FHL, as a weak plantarflexion muscle, was also evident contracting during ankle flexion. Isolated contraction and consequential thickening of the FHL muscle squeezed the fatty extension distally. Tunnelling under the posterior fat, it ultimately appeared to force the distal wedge into the retrocalcaneal bursa. Additionally, the FHL forms a stiff anterior boundary on plantarflexion.

Ultrasound images allowed measurement of the movement of Kager's fat pad. Images were captured with the subject prone and the foot in a position of maximum plantarflexion, the neutral position, and maximum dorsiflexion. The distance between the distal wedge and the Enthesis Proximal Point was measured to quantify this movement. These results are accompanied by a measure of the flexion angle (between the long axis of the lower leg and the foot) in parenthesis (Table 5.3.1, Figure 5.3.1).

Table 5.3.1: The distance (mm) of the BPW from the Enthesis Proximal Point. The angle of ankle flexion is noted in parenthesis.

Distance between BPW and EPP (mm)						
	Subject					Mean
	1	2	3	4	5	
Maximum dorsiflexion	11.4 (90)	10.5 (66)	13.3 (64)	13.8 (82)	8.0 (72)	11.4
Neutral	10.1 (90)	6.9 (90)	9.6 (90)	11.8 (90)	5.5 (90)	8.8
Maximum plantarflexion	9.0 (144)	6.9 (140)	7.4 (140)	1.5 (162)	5.5 (135)	6.1

When the Achilles tendon was loaded, the movements reported in Table 5.3.1 for an unloaded Achilles tendon were accentuated. In particular, the BPW was seen to move further into the retrocalcaneal bursa, typically moving to a position adjacent to the most proximal point of the enthesis. On dorsiflexion, the fat pad was expelled from the retrocalcaneal bursa to a greater extent than previously witnessed. These results are evident in Table 5.3.2. In Figure 5.3.2 these results are compared graphically to those achieved when the Achilles tendon was unloaded.

Table 5.3.2: The distance (mm) of the BPW relative to the Enthesis Proximal Point when the Achilles tendon is loaded. The angle of ankle flexion is noted in parenthesis.

Distance between BPW and EPP (mm)						
	Subject					Mean
	1	2	3	4	5	
Maximum dorsiflexion	15.7 (62)	11.7 (66)	13.7 (64)	12.4 (82)	9.8 (64)	12.7
Neutral	15.1 (90)	11.7 (90)	11.1 (90)	12.6 (90)	7.6 (90)	11.6
Maximum plantarflexion	4.9 (130)	1.4 (140)	5.9 (138)	5.7 (156)	2.3 (138)	4

5.3.1.1 Posterior Displacement of the Achilles Tendon:

Despite moving in to the retrocalcaneal bursa, the BPW was not found to increase the lever arm in any of the subjects.

5.3.1.2 The Insertional Angle:

The insertional angle was examined in three subjects using MRI. The insertional angle was measured initially with the foot in maximum dorsiflexion, and was measured thereafter at intervals of 10 degrees of flexion (Table 5.3.3, Figure 5.3.3).

Table 5.3.3: The variation of the insertional angle (degrees) with a change in the ankle angle (degrees, displayed in parenthesis).

Variation of Insertional Angle (Deg) with Ankle Angle (Deg)			
	Subject		
	1	2	3
Dorsiflexion	0 (82)	0 (85)	0 (83)
	10 (92)	0 (95)	0 (93)
	15.5 (102)	11 (105)	4 (103)
	21 (112)	19 (105)	11 (113)
	22 (122)	28 (125)	22 (123)
	27 (132)	34 (135)	-
Plantarflexion	29 (142)	36 (145)	-

5.3.2 The Lubrication of Kager's Fat Pad:

5.3.2.1 Ra Values:

The surface roughness values, Ra, of both the glass and PMMA bearing surfaces were measured using a Form Talysurf Series 2 machine (Taylor-Hobson Ltd., UK). Four recordings along a 10mm length were taken, and the mean calculated. These results are displayed in Table 5.3.4:

Table 5.3.4: The Ra values (μm) for the glass and PMMA surfaces:

Surface Roughness, Ra (μm)		
	PMMA	**Glass**
Test 1	0.380	0.058
Test 2	0.104	0.040
Test 3	0.300	0.024
Test 4	0.404	0.013
Mean	**0.297**	**0.034**

5.3.2.2 Apparatus I:

Bovine synovial membrane was examined using Apparatus 1 in order to successfully validate the equipment. The arm rotation was measured by the potentiometer voltage change, with this data being processed following the above protocol to derive the coefficient of friction. The Sommerfeld number was also calculated, and the relationship between the two parameters plotted in the format of the Stribeck curve (Figure 5.3.4). The positive trend line of this curve is indicative of fluid film lubrication.

The coefficient of friction is greater, however, than that previously reported by Cooke et al **[183, 189]** (Figure 5.3.4, blue line). In addition, these values are also approximately 1 order of magnitude outside the range typically expected in such lubrication regimes **[196]**. Thus, the apparatus was modified to reduce the inherent friction, as detailed earlier in this chapter.

5.3.2.3 Apparatus 2:

Apparatus 2 was also validated using bovine synovial membrane. These results were processed as above, and the Stribeck representation is displayed in Figure 5.3.5. These results are closely comparable both with the previous data **[183, 189]** and the typical values of the lubrication regimes reported **[196]**, and thus the apparatus was considered validated.

The bovine fat pad experiments used both PMMA and glass discs as conjoining surfaces. The results are displayed in Figure 5.3.6 & 5.3.7 respectively. The former indicates a regime of predominantly fluid film lubrication with the positive gradient. However, as the Sommerfeld number decreases, the increase in coefficient of friction is indicative of mixed lubrication. In Figure 5.3.7, the glass bearing surface appears to exhibit solely fluid film lubrication.

5.3.3 Mechanical Loading:

The mechanical model was tested with a fresh bovine fat pad positioned between the tendon and the superior tuberosity, replicating *in vivo* conditions. Due to the fat pad

drying out and degrading relatively quickly during the experiment, only 2 repetitions of each experiment were performed as the supply of tissue was limited. In addition, Profiles 1 & 4 were excluded from the study as it was deemed that the fat pad was unlikely to affect the load borne due to the geometry of the contact.

The pressure experienced on the superior tuberosity was recorded on the pressure sensitive film covering its surface during application of a 0.4kN tensile load to the tendon. By comparing the colour of the film to a series of calibration scale, the pressure (PSI) recorded was determined (Table 5.3.5(a)). This pressure was converted into SI units (kPa)(Table 5.3.5(b)).

Table 5.3.5(a): The pressure (PSI) recorded on the superior tuberosity surface when in contact with bovine flexor tendon (load = 0.4kN). The model included bovine fat pad.

	Pressure (PSI)				
	30° DRF	15° DRF	Neutral	15° PLF	30° PLF
Profile 2					
Test 1	83	83	54	0	0
Test 2	83	83	61	0	0
Profile 3					
Test 1	114	83	78	69	0
Test 2	114	83	69	61	0

Table 5.3.5(b): The pressure (kPa) recorded on the superior tuberosity surface when in contact with bovine flexor tendon (load = 0.4kN). The model included bovine fat pad.

	Pressure (kPa)				
	30° DRF	15° DRF	Neutral	15° PLF	30° PLF
Profile 2					
Test 1	570	570	370	0	0
Test 2	570	570	420	0	0
Profile 3					
Test 1	790	570	540	480	0
Test 2	790	570	480	420	0

The contact area was then measured from the pressure sensitive film (Table 5.3.6a)) to allow the distributed load on the superior tuberosity to be calculated (Table 5.3.6(b)).

Table 5.3.6(a): The contact area (m^2) between the superior tuberosity and the fat pad.

	Contact area x 10^{-4} (m^2)				
	30° DRF	15° DRF	Neutral	15° PLF	30° PLF
Profile 2					
Test 1	4.12	1.30	0.65	0	0
Test 2	4.12	1.40	0.65	0	0
Profile 3					
Test 1	3.86	2.70	1.30	0.65	0
Test 2	4.18	2.70	1.40	0.70	0

Table 5.3.6(b): The distributed load (N) experienced on the superior tuberosity surface.

	Distributed load (N)				
	30° DRF	15° DRF	Neutral	15° PLF	30° PLF
Profile 2					
Test 1	82.4	82.4	24.2	0	0
Test 2	96.7	88.1	27.3	0	0
Mean	**89.6**	**85.3**	**25.8**	**0**	**0**
Profile 3					
Test 1	314	155	69.9	31.4	0
Test 2	329	155	66.6	29.4	0
Mean	**321**	**155**	**68.4**	**30.4**	**0**

The effect of Kager's fat pad on the pressure and distributed load experienced by the superior tuberosity was then determined by comparing the values recorded with the fat pad (Tables 5.3.5(b) & 5.3.6(b)) against those where the fat pad was not included (Tables 3.3.9 and 3.3.10(b)). These results are shown in Table 5.3.7 (Figures 5.3.8 & 5.3.9), and Table 5.3.8 (Figures 5.3.10 & 5.3.11) respectively.

Table 5.3.7: The difference in pressure (kPa) experienced on the superior tuberosity surface due to the fat pad.

	Difference in pressure (kPa)				
	30° DRF	15° DRF	Neutral	15° PLF	30° PLF
Profile 2					
Mean	**0**	**0**	**-195**	**0**	**0**
Profile 3					
Mean	**0**	**0**	**-59.5**	**-60**	**0**

Table 5.3.8: The difference in distributed load (N) experienced on the superior tuberosity surface due to the fat pad.

	Difference in distributed load (N)				
	30° DRF	15° DRF	Neutral	15° PLF	30° PLF
Profile 2					
Mean	0	0	-18.2	0	0
Profile 3					
Mean	0	0	-29.8	0	0

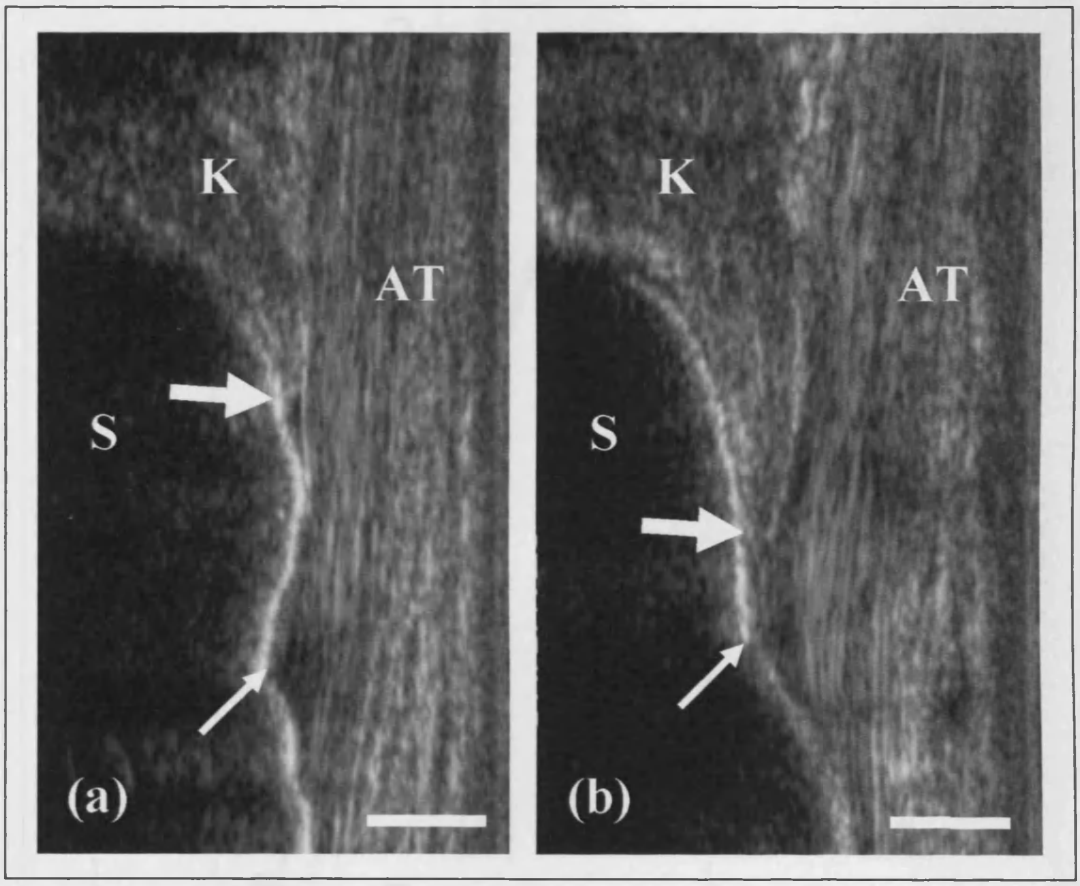

Figure 5.3.1: Sagittal US images of the Achilles tendon enthesis organ demonstrating movement of Kager's fat pad. (a) With the foot in the dorsiflexed position, the fat pad is expelled from the retrocalcaneal bursa. (b) With the foot in the plantarflexed position, the fat pad has moved in to the retrocalcaneal bursa. AT = Achilles tendon, K = Kager's fat pad, S = Superior Tuberosity, Small arrow = Enthesis Proximal Point, Large arrow = Leading edge of fat pad, Scale bar = 3mm.

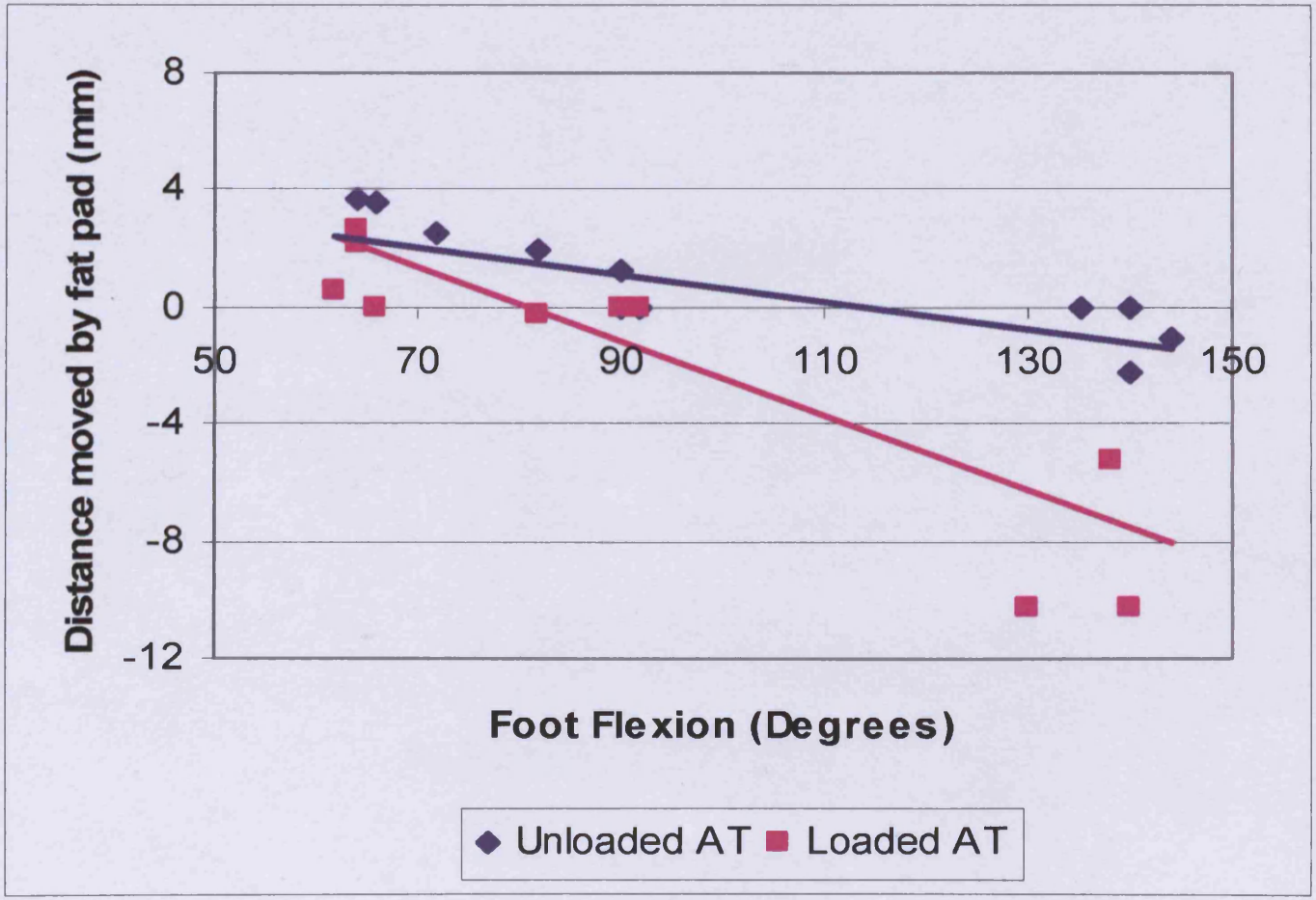

Figure 5.3.2: Graphical representation of the increased movement of Kager's fat pad when the Achilles tendon is loaded. The Y-axis reflects the normalised distance moved by Kager's fat pad from when in the neutral position (e.g. -4mm = 4mm distally, into the retrocalcaneal bursa). Unloaded Achilles tendon: R^2 = 0.63; Loaded Achilles tendon: R^2 = 0.80.

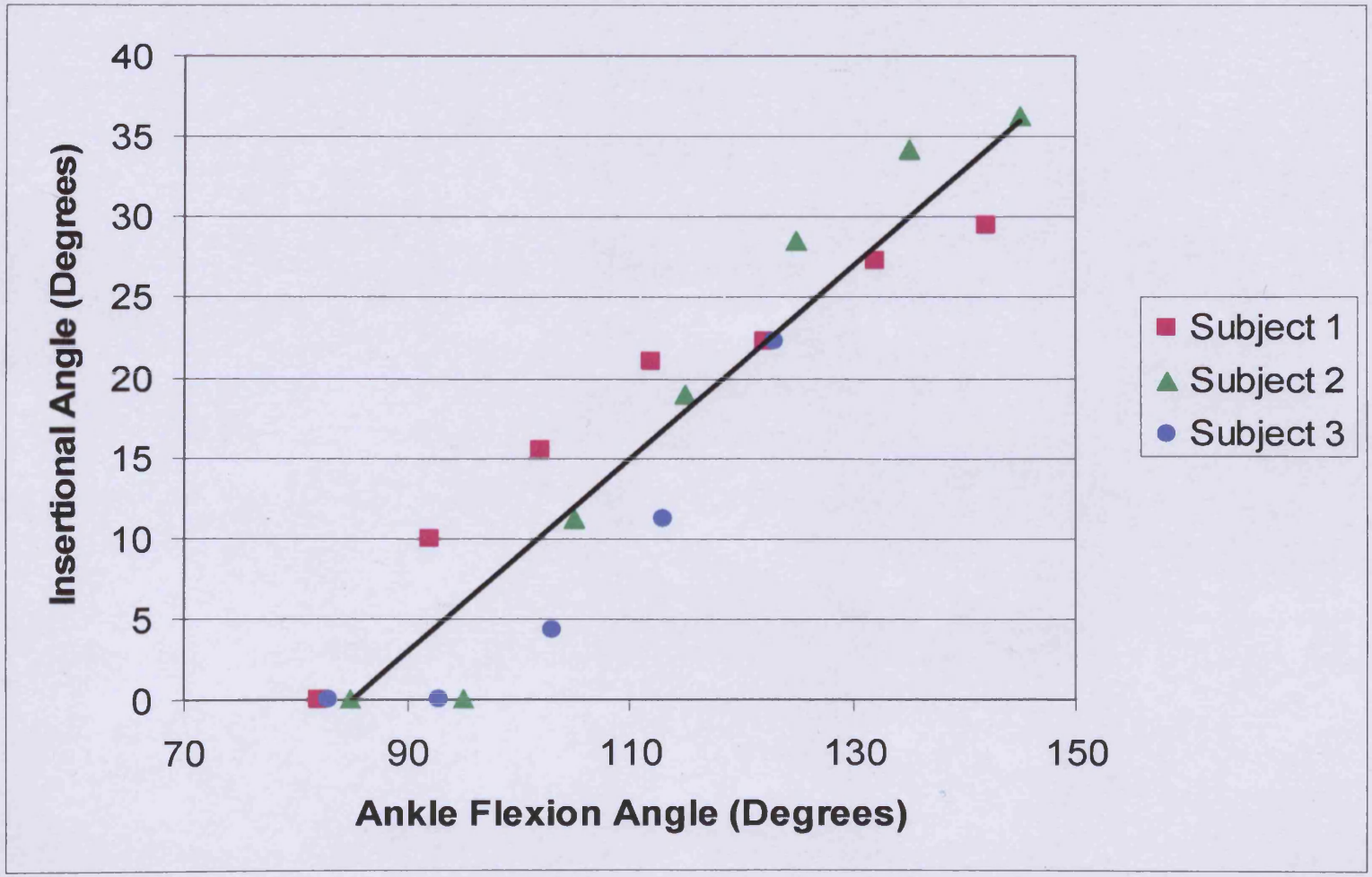

Figure 5.3.3: Ankle flexion angle vs insertional angle of 3 subjects. A linear trend line ($R^2 = 0.90$) indicates that the insertional angle is proportional to the angle of ankle flexion

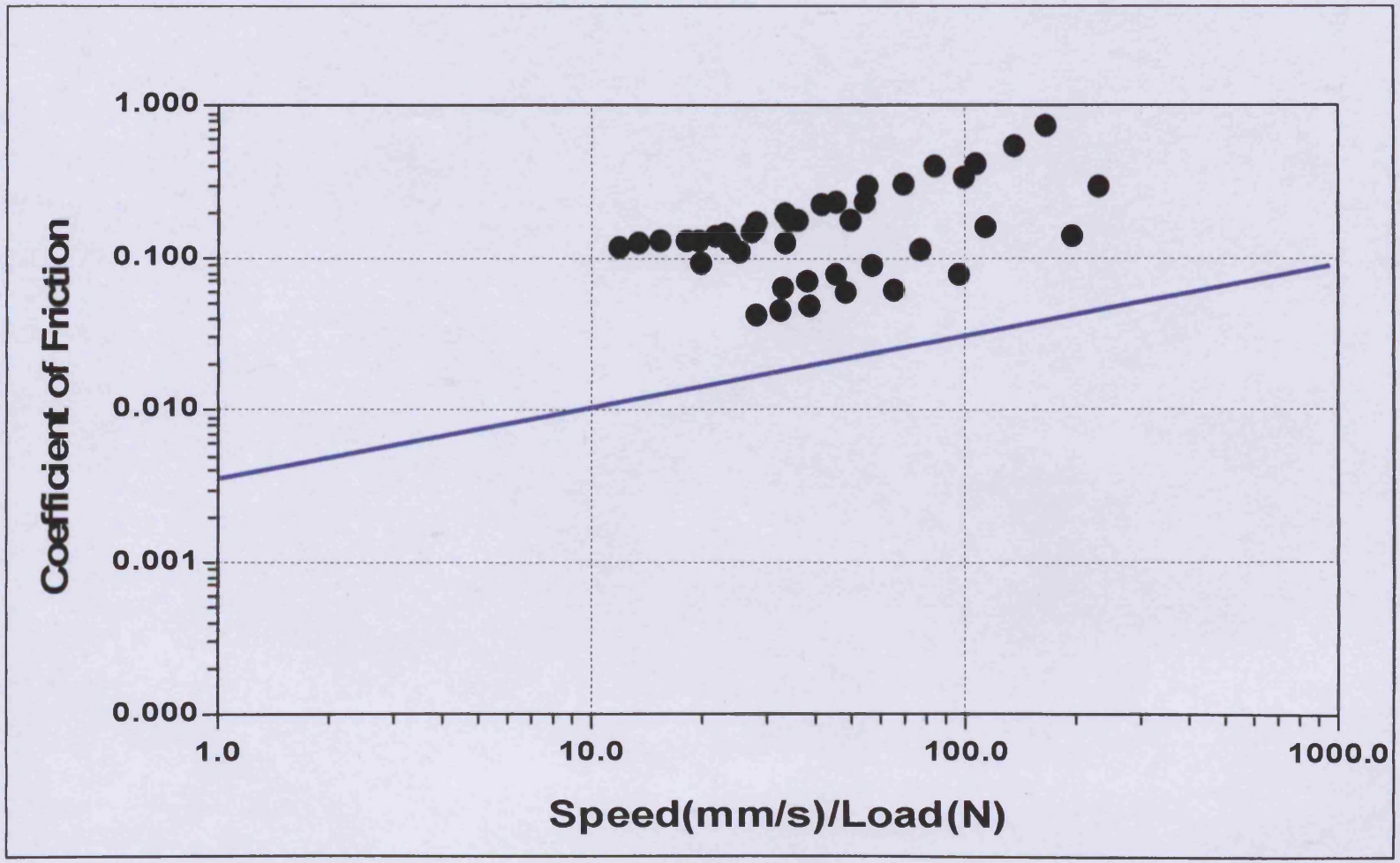

Figure 5.3.4: Stribeck plot for bovine synovial membrane against PMMA counterface using Apparatus 1. These results are compared to the previously reported **[183, 189]** results (blue line) to provide validation of the apparatus.

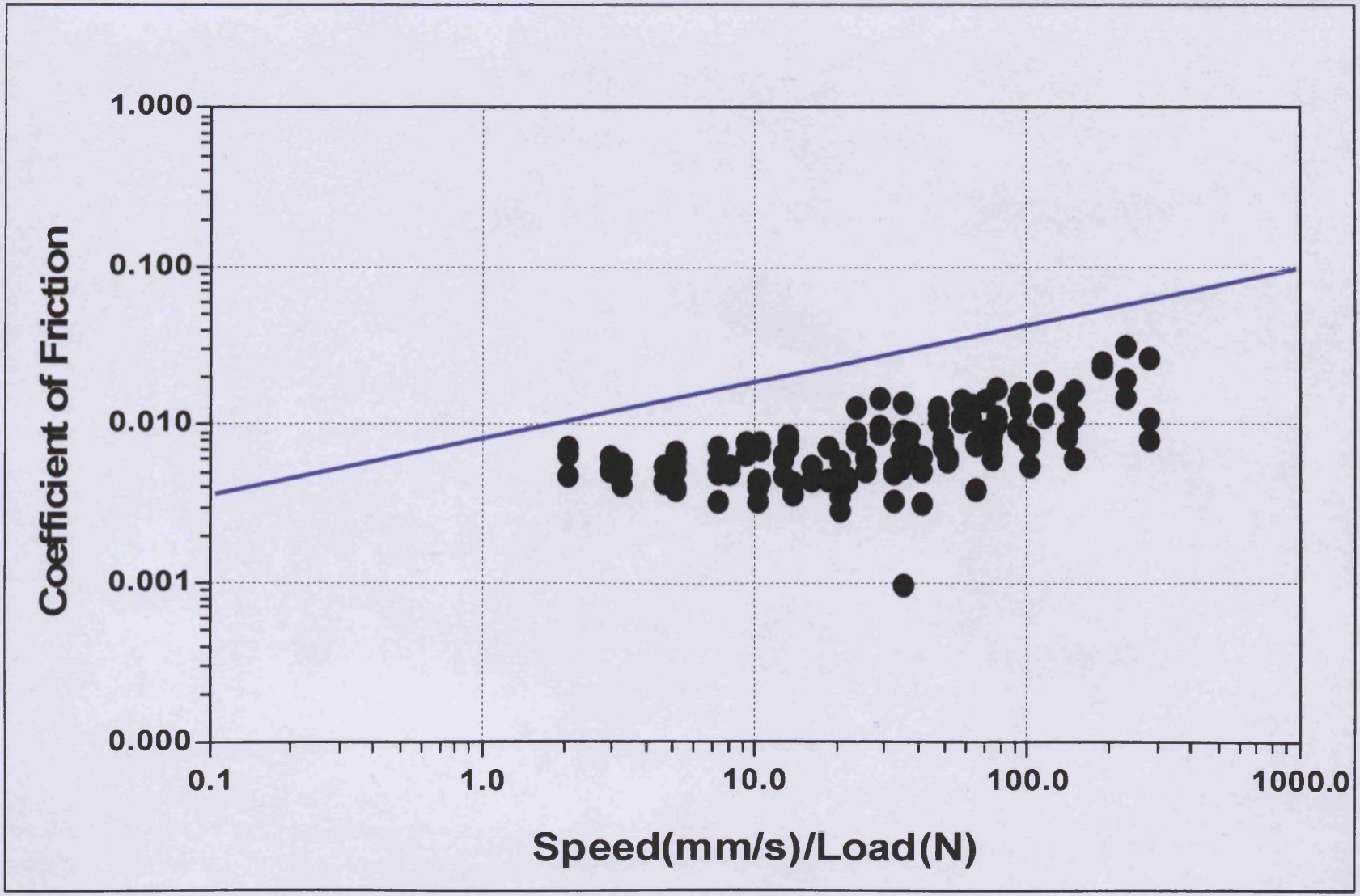

Figure 5.3.5: Stribeck plot for bovine synovial membrane against PMMA counterface using Apparatus 2. This is compared to the previously published **[183, 189]** results (blue line) to act as validation for the apparatus.

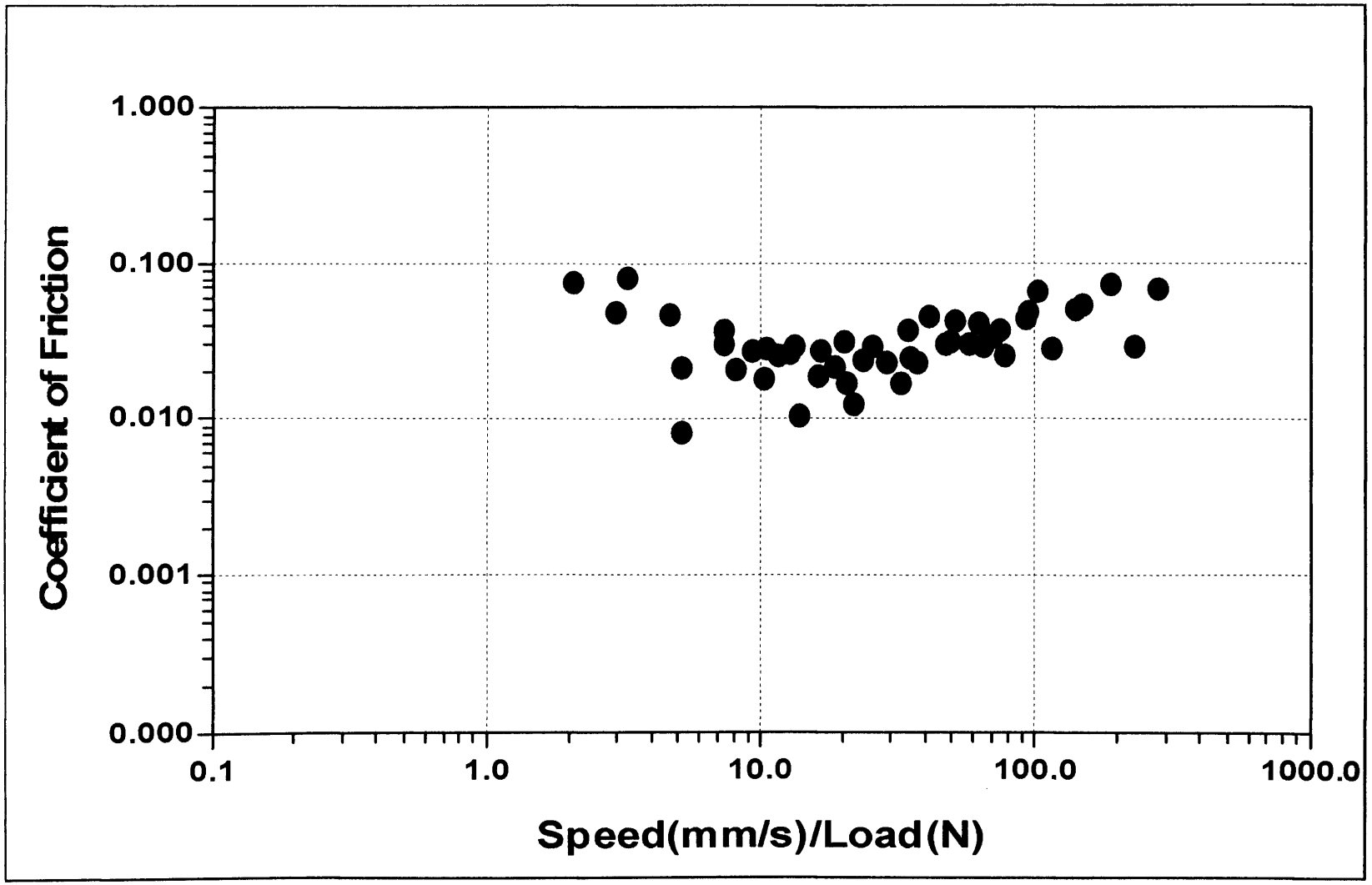

Figure 5.3.6: Stribeck plot for bovine fat pad against PMMA counterface using Apparatus 2. This bathtub curve may be representative of the transition between mixed and fluid film lubrication when compared to the Stribeck curve (Figure 5.2.5).

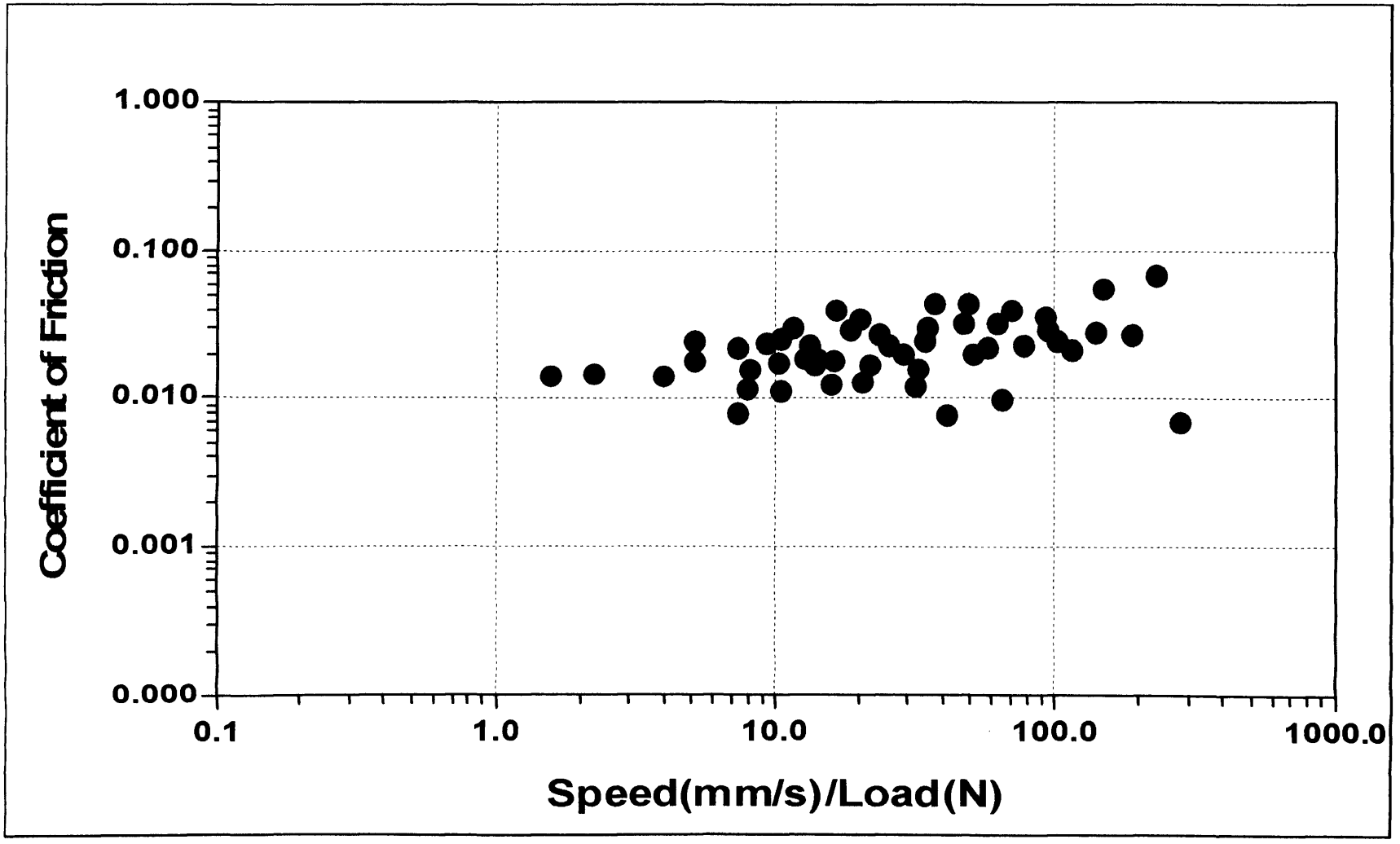

Figure 5.3.7: Stribeck plot for bovine fat pad against glass counterface using Apparatus 2. A linear plot is indicative of pure fluid film lubrication when compared to the Stribeck curve (Figure 5.2.5).

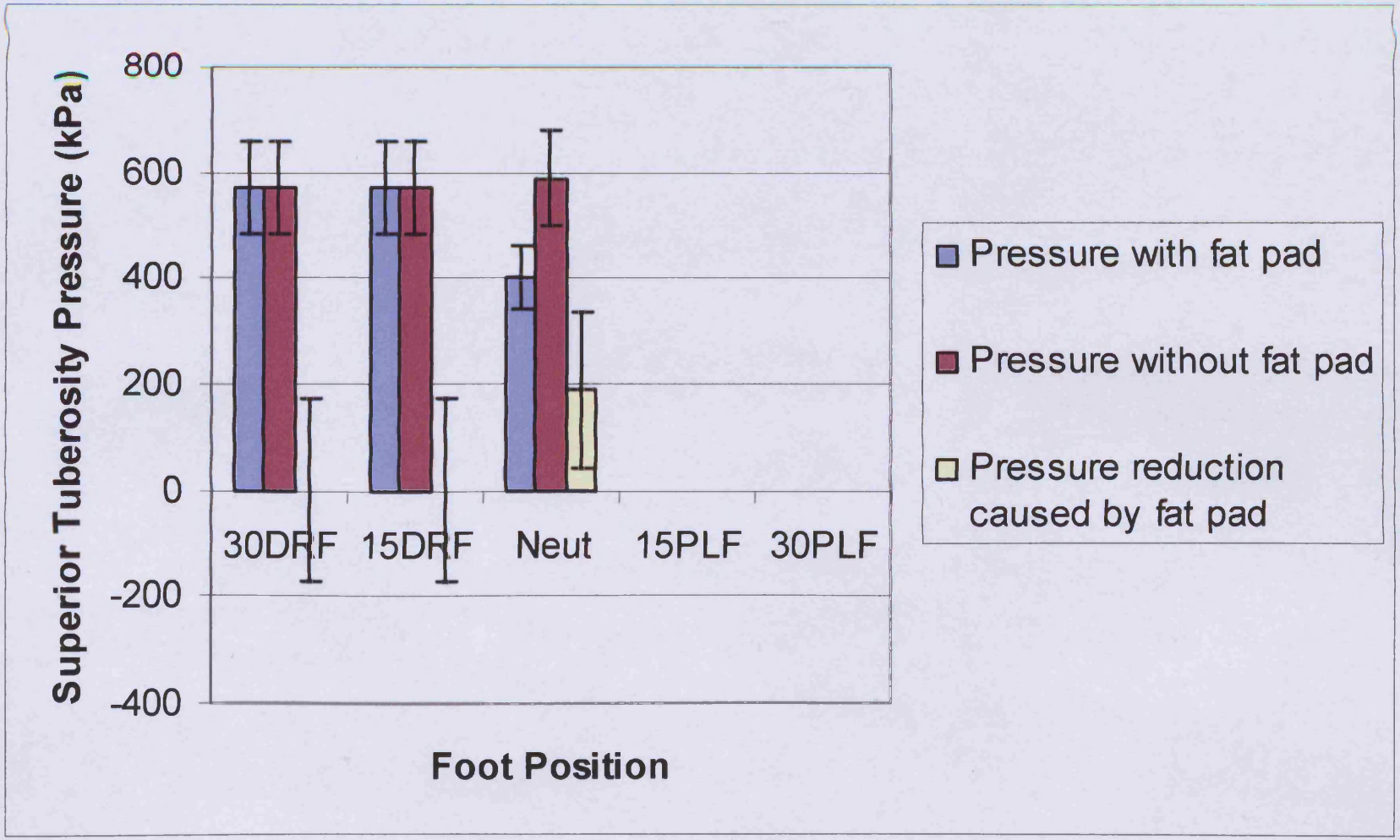

Figure 5.3.8: Comparison of the effect of bovine fat pad on the pressure on Profile 2. Error bars for measured pressure = ±15%. Error bars for pressure reduction = maximum and minimum possible error following calculation.

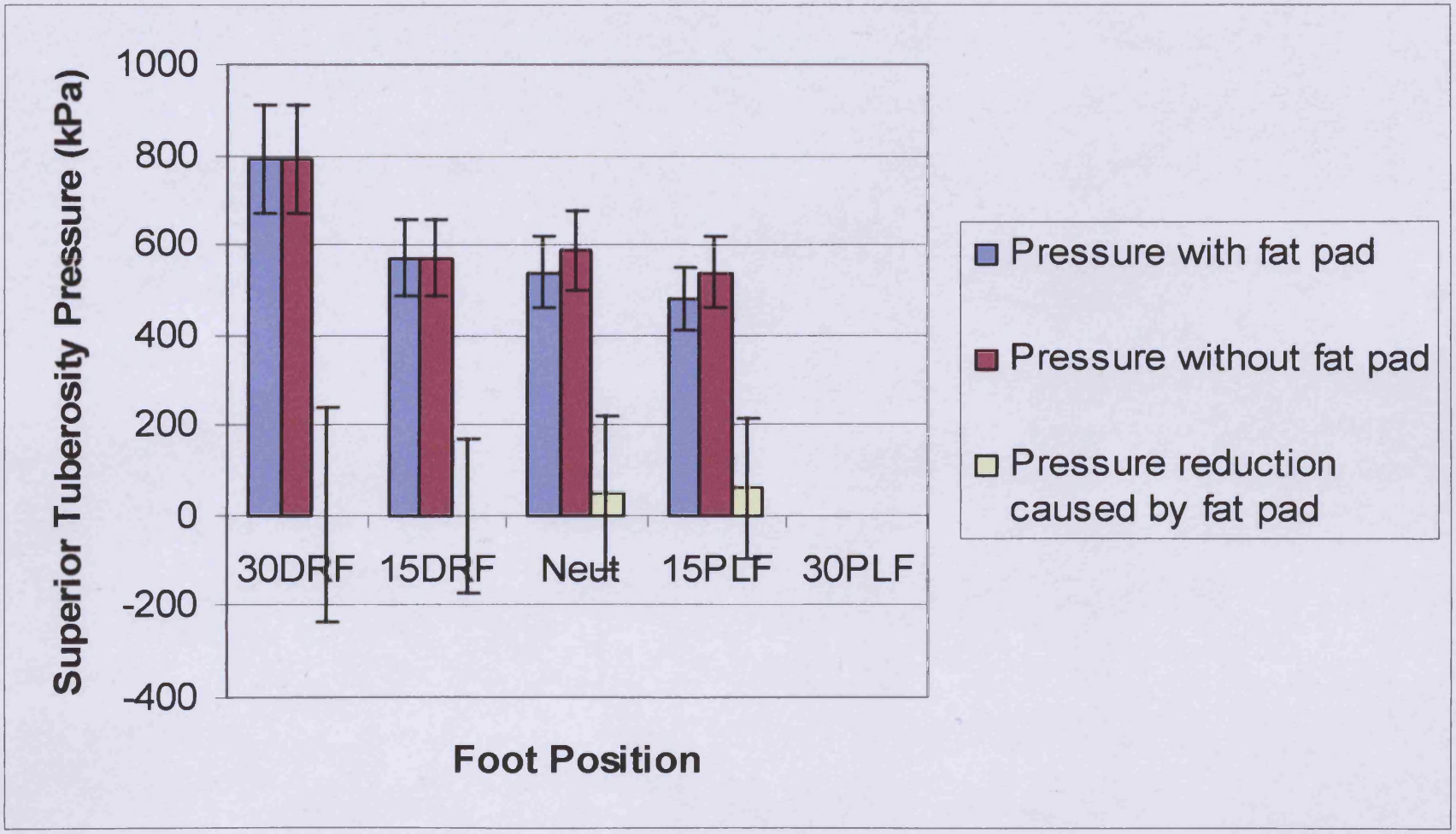

Figure 5.3.9: Comparison of the effect of bovine fat pad on the pressure on Profile 3. Error bars for measured load = ± 15%. Error bars for pressure reduction = maximum and minimum possible error following calculation.

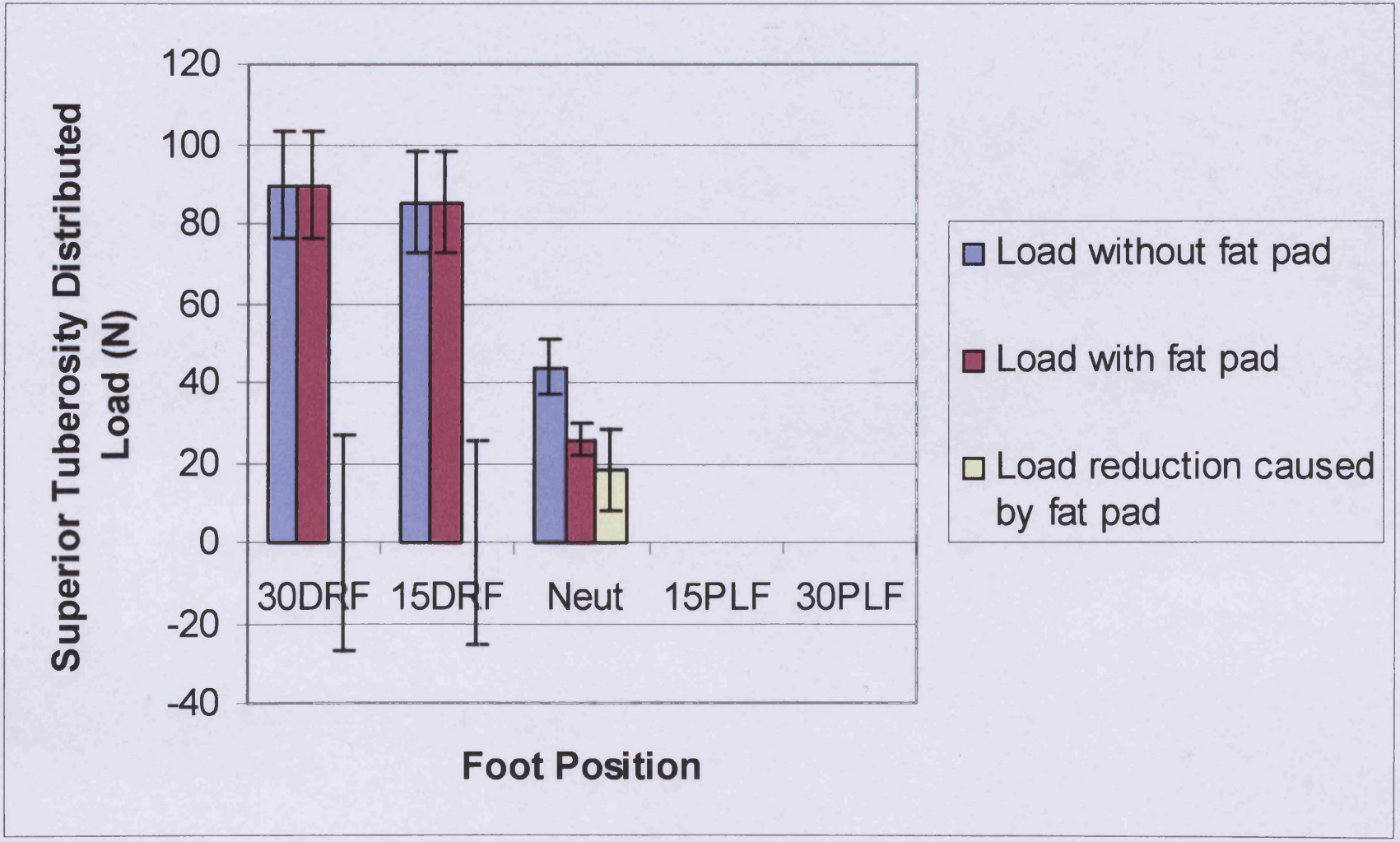

Figure 5.3.10: Comparison of the effect of bovine fat pad on the distributed load on Profile 2. Error bars for measured load = ± 15%. Error bars for pressure reduction = maximum and minimum possible error following calculation.

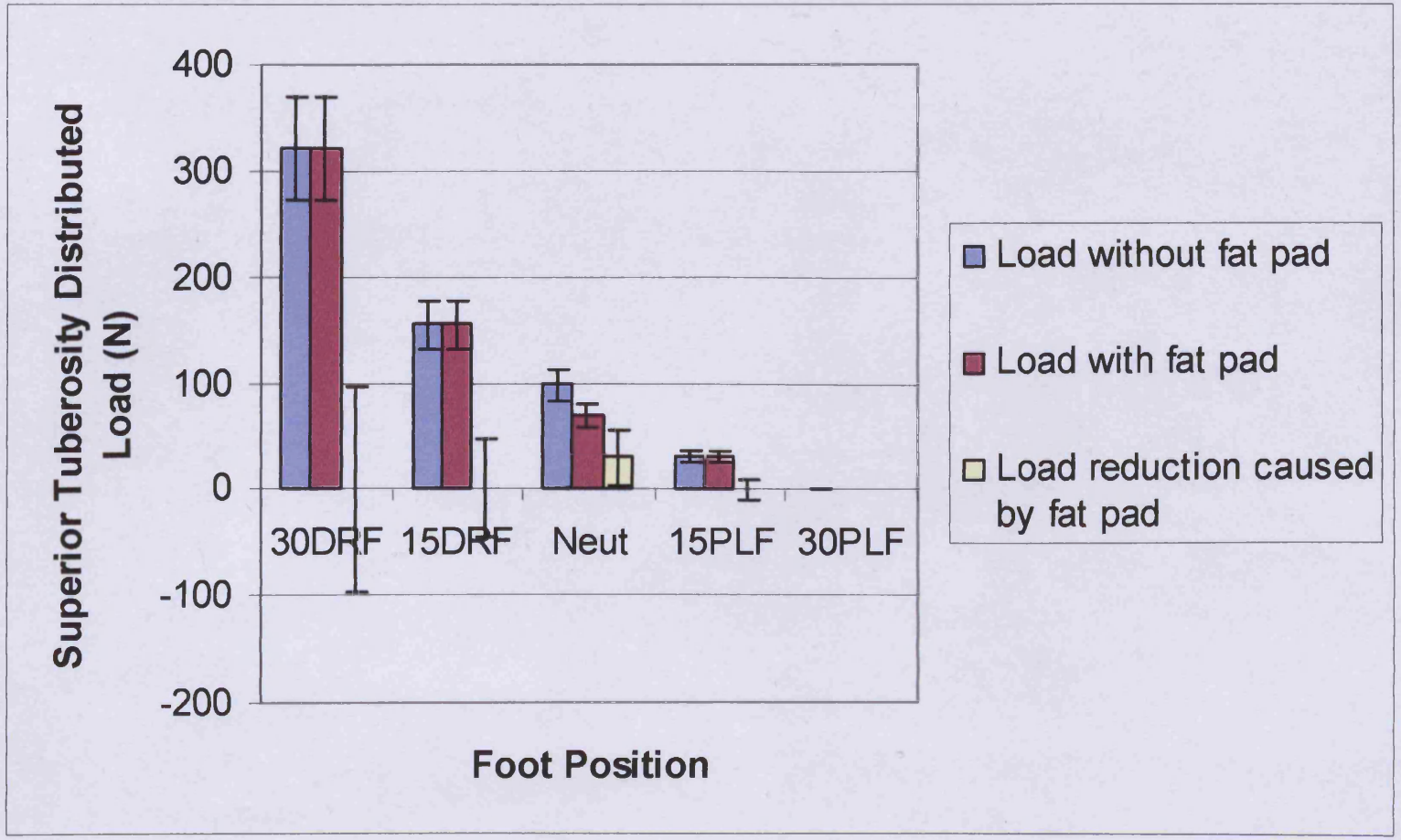

Figure 5.3.11: Comparison of the effect of bovine fat pad on the distributed load on Profile 3. Error bars for measured load = ± 15%. Error bars for pressure reduction = maximum and minimum possible error following calculation.

5.4 Discussion

Through the use of dynamic ultrasound, differences in the 3 distinct regions of Kager's fat pad have been identified.

When the subject was in the prone position and the Achilles tendon unloaded, plantarflexion of the foot caused the BPW to move into the retrocalcaneal bursa. This movement halved the distance between the BPW and the enthesis in comparison to its position at dorsiflexion. When the subject was standing and the Achilles tendon was loaded, the BPW protruded even further into the retrocalcaneal bursa. This suggests that BPW movement may be gravity-controlled.

Examination of the US movie files showed that BPW movement may be as a consequence of the retrocalcaneal bursa moving nearer to the BPW on ankle flexion, rather than the BPW actively moving in to the bursa. Movement of the retrocalcaneal bursa occurred as a consequence of the antero-superior rotation of the calcaneus on plantarflexion. The rotation of the calcaneus also lifted Kager's fat pad, causing a change in the shape of Kager's triangle on plantarflexion. Fat pad deformation is likely to cause the transformation of the paratenon boundary from an inverted-J to the L-shape. On being lifted, Kager's fat pad contacts both the hard posterior surface of the tibia and the rigid, contracted FHL muscle belly. Thus, all the borders of Kager's fat pad are, with the exception of the Achilles tendon, solid, meaning any movement must be either posteriorly, or in forcing the BPW in to the retrocalcaneal bursa. On loading the Achilles tendon, this too becomes a rigid boundary. Thus, the BPW is the only remaining mobile aspect, which explains the increased distal movement observed during loading.

The BPW movement also appears to be influenced by flexor hallucis longus contraction. On FHL contraction, the FHL-associated fat pad appears to be squeezed distally. As the FHL-associated fat pad and BPW are linked by the former tunnelling under the Achilles tendon-associated fat pad, the BPW is forced in to the retrocalcaneal bursa. Such reliance upon FHL contraction may explain the characteristic distal prominence of the muscle belly in comparison to the tendinous

appearance of the neighbouring flexor digitorum longus and tibialis posterior **[1]**. The efficiency of the FHL-associated fat pad movement again appears to be increased by its surrounding structures. Forming the anterior boundary of the FHL-associated fat pad, the talus opposes movement anteriorly, whilst the FHL tendon sheath is likely to resist FHL-associated fat pad movement in a medial, lateral and posterior direction. With the FHL muscle belly opposing proximal movement, the FHL-associated fat pad can only move in a distal direction, consequently forcing the BPW in to the retrocalcaneal bursa.

The BPW may also be sucked in to the retrocalcaneal bursa. With the insertional angle increasing on plantarflexion, an increase in volume of the retrocalcaneal bursa is expected. It is likely that, in engulfing the posterior surface of the calcaneus, the deep fascia and paratenon of the Achilles tendon form an air-tight seal around the bursa. Thus, it is hypothesised that Kager's fat pad is sucked in to the bursa to equalise the pressure. This is in accordance with the previous speculation that Kager's fat pad may act as a 'variable plunger' **[152]**. Equally, as the pressure increases on returning the foot to the neutral position, the BPW is expelled from the retrocalcaneal bursa.

The lubrication between the BPW and the calcaneus was examined experimentally using a specially fabricated apparatus and a fresh bovine fat pad. First, however, validation of this apparatus was necessary. This was achieved by comparing the results of Apparatus 1 (Figure 5.3.4) with those previously published (Figure 5.4.1). Whilst the results of both Cooke **[183, 189]** and Apparatus 1 were - when compared to the Stribeck Curve (Figure 5.2.5), indicative of the fluid film lubrication regime, it was clear that the coefficient of friction measured using Apparatus 1 was approximately 1 order of magnitude greater. Additionally, whilst the results of Cooke et al. **[183, 189]** fall within the range typical of fluid film lubrication **[196]**, the coefficient of friction determined using Apparatus 1 - from 0.1–1 – was again an order of magnitude greater. Thus it was concluded that the apparatus influenced the level of friction measured.

A distinct division within the results was evident in Figure 5.3.4. This was likely to be caused by the different testing conditions produced when the specimen position was moved further away from the pivot to increase the sliding speed. The decreased

coefficient of friction corresponded to a fresh application of synovial fluid upon changing the specimen position, thus significantly lower levels of friction were recorded. It was noted that this was an inappropriate method by which to replenish the supply of synovial fluid, and thus the protocol was changed to avoid recurrence of this problem.

So, whilst the correct lubrication regime was identified using this apparatus, it was determined that the levels of friction within the system significantly influenced the coefficient of friction measured. Thus, a number of modifications were made to the Apparatus (as detailed in 5.2, Materials and Methods) in order to minimise the inherent friction. These modifications resulted in the fabrication of Apparatus 2.

Apparatus 2 (Figure 5.3.5) was successfully validated against both the results of Cooke **[183, 189]** (Figure 5.4.1) and the known coefficient of friction values **[196]**. The friction within the system was significantly reduced partly by over-engineering the apparatus. By avoiding component bending and torsion within the apparatus, the angle of the specimen relative to the counterface is likely to have remained consistent, thus avoiding the breakdown of the fluid-film layer. Care was also taken to reduce the friction within the ball bearing, and to ensure that the disc remained covered with a uniform layer of synovial fluid.

Following successful validation, Apparatus 2 was used to approximate the lubrication regime between Kager's fat pad and the calcaneus. Bovine fat pad was tested against both PMMA and glass, replicating the *in vivo* conjuncture. The relationship of the coefficient of friction and the reduced Sommerfeld number was plotted (Figure 5.3.6 & 5.3.7). The positive trend-line gradient of these Figures is, on comparison with the Stribeck curve (Figure 5.2.2), representative of fluid film lubrication. The coefficient of friction of 0.01 is further confirmation of this lubrication regime. As similar results were achieved when using both the glass and PMMA surfaces, it can be assumed that the fluid film regime predominated. Generated due to an increase in pressure, this lubrication regime means that the two surfaces are completely separated, thus avoiding adhesive and abrasive wear. Consequently, surface degeneration of the periosteal fibrocartilage as Kager's fat pad continually slides over it on ankle flexion is presumably decreased, thus probably reducing inflammation and injury.

There was also evidence of mixed lubrication at the fat pad conjuncture, in particular with the PMMA surface (Figure 5.3.6). Here, the bath tub curve indicates a transition from fluid film to mixed lubrication, as the fluid film layer breaks down at lower speeds or higher loads (i.e. a low Sommerfeld number). This deterioration was encouraged with the PMMA counterface, as this surface is rougher than glass (Table 5.3.5). A similar break-down of the layer would be expected to occur in vivo when the sliding speed tends towards zero. This has previously been reported in synovial joints **[161, 197-200]**, where the surface roughness (1-6μm **[201]**) is more comparable to PMMA than glass. As no data regarding the periosteal fibrocartilage roughness could be collected due to concerns of equipment contamination, however, such occurrences in the Achilles tendon enthesis organ can only be speculated. Such a change of lubrication regime would cause an increase in friction, however, and thus probably wear.

The specimen is likely to experience degeneration over the course of the experiment, due both to dehydration and wearing. Thus, it is likely that this affected the lubrication regime, encouraging mixed lubrication. Whilst a new fat pad specimen was used for the glass and then PMMA counterface, no further replacements were possible due to a limited supply. The leakage and evaporation of synovial fluid would also have increased the coefficient of friction between the specimen and the disc. A brush was used to ensure an even distribution of the fluid over the disc, whilst additional fluid was added as appropriate. However, a limited supply of synovial fluid did mean the quantity administered was restricted. Attempts were made to minimise the effect of this degeneration on the hypothesised lubrication regime by alternating tests between small and then large Sommerfeld numbers. Thus, both extremes of the hypothesised Stribeck curve would be affected.

The viscosity of the synovial fluid could also have affected the lubrication regime, as it is a parameter included in the Sommerfeld number. However, due to the problems of measuring the viscosity of synovial fluid due to shear thinning **[183, 189]**, the reduced Sommerfeld number was instead adopted. The laboratory temperature was, however, kept at approximately 18°C to ensure the synovial fluid viscosity was consistent throughout the entire study. Unfortunately it was not possible to perform

the experiments at a temperature closer to body temperature, and thus more accurately replicate the in vivo temperature. This was due to restrictions of the laboratory suitable for such experiments. Employing a stand-alone heater was considered, although a lack of control, and thus consistency, of the room temperature meant this was not viable.

Whilst fluid film lubrication has been identified, the obvious simplifications mean that the experiment is clearly limited, and thus caution should be exercised when extrapolating these results to the human environment. The approximation of glass and PMMA to periosteal fibrocartilage (the articulating tissue covering the calcaneus) is clearly crude, and has never been reported. However, these surfaces have been approximated to the articular cartilage of the synovial joint **[183, 189]**, although the similarity in roughness between these 2 soft tissues is unknown. However, it is likely that the formation of fluid film lubrication is likely to have been encouraged by the flatter profile of the discs in comparison to that of the in-vivo bone geometry. Equally, it should be remember that this mode of lubrication could have developed due to differences in fat pad characteristics rather than the change in the counterface alone **[189]**.

The mechanical influence of Kager's fat pad within the Achilles tendon enthesis organ was examined using the mechanical model detailed in Chapter 3. The 4 different superior tuberosity profiles fabricated earlier were again used to represent the range of superior tuberosity shape observed histologically. A fresh bovine flexor tendon was attached to the model by a wedge grip, whilst the proximal end was attached to a tensometric tensile testing machine. A fresh bovine fat pad was positioned between the tendon and bone, in an *in vivo* position as verified against ultrasound images.

Of the 4 profiles fabricated, the effect of the bovine fat pad was only examined on Profiles 2 and 3. The other 2 profiles were excluded from the study in order to preserve the soft tissue. The shape of Profile 1 (representative of a superior tuberosity post-Haglund's correction) was such that there was sufficient space between the tendon and bone for the fat pad to deform to such an extent so as not to resist the tendon. Profile 4 was such that the fat pad was also ineffective, with it posteriorly

displacing the tendon to such an extent that it bypassed the fat pad in all positions of ankle flexion.

The fat pad was influential on the pressure borne by the superior tuberosity of Profiles 2 & 3. Contact between the fat pad and tendon whilst the foot was in the neutral position caused a 30% reduction in pressure on the superior tuberosity surface of Profile 2. This equated to a 39% reduction in loading. When this Profile was dorsiflexed, however, the fat did not fit between the tendon and bone and thus there was not a reduction in pressure on the superior tuberosity. On plantarflexion, the tendon did not pressurise the superior tuberosity, but the latter structure did appear to avoid the former bending. The fat pad caused a 15% pressure reduction in the neutral and 15°PLF position when using Profile 3. This equated to a 30% reduction in load in the neutral position. Due to the contact area, however, there was not a reduction in loading at 15°PLF. Again, on dorsiflexion the fat pad did not fit between the two structures, as observed *in vivo*.

The insertional angle between the tendon and bone increased when plantarflexed, with the threaded rod accurately mimicking the restriction of bow-stringing as achieved by the deep fascia and paratenon *in vivo*. Whilst not load bearing during plantarflexion, however, it did appear that the fat pad was acting to resist excessive bending of the slack tendon. This could be important, as it would appear to avoid the collagen fibres in the tendon midsection bending excessively, an action that may increase the vulnerability of this region.

Whilst the peak reduction in loading on the superior tuberosity as a consequence of the fat pad (39%) was similar to that by the knee menisci (40 – 60%) **[179, 192, 202]**, overall the reduction in loading at the ankle joint is less than the knee joint. This was expected as fibrosis (which develops to resist external loading **[28, 165-168]**) is only evident in the distal tip of Kager's fat pad, which is in contrast to the predominantly fibrous knee meniscus **[25, 26, 203, 204]**. Similarly, Kager's pad has less fibrosis than the calcaneal fat pad, which is thought to bear 70% of the body weight **[175]** on heel strike.

These results are indicative of Kager's fat pad reducing the pressure and load in some instances on the superior tuberosity, and thus probably protecting the surfaces of both the calcaneus and the Achilles tendon when under compression. Ideally human Kager's fat pad would have been used for the experiments, as it is likely that the material properties of the bovine tissue differ in comparison. Perhaps more importantly, the shape of the bovine fat pad was not akin to Kager's fat pad. Whilst Kager's fat pad includes a specialised mobile wedge, the bovine fat pad was simply a mass of fatty tissue that lacked shape. Thus, whilst the BPW of Kager's fat pad can fit between the tendon and bone even at small angles of insertion, the bovine fat pad could not. Therefore, whilst the bulk of the bovine fat pad was positioned correctly when compared to the ultrasound, the position of the BPW was not replicated despite attempts to cut the fat pad into shape. This is likely to explain why, where contact was expected, it was not observed.

The accuracy of the results was influenced by the use of the pressure sensitive paper. This has a quoted manufacturer accuracy of ±15%. Additionally, the method of measuring the pressure recorded was also subject to error, as it relied upon comparison of the colour of the film to a calibration scale. However, this technique was still regarded as the most accurate and practical solution possible, having also considered the use of photoelastic film and springs. Modelling this setup computationally was also excluded due to the lack of material data on the Achilles tendon enthesis organ components, and the complexity of modelling the movement of Kager's fat pad in particular.

The temperature and humidity (28°C; 75% humidity) within the laboratory were factored into the calibration scale for the pressure sensitive paper. The conditions are likely, however, to affect the properties of the tendon, the synovial fluid and the fat pad. Whilst the conditions were stable throughout the experiment, it is inevitable that the soft tissues would have dried out, and a quantity of the synovial fluid evaporated. This was recognised and actions were taken to try to minimise the subsequent problems. Unfortunately the sample size could not be increased due to a lack of tissue, and thus the results are not statistically significant

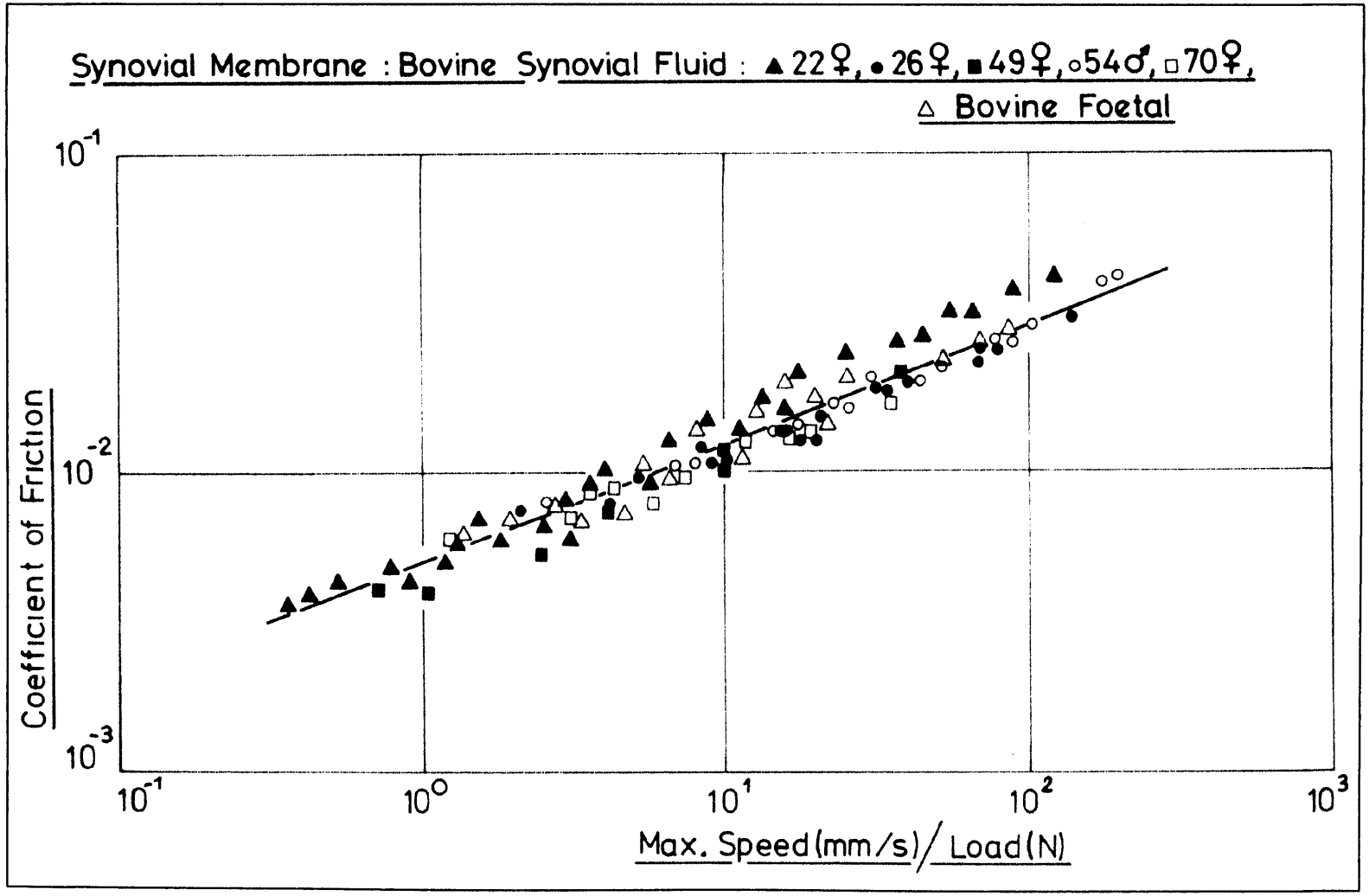

Figure 5.4.1: The results of Cooke et al. **[183, 189]** describing the lubrication of bovine synovial membrane. This result was used as validation of the new apparatus.

5.5 Conclusions

The following conclusions can be drawn from the work in this chapter:

1. Three mechanisms were hypothesised as being responsible for the movement of Kager's fat pad, and in particular the bursal-protruding wedge: the FHL-associated fat pad pushing the BPW into the retrocalcaneal bursa on plantarflexion; the BPW moving to equalise a change in the retrocalcaneal bursa pressure caused by ankle flexion; passive movement of the BPW as the retrocalcaneal bursa moves towards it on ankle flexion.

2. In contrast to previous reports, Kager's fat pad did not appear to increase the length of the Achilles tendon lever arm.

3. Movement of the BPW in to the retrocalcaneal bursa to equalise the pressure may act to avoid synovial fluid degeneration.

4. The movement of the BPW into the retrocalcaneal bursa appears to generate fluid-film lubrication. Thus, the conjoining surfaces of Kager's fat pad and the calcaneus are likely to be protected by a layer of lubricating fluid, probably synovial fluid.

5. The fat pad can reduce the pressure and load on the superior tuberosity by approximately one-third. This reduction is dependant on the superior tuberosity size and the foot position, and also relies upon the BPW fitting between the superior tuberosity and the Achilles tendon.

6, General Discussion

6.1 General Discussion

Whilst the previously reported mechanical advantage of Kager's fat pad **[109, 144, 152]** was not observed, the tissue was seen to resist the Achilles tendon – and thus prevent collagen fibre-bending - when in unloaded plantarflexion. The fat pad appeared to support congruency of the adjoining tendon and bone in a manner similar to the knee meniscus **[205]**. The knee meniscus ensures congruency between the tibial plateau and femoral condyles and, like Kager's fat pad, has been described as a 'space filler' **[205]**. Whilst the exact stabilising role of neither the knee meniscus **[177]** nor Kager's fat pad has yet been established, both are held in place by a series of fibrous anchors.

Excessive bending of the Achilles tendon at the enthesis is avoided by the deep fascia/paratenon connecting to the calcaneus. In loaded plantarflexion, the Achilles tendon would be expected to take the shortest possible route between the muscle and bone on application of a contractile force. However, the deep fascia/paratenon restricts this 'bow-stringing' (Figure 6.1.1), effectively controlling the Achilles tendon insertional angle. In directing the route of the tendon, the deep fascia/paratenon could be considered to be acting as a pulley - in addition to the superior tuberosity and enthesial fibrocartilage **[31]**. Hence, care should be given to avoid weakening the deep fascia/paratenon when surgically managing hind foot disorders. Where the deep fascia/paratenon is involved during surgical procedures such as Achilles tendon reattachment, efforts should be made to ensure that it is appropriately re-established prior to closing of the wound, and thus to allow the continuation of its function post-operatively.

Equally, removal of the superior tuberosity may increase the likelihood of enthesis injury due to the promotion of collagen fibre bending. Whilst superior tuberosity excision is not likely to increase significantly the shear stress and thus risk of enthesis failure, interestingly the bony spurs (enthesophytes) previously reported in the distal part of the enthesis have been hypothesised to increase the area of attachment **[206]**, and thus presumably increase the ultimate tensile strength. The relationship between these enthesophytes and the superior tuberosity prominence does, however, need

further investigation across a greater number of specimens. A detailed computational examination would also provide data on the likely areas of maximum tension within the enthesis. By changing a number of parameters such as the direction of loading and the superior tuberosity prominence, correlation could be sought with the presentation of enthesophytes cadaverically. However, before theoretical models of sufficient accuracy can be developed, the properties of the tissues of the Achilles tendon enthesis organ need to be determined.

The action of the pulleys identified within the Achilles tendon enthesis organ may increase the strain on the tendon by increasing the tensile force. Should this occur, the work done by the muscles to cause this extension is stored as energy within the tendon **[207]**, due to the tendons elasticity **[65]**. This energy is then released on removal of the contractile force, thereby reducing the energy that would otherwise be necessary for the desired skeletal movement **[207]**. Animals are also known to exploit these elastic properties, increasing their jumping ability due to the elastic recoil of a tendon being much faster than that of a muscle **[207]**. Therefore, in increasing the strain on the Achilles tendon, a large superior tuberosity is likely to improve efficiency.

In addition to the biomechanical role of the superior tuberosity, the role of Kager's fat pad was also examined. An extension of the deep fascia/paratenon and a synovial membrane invagination appear to be responsible for creating three functionally different regions within Kager's fat pad. The regions, based upon their location, have been termed:

- The bursal protruding wedge (BPW)
- The FHL-associated fat pad
- The Achilles tendon associated fat pad

The ability of the BPW to move independently from the remaining bulk of Kager's fat pad is probably due to the synovial invagination. Where a large superior tuberosity - and thus a small Achilles tendon insertional angle - were present, a synovial invagination was obvious. This possibly aided the BPW to extend and thus slide around the superior tuberosity and into the retrocalcaneal bursa. Where the superior

tuberosity was less prominent, BPW movement was relatively limited as it comfortably reached the most distal point within the bursa. In such instances, a synovial invagination was not evident. Thus, it appears that the synovial invagination is crucial in allowing BPW movement, and subsequently influences the biomechanics of the Achilles tendon enthesis organ, although a more thorough study is necessary.

Three mechanisms have been hypothesised as being responsible for the movement of the BPW in to the retrocalcaneal bursa. BPW movement may be solely or partly caused by the antero-superior rotation of the calcaneus, by being sucked into the bursa to equalise pressure, or by being pushing by the FHL-associated fat. As FHL contraction increases BPW movement, injury to the former may inhibit BPW movement and thus may be a previously unconsidered cause of posteromedial heel pain **[208]**. Such examples may include the accumulation of fluid around the tendon of FHL **[209-211]**, or the reported FHL-entrapment associated with an enlarged os trigonum **[149, 209]**. BPW movement may be further inhibited by injuries to the FHL tendon caused at plantarflexion, such as those that occur in ballet dancers en pointe, in soccer players (ball-kicking results in forced plantarflexion), or in athletes engaged in downhill running **[149, 209]**.

It appeared that the wedge-shape of the BPW was potentially crucial to its biomechanical role, as it allowed the structure to move between the Achilles tendon and calcaneus even when the insertional angle was negligible. However, it was not possible to mimic this geometry when mechanically modelling the enthesis organ, and thus BPW movement was restricted. This meant that the BPW affected only 2 angles of ankle flexion (neutral position; 15 degrees PLF). However, the reduction of superior tuberosity pressure was dependant on both its size and the position of the BPW, with pressure reductions in some instances as significant as 30%.

The compressive load on the surface of the superior tuberosity was derived by considering the area of contact. The largest superior tuberosity, Profile 4, experienced a compressive load of 100% the magnitude of the Achilles tendon tensile load when in dorsiflexion. This was 8-fold greater than the smallest tuberosity when in an identical loading environment. This data was, in tandem with other results (Figures 5.3.6 & 5.3.7), used to further interrogate the lubrication regime *in vivo* between the

fat pad and the calcaneus, although the two experimental environments differed (i.e. the Stribeck curve relies upon a speed to generate a lubrication regime, whereas the mechanical model statistically measured force statically).

When calculating the reduced Sommerfeld number for the apparent in vivo conditions (compressive load ranging between 0-300N; sliding speed 0-15mm/s), it is evident that the minimum Sommerfeld number achieved experimental typically exceeded this. However, when considering the conjoining surface most similar to in vivo conditions (i.e. articular cartilage) (PMMA, Figure 5.3.6), it would appear from the rising trend of data at a low Sommerfeld number that the regime is likely to be mixed lubrication during the majority of the gait cycle. Whilst this regime is expected to degenerate further where the speed tends toward zero and/or the load increases (i.e. plantarflexion, dorsiflexion), where the load tends towards zero (i.e. plantarflexion), it appears possible for fluid-film lubrication to develop. Thus, it would suggest that the conjunction is lubricated partially by fluid-film at plantarflexion during the gait cycle, though this is likely to break down during load bearing. The effect of this break-down is likely to be minimised, however, as hyaluronic acid (HA) within synovial fluid acts as a wetting agent, and thus a dry contact is likely to be avoided (i.e. boundary lubrication will occur).

The generation of a temporary fluid film layer of lubricant on the protrusion of the BPW into the retrocalcaneal bursa is likely to minimise the risk of degradation of the conjoining tissues during contact **[201, 212]**. By potentially spreading the synovial fluid held within the bursa, the role of the BPW would be analogous to that of the knee meniscus **[29]**. Here, a 20% increase in friction reported following meniscectomy **[29]**.

The biomechanics of the Achilles tendon enthesis organ is also influenced by the physiology of the fat pad. In particular, the synovial membrane evident covering the BPW is likely to be important in the production of synovial fluid. Thus, excision of the BPW during arthroscopy is likely to inhibit the supply of synovial fluid to the Achilles tendon enthesis organ. The importance of synovial fluid – and in particular HA - is appreciated when considering the pain relief from osteoarthritis following its injection in to the synovial cavity **[213, 214]**. Thus, supply of synovial fluid from the

membrane appears important. It should also be noted that following total hip replacement the concentration of HA in synovial fluid reduces **[215, 216]**. Thus, the biotriobology of the Achilles tendon enthesis organ may be affected by removing components other than just Kager's fat pad. BPW excision may also cause degeneration of the synovial fluid, by inducing conditions such as synovial ischaemia and hypoxia **[217]** if the hypothesised retrocalcaneal pressure change can not be equalised.

The viscosity of the synovial fluid is also known to influence the rheological characteristics at the conjuncture **[201, 212]**. A reduction in viscosity is, in line with the Sommerfeld number, likely to increase the coefficient of friction. A reduction in viscosity may be caused either by inflammation or **[218, 219]** an increase in temperature (as seen in bovine serum) **[160]**. Such a reduction in viscosity has been reported to increase the likelihood of fissures on the surface of articular cartilage **[219]**, which may be a precursor to inflammation and thus injury **[174]**. Wear may also be responsible for the degeneration of the periosteal and sesamoidal fibrocartilages reported by Rufai et al **[32]** which, the authors suggest, may be a cause of retrocalcaneal bursitis. Thus, it follows that as a consequence of poorer lubrication, larger tuberosities may be prone to an increased prevalence of retrocalcaneal bursitis, and possibly other hindfoot disorders such as Haglund's disease.

Presuming that the same lubrication regime was present at the fat pad-tendon conjunction, it would appear possible that all the surfaces within the Achilles tendon enthesis organ could at least temporarily be coated with synovial fluid at some instance during the gait cycle. This has additional benefits alongside minimising the friction as it also protects against enzymic digestion, aids osmosis between the joint and the blood supply, and provides the cartilage with nutrition **[29]**. Thus, the lubrication regime and so the BPW appears crucial in performing a number of functions.

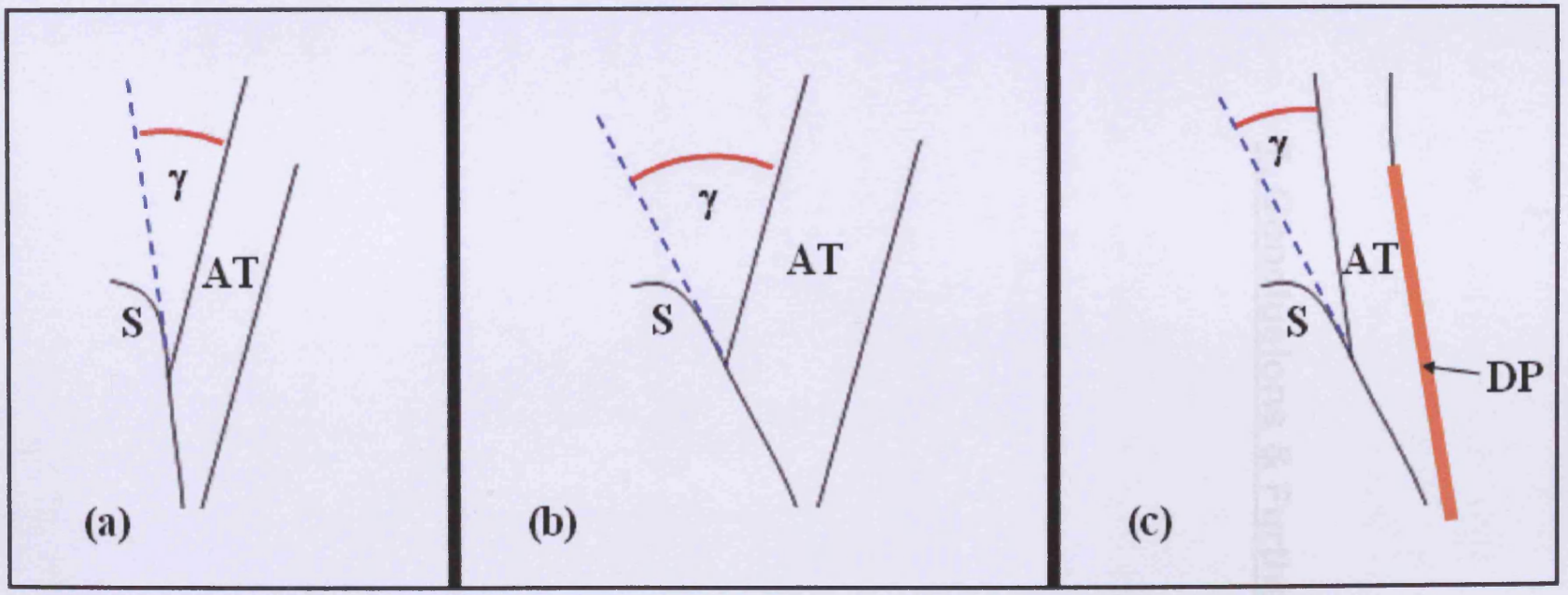

Figure 6.1.1: Schematic representation of how the deep fascia/paratenon (DP) maintains a consistent insertional angle (γ) between the Achilles tendon (AT) and the superior tuberosity (S). (a) A schematic representation of the foot in the neutral position (b) With the foot in plantarflexion, the insertinoal angle increases without the deep fascia/paratenon (c) The deep fascia/paratenon ensures the insertional angle remains consistent.

7, Conclusions & Further Work

7.1 Conclusions

The work in this thesis has investigated the biomechanics of a number of components of the enthesis organ. The influence of these factors upon the Achilles tendon enthesis organ has then been discussed. The conclusive points drawn are listed below.

- A method of microscopic examination of the superior tuberosity has been devised that would appear to allow for reproducible quantification of its size.

- Whilst the superior tuberosity was seen to mechanically advantage the Achilles tendon by increasing the lever arm, calcaneal resection to cure Haglund's disease causes only a negligible increase in the enthesis shear stress.

- Both the superior tuberosity and the deep fascia/paratenon are important structures in controlling the angle at which the Achilles tendon attaches to the calcaneus.

- The load exerted on to the surface of the superior tuberosity was found to depend upon both the foot position and the tuberosity size. The equal and opposite reaction expected upon the Achilles tendon may influence the rate of surface degeneration. This load is reduced, however, in instances where Kager's fat pad is between the two structures, and thus may reduce the wearing of the surfaces at the conjunction.

- Microscopic examination of Kager's fat pad identified a number of features that appear to promote independence of 3 separate regions. The most specialised region, the bursal-protruding wedge, was seen moving into and out of the retrocalcaneal bursa on ankle flexion.

- BPW movement is possibly controlled by 3 mechanisms, and thus restriction of any of these may be an indirect cause of hindfoot pain.

- The BPW may move into the retrocalcaneal bursa to avoid a change in pressure which may otherwise cause synovial fluid degradation and thus an increased rate of wear.

- The synovial membrane covering this wedge is likely to be a significant and important source of the synovial fluid within the retrocalcaneal bursa.

- Protecting the Achilles tendon enthesis organ, the movement of the BPW may act to generate a lubrication regime of which the exact specifications are likely to depend upon the superior tuberosity size.

- Lubrication regime breakdown is likely on dorsiflexion, creating boundary lubrication, which potentially influences the rate of wear and thus degeneration of the surfaces at the conjunction.

- Kager's fat pad may also aid in the rehabilitation of the Achilles tendon, appearing to protect the blood flow through vessels bridging the interface that was evident at Achilles tendonitis.

Thus, in performing the first examination of the biomechanics of the Achilles tendon enthesis organ, this work has identified the importance of, in particular, Kager's fat pad. It would appear that, like the knee meniscus previously, excision of this tissue may be ill-advised, denying the Achilles tendon enthesis organ biomechanical functions that this variable space filler was not previously considered performing. Further work is necessary, however, to develop these hypotheses.

7.2 Further Work

The aim of the work presented in this thesis was to provide an overview of the biomechanics of the Achilles tendon enthesis organ. In achieving this aim, a number of aspects have been identified that would benefit from further development.

7.2.1 Superior Tuberosity Biomechanics:

7.2.1.1 Superior Tuberosity Quantification:

A new method of quantifying the superior tuberosity size was devised in this thesis due to the poor results reported with the existing methods. A microscopic technique allows for an image of higher resolution to be used when examining the tuberosity, and thus possibly increasing the accuracy of the measurement. Importantly in this work, however, whilst this method appeared successful it was only validated against other novel methods, as no 'gold standard' exists. Thus, an additional cadaveric study is required to more thoroughly investigate the reliability and accuracy of this method. Once this has achieved statistical accuracy, the method should be used on macroscopic images as used in clinical practice. If this successfully evaluates the superior tuberosity macroscopically, cases of Haglund's disease should be examined. Should the method still be achieving success, use in a clinical environment may then be considered. Clearly, however, this requires significant time and development, and possibly a number of minor modifications.

7.2.1.2 Achilles Tendon Injury:

Whilst the mechanical model in this thesis recognised that the superior tuberosity size caused a significant variation in the compressive load recorded at the contact with the Achilles tendon, a more accurate representation of the in vivo environment is required to investigate the physiological effects.

Initially, a more sophisticated model is required to further investigate the areas of stress and strain in both the superior tuberosity and Achilles tendon. This is probably best achieved by the development of a computational model, as this will allow for accurate geometry and material property data. Whilst the initial geometrically-

accurate two-dimensional model produced during this study provides an ideal starting position, the incomplete nature of the material property data describing the tissues in the enthesis organ would delay such a study. Validation of the eventual results can be performed by fabrication of a mechanical model similar to that used in this work.

In parallel with a computational evaluation of the enthesis organ, the effect of loading on the contacting surfaces also needs to be developed. Currently only 1 publication has examined the histopathology of the Achilles tendon insertional region **[32]**, and this did not consider the effect of mechanical loading. Such a study would be important in determining the effect of any increase in stress or strain on the contacting surfaces.

7.2.1.3 Surgical Correction of Haglund's Disease:

The effect on the strength of the enthesis following resection of the superior tuberosity needs to be examined. As identified in this work, the superior tuberosity is influential in controlling the insertional angle of the tendon, and thus the angle of principle load. Whilst the removal of the superior tuberosity will undoubtedly change this angle, the consequences of this both directly on the strength of the union, and indirectly on the bending on the collagen fibres, needs to be examined. Again, this is probably most accurately achieved computationally, as described above.

7.2.2 Kager's Fat Pad Biomechanics:

7.2.2.1 Size & Movement:

Whilst it appeared that the size and movement of Kager's fat pad was dependant on the size of the superior tuberosity, the sample size used in this study was too small to statistically confirm these observations. A more detailed study to statistically confirm these observations would be beneficial. Equally, identification of the parameters that affect both the size and movement of the fat pad is necessary to allow roles such as the load bearing of the tissue to be better understood. Matching this data to hind foot pain may provide a useful relationship by which to identify such disorders.

7.2.2.2 Lubrication:

Whilst the lubrication regime between the fat pad and the calcaneus is likely to be important in determining the rate of wear on the conjoining surfaces, no previous studies have examined the effect of repeated sliding over a fibrocartilage surface. Such a study would be beneficial in determining the importance of maintaining the fluid-film layer that was predicted in this work.

Similar to the Achilles tendon-calcaneus conjuncture, the iliotibial band and lateral epicondyle condyle conjuncture is frequently a site of overuse injury (iliotibial band syndrome). Thus, examining the lubrication regime of tendon against bone/fibrocartilage may allow for the development of methods by which to prevent microsawing and thus overuse injuries. The effect of the tendon being loaded should also be examined, as proteoglycan exudation may be an important lubrication process.

Whilst the reduced Sommerfeld number was used in this work, the importance of temperature in affecting the lubrication regime has previously been overlooked. Whilst a temperature increase in the ankle joint is highly likely during exercise, the extent to which the lubrication regime degenerates is unclear, but may influence the prevalence of Achilles tendon overuse injuries reported. Thus, this study should be repeated incorporating a method by which to control the ambient temperature.

7.2.2.3 Load Bearing:

The significance of the reduction in load bearing discussed in this work is ultimately dependant upon the effect this has on the bearing surfaces. Should greater pathology be observed on higher load bearing, then clearly the retention of Kager's fat pad should be considered. Further investigation is required in to the effect of Kager's fat pad on the loading at the conjuncture, however, as this study relied upon an apparatus with a number of simplifications. This is probably best modelled computationally, although the same restrictions as discussed above (section 7.2.2.1) will apply to such a model.

7.2.3 The Rehabilitative Role of Kager's Fat Pad:

Kager's fat pad was observed as having an increased blood supply during Achilles tendon inflammation, which may serve to transfer nutrients and thereby encourage regeneration. These vessels are, however, currently severed when surgically reducing Achilles tendon inflammation (a procedure termed tendon stripping) **[45]**. Whilst, unsurprisingly, the inflammation reduces, it is possible that the tendon is weakened by encouraging avascularity **[21, 38, 39, 42, 44, 46, 59]**. Investigation is necessary to determine the extent, if any, of such weakening.

7.2.4 The Paratenon and Deep Fascia:

The work in this study has hypothesised the importance of the paratenon and deep fascia in controlling the angle of Achilles tendon insertion on plantarflexion. Further study in to the variation in shape and size of these tissues is necessary to determine whether this may be a previously unconsidered cause of posterior heel pain.

8, References

1 Standring, S. *Gray's Anatomy: the Anatomical Basis of Clinical Practice*. 2005, Edinburgh: Elsevier/Churchill Livingstone.

2 Kulund, D. N. *The Athlete Injuries*. 1988, Philadelphia: JB Lippincott.

3 Benjamin, M. and McGonagle, D. The anatomical basis for disease localisation in seronegative spondyloarthropathy at entheses and related sites. *J Anat*, 2001, **199** (Pt 5), 503-526.

4 Benjamin, M., Kumai, T., Milz, S., et al. The skeletal attachment of tendons--tendon "entheses". *Comp Biochem Physiol A Mol Integr Physiol*, 2002, **133** (4), 931-945.

5 Benjamin, M., Moriggl, B., Brenner, E., et al. The "enthesis organ" concept: why enthesopathies may not present as focal insertional disorders. *Arthritis Rheum*, 2004, **50** (10), 3306-3313.

6 Benjamin, M., Redman, S., Milz, S., et al. Adipose tissue at entheses: the rheumatological implications of its distribution. A potential site of pain and stress dissipation? *Ann Rheum Dis*, 2004, **63** (12), 1549-1555.

7 Benjamin, M., Toumi, H., Ralphs, J. R., et al. Where tendons and ligaments meet bone: attachment sites ('entheses') in relation to exercise and/or mechanical load. *J Anat*, 2006, **208** (4), 471-490.

8 de Palma, L., Marinelli, M., Meme, L., et al. Immunohistochemistry of the enthesis organ of the human Achilles tendon. *Foot Ankle Int*, 2004, **25** (6), 414-418.

9 Moriggl, B., Kumai, T., Milz, S., et al. The structure and histopathology of the "enthesis organ" at the navicular insertion of the tendon of tibialis posterior. *J Rheumatol*, 2003, **30** (3), 508-517.

10 Ritchlin, C. T. Pathogenesis of psoriatic arthritis. *Curr Opin Rheumatol*, 2005, **17** (4), 406-412.

11 Robson, M. D., Benjamin, M., Gishen, P., et al. Magnetic resonance imaging of the Achilles tendon using ultrashort TE (UTE) pulse sequences. *Clin Radiol*, 2004, **59** (8), 727-735.

12 Tan, A. L., Toumi, H., Benjamin, M., et al. Combined high-resolution magnetic resonance imaging and histology to explore the role of ligaments and tendons in the phenotypic expression of early hand osteoarthritis. *Ann Rheum Dis*, 2006,

13 Baeten, D., Kruithof, E., De Rycke, L., et al. Diagnostic classification of spondylarthropathy and rheumatoid arthritis by synovial histopathology: a prospective study in 154 consecutive patients. *Arthritis Rheum*, 2004, **50** (9), 2931-2941.

14 Wren, T. A., Yerby, S. A., Beaupre, G. S., et al. Mechanical properties of the human Achilles tendon. *Clin Biomech (Bristol, Avon)*, 2001, **16** (3), 245-251.

15 Byers, G. E., 3rd and Berquist, T. H. Radiology of sports-related injuries. *Curr Probl Diagn Radiol*, 1996, **25** (1), 1-49.

16 Best, T. M. and Garrett, W. E. Basic Science of soft tissue: Muscle and tendon. 1994, In *Orthopaedic Sports Medicine* (Ed. J. C. DeLee and D. Drez), Philadelphia: WB Saunders.1-45

17 Safran, M. R., Garrett, W. E., Jr., Seaber, A. V., et al. The role of warm-up in muscular injury prevention. *Am J Sports Med*, 1988, **16**, 123-129.

18 Lin, R., Chang, G. and Chang, L. Biomechanical properties of muscle-tendon unit under high-speed passive stretch. *Clin Biomech (Bristol, Avon)*, 1999, **14** (6), 412-417.

19 Haglund, P. Beitrag zur klinik der Achillessehne. *Z Orthop Chir*, 1928, **49**, 4.

20 Jarde, O., Quenot, P., Trinquier-Lautard, J. L., et al. Haglund disease treated by simple resection of calcaneus tuberosity. An angular and therapeutic study. Apropos of 74 cases with 2 years follow-up. *Rev Chir Orthop Reparatrice Appar Mot*, 1997, **83** (6), 566-573.

21 Schmidt-Rohlfing, B., Graf, J., Schneider, U., et al. The blood supply of the Achilles tendon. *Int Orthop*, 1992, **16** (1), 29-31.

22 Sella, E. J., Caminear, D. S. and McLarney, E. A. Haglund's syndrome. *J Foot Ankle Surg*, 1998, **37** (2), 110-114; discussion 173.

23 Orava, S. and Leppilahti, J. Overuse Injuries of Tendons in Athletes. 1999, In *European Instructional Course Lectures.* (Ed. R. Jakob, P. Fulford and F. Horan), London: The British Editorial Society of Bone and Joint Surgery.

24 Canoso, J. J. The premiere enthesis. *J Rheumatol*, 1998, **25** (7), 1254-1256.

25 Caldwell, J. G. L., Allen, A. A. and Fu, F. H. Functional anatomy and biomechanics of the meniscus. *Op Tech Sports Med*, 1994, **2** (3), 152-163.

26 Allen, A. A., Caldwell, G. L. and Fu, F. H. Anatomy and biomechanics of the meniscus. *Op Tech Sports Med*, 1995, **5**, 2-9.

27 Louis-Ugbo, J., Leeson, B. and Hutton, W. C. Tensile properties of fresh human calcaneal (Achilles) tendons. *Clin Anat*, 2004, **17** (1), 30-35.

28 Miller-Young, J. E., Duncan, N. A. and Baroud, G. Material properties of the human calcaneal fat pad in compression: experiment and theory. *J Biomech*, 2002, **35** (12), 1523-1531.

29 Barnett, C. H., Davies, D. V. and MacConaill, M. A. *Synovial joints: Their structure and mechanics*. 1961, London: Longman.

30 Dolgo-Saburoff, B. Uber Ursprung und Insertion der Skeletmuskeln. *Anat Anz*, 1929, **68**, 80 - 87.

31 Milz, S., Rufai, A., Buettner, A., et al. Three-dimensional reconstructions of the Achilles tendon insertion in man. *J Anat*, 2002, **200** (Pt 2), 145-152.

32 Rufai, A., Ralphs, J. R. and Benjamin, M. Structure and histopathology of the insertional region of the human Achilles tendon. *J Orthop Res*, 1995, **13** (4), 585-593.

33 O'Brien, M. Functional anatomy and physiology of tendons. *Clin Sports Med*, 1992, **11** (3), 505-520.

34 Dykyj, D. and Jules, K. T. The clinical anatomy of tendons. *J Am Podiatr Med Assoc*, 1991, **81** (7), 358-365.

35 Jozsa, L. G. and Kannus, P. *Human Tendons. Anatomy, Physiology and Pathology*. 1997, Champaigne: Human Kinetics.

36 Wallenbock, E., Lang, O. and Lugner, P. Stress in the Achilles tendon during a topple-over movement in the ankle joint. *J Biomech*, 1995, **28** (9), 1091-1101.

37 Oxlund, H. Relationships between the biomechanical properties, composition and molecular structure of connective tissues. *Connect Tissue Res*, 1986, **15** (1-2), 65-72.

38 Carr, A. J. and Norris, S. H. The blood supply of the calcaneal tendon. *J Bone Joint Surg Br*, 1989, **71** (1), 100-101.

39 Ahmed, I. M., Lagopoulos, M., McConnell, P., et al. Blood supply of the Achilles tendon. *J Orthop Res*, 1998, **16** (5), 591-596.

40 Karcz, M. J., Skawina, A., Gorczyca, J., et al. The arterial vascularisation of the human calcaneus (Achilles) tendo during the prenatal development. *Folia Morphol (Warsz)*, 1996, **55** (4), 306-308.

41 Niculescu, V. and Matusz, P. The clinical importance of the calcaneal tendon vasculature (tendo calcaneus). *Morphol Embryol (Bucur)*, 1988, **34** (1), 5-8.

42 Astrom, M. and Westlin, N. Blood flow in the human Achilles tendon assessed by laser Doppler flowmetry. *J Orthop Res*, 1994, **12** (2), 246-252.

43 Langberg, H., Bulow, J. and Kjaer, M. Blood flow in the peritendinous space of the human Achilles tendon during exercise. *Acta Physiol Scand*, 1998, **163** (2), 149-153.

44 Lagergren, C. and Lindholm, A. Vascular distribution in the Achilles tendon; an angiographic and microangiographic study. *Acta Chir Scand*, 1959, **116** (5-6), 491-495.

45 Lesic, A. and Bumbasirevic, M. Disorders of the Achilles tendon. *Current Orthopaedics*, 2004, **18** (1), 63-75.

46 Zantop, T., Tillmann, B. and Petersen, W. Quantitative assessment of blood vessels of the human Achilles tendon: an immunohistochemical cadaver study. *Arch Orthop Trauma Surg*, 2003, **123** (9), 501-504.

47 Schatzker, J., Branemark, P.I., Intravital observations on the microvascular anatomy and microcirculation of the tendon. *Acta Orthop Scand (Suppl)*, 1969, **126**, 1-23.

48 Stein, V., Laprell, H., Tinnemeyer, S., et al. Quantitative assessment of intravascular volume of the human Achilles tendon. *Acta Orthop Scand*, 2000, **71** (1), 60-63.

49 Astrom, M. and Westlin, N. Blood flow in chronic Achilles tendinopathy. *Clin Orthop Relat Res*, 1994, (308), 166-172.

50 Theobald, P., Benjamin, M., Nokes, L., et al. Review of the vascularisation of the human Achilles tendon. *Injury*, 2005, **36** (11), 1267-1272.

51 Barfred, T. Kinesiological comments on subcutaneous ruptures of the Achilles tendon. *Acta Orthop Scand*, 1971, **42** (5), 397-405.

52 Curwin, S. and Stanish, W. D. *Tendinitis: Its etiology and treatment.* 1984, Lexington, MA: Collamore Press.

53 Plotz, E. Funktioneller Bau und funktionelle Anpassung det Gleitsehnen. *Z Orthop*, 1938, **67**, 212-234.

54 Clement, D. B., Taunton, J.E., Smart, G.W., Achilles tendinitis and peritendinitis: Etiology and treatment. *Am J Sports Med*, 1984, **12**, 179-184.

55 Koch, S. and Tillmann, B. The distal tendon of the biceps brachii. Structure and clinical correlations. *Ann Anat*, 1995, **177** (5), 467-474.

56 Jorza LG and Kannus P *Human Tendons: Anatomy, Physiology and Pathology*. 1997, Champaigne: Human Kinetics.

57 Clancy, W. G., Jr., Neidhart, D. and Brand, R. L. Achilles tendonitis in runners: a report of five cases. *Am J Sports Med*, 1976, **4** (2), 46-57.

58 Davidsson, L., Salo, M., Pathogenesis of subcutaneous tendon ruptures. *Acta Chir Scand*, 1969, **135**, 209-215.

59 Astrom, M. Laser Doppler flowmetry in the assessment of tendon blood flow. *Scand J Med Sci Sports*, 2000, **10** (6), 365-367.

60 Laine, V. A. I., Vaino, K.J., Spontaneous ruptures of tendons in rheumatoid arthritis. *Acta Orthop Scand*, 1955, **24** (250-257),

61 Reinherz, R. P., Granoff, S. R. and Westerfield, M. Pathological afflictions of the Achilles tendon. *J Foot Surg*, 1991, **30**, 117-121.

62 Campbell, P., Lawton, J.O., Spontaneous rupture of the Achilles tendon: pathology and management. *Br J Hosp Med*, 1993, **50** (321-325),

63 Komi, P. V., Fukashiro, S. and Jarvinen, M. Biomechanical loading of Achilles tendon during normal locomotion. *Clin Sports Med*, 1992, **11** (3), 521-531.

64 Ker, R. F., Alexander, R. M. and Bennett, M. B. Why are mammalian tendons so thick. *J Zool*, 1988, **216**, 309-324.

65 Nordin, M. and Frankel, V. H. *Basic biomechanics of the musculoskeletal system*. 2001, Baltimore: Lippincott Williams & Wilkins.

66 Ciullo, J. V. and Zarins, B. Biomechanics of the musculotendinous unit: relation to athletic performance and injury. *Clin Sports Med*, 1983, **2** (1), 71-86.

67 Fung, Y. C. *Biomechanics: Mechanical Properties of Living Tissue*. 1981, New York: Springer-Verlag.

68 Fyfe, I. and Stanish, W. D. The use of eccentric training and stretching in the treatment and prevention of tendon injuries. *Clin Sports Med*, 1992, **11** (3), 601-624.

69 Elliott, D. H. Structure and Function of Mammalian Tendon. *Biol Rev Camb Philos Soc*, 1965, **40**, 392-421.

70 Hess, G. P., Cappiello, W. L., Poole, R. M., et al. Prevention and treatment of overuse tendon injuries. *Sports Med*, 1989, **8** (6), 371-384.

71 Renstrom, P. and Johnson, R. J. Overuse injuries in sports. A review. *Sports Med*, 1985, **2** (5), 316-333.

72 Hansen, K. A., Weiss, J. A. and Barton, J. K. Recruitment of tendon crimp with applied tensile strain. *J Biomech Eng*, 2002, **124** (1), 72-77.

73 Waggett, A. D., Ralphs, J. R., Kwan, A. P., et al. Characterization of collagens and proteoglycans at the insertion of the human Achilles tendon. *Matrix Biol*, 1998, **16** (8), 457-470.

74 Amiel, D., Chu, C. R. and Lee, J. Effect of loading on metabolism and repair of tendons and ligaments. 1995, In *Repetitive Motion Disorders of the Upper Extremity* (Ed. S. C. Gordon, S. J. Blair and L. J. Fine), Rosemont, Illinois: AAOS.217 - 230

75 Akeson, W. H., Woo, S. L., Amiel, D., et al. The biology of ligaments. 1984, In *Rehabilitation of the Injured Knee* (Ed. F. J. Funk and L. Y. Hunter), St. Louis: Mosby.93-148

76 Butler, D. L., Grood, E. S., Noyes, F. R., et al. Biomechanics of ligaments and tendons. *Exerc Sport Sci Rev*, 1978, **6**, 125-181.

77 Plecko, M. and Passl, R. Rupture of the Achilles tendon. *J Finn Orthop Trauma*, 1991, **14**, 201-204.

78 Buchanan, C. I. and Marsh, R. L. Effects of exercise on the biomechanical, biochemical and structural properties of tendons. *Comp Biochem Physiol A: Mol Integr Physiol*, 2002, **133** (4), 1101-1107.

79 Ying, M., Yeung, E., Li, B., et al. Sonographic evaluation of the size of Achilles tendon: the effect of exercise and dominance of the ankle. *Ultrasound Med Biol*, 2003, **29** (5), 637-642.

80 Rosager, S., Aagaard, P., Dyhre-Poulsen, P., et al. Load-displacement properties of the human triceps surae aponeurosis and tendon in runners and non-runners. *Scand J Med Sci Sports*, 2002, **12** (2), 90-98.

81 Renstrom, P. and Kannus, P. Prevention of sports injuries. 1991, In *Sports Medicine* (Ed. R. H. Strauss), Philadelphia: W.B. Saunders.pp 307-329

82 Komi, P. V. Physiological and biomechanical correlates of muscle function: Effects of muscle structure and stretch-shortening cycle on force and speed. 1984, In *Exercise and sports sciences reviews* (Ed. R. H. Terjung), Lexington, MA: DC Heath.81-123

83 Snook, G. A. Achilles tendon tenosynovitis in long-distance runners. *Med Sci Ports*, 1972, **4**, 155-158.

84 Leach, R. E. Achilles tendinitis. *Am J Sports Med*, 1981, **9**, 93-98.

85 Cretnik, A. and Frank, A. Incidence and outcome of rupture of the Achilles tendon. *Wien Klin Wochenschr*, 2004, **116** (Suppl 2), 33-38.

86 Maffulli, N., Waterston, S. W., Squair, J., et al. Changing incidence of Achilles tendon rupture in Scotland: a 15-year study. *Clin J Sport Med*, 1999, **9** (3), 157-160.

87 Ferretti, A., Ippolito, E., Mariani, P., et al. Jumper's knee. *Am J Sports Med*, 1983, **11** (2), 58-62.

88 Eckstein, F., Jacobs, C. R. and Merz, B. R. Mechanobiological adaptation of subchondral bone as a function of joint incongruity and loading. *Med Eng Phys*, 1997, **19** (8), 720-728.

89 Frank, C., McDonald, D. and Shrive, N. Collagen fibril diameters in the rabbit medial collateral ligament scar: a longer term assessment. *Connect Tissue Res*, 1997, **36** (3), 261-269.

90 Frank, C., McDonald, D., Bray, D., et al. Collagen fibril diameters in the healing adult rabbit medial collateral ligament. *Connect Tissue Res*, 1992, **27** (4), 251-263.

91 Frank, C., Woo, S. L., Amiel, D., et al. Medial collateral ligament healing. A multidisciplinary assessment in rabbits. *Am J Sports Med*, 1983, **11** (6), 379-389.

92 Rho, J. Y., Ashman, R. B. and Turner, C. H. Young's modulus of trabecular and cortical bone material: ultrasonic and microtensile measurements. *J Biomech*, 1993, **26** (2), 111-119.

93 Gao, J. and Messner, K. Quantitative comparison of soft tissue-bone interface at chondral ligament insertions in the rabbit knee joint. *J Anat*, 1996, **188 (Pt 2)**, 367-373.

94 Evans, E. J., Benjamin, M. and Pemberton, D. J. Variations in the amount of calcified tissue at the attachments of the quadriceps tendon and patellar ligament in man. *J Anat*, 1991, **174**, 145-151.

95 Pidaparti, R. M. and Burr, D. B. Collagen fiber orientation and geometry effects on the mechanical properties of secondary osteons. *J Biomech*, 1992, **25** (8), 869-880.

96 Frasca, P., Harper, R. A. and Katz, J. L. Collagen fiber orientations in human secondary osteons. *Acta Anat (Basel)*, 1977, **98** (1), 1-13.

97 Ascenzi, A. and Bonucci, E. The compressive properties of single osteons. *Anat Rec*, 1968, **161** (3), 377-391.

98 Clark, J. and Stechschulte, D. J., Jr. The interface between bone and tendon at an insertion site: a study of the quadriceps tendon insertion. *J Anat*, 1998, **192 (Pt 4)**, 605-616.

99 Noyes, F. R., DeLucas, J. L. and Torvik, P. J. Biomechanics of anterior cruciate ligament failure: an analysis of strain-rate sensitivity and mechanisms of failure in primates. *J Bone Joint Surg Am*, 1974, **56** (2), 236-253.

100 McMinn, R. M. H., Hutchings, R. T. and Logan, B. M. *Colour atlas of foot and ankle anatomy. 2nd Edition.* 1996, London: Mosby Wolfe.

101 Myerson, M. S. and McGarvey, W. Disorders of the Achilles insertion and Achilles tendonitis. *AAOS Instructional Course Lectures*, 1999, **48**,

102 Frey, C., Rosenberg, Z., Shereff, M. J., et al. The retrocalcaneal bursa: anatomy and bursography. *Foot Ankle*, 1992, **13** (4), 203-207.

103 Prinyaroj, P. and Prasartritha, T. Retrocalcaneal bursitis: its correlation with retrocalcaneal angle and treatment. *J Med Assoc Thai*, 1986, **69** (4), 216-223.

104 Fowler, A. and Philip, J. F. Abnormality of the calcaneus as a cause of painful heel. *Br J Surg*, 1945, **32**, 494-498.

105 Notari, M. A. and Mittler, B. E. An investigation of Fowler-Philip's angle in diagnosing Haglund's deformity. *J Am Podiatry Assoc*, 1984, **74** (10), 486-489.

106 Keck, S. W. and Kelly, P. J. Bursitis of the Posterior Part of the Heel; Evaluation of Surgical Treatment of Eighteen Patients. *J Bone Joint Surg Am*, 1965, **47**, 267-273.

107 Fuglsang, F. and Torup, D. Bursitis retrocalcanearis. *Acta Orthop Scand*, 1961, **30**, 315-323.

108 Steffensen, J. and Evensen, A. Bursitis retrocalcanea achilli. *Acta Orthop Scand*, 1958, **80**, 1947-1953.

109 Ruch, J. A. Haglund's disease. *J Am Podiatry Assoc*, 1974, **64** (12), 1000-1003.

110 Maynou, C., Mestdagh, H., Dubois, H. H., et al. Is calcaneal osteotomy justified in Haglund's disease? *Rev Chir Orthop Reparatrice Appar Mot*, 1998, **84** (8), 734-738.

111 Chauveaux, D., Liet, P., Le Huec, J. C., et al. A new radiologic measurement for the diagnosis of Haglund's deformity. *Surg Radiol Anat*, 1991, **13** (1), 39-44.

112 Heneghan, M. A. and Pavlov, H. The Haglund painful heel syndrome. Experimental investigation of cause and therapeutic implications. *Clin Orthop*, 1984, (187), 228-234.

113 Burhenne, L. J. and Connell, D. G. Xeroradiography in the diagnosis of the Haglund syndrome. *Can Assoc Radiol J*, 1986, **37** (3), 157-160.

114 Lowdon, A., Bader, D. L. and Mowat, A. G. The effect of heel pads on the treatment of Achilles tendinitis: a double blind trial. *Am J Sports Med*, 1984, **12** (6), 431-435.

115 Noyes, F. R., Nussbaum, N. S., Torvik, P. J., et al. Biomechanical and ultrastructural changes in ligaments and tendons after local corticosteroid injections [abstract]. *J Bone Joint Surg Am*, 1975, **57A**, 876.

116 Anastassiades, T. and Dziewiatkowski, D. The effect of cortisone on the metabolism of connective tissues in the rat. *J Lab Clin Med*, 1970, **75** (5), 826-839.

117 Unverferth, L. J. and Olix, M. L. The effect of local steroid injections on tendon. *J Sports Med*, 1973, **1** (4), 31-37.

118 Melmed, E. P. Spontaneous bilateral rupture of the calcaneal tendon during steroid therapy. *J Bone Joint Surg Br*, 1965, **47**, 104-105.

119 Sweetnam, R. Corticosteroid arthropathy and tendon rupture. *J Bone Joint Surg Br*, 1969, **51** (3), 397-398.

120 Zadek, I. An operation for the cure of achillobursitis. *Am J Surg*, 1939, **43** (2), 542-546.

121 van Dijk, C. N., van Dyk, G. E., Scholten, P. E., et al. Endoscopic calcaneoplasty. *Am J Sports Med*, 2001, **29** (2), 185-189.

122 Stephens, M. M. Haglund's deformity and retrocalcaneal bursitis. *Orthop Clin North Am*, 1994, **25** (1), 41-46.

123 Friedman, B., Jones, J., Chaves-Munoz, G., et al. *Principles of MRI.* 1990, Maidenhead: McGraw-HIll.

124 Angermann, P. Chronic retrocalcaneal bursitis treated by resection of the calcaneus. *Foot Ankle*, 1990, **10** (5), 285-287.

125 Malay, D. Heel surgery. 1992, In *Comprehensive Textbook of Foot Surgery (2nd ed.)* (Ed. E. McGlamry, A. Banks and M. Downey), Baltimore: Williams & Wilkins.431-455

126 Sergio, F. Haglund's disease: notes on clinical diagnosis and surgical technique. *Foot and Ankle Surgery*, 1997, **3** (4), 175-181.

127 Biermann, H. Die Knocken bildung im Bereich Periostaler-Diaphysar Sehnen- und Bandansatze. *Zeitschrift fur Zellforschung und mikroskopische Anatomie*, 1957, **46**, 635-671.

128 Benjamin, M. and Ralphs, J. R. Fibrocartilage in tendons and ligaments--an adaptation to compressive load. *J Anat*, 1998, **193 (Pt 4)**, 481-494.

129 Knese, K. H. Stutzgewebe und Skelettsystem. 1979, In *Handbuch der mikroskopischen Anatomie des Menschen II/5* (Ed. W. von Mllendorff and W. Bargmann), Berlin: Springer.1 - 938

130 Benjamin, M., Evans, E. J. and Copp, L. The histology of tendon attachments to bone in man. *J Anat*, 1986, **149**, 89-100.

131 Benjamin, M., Ralphs, J. R., Shibu, M., et al. Capsular tissues of the proximal interphalangeal joint: normal composition and effects of Dupuytren's disease and rheumatoid arthritis. *J Hand Surg [Br]*, 1993, **18** (3), 371-376.

132 Frowen, P. and Benjamin, M. Variations in the quality of uncalcified fibrocartilage at the insertions of the extrinsic calf muscles in the foot. *J Anat*, 1995, **186 (Pt 2)**, 417-421.

133 Knese, K. H. and Biermann, H. [Osteogenesis in tendon and ligament insertions in the area of the original chondral apophyses.]. *Z Zellforsch Mikrosk Anat*, 1958, **49** (2), 142-187.

134 Benham, P. P., Crawford, R. J. and Armstrong, C. G. *Mechanics of Engineering Materials*. 1996, London: Prentice Hill.

135 Milz, S., Schluter, T., Putz, R., et al. Fibrocartilage in the transverse ligament of the human atlas. *Spine*, 2001, **26** (16), 1765-1771.

136 Vogel, K. G. and Koob, T. J. Structural specialization in tendons under compression. *Int Rev Cytol*, 1989, **115**, 267-293.

137 Gillard, G. C., Reilly, H. C., Bell-Booth, P. G., et al. The influence of mechanical forces on the glycosaminoglycan content of the rabbit flexor digitorum profundus tendon. *Connect Tissue Res*, 1979, **7** (1), 37-46.

138 Benjamin, M., Qin, S. and Ralphs, J. R. Fibrocartilage associated with human tendons and their pulleys. *J Anat*, 1995, **187 (Pt 3)**, 625-633.

139 Heinegard, D. and Oldberg, A. Glycosylated matrix proteins. 1993, In *Connective Tissue and its Heritable Disorders* (Ed. P. M. Royce and B. Steinmann), New York: Wiley-Liss.

140 Weston, W. J. The bursa deep to tendo achillis. *Australas Radiol*, 1970, **14** (3), 327-331.

141 Resnick, D. and Niwayama, G. Anatomy of individual joints. 1981, In *Diagnosis of Bone and Joint Disorders* (Ed. D. Resnick and G. Niwayama), Philadelphia: W.B. Saunders.44-174

142 Sutro, C. J. The os calcis, the tendo-achilles and the local bursae. *Bull Hosp Joint Dis*, 1966, **27** (2), 76-89.

143 Jorza, L. G. and Kannus, P. *Human Tendons. Anatomy, Physiology and Pathology*. 1997, Champaigne: Human Kinetics.

144 Arndt, A. N., Komi, P. V., Bruggemann, G. P., et al. Individual muscle contributions to the in vivo Achilles tendon force. *Clin Biomech (Bristol, Avon)*, 1998, **13** (7), 532-541.

145 Canoso, J. J., Stack, M. T. and Brandt, K. D. Hyaluronic acid content of deep and subcutaneous bursae of man. *Ann Rheum Dis*, 1983, **42** (2), 171-175.

146 Schweitzer, M. E. and Karasick, D. MR Imaging of Disorders of the Achilles Tendon. *Am. J. Roentgenol.*, 2000, **175** (3), 613-625.

147 Dreeben, S. Heel Pain. 1994, In *Orthopaedic knowledge update: foot and ankle* (Ed. L. D. Lutter, M. Mizel and G. B. Pfeffer), Rosemont, IL: AAOS.171-191

148 Ly, J. Q. and Bui-Mansfield, L. T. Anatomy of and abnormalities associated with Kager's fat Pad. *AJR Am J Roentgenol*, 2004, **182** (1), 147-154.

149 Theobald, P., Bydder, G., Dent, C., et al. The functional anatomy of Kager's fat pad in relation to retrocalcaneal problems and other hindfoot disorders. *J Anat*, 2006, **208** (1), 91-97.

150 Theobald, P., Bydder, G., Nokes, L., et al. The functional significance of Kager's fat pad in relation to the Achilles tendon. *J Anat*, 2006, **208** (3), 407-408.

151 Canoso, J. J., Wohlgethan, J. R., Newberg, A. H., et al. Aspiration of the retrocalcaneal bursa. *Ann Rheum Dis*, 1984, **43** (2), 308-312.

152 Canoso, J. J., Liu, N., Traill, M. R., et al. Physiology of the retrocalcaneal bursa. *Ann Rheum Dis*, 1988, **47**, 910-912.

153 Shaw, H. M., Santer, R. M., Watson, A., et al. The innervation of the enthesis organ of the rat Achilles tendon. *J Anat*, 2006, **208** (3), 402.

154 Merrilees, M. J. and Flint, M. H. Ultrastructural study of tension and pressure zones in a rabbit flexor tendon. *Am J Anat*, 1980, **157** (1), 87-106.

155 Trew, M. and Everett, T. *Human Movement*. 2001, London: Churchill Livingstone.

156 Kuo, P. L., Li, P. C. and Li, M. L. Elastic properties of tendon measured by two different approaches. *Ultrasound Med Biol*, 2001, **27** (9), 1275-1284.

157 Thermann, H., Frerichs, O., Biewener, A., et al. [Biomechanical studies of human Achilles tendon rupture]. *Unfallchirurg*, 1995, **98** (11), 570-575.

158 Ploetz, E. Funktioneller Bau und funktionelle Anpassung det Gleitsehnen. *Z Orthop*, 1938, **67**, 212-234.

159 Dvir, Z. *Clinical Biomechanics*. 2000, London: Churchill Livingstone.

160 Cooke, A. F., Dowson, D. and Wright, V. The rheology of synovial fluid and some potential synthetic lubricants for degenerate synovial joints. *Engng Med*, 1978, 7, 66-72.

161 McCutchen, C. W. Why did nature make synovial fluid slimy? *Clin Orthop Relat Res*, 1969, **64**, 18-20.

162 Blechschmidt, E. The structure of the calcaneal padding. *Foot Ankle*, 1982, **2** (5), 260-283.

163 Jorgensen, U. and Bojsen-Moller, F. Shock absorbency of factors in the shoe/heel interaction--with special focus on role of the heel pad. *Foot Ankle*, 1989, **9** (6), 294-299.

164 Jahss, M. H., Michelson, J. D., Desai, P., et al. Investigations into the fat pads of the sole of the foot: anatomy and histology. *Foot Ankle*, 1992, **13** (5), 233-242.

165 Hsu, T. C., Wang, C. L., Shau, Y. W., et al. Altered heel-pad mechanical properties in patients with Type 2 diabetes mellitus. *Diabet Med*, 2000, **17** (12), 854-859.

166 Ker, R. F., Bennett, M. B., Alexander, R. M., et al. Foot strike and the properties of the human heel pad. *Proc Inst Mech Eng [H]*, 1989, **203** (4), 191-196.

167 Paul, I. L., Munro, M. B., Abernethy, P. J., et al. Musculo-skeletal shock absorption: relative contribution of bone and soft tissues at various frequencies. *J Biomech*, 1978, **11** (5), 237-239.

168 Cavanagh, P. R., Valiant, G. A. and Misevich, K. W. Biological aspects of modeling shoe/foot interaction during running. 1984, In *Sport Shoes and Playing Surfaces.* (Ed. E. C. Frederick), Illinois: Human Kinetics Publishers.24-46

169 Robbins, S. E., Gouw, G. J. and Hanna, A. M. Running-related injury prevention through innate impact-moderating behavior. *Med Sci Sports Exerc*, 1989, **21** (2), 130-139.

170 Buschmann, W. R., Hudgins, L. C., Kummer, F., et al. Fatty acid composition of normal and atrophied heel fat pad. *Foot Ankle*, 1993, **14** (7), 389-394.

171 De Clercq, D., Aerts, P. and Kunnen, M. The mechanical characteristics of the human heel pad during foot strike in running: an in vivo cineradiographic study. *J Biomech*, 1994, **27** (10), 1213-1222.

172 Ghost, P. and Taylor, T. The knee joint meniscus: A fibrocartilage of some distinction. *Clin Orthop Relat Res*, 1987, **224**, 52-63.

173 Aspden, R. M., Yarker, Y. E. and Hukins, D. W. Collagen orientations in the meniscus of the knee joint. *J Anat*, 1985, **140 (Pt 3)**, 371-380.

174 Kerin, A. J., Coleman, A., Wisnom, M. R., et al. Propagation of surface fissures in articular cartilage in response to cyclic loading in vitro. *Clin Biomech (Bristol, Avon)*, 2003, **18** (10), 960-968.

175 Jorgensen, U. and Ekstrand, J. Significance of heel pad confinement for the shock absorption at heel strike. *Int J Sports Med*, 1988, **9** (6), 468-473.

176 Cavanagh, P. R. and Lafortune, M. A. Ground reaction forces in distance running. *J Biomech*, 1980, **13** (5), 397-406.

177 Lumsden, J. M., Caron, J. P., Steffe, J. F., et al. Apparent viscosity of the synovial fluid from mid-carpal, tibiotarsal, and distal interphalangeal joints of horses. *Am J Vet Res*, 1996, **57** (6), 879-883.

178 Fukubayashi, T. and Kurosawa, H. The contact area and pressure distribution pattern of the knee. A study of normal and osteoarthrotic knee joints. *Acta Orthop Scand*, 1980, **51** (6), 871-879.

179 Seedholm, B. B., Takeda, T., Tsubuku, M., et al. Mechanical factors and patellofemoral osteoarthrosis. *Ann Rheum Dis*, 1979, **38** (4), 307-316.

180 Walker, P. S. and Erkman, M. J. The role of the menisci in force transmission across the knee. *Clin Orthop Relat Res*, 1975, (109), 184-192.

181 Jones, E. S. Joint Lubrication. *Lancet*, 1934, **223** (5783), 1426-1427.

182 Jones, E. S. Joint Lubrication. *Lancet*, 1936, **227** (5879), 1043-1045.

183 Cooke, A. F., Dowson, D. and Wright, V. Lubrication of synovial membrane. *Ann Rheum Dis*, 1976, **35** (1), 56-59.

184 Weightman, B. O., Paul, I. L., Rose, R. M., et al. A comparative study of total hip replacement prostheses. *J Biomech*, 1973, **6** (3), 299-306.

185 Zhang, M. and Mak, A. F. In vivo friction properties of human skin. *Prosthet Orthot Int*, 1999, **23** (2), 135-141.

186 Kenins Influence of fibre type and moisture on measured fabric-to-skin friction. *Textile Res J*, 1994, **64** (12), 722-728.

187 Bhushan, B., Wei, G. and Haddad, P. Friction and wear studies of human hair and skin. *Wear*, 2005, **259** (7-12), 1012-1021.

188 El-Shimi, A. F. In vivo skin friction measurements. *J Soc Cosmet Chem*, 1977, **28**, 37-51.

189 Cooke, A. F. Lubrication of synovial membrane. 1981, In *Introduction to the biomechanics of joints and joint replacement* (Ed. D. Dowson and V. Wright), London: Mechanical Engineering Publications Ltd.154-158

190 Fithian, D. C., Kelly, M. A. and Mow, V. C. Material properties and structure-function relationships in the menisci. *Clin Orthop Relat Res*, 1990, (252), 19-31.

191 Voloshin, A. S. and Wosk, J. Shock absorption of meniscectomized and painful knees: a comparative in vivo study. *J Biomed Eng*, 1983, **5** (2), 157-161.

192 Krause, W. R., Pope, M. H., Johnson, R. J., et al. Mechanical changes in the knee after meniscectomy. *J Bone Joint Surg Am*, 1976, **58** (5), 599-604.

193 Fukubayashi, T., Torzilli, P. A., Sherman, M. F., et al. An in vitro biomechanical evaluation of anterior-posterior motion of the knee. Tibial displacement, rotation, and torque. *J Bone Joint Surg Am*, 1982, **64** (2), 258-264.

194 Shoemaker, S. C. and Markolf, K. L. The role of the meniscus in the anterior-posterior stability of the loaded anterior cruciate-deficient knee. Effects of partial versus total excision. *J Bone Joint Surg Am*, 1986, **68** (1), 71-79.

195 Jorgensen, U. Achillodynia and loss of heel pad shock absorbency. *Am J Sports Med*, 1985, **13** (2), 128-132.

196 Thomopoulos, S., Williams, G. R., Gimbel, J. A., et al. Variation of biomechanical, structural, and compositional properties along the tendon to bone insertion site. *J Orthop Res*, 2003, **21** (3), 413-419.

197 Forster, H. and Fisher, J. The influence of loading time and lubricant on the friction of articular cartilage. *Proc Inst Mech Eng [H]*, 1996, **210** (2), 109-119.

198 Walker, P. S., Dowson, D., Longfield, M. D., et al. Lubrication of human joints. *Ann Rheum Dis*, 1969, **28** (2), 194.

199 Walker, P. S., Dowson, D., Longfield, M. D., et al. "Boosted lubrication" in synovial joints by fluid entrapment and enrichment. *Ann Rheum Dis*, 1968, **27** (6), 512-520.

200 Scholes, S. C., Unsworth, A., Hall, R. M., et al. The effects of material combination and lubricant on the friction of total hip prostheses. *Wear*, 2000, **241** (2), 209-213.

201 Dowson, D. and Wright, V. *Introduction to the biomechanics of joints and joint replacement*. 1981, London: Mechanical Engineering Publications Ltd.

202 Shrive, N. G., O'Connor, J. J. and Goodfellow, J. W. Load-bearing in the knee joint. *Clin Orthop Relat Res*, 1978, (131), 279-287.

203 Aagaard, H. and Verdonk, R. Function of the normal meniscus and consequences of meniscal resection. *Scand J Med Sci Sports*, 1999, **9** (3), 134-140.

204 Bessette, G. C. The meniscus. *Orthopedics*, 1992, **15** (1), 35-42.

205 Warren, R. F., Arnoczky, S. P. and Wickiewicz, T. L. Anatomy of the knee. 1986, In *The lower extremity and spine in sports medicine* (Ed. J. A. Nicholas and E. B. Hershman), St Louis: Mosby.

206 Benjamin, M., Rufai, A. and Ralphs, J. R. The mechanism of formation of bony spurs (enthesophytes) in the achilles tendon. *Arthritis Rheum*, 2000, **43** (3), 576-583.

207 Alexander, R. M. Human elasticity. *Phys. Educ.*, 1994, **29**, 358-362.

208 Narvaez, J. A., Cerezal, L. and Narvaez, J. MRI of sports-related injuries of the foot and ankle: part 1. *Curr Probl Diagn Radiol*, 2003, **32** (4), 139-155.

209 Lo, L. D., Schweitzer, M. E., Fan, J. K., et al. MR imaging findings of entrapment of the flexor hallucis longus tendon. *AJR Am J Roentgenol*, 2001, **176** (5), 1145-1148.

210 Lohman, M., Kivisaari, A., Vehmas, T., et al. MRI abnormalities of foot and ankle in asymptomatic, physically active individuals. *Skeletal Radiol*, 2001, **30** (2), 61-66.

211 Bureau, N. J., Cardinal, E., Hobden, R., et al. Posterior ankle impingement syndrome: MR imaging findings in seven patients. *Radiology*, 2000, **215** (2), 497-503.

212 Hutchings, I. M. *Tribology: Friction and wear of engineering materials.* 1992, Oxford: Butterworth Heinemann.

213 Aggarwal, A. and Sempowski, I. P. Hyaluronic acid injections for knee osteoarthritis. Systematic review of the literature. *Can Fam Physician*, 2004, **50**, 249-256.

214 Balazs, E. A. Analgesic effect of elastoviscous hyaluronan solutions and the treatment of arthritic pain. *Cells Tissues Organs*, 2003, **174** (1-2), 49-62.

215 Mazzucco, D., McKinley, G., Scott, R. D., et al. Rheology of joint fluid in total knee arthroplasty patients. *J Orthop Res*, 2002, **20** (6), 1157-1163.

216 Yamada, H., Morita, M., Henmi, O., et al. Hyaluronan in synovial fluid of patients with loose total hip prosthesis. Comparison with hyaluronan in patients with hip osteoarthritis and idiopathic osteonecrosis of femoral head. *Arch Orthop Trauma Surg*, 2000, **120** (9), 521-524.

217 Cory, C. Z., Jones, M. D., James, D. S., et al. The potential and limitations of utilising head impact injury models to assess the likelihood of significant head injury in infants after a fall. *Forensic Sci Int*, 2001, **123** (2-3), 89-106.

218 Hogan, D. B. and Pritzker, K. P. Synovial fluid analysis--another look at the mucin clot test. *J Rheumatol*, 1985, **12** (2), 242-244.

219 Kafka, V. Surface fissures in articular cartilage: effect of pathological changes in synovial fluid. *Clin Biomech (Bristol, Avon)*, 2002, **17** (9-10), 713-715.

Appendix A, Thesis Appendices

A.1 Positions of Ankle Flexion

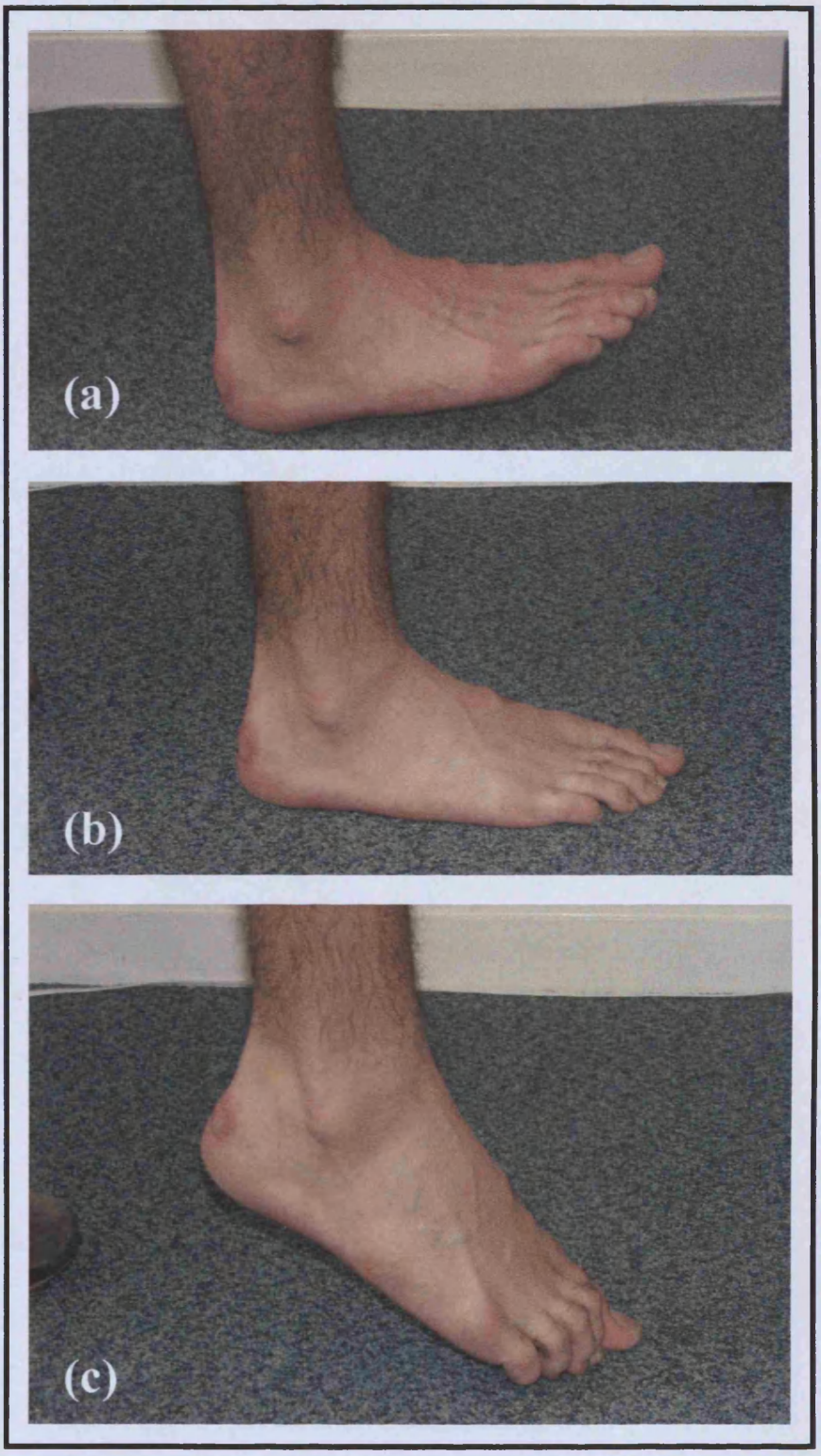

Appendix A.1: The positions of ankle flexion. (a) The foot in dorsiflexion. (b) The foot in the neutral position. (c) The foot in plantarflexion.

A.2 Rotary Microtome

Appendix A.2: A rotary microtome similar to that used in preparing the histological specimens

A.3 Superior Tuberosity Measurement – Example Calculation

A.3.1 Technique 1:

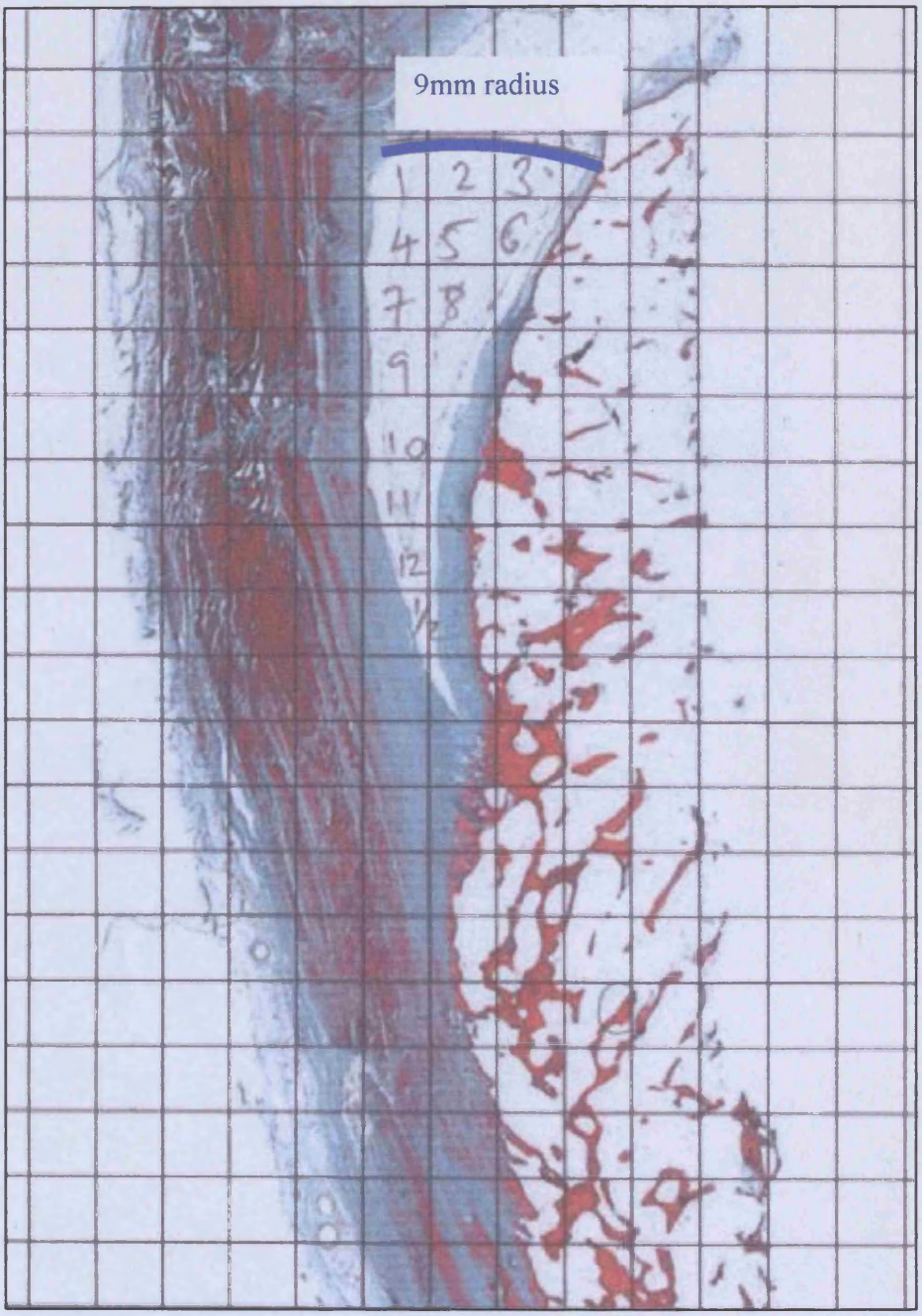

Appendix A.3.1: Measuring the superior tuberosity size (Specimen 4, Sample Point 2) using Technique 1. The histological section has had an electronic grid overlaid, where each division = 1mm. The area between the Apparent Achilles tendon axis and the superior tuberosity within a 9mm radius = $12.5mm^2$ = 12.5×10^{-6} m^2. The reciprocal of this area = 8×10^4 m^{-1}.

A.3.2 Technique 2:

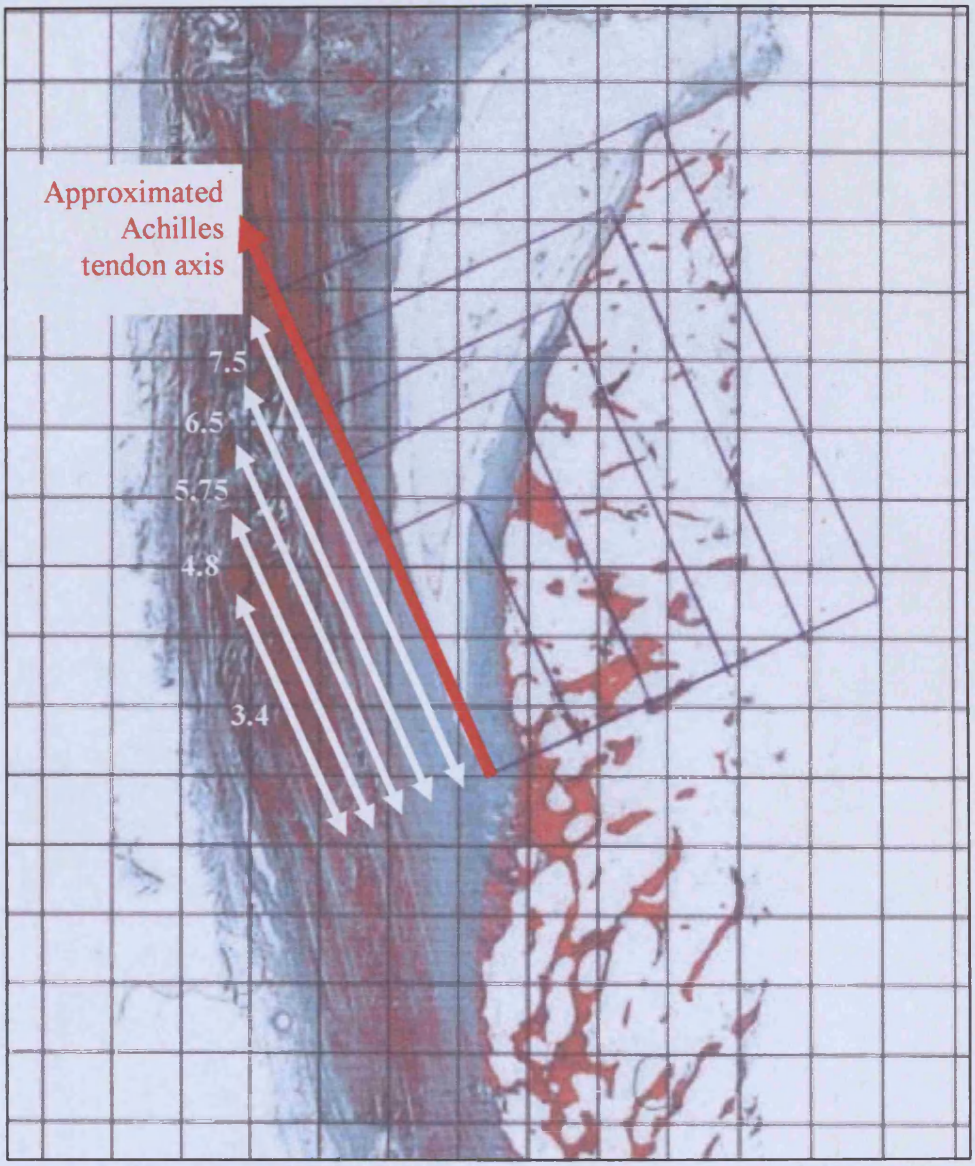

Appendix A.3.2: Measuring the superior tuberosity size (Specimen 4, Sample Point 2) using Technique 2. The histological section has had an electronic grid overlaid, where each division = 1mm. The summated superior tuberosity gradient over 5mm = 3.4 + 4.8 + 5.8 + 6.5 + 7.5 = 28

A.3.3 Technique 3:

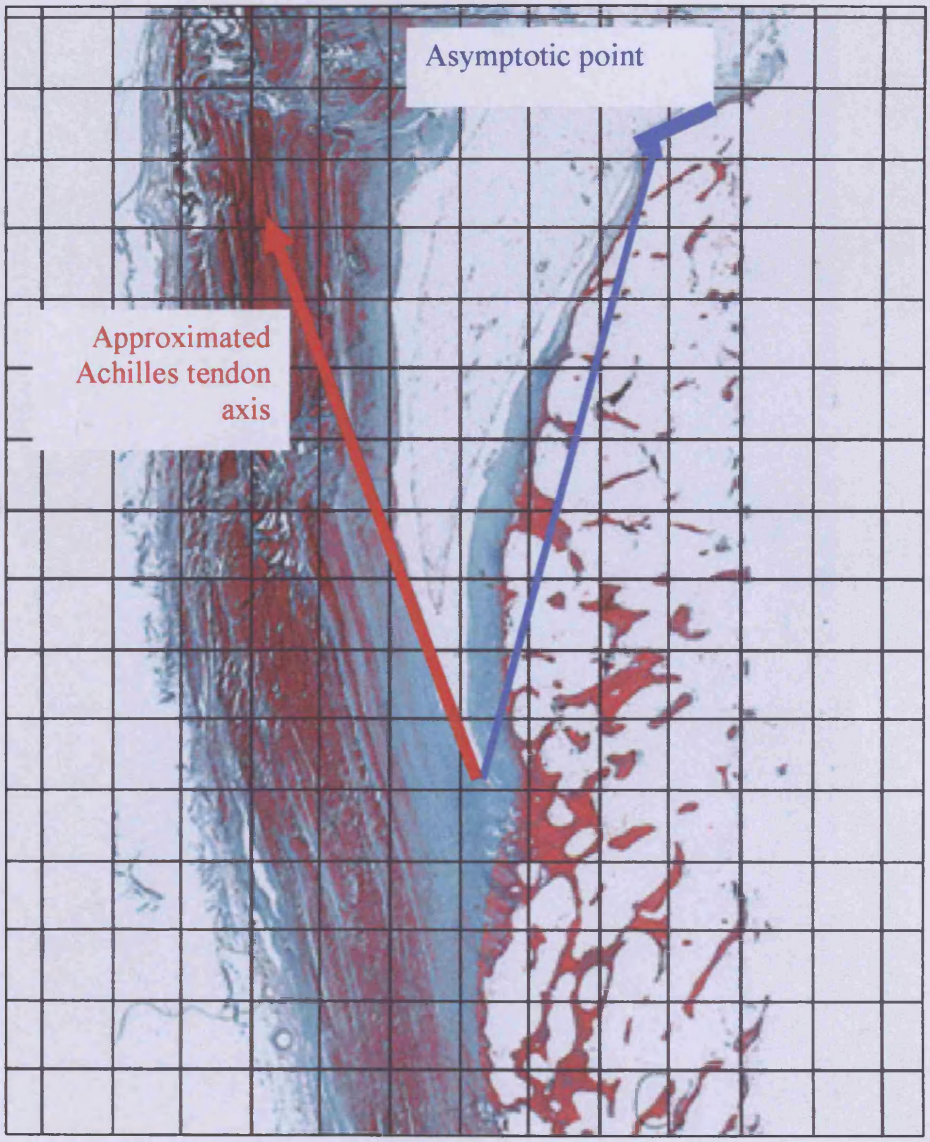

Appendix A.3.3: Measuring the superior tuberosity size (Specimen 4, Sample Point 2) using Technique 3. The histological section has had an electronic grid overlaid, where each division = 1mm. The angle subtended between the asymptotic point and the Approximated Achilles tendon axis is 38^{O}. The repriocal of this angle is 26×10^{-3}.

A.4 The Principles of MRI

Magnetic resonance imaging is a very sophisticated technique based on complex theory. Whilst outside the scope of this Thesis, a brief and simplified account is given below. Should a more detailed account be desired, a number of textbooks cover this area in great detail.

There are millions of hydrogen atoms throughout the human body, all of which have a magnetic charge due to their nucleus having a single proton. These hydrogen atoms are known to spin in random orientations which, coined with their large magnetic charge, is utilised to produce MRI's. An MRI machine consists of, amongst other components, a large superconducting magnet, creating a very intense magnetic field running down the centre of the bore. As the patient is in the supine position within the bore, their hydrogen atoms align along this magnetic field. Aligning in the direction of either the patient's head or feet, the vast majority of atoms cancel one another out - that is, one lined up towards the head is cancelled by one towards their feet. The MRI machine then focuses a hydrogen-specific radio frequency (RF) pulse to this area, which is absorbed by the atoms. This energy then makes the free, unmatched atoms spin in a particular frequency and direction. The specific frequency of resonance is calculated based upon the particular tissue being imaged, and the strength of the main magnetic field. The hydrogen atoms return to their natural alignment within the magnetic field when the RF pulse is turned off, releasing the excess stored energy. This energy is picked up by the surrounding coil in the MR machine in the form of mathematical data, which is then converted computationally using a Fourier transform to produce the magnetic resonance image.

The ability of the MRI machine to produce sequential images, and images in different planes whilst the patient is stationary, is a great benefit of the technique. This is possible due to the gradient magnets within the machine. There are 3 gradient magnets that produce a magnetic field considerably weaker than that of the main magnetic field. The magnets are arranged such that when they are turned on and off very rapidly in a specific manner, they alter the main magnetic field on a very local

level. Normal and abnormal tissue responds differently to this slight alteration, which gives rise to the differentiation visible on the MRI.

A.5 Pressure Sensitive film Calibration

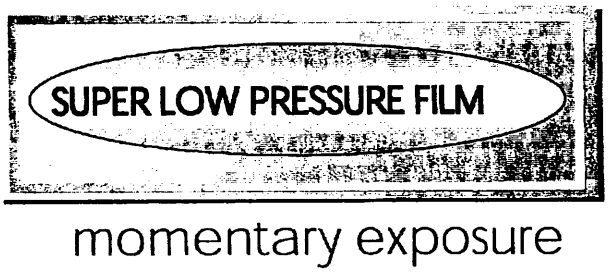

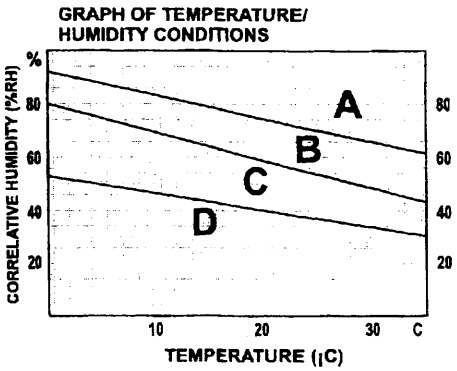

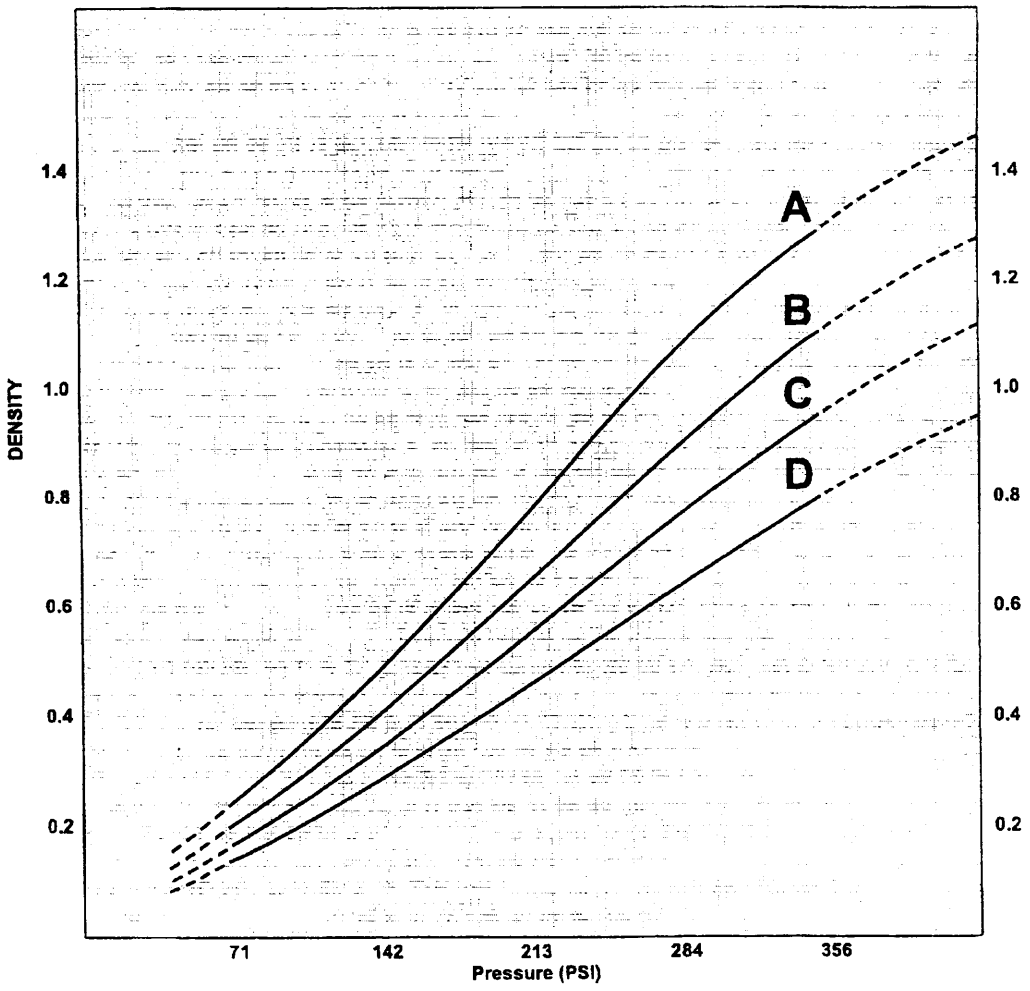

- 8 -

Appendix A.5: The calibration scale used to determine the pressure experienced at the contact.

A.6 Finite Element Model

The mechanical model geometry has been simplified to allow for computational modelling. The superior tuberosity has been modelled as a fixed curve, against which the Achilles tendon can slide over to allow for tendon strain. An irregular, quadrilateral mesh was used to allow maximum conformation of the mesh to the geometry. The material property data of the Achilles tendon were gathered from a variety of sources.

The complexity of the contact, however, is one of the reasons for this model not being completed. Movement of the tendon at the superior tuberosity interface was initially restricted in the x-direction, whilst allowed in the y-direction, and thus allowing the tendon a degree of movement when loaded. This, however, considerably effected the deformation of the model, and thus was probably the reason for the poor results. To improve the modelling of the contact, the use of interface elements was attempted. As the software did not allow for sliding across the contact between the interface elements, the model data file had to be manipulated to represent the contact. Thus, a series of springs were modelled between the interface elements that were stiff perpendicular to the superior tuberosity surface (to represent the deep fascia/paratenon) whilst being weak parallel to the superior tuberosity surface (to allow for sliding).

In addition, the lack of material properties describing the tissues of the enthesis organ would have significantly limited the accuracy of the model. Hopefully, when such data becomes available, these models can be developed to examine the how the stress at the enthesis depends on both the ankle angle and superior tuberosity size.

A.6.1 Profile 2:

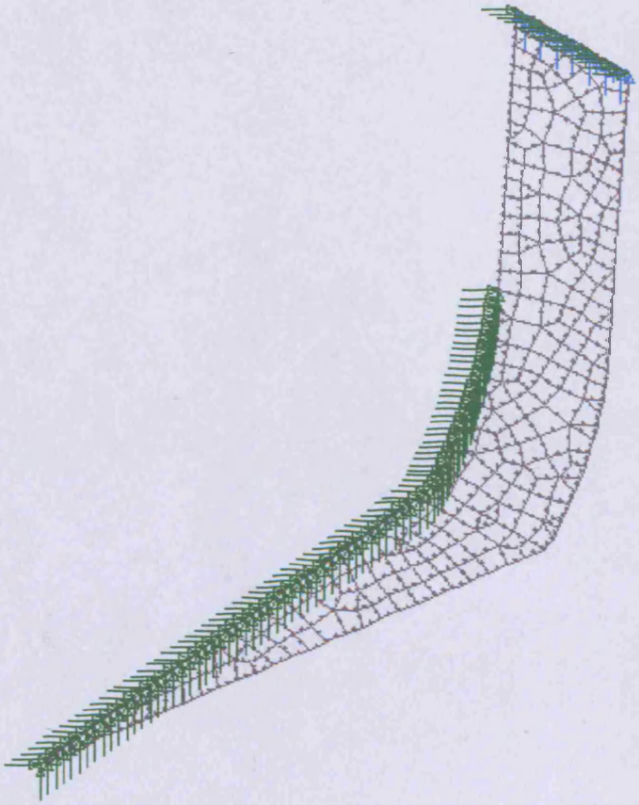

Appendix A.6.1.1: Lusas FE model of Profile 2 at 30° dorsiflexion. The contact between the Achilles tendon and the superior tuberosity was modelled initially by prohibiting tendon displacement in the x-direction. The green arrows indicate the fixed nodes of the superior tuberosity, whilst the blue arrows indicate the distributed tensile load placed upon the Achilles tendon.

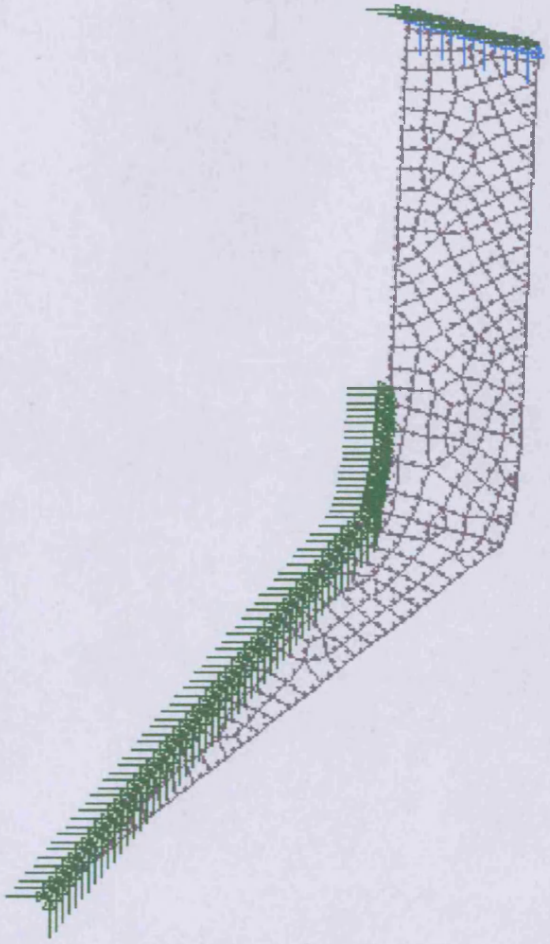

Appendix A.6.1.2: Lusas FE model of Profile 2 at 15° dorsiflexion. The green arrows indicate the fixed nodes, whilst the blue arrows indicate the distributed tensile load placed upon the Achilles tendon.

A.6.2 Profile 3:

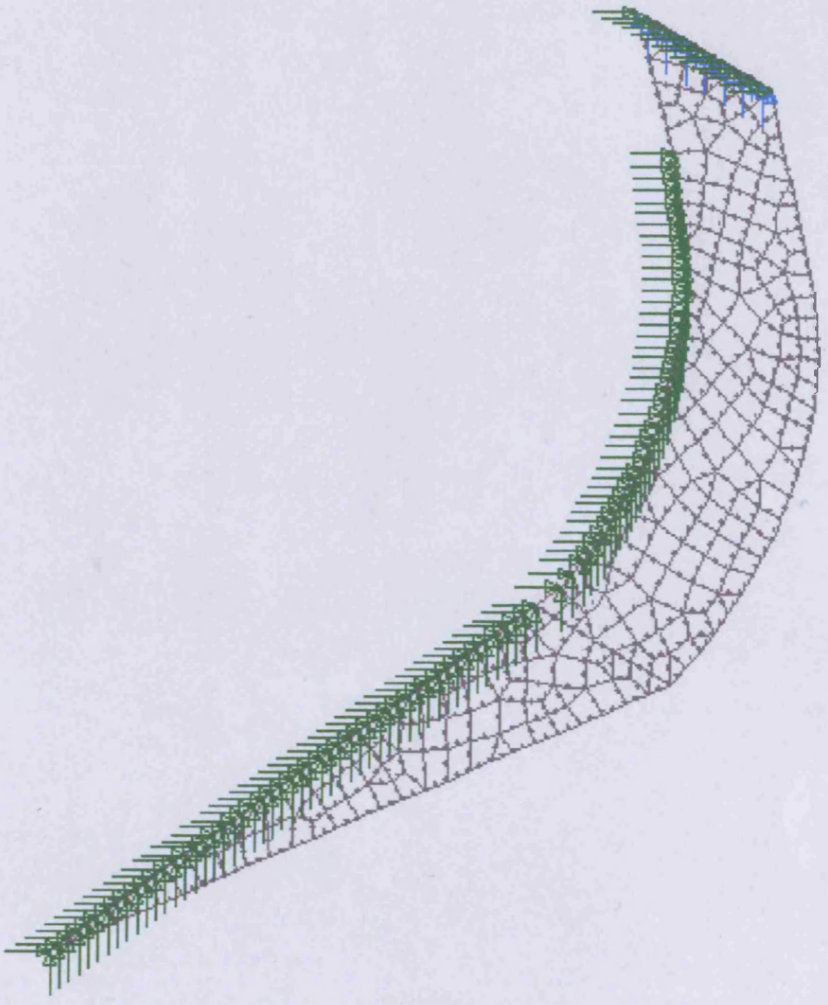

Appendix A.6.2.1: Lusas FE model of Profile 3 at 30° dorsiflexion. The green arrows indicate the fixed nodes, whilst the blue arrows indicate the distributed tensile load placed upon the Achilles tendon.

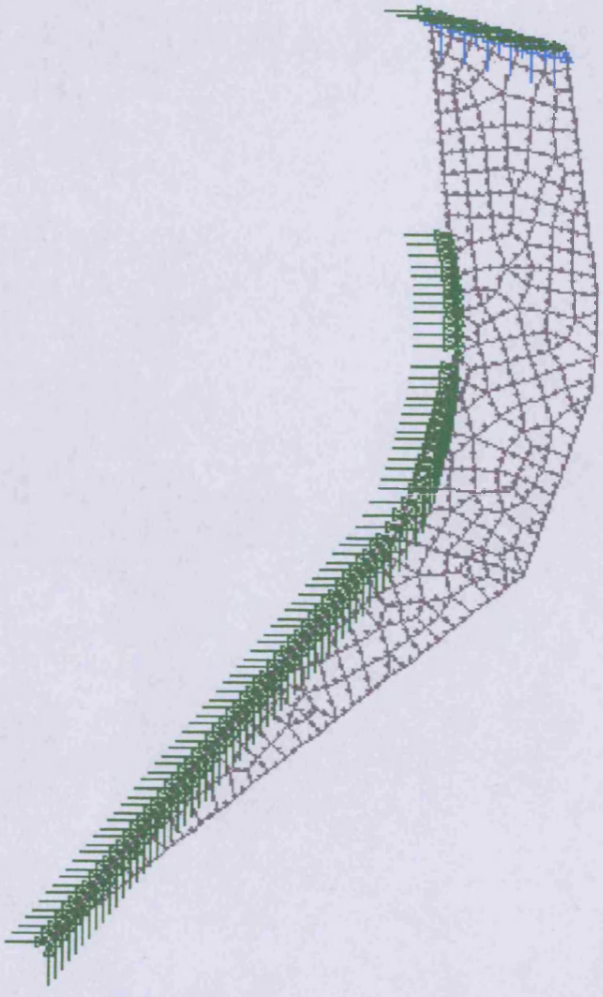

Appendix A.6.2.2: Lusas FE model of Profile 3 at 15° dorsiflexion. The green arrows indicate the fixed nodes, whilst the blue arrows indicate the distributed tensile load placed upon the Achilles tendon.

A.6.3 Profile 4

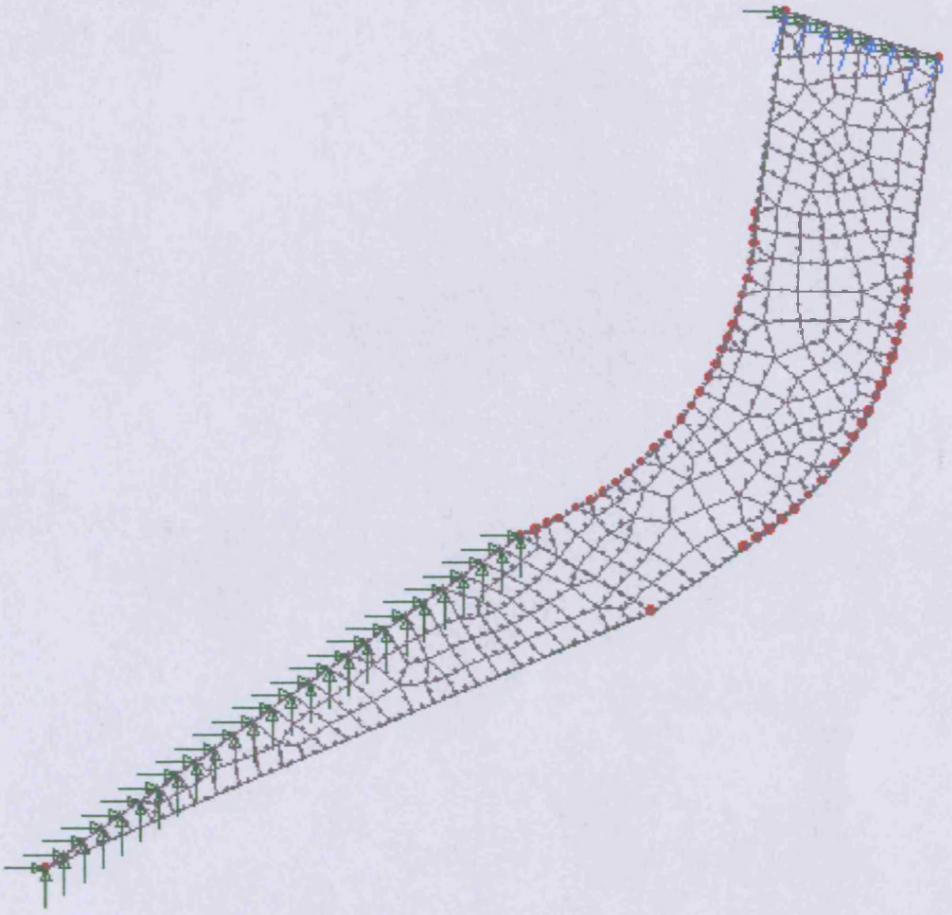

Appendix A.6.3.1: Lusas FE model of Profile 4 at 30° dorsiflexion. The contact was modelled in a more sophisticated manner in order to improve the deformation characteristics of the tendon following loading. The green arrows indicate the fixed nodes, whilst the blue arrows indicate the distributed tensile load placed upon the Achilles tendon.

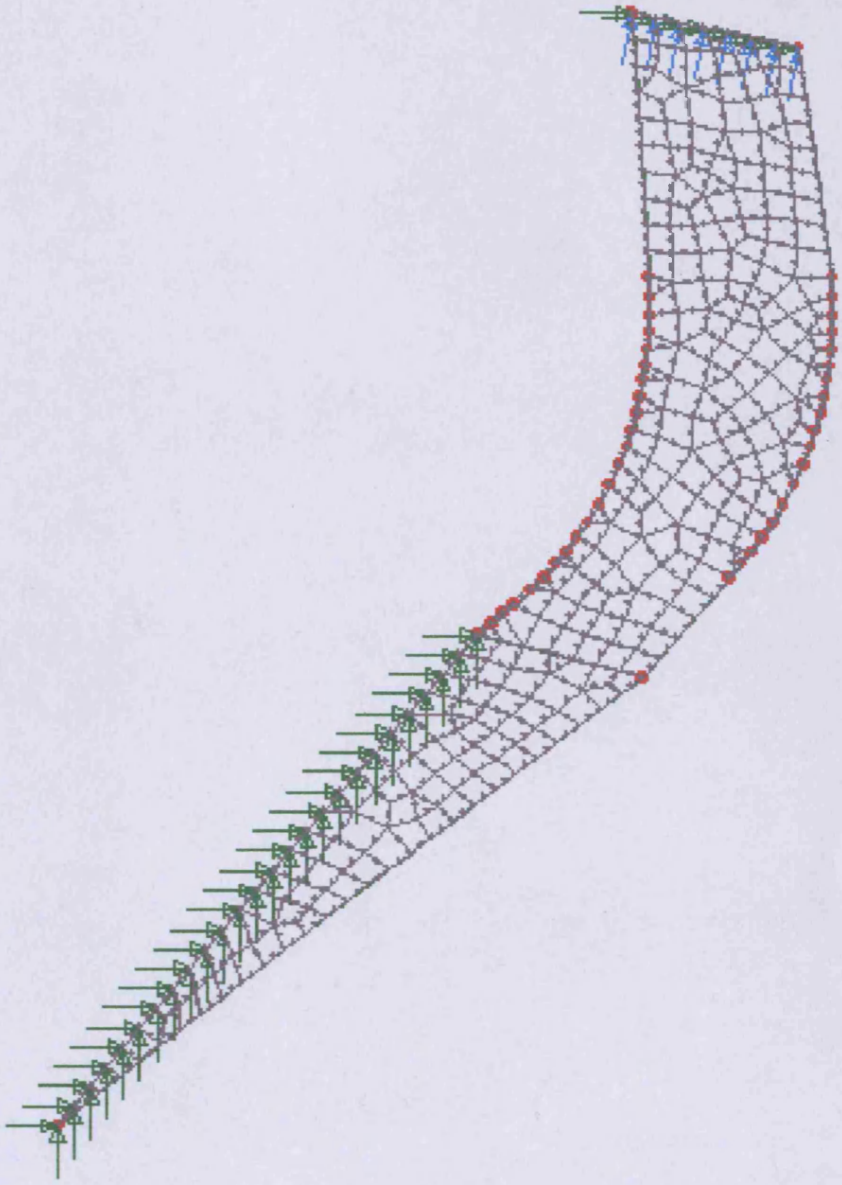

Appendix A.6.3.2: Lusas FE model of Profile 4 at 15° dorsiflexion. The green arrows indicate the fixed nodes, whilst the blue arrows indicate the distributed tensile load placed upon the Achilles tendon.

A.7 The Principles of Ultrasound

Ultrasound imaging relies upon principles similar to the echolocation systems used by bats, whales and dolphins, as well as the SONAR navigation system used by submarines. Through the emission of a series of high frequency sound waves, in tandem with their echoes, information may be gleaned about the surrounding structures.

Ultrasound utilises the piezoelectric effect to generate and send high-frequency sound pulses into the body. The pulses are generated within a transducer, by one or more piezoelectric crystals. When these crystals are excited with an electrical current, the crystals rapidly change shape causing the generation of an ultrasonic pulse, which is directed into the body. Multiple-crystal transducers are advantageous as the ultrasonic beam can be directed by changing the timing in which each element gets pulsed, thus creating a higher resolution of image. An acoustic lens within the transducer additionally focussed the emitted waves.

The shape of the transducer determines the size of the field of view, and thus the size of the acquired image. In diagnosis, this may be of particular importance to allow for the examination of a number of surrounding tissues. Equally important in aiding diagnosis is the depth to which the sound waves penetrate - and thus the depth of the image produced, as well as the final image resolution. These factors are both governed by the frequency of the transducer, which typically ranges between 1 to 20 megahertz (MHz). An increase in frequency produces an image of higher resolution, although of reduced depth. Hence a compromise must be sought in order to obtain the desired image.

The piezoelectric principle also works in reverse. Hence, the transducer can also be used to record received ultrasonic waves. It is this principle that underpins the US technique. On reaching a boundary between two tissues, a number of sound waves are reflected back to the transducer. This causes deformation of the piezoelectric crystals, causing the release of an electrical current. However, only a minority of waves are reflected at the first tissue boundary, meaning that the remaining waves are free to

travel deeper into the body. At each tissue boundary reached thereafter, a number of waves are reflected, although the depth to which the waves travel is ultimately determined by the transducer frequency.

The time taken for each echo to return to the transducer is recorded by the US machine. The central processing unit of the US machine can then calculate the distance of a particular boundary from the transducer, in the knowledge that the speed of sound in tissue equals 1540m/s. This data can then be displayed on a screen as a two-dimensional image, with the different distances and intensities being represented by a shade of colour, typically white.

A.8 Coefficient of Friction – Example Calculation

Below is an example calculation to determine the coefficient of friction of fat pad vs bone, run against the plastic counterface (Figure 5.3.6). The data used is from the experiment at 21mm/s, with a 0.5N load applied:

ΔV = 0.0462V

D_S = Distance from pivot to spring = 105mm

D_H = Distance from pivot to holder = 260mm

N_H, L = Normal load applied to holder = 0.5N

V = 21 mm/s

Equation 5.2.1: $F_S = kx = 0.02x$

Equation 5.2.2(a): $\theta = \frac{\Delta V}{0.03} = \frac{0.0462}{0.03} = 1.54$

Equation 5.2.2(b): $x = \frac{2\pi D_S \theta}{360} = \frac{2\pi \times 105 \times 1.54}{360} \approx 2.82$

∴ Equation 5.2.1: $F_S = kx = 0.02 \times 2.82 = 0.0564$

Equation 5.2.3(a): $F_H = \frac{F_S D_S}{D_H} = \frac{0.0564 \times 105}{260} = 0.0228$

Equation 5.2.3(b): $\mu = \frac{F_H}{N_H} = \frac{0.0228}{0.5} = 0.0456$

Equation 5.2.4: $S = \frac{V}{L} = \frac{21}{0.5} = 42 mms^{-1}N^{-1}$

The resultant plot can be identified on Figure 5.3.6 as:

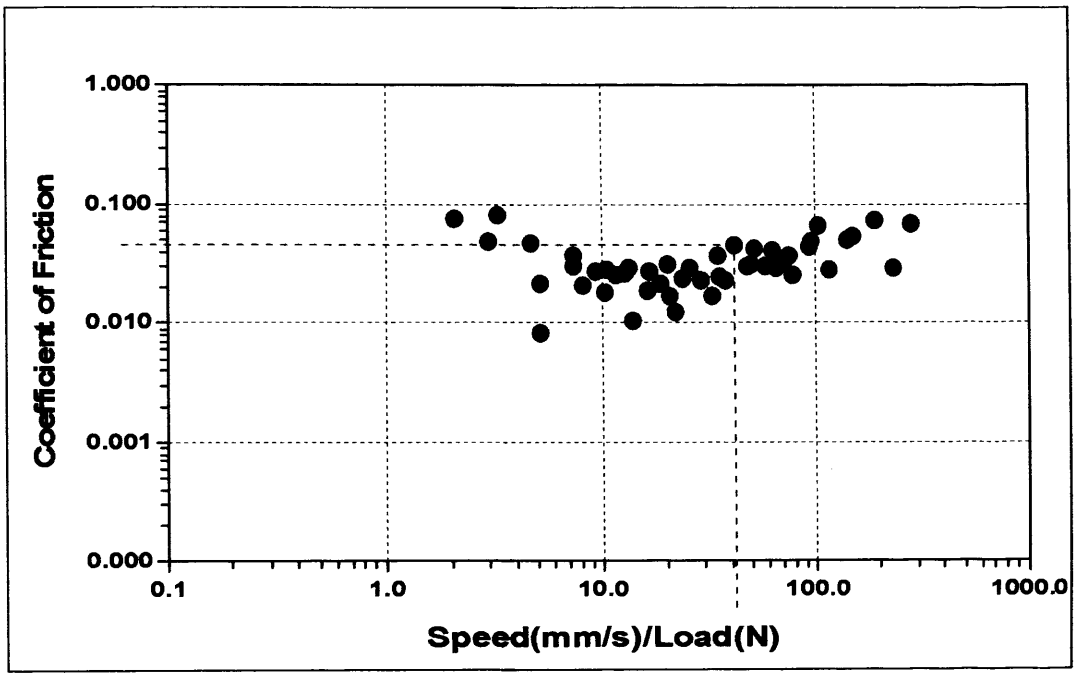

A.9 Surface Roughness

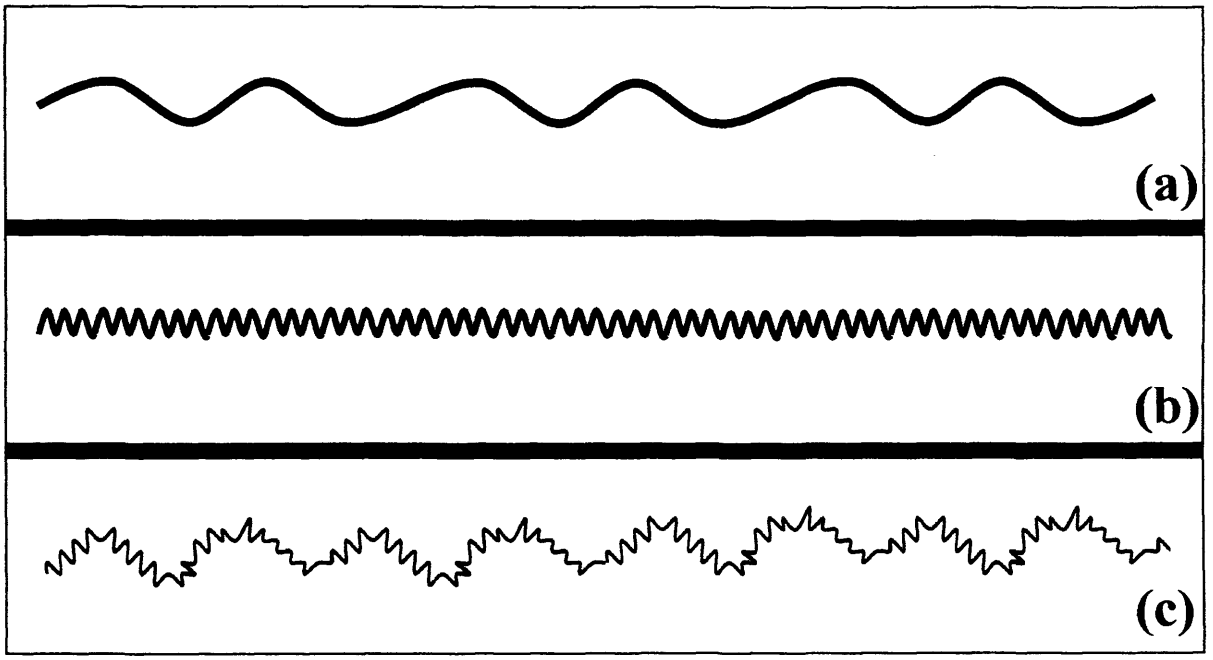

Appendix A.9: Distinguishing between a rough surface and a wavy surface is important in the field of tribology. (a) A wavy surface (b) A rough surface (c) A rough, wavy surface.

Appendix B, Thesis Publications

B.1 Journal Publications

B.1.1. Review of the vascularisation of the human Achilles tendon:

Theobald, P., Benjamin, M., Nokes, L. and Pugh, N. Review of the vascularisation of the human Achilles tendon. *Injury*, 2005, **36** (11), 1267-1272.

Injury, Int. J. Care Injured (2005) 36, 1267–1272

ELSEVIER

INJURY
INTERNATIONAL JOURNAL OF THE CARE OF THE INJURED

www.elsevier.com/locate/injury

REVIEW

Review of the vascularisation of the human Achilles tendon

P. Theobald [a,*], M. Benjamin [b], L. Nokes [c], N. Pugh [d]

[a] *Research Office, Cardiff School of Engineering, Queens Building, The Parade, P.O. Box 925, Cardiff, CF24 0YF, UK*
[b] *Cardiff School of Biosciences, Museum Avenue, P.O. Box 911, Cardiff, CF10 3US, UK*
[c] *Cardiff School of Engineering, Queens Building, The Parade, P.O. Box 925, Cardiff, CF24 0YF, UK*
[d] *Medical Physics and Clinical Engineering Directorate, University Hospital Wales, Heath Park, Cardiff, CF14 4XW, UK*

KEYWORDS
Vascularisation;
Achilles tendon;
Ruptures;
Review;
Bloodflow

Summary A region of avascularity mid-way along the length of the Achilles tendon has long been associated with rupture. Whilst it is agreed that this region is the location most common to rupture, the exact vascular distribution appears unclear. Regions of avascularity identified within the tendon have included the origin and insertion, as well as the midsection.

This review aims to analyse critically and summarise all previous studies of the vascularisation of the healthy human Achilles tendon, in order to determine the most likely region of avascularity and, thereby establish whether a relationship exists between vascularisation and rupture.

Whilst no definitive conclusion was reached, it was concluded that the vascularisation does affect the tensile strength and so rupture vulnerability of the healthy Achilles tendon, although it is unlikely to be either the sole, or most significant, contributor. Other factors, such as thinning and twisting of the tendon at the midsection are mechanical influences that will increase the incidence of rupture by increasing the concentration of stress.

Contents

* Corresponding author.
E-mail address: theobaldps@cardiff.ac.uk (P. Theobald).

0020-1383/$ – see front matter © 2005 Elsevier Ltd. All rights reserved.
doi:10.1016/j.injury.2005.02.012

Introduction

The Achilles tendon provides a connective tissue linkage between gastrocnemius and soleus muscles and the os calcis and is a common cause of complaint in athletes,[11,23,39] with injuries such as Achilles peritendinitis. Approximately 7 per 100,000 males experience Achilles tendon rupture[12,25]—typically at the midsection,[8,20,32] which is believed to coincide with a zone of avascularity.[1,9,19,36,40,45]

Whilst many studies have attempted to solve the relationship between the blood supply to the Achilles tendon and the location most vulnerable to rupture,[1,3,4,9,19,36,45] a range of possible theories and solutions has been reported.

Anatomy of the Achilles tendon

Fusing with the gastrocnemius muscle proximally, the Achilles tendon is of a broad, flat shape near its origin. The length of this attachment ranges from 11–26 cm, with the attachment formed by the fusion of the soleus muscle to the anterior surface of gastrocnemius being 3–11 cm in length.[13] The midsection of the tendon is thinner and rounder than its origin, before expanding and attaching to the calcaneus in a shape of a delta.[16]

The Achilles tendon comprises bundles of collagen fibrils, each wrapped in endotenon, which in turn are enveloped by an epitenon. Further protection and stability is provided to the Achilles tendon by the paratenon, a layer of thin, areolar tissue wrapped around the epitenon.[44]

In spanning between the muscle and bone, the fibres of the Achilles tendon spiral by up to 90°,[16,27,40] producing an area of concentrated stress[16]—the extent of this rotation is determined by the position of fusion between the two muscles, with a more distal fusion resulting in more rotation.[16] In twisting, the tendon is being wrung, causing constriction of the vascular networks. Twisting does, however, result in less fibre buckling when the tendon is lax and less deformation of individual strands when under tension, thereby reducing both fibre distortion and interfibre friction, so increasing strength.[1]

Stress concentrations are believed to cause avascularity,[31] which in turn is believed to be a factor in tendon rupture,[1,3,4,9,19,36,45] either due to a direct reduction in tendon strength,[10,14,19,24] or by indirectly triggering rupture through events such as degenerative change.[1,30,45] Other authors, however, suggest that there is no correlation between the two.[36]

The location at which rupture is likely to occur is in little doubt, with regions 2–6,[20] 4–7,[32] or 3–5 cm[8] proximal to the calcaneal insertion reported as the most frequent. The aetiology of rupture in this region, however, remains unclear,[5] although investigations suggest that a significant cause of rupture of the Achilles tendon may be repeated microtrauma.[2,26,32,44]

Anatomy of the blood supply

Supplying the length of the Achilles tendon are vessels of the anterior paratenon, deriving from the posterior tibial artery.[1,9,17,36] The peroneal artery, probably through anastomoses with the posterior tibial artery, makes small contributions; the anterior tibial artery appears not to be involved.[1]

Whilst the paratenon is known to be a highly vascular tissue,[9] disagreement exists as to whether the vessels are uniformly distributed throughout its length,[9] or allow for greater blood flow at the site of insertion.[36] It has been reported that the paratenon contributes only 35% of the total supply to the midsection of the rabbit Achilles tendon,[29] implying that the remaining 65% must be supplied through the additional sources that vascularise the tendon insertion and origin. This contrasts with the human Achilles tendon, however, which is thought to be vascularised primarily by the paratenon.

The proximal third of the tendon receives additional blood supply through vessels of the muscle bellies continuing into the endotenon, although this contribution is not believed to be significant.[1,19,21,24,35,45] The distal third of the tendon receives additional vascularisation, the majority of which is supplied by vessels of less than 300 μm in diameter[19] of the rete arteriosum calcaneare, fed by the fibular and posterior tibial arteries. This supply starts at the margin of the insertion, continuing proximally up the endotenon for approximately 2 cm.[1,17,19,24,35,45]

Vascular supply development

Whilst blood flow is known to decrease with age,[4] it has also been shown that the relative blood sup-

plies of the different zones of tissue vary with age. The most intensively vascularised zone of the foetal Achilles tendon–muscle–bone complex is the tendon insertion, whereas in samples aged 30 years and over the most intensely vascularised zone is at the tendon origin. The middle part of the tendon is the least vascularised at all ages.[30]

Distribution of the blood supply

Reports regarding the distribution of blood supply to the Achilles tendon vary considerably—regions of avascularity have been found in the insertion,[3,4,9,21] mid-section,[19,40,45] insertion and mid-section[1,9] and mid-section and origin.[36] These results and the techniques used are summarised in Table 1.

Ahmed et al.[1] reported that the insertional region of the human Achilles tendon is the most vascularised region, measuring the vascularity of only eight Achilles tendons by calculating the vessel surface area on histological sections. This protocol has been criticised due to the likelihood of the small vessels' collapsing—and it is also deemed likely that the majority of insertional vessels are smaller than those throughout the remainder of the tendon,[9,30,36,45] so appearing invisible when examined microscopically.[45] Immunohistochemical results found the tendon origin to be the most vascularised region,[45] although a wide range of values was reported for each location.

Angiography allows vascularisation to be measured by identifying blood vessels radiographically. Following such a protocol, it is important to check that the medium has reached all vessels of the tendon so ensuring an accurate representation: concerns have previously been expressed[1] about protocols that do not successfully clear clotted blood from the vessels before injecting the medium.[9,19,36] Injection pressure should also be controlled, so as to avoid a false-positive result, where vessels that do not exist are shown to be present. Reporting an injection pressure of between 130 and 170 mmHg, Lagergren and Lindholm[19] do not appear to have controlled this. Whilst Stein et al.[40] controlled the pressure at which radioisotope was injected, no detail was given of how the medium resisted the pressure applied when dissecting the tendon into 1 cm long sections. It appears plausible that medium could have leaked from the specimen on dissection. It was found that the midsection was the poorest area of vascularisation, increasing both distally and proximally, reaching approximately a five-fold increase in vascularisation density at the extremes, compared with the midsection.[40]

Measuring the blood flow through the Achilles tendon is another method to quantify vascularisation; radioisotope scanning, laser Doppler flowmetry (LDF) and power Doppler are all such techniques. Radioisotope scanning calculates blood flow by measuring the clearance rate of an injected isotope, a relationship solely dependant on the flow of blood.[15,42,43] Using ^{133}Xe, blood flow was found to

Table 1 Summary of studies reporting regions of human Achilles tendon vascularisation

Author	Technique	Result	
		Most vascularisation	Least vascularisation
Ahmed et al.[1]	Histological blood vessel density—quantitative study	Insertion	Mid-section and origin
Astrom[3]	Qualitative laser Doppler flowmetry study	Mid-section and origin	Insertion
Astrom and Westlin[4]	Quantitative laser Doppler flowmetry study	Mid-section and origin	Insertion
Carr and Norris[9]	Angiographic qualitative study (of vessels greater than 20 μm diameter)	Insertion	Mid-section
Lagergren and Lindholm[19]	Angiographic qualitative study	Origin and Insertion	Mid-section
Langberg et al.[21]	Radioisotope tracking of tendon blood flow—quantitative study	Mid-section	Insertion
Schmidt-Rohlfing et al.[36]	Epoxy resin injections highlighting vessels—qualitative study	Origin	Mid-section and outer distal section
Silvestri et al.[37]	Qualitative power Doppler study	No flow recorded	No flow recorded
Stein et al.[40]	Quantitative intravascular volume	Origin	Mid-section
Zantop et al.[45]	Immunohistochemical quantitative vascular density study	Origin	Mid-section

be greater 5 cm proximal to the calcaneal insertion than at 2 cm proximal.[21] Whilst other studies have looked at the blood vessel distribution rather than the blood flow, none has found the tendon midsection to be more highly vascularised than the insertion. These unusual results may be explained by the tendency of the technique to produce false-negative or false-positive results. Should the injection pressure be too high, or a vessel damaged due to post-mortem degradation, the medium can be pressed into the paravasal space, thereby indicating vessels that do not exist, producing a false-positive result. A false-negative result is observed when blood vessels that are present are not identified, due to insufficient volume of solution, insufficient solution pressure, premature hardening, or blockage.[45] Along with these disadvantages, the technique is invasive, time-consuming and cumbersome, and so has very limited clinical use.[4]

Laser Doppler flowmetry returns similar results to radioisotope clearance,[28,38] despite the success of the Doppler technique in detecting blood vessels within healthy Achilles tendon being questioned, due to their low metabolic activity and high resistance.[6] Introduced in 1975,[41] LDF has been used to determine that blood flow varies with respect to loading and gender,[4] and is inversely correlated with age.[4,15] Whilst said to be harmless,[3,4] this technique is mainly a research tool,[3] again due to the invasive and impractical nature requiring a probe to be inserted percutaneously. Using this technique, blood flow is seen to reduce near the tendon insertion,[4] although no comparison is possible with values yielded by other studies, due to the expression of results in non-standard units, in the belief that expressing in absolute units may give a false impression. Whilst the technique continuously measures blood flow, only a small volume of tissue (approximately 1 mm^3) can be measured due to limited light penetration. Other factors are likely to introduce inconsistency, including variations in signal due to bleeding and gross body movement.[3]

The power Doppler technique has advantages over both pulsed and colour Doppler,[34] due to being more sensitive to small and tortuous vessels of superficial structures.[37] Neither Silvestri et al.[37] nor Reiter et al.[33] could report any reading of blood flow through the healthy adult Achilles tendon, a fact that has never previously been questioned.[3,4,21] In cases of pathology, however, vessels are evident originating from the peritendinous soft tissue near the insertion, indicating an increased blood flow—manifest as swelling—and also a decrease in blood vessel resistance.[18,33,37] On completion of treatment, the blood flow again became untraceable.

Effect of non-uniform vascular distribution

Table 1 demonstrates that the exact vascular distribution in the Achilles tendon is still unknown. The majority of authors, however, believe that blood supply to the midsection is the poorest of the entire tendon.[1,9,19,36,40,45] Such avascularity is believed either directly to decrease tensile strength,[10,14,19,24] or indirectly to weaken the tendon through degenerative change,[1,30,45] hence, increasing the likelihood of rupture.[1,3,4,9,19,36,45]

Indeed, rupture occurs most commonly in the tendon's midsection[8,20,32] and a correlation was suggested over 40 years ago,[19] gaining wide acceptance.[9,19,24,45] It does not, however, have unanimous support—Schmidt-Rohlfing et al.[36] found two regions of avascularity, though only one is the site of rupture, so negating any connection. Support for this argument is provided by authors who also found avascularity in regions other than the midsection.[1,3,4,21,30] A more likely source of rupture may be due to the structural disturbance induced when the tendon is stressed.[36]

Effect of exercise on blood flow

During exercise, the blood flow within the peritendinous area of the Achilles tendon was found significantly to increase—a 2.5-fold increase was evident 2 cm proximal to insertion, whereas a four-fold increase was evident 5 cm proximally.[21] This increased flow as a result of exercise is unaltered by age.[22] Whilst this result indicates increased flow within the peritendinous area, it did not measure the blood flow within the tendon. It has been seen, however, that the blood flow within the canine Achilles tendon increases with exercise, suggesting that an increase in peritendinous flow does lead to an increase in tendon blood flow.[7]

Measuring the blood flow both within and around the Achilles tendon, an increase was found after a prolonged period of overloading by dynamic exercise and that the ratio between flow within and around the tendon was unaltered.[21] Somewhat in contrast to this view, blood flow in the tendon decreased when measured with LDF during passive stretch, or active contraction, of the triceps surae.[4] There was a large variation between individuals and, furthermore, it was clear that a decrease in local blood flow during isometric contraction was pronounced only when a tourniquet was inflated around the exercising limb, interrupting the vascular supply.[21]

Conclusion

The exact vascularisation of the healthy human adult Achilles tendon is still unknown, with variations depending on the measurement technique used. There appears to be general acceptance that avascularity is predominant in the mid-section of the tendon, and that this is likely to be a factor in tendon rupture. Other factors, such as the thinning and twisting of the tendon in its midsection, are mechanical influences that will increase the stress within that region, and so predispose to rupture.

Conflict of interest statement

No author has gained any financial benefits from writing this paper.

References

1. Ahmed IM, Lagopoulos M, McConnell P, et al. Blood supply of the Achilles tendon. J Orthop Res 1998;16:591–6.
2. Arner O, Lindholm A, Orell SR. Histological changes in subcutaneous rupture of the Achilles tendon; a study of 74 cases. Acta Chir Scand 1959;116:484–90.
3. Astrom M. Laser Doppler flowmetry in the assessment of tendon blood flow. Scand J Med Sci Sports 2000;10:365–7.
4. Astrom M, Westlin N. Blood flow in the human Achilles tendon assessed by laser Doppler flowmetry. J Orthop Res 1994;12: 246–52.
5. Barfred T. Kinesiological comments on subcutaneous ruptures of the Achilles tendon. Acta Orthop Scand 1971;42:397–405.
6. Breidhal WH, Stafford Johnson DB, Newman JS, Adler RS. Power Doppler sonography in tenosynovitis: significance of the peritendinous hypoechoic rim. J Ultrasound Med 1998;17: 107.
7. Bülow J, Tondevold E. Blood flow in different adipose tissue depots during prolonged exercise in dogs. Pflügers Arch 1982;392:235–8.
8. Campbell P, Lawton JO. Spontaneous rupture of the Achilles tendon: pathology and management. Br J Hosp Med 1993;50: 321–5.
9. Carr AJ, Norris SH. The blood supply of the calcaneal tendon. J Bone Joint Surg Br 1989;71B:100–1.
10. Clancy Jr WG, Neidhart D, Brand RL. Achilles tendonitis in runners: a report of five cases. Am J Sports Med 1976;4:46–57.
11. Clement DB, Taunton JE, Smart GW. Achilles tendinitis and peritendinitis: etiology and treatment. Am J Sports Med 1984;12:179–84.
12. Cretnik A, Frank A. Incidence and outcome of rupture of the Achilles tendon. Wien Klin Wochenschr 2004;116:33–8.
13. Curwin S, Stanish WD. Tendinitis: its etiology and treatment. Lexington: Collamore Press, 1984.
14. Davidsson L, Salo M. Pathogenesis of subcutaneous tendon ruptures. Acta Chir Scand 1969;135:209–15.
15. Hastad K, Larsson LG, Lindholm A. Clearance of radiosodium after local deposit in the Achilles tendon. Acta Chir Scand 1959;116:251–5.
16. Jorza LG, Kannus P. Human tendons: anatomy, physiology and pathology. Human kinetics. Champaigne; 1997.
17. Karcz MJ, Skawina A, Gorczyca J, Danilewicz M. The arterial vascularisation of the human calcaneus (Achilles) tendo during the prenatal development. Folia Morphol (Warsz) 1996;55:306–8.
18. Klippel JH, Dieppe PA. Rheumatology. St. Louis: Mosby-Year Book, 1994.
19. Lagergren C, Lindholm A. Vascular distribution in the Achilles tendon; an angiographic and microangiographic study. Acta Chir Scand 1958–1959;116:491–5.
20. Laine VAI, Vaino KJ. Spontaneous ruptures of tendons in rheumatoid arthritis. Acta Orthop Scand 1955;24:250–7.
21. Langberg H, Bulow J, Kjaer M. Blood flow in the peritendinous space of the human Achilles tendon during exercise. Acta Physiol Scand 1998;163:149–53.
22. Langberg H, Olesen J, Skovgaard D, Kjaer M. Age related blood flow around the Achilles tendon during exercise in humans. Eur J Appl Physiol 2001;84:246–8.
23. Leach RE. Achilles tendinitis. Am J Sports Med 1981;9:93–8.
24. Lesic A, Bumbasirevic M. Disorders of the Achilles tendon. Curr Orthop 2004;18:63–75.
25. Maffuli N, Waterston SW, Squair K, et al. Changing incidence of Achilles tendon rupture in Scotland: a 15 years study. Clin Sports Med 1999;9:157–60.
26. Mayer L. The physiological method of tendon transplantation. Surg Gynecol Obstet 1916;22:183–97.
27. McGlamry ED. Fundamentals of foot surgery. Baltimore: Williams and Wilkins, 1987.
28. Monteiro AA, Svensson H, Bornmyr S, et al. Comparison of ^{133}Xe clearance and laser Doppler flowmetry in assessment of blood flow changes in human masseter muscle induced by isometric contraction. Arch Oral Biol 1989;35:779–86.
29. Naito M, Ogata K. The blood supply of the tendon with a paratenon: an experimental study using hydrogen washout technique. Hand 1983;15:9–14.
30. Niculescu V, Matusz P. The clinical importance of the calcaneal tendon vasculature (tendo calcaneus). Morphol Embryol (Bucur) 1988;34:5–8.
31. Plotz E. Funktioneller Bau und funktionelle Anpassung det Gleitsehnen. Z Orthop 1938;67:212–34.
32. Reinherz RP, Granoff SR, Westerfield M. Pathological afflictions of the Achilles tendon. J Foot Surg 1991;30:117–21.
33. Reiter M, Ulreich N, Dirisamer A, et al. Colour and power Doppler sonography in symptomatic Achilles tendon disease. Int J Sports Med 2004;25:301–5.
34. Rubin JM, Bude RO, Carson PL, et al. A potentially useful alterative to mean frequency-based color Doppler US. Radiology 1994;190:853.
35. Schatzker J, Branemark PI. Intravital observations on the microvascular anatomy and microcirculation of the tendon. Acta Orthop Scand (Suppl) 1969;126:1–23.
36. Schmidt-Rohlfing B, Graf J, Schneider U, Niethard FU. The blood supply of the Achilles tendon. Int Orthop 1992;16:29–31.
37. Silvestri E, Biggi E, Molfetta L, et al. Power Doppler analysis of tendon vascularisation. Int J Tissue React 2003;25: 149–58.
38. Skraphedinsson JO, Harding H, Thoren P. Repeated measurements of cerebral blood flow in rats. Comparison between the hydrogen clearance method and laser Doppler flowmetry. Acta Physiol Scand 1988;134:133–42.
39. Snook GA. Achilles tendon tenosynovitis in long-distance runners. Med Sci Sports 1972;4:155–8.
40. Stein V, Laprell H, Tinnemeyer S, Peterson W. Quantitative assessment of intravascular volume of the human Achilles tendon. Acta Orthop Scand 2000;71:60–3.

41. Stern MD. In vivo evaluation of microcirculation by coherent light scattering. Nature 1975;254:56–8.
42. Walder DN. The local clearance of radioactive sodium from muscle in normal subjects and those with periferal vascular diseases. Clin Sci 1953;12:153.
43. Walder DN. The relationship between blood flow, capillary surface area and sodium clearance in muscle. Clin Sci 1955;14:303.
44. Williams JGP. Achilles tendon lesions in sport. Sports Med 1986;3:114–35.
45. Zantop T, Tillmann B, Petersen W. Quantitative assessment of blood vessels of the human Achilles tendon: an immunohistochemical cadaver study. Arch Orthop Trauma Surg 2003;123:501–4.

B.1.2. The Functional Anatomy of Kager's Fat Pad in Relation to Retrocalcaneal Problems and other Hindfoot Disorders:

Theobald, P., Bydder, G., Dent, C., Nokes, L., Pugh, N. and Benjamin, M. The functional anatomy of Kager's fat pad in relation to retrocalcaneal problems and other hindfoot disorders. *J Anat*, 2006, **208** (1), 91-97.

J. Anat. (2006) 208, pp91–97

The functional anatomy of Kager's fat pad in relation to retrocalcaneal problems and other hindfoot disorders

P. Theobald,[1] G. Bydder,[2] C. Dent,[3] L. Nokes,[1] N. Pugh[4] and M. Benjamin[5]

[1]*Institute of Medical Engineering and Medical Physics,* [3]*Department of Orthopaedics, and* [5]*School of Biosciences, Cardiff University, UK*

[2]*Department of Radiology, University of California, San Diego, USA*

[4]*Medical Physics and Clinical Engineering Directorate, University Hospital Wales*

Abstract

Kager's fat pad is a mass of adipose tissue occupying Kager's triangle. By means of a combined magnetic resonance imaging, ultrasound, gross anatomical and histological study, we show that it has three regions that are closely related to the sides of the triangle. Thus, it has parts related to the Achilles and flexor hallucis longus (FHL) tendons and a wedge of fat adjacent to the calcaneus. The calcaneal wedge moves into the bursa during plantarflexion, as a consequence of both an upward displacement of the calcaneus relative to the wedge and a downward displacement of the wedge relative to the calcaneus. During dorsiflexion, the bursal wedge is retracted. The movements are promoted by the tapering shape of the bursal wedge and by its deep synovial infolds. Fibrous connections linking the fat to the Achilles tendon anchor and stabilize it proximally and thus contribute to the motility of its tip. We conclude that the three regions of Kager's fat pad have specialized functions: an FHL part which contributes to moving the bursal wedge during plantarflexion, an Achilles part which protects blood vessels entering this tendon, and a bursal wedge which we suggest minimizes pressure changes in the bursa. All three regions contribute to reducing the risk of tendon kinking and each may be implicated in heel pain syndromes.

Key words Achilles tendon; bursa; enthesis; enthesopathy; Haglund's deformity; Kager's triangle; retrocalcaneal bursitis.

Introduction

Kager's (pre-Achilles) fat pad is a mass of adipose tissue lying within Kager's triangle that is well known to rheumatologists, radiologists, orthopaedic surgeons and sports medicine specialists alike. It appears in radiographs as a sharply marginated, radiolucent area bordered anteriorly by flexor hallucis longus (FHL), posteriorly by the Achilles tendon and inferiorly by the calcaneus (Ly & Bui-Mansfield, 2004). The ankle joint lies at the antero-inferior corner of the triangle and posterolaterally it is continuous with the retrocalcaneal bursa. Curiously, the triangle itself usually receives more attention than the fat within it, as it is a well-recognized radiological landmark that is commonly used as a reference frame in evaluating problems with the ankle joint and with the Achilles and FHL tendons (Ly & Bui-Mansfield, 2004). This lack of attention to the fat pad itself reflects an insufficient understanding of its functional significance and whether any alteration to its mechanics could bear on injury and pathology posterior to the ankle joint. It has been suggested that Kager's fat pad acts as a variable space filler and conveys a mechanical advantage on the Achilles tendon insertion, by moving into the retrocalcaneal bursa during plantarflexion (Canoso et al. 1988). By entering the bursa in this position, it is thought that the fat increases the lever arm of the tendon (Canoso et al. 1988). In the present paper, we have used a combined anatomical, ultrasound (US), magnetic resonance imaging (MRI) and histological study to explain how the tip of the fat pad moves into the bursa. We suggest that the presence of distinctive regions of fat within Kager's triangle provides a novel basis for understanding rheumatological disorders in the region.

Correspondence
Professor Michael Benjamin, School of Biosciences, Cardiff University, Museum Avenue, Cardiff CF10 3US, UK. T/F: +44 (0)2920 875041; E: Benjamin@cardiff.ac.uk

Accepted for publication *13 October 2005*

Materials and methods

Macroscopic investigations

MRI study

MRI was performed at the University of California San Diego. The right foot of three normal male volunteers (age 31, 51 and 60 years) was imaged in three positions [maximum dorsiflexion, maximum plantarflexion and the anatomical (neutral) position] whilst the subjects were in the supine position and the images were acquired in three orthogonal planes. All the ankle movements were performed passively by strapping the forefoot to a stand. No volunteer had any history of significant injury to the Achilles tendon or ankle, and all three were asymptomatic. T_1-weighted, non-fat-saturated conventional spin echo scans were obtained using a 1.5-T MR scanner (Siemens, Erlangen, Germany). The matrix size was 512 × 384, the field of view 18 cm, repetition time 480 ms, echo time 12 ms and slice thickness was 3 mm with zero gap.

US study

Ultrasound examination of the Achilles tendon region and Kager's fat pad was performed using a Toshiba Aplio scanning machine (Toshiba Medical Systems Europe, Zoetermeer, the Netherlands) at the University Hospital of Wales (Medical Physics and Clinical Engineering Directorate, UHW, Cardiff, UK) by an experienced sonographer (N.P.). One foot from each of four volunteers (three males, one female; age range 24–57 years) was scanned in the three different positions that are described above. Subjects were examined both when prone (non-load-bearing) and when standing (load-bearing). All ankle movements in the standing position were performed actively and under load. However, movements in the prone position were performed both actively without load and passively by an assistant moving the subject's foot. The degree of flexion was measured using a goniometer.

Gross anatomical examination

Six elderly perfusion-fixed dissecting room cadavers (three males, three females, ages 71–101 years) donated to Cardiff University for anatomical examination were used to study the gross anatomy of the fat pad.

Microscopic investigations

The central third of the Achilles tendon enthesis was removed from six formalin-fixed, dissecting room cadavers (three males, three females, ages 63–87 years) and processed for routine histology. The specimens were thus postfixed in 10% neutral buffered formal saline for 1 week, decalcified in 2% nitric acid, dehydrated in graded alcohols and embedded in paraffin wax. Serial sagittal sections were cut at 8 μm throughout each block and 12 sections were mounted on glass slides at 500-μm intervals. The sections were stained with Masson's trichrome, haematoxylin & eosin, or toluidine blue.

Results

Macroscopic studies

Three regions of Kager's fat pad could be discerned by combining the information gleaned from the gross anatomical, MRI and US studies. These are referred to as a large, superficial 'Achilles-associated part', a deep 'FHL-associated part' and a 'calcaneal bursal wedge' or tongue (Figs 1 and 2). The Achilles-associated part of Kager's fat pad lay immediately anterior to the tendon and the FHL-associated part was enclosed within the tendon sheath (Fig. 1b). In the sagittal plane, the FHL part of Kager's pad could be seen extending in an inverted J-shaped (dorsiflexed foot; Fig. 1b) or L-shaped (plantarflexed foot; Fig. 2a) fashion under the Achilles-associated fat, fusing with the latter and thus forming the calcaneal bursal wedge. This distal wedge was free of all connections to the Achilles tendon and extended into the retrocalcaneal bursa in a plantarflexed foot (Fig. 2). This bursal movement occurred during both active and passive plantarflexion, but was more pronounced when the foot was actively plantarflexed under load. Immediately proximal to the bursal wedge, the fat was firmly anchored to the Achilles tendon (Figs 2b and 3a). Small blood vessels passed in a tortuous fashion through the Achilles-associated fat (Figs 3b and 4a) and were identified in dissections as branches of the posterior tibial and peroneal arteries. The former lay superficially and were found in its inferior and medial aspects; the latter were deeper and typical of the superior and lateral regions. MRI in the axial plane revealed that the paratenon extends around the Achilles-associated part of Kager's fat pad, thereby holding the fat next to the tendon (Fig. 4b).

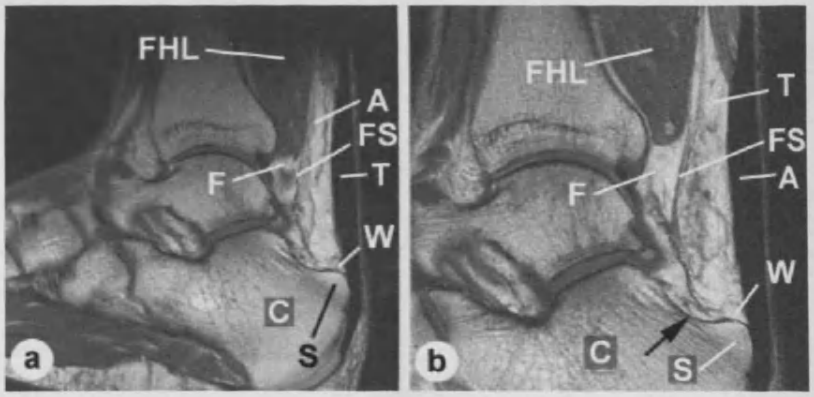

Fig. 1 Macroscopic anatomy of Kager's fat pad – MRIs. (a) An MRI of a dorsiflexed foot imaged in the sagittal plane to show the three regions of the fat pad: the Achilles-associated part (A) lying immediately anterior to the Achilles tendon (T), the FHL-associated part (F) enclosed within the fascial sheath (FS), which extends from below the muscle belly of flexor hallucis longus (FHL), and the calcaneal bursal wedge (W). C, calcaneus; S, superior tuberosity. (b) A higher magnification view of an MRI adjacent to that featured in (a) showing the three regions of the fat pad. It demonstrates how the FHL-associated fat passes beneath the Achilles-associated fat (arrow) in a J-shaped curve to fuse with it and form the bursal wedge. Note how the FHL-associated fat is enclosed within an extension of the fascia that surrounds FHL and becomes its tendon sheath.

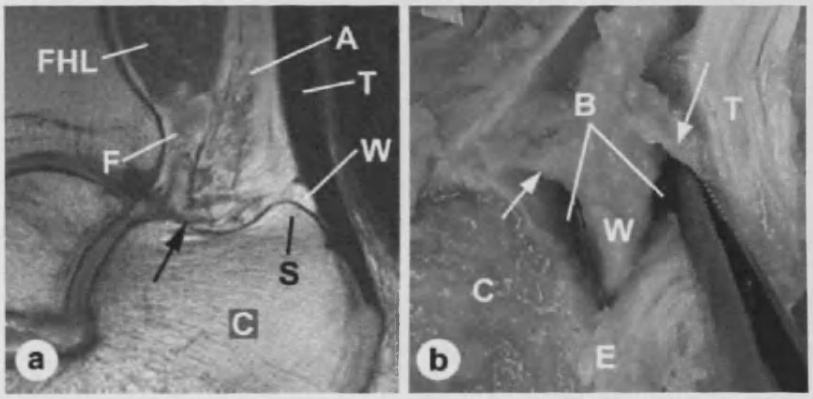

Fig. 2 Macroscopic anatomy of Kager's fat pad. (a) An MRI of a plantarflexed foot (same subject as in Fig. 1) imaged in the sagittal plane. It shows how the bursal-protruding wedge of fat (W) has moved into the retrocalcaneal bursa, by passing over the superior tuberosity (S) of the calcaneus (C). Note how the tendon and muscle regions of the fat have been moulded into a new shape by foot movements. The FHL-associated fat (F) now makes a sharp inverted L-shaped bend (arrow) before fusing with the Achilles-associated fat (A). The Achilles fat is much wider distally than in a dorsiflexed foot. When the FHL and Achilles fat fuse together, they form the bursal wedge. T, Achilles tendon. (b) A hemisected Achilles tendon from a dissecting room cadaver, showing the bursal wedge of Kager's fat pad protruding into the retrocalcaneal bursa (B) near the tendon enthesis (E). The fat is anchored anteriorly and posteriorly by fibrous bands (arrows).

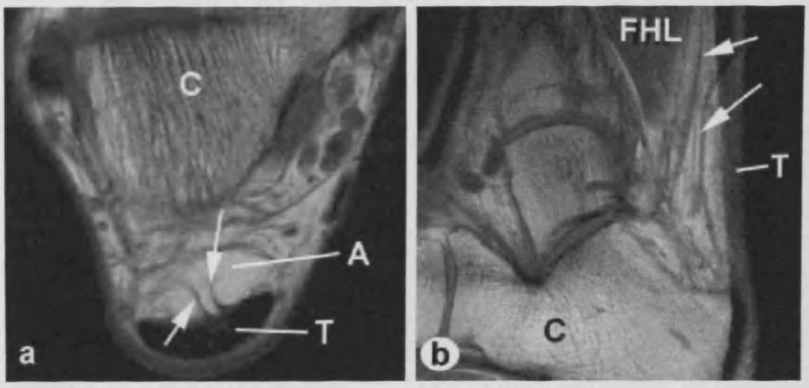

Fig. 3 Macroscopic anatomy of Kager's fat pad – MRIs. (a) An axial plane image showing two conspicuous fibrous anchors (arrows) connecting the fat pad to the Achilles tendon (T) immediately proximal to the bursal wedge of fat. C, calcaneus; A, Achilles-associated fat. (b) A sagittal image to show the prominent blood vessels (arrows) passing through the Achilles-associated fat. FHL, flexor hallucis longus.

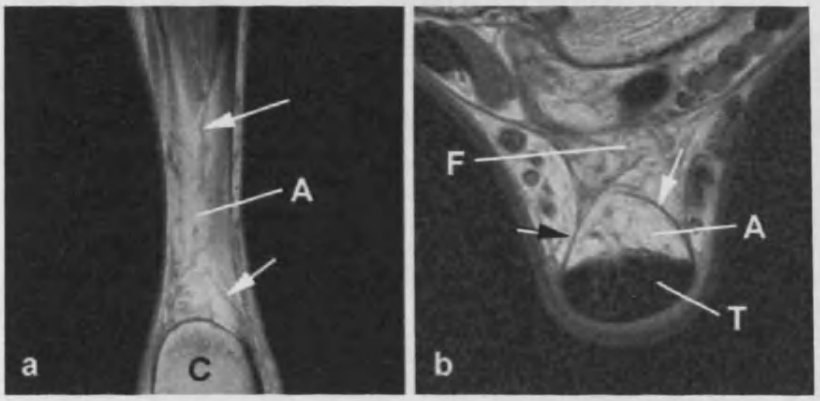

Fig. 4 Macroscopic anatomy of Kager's fat pad – MRIs. (a) A coronal plane image through the Achilles-associated fat (A), immediately anterior to the Achilles tendon, showing blood vessels coursing through the fat (arrows). The tendon itself is not visible. (b) An axial plane image showing how Achilles-associated fat (A) is enclosed within the false tendon sheath (arrows) which surrounds the Achilles tendon (T). C, calcaneus; F, FHL-associated fat.

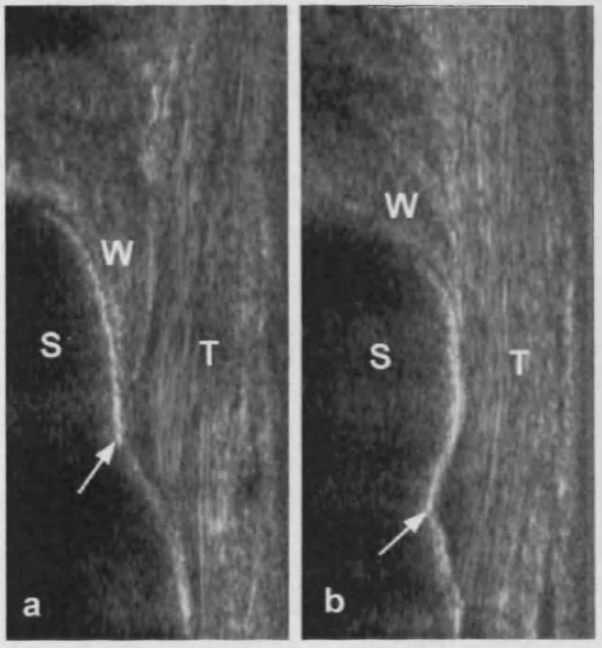

Fig. 5 Ultrasound images of the Achilles tendon enthesis from a subject standing (a) on his toes in a load-bearing, plantarflexed foot and (b) in the anatomical (neutral) position. Note that in a plantarflexed foot, the bursal wedge of Kager's fat pad (W) extends completely into the bursa as far as the enthesis itself (arrows). Consequently, the superior tuberosity of the calcaneus (S) is in direct contact with the fat and this in turn directly touches the Achilles tendon (T). When the foot is returned to the neutral position, the fat pad is retracted and the tendon and bone now touch each other directly.

A change in the position of the calcaneal bursal wedge was evident ultrasonically with ankle movements (Fig. 5). On plantarflexion, the wedge of fat moved distally into the furthest extremities of the retrocalcaneal bursa, and this movement was further accentuated by an upward displacement of the superior tuberosity. The fat extended completely into the bursa, until it reached the enthesis itself (Fig. 5a). It retracted on returning the foot to the anatomical (neutral) position (Fig. 5b). The maximum range of excursion between full active plantarflexion and full dorsiflexion was approximately 4 mm in the non-load-bearing foot and 10–12 mm during load-bearing. By studying US movie files of active plantarflexion under load, it was clear that movements of the calcaneal bursal wedge also resulted from concentric contractions of FHL. As the muscle thickened, it moved ('pumped') the FHL-associated fat – which in turn moved the bursal wedge as the final link in a kinetic chain. However, the rapidity of the final phase of bursal-wedge movement suggested that the fat was also sucked into the bursa as the insertional angle between the Achilles tendon and the calcaneus increased on plantarflexion.

Microscopic studies

A posterior synovial invagination partly divided the calcaneal bursal wedge from the remainder (Fig. 6a). Fibrous strands anchoring the Achilles tendon to the fat were occasionally seen and attached to the pad in the region of the invaginations (Fig. 6a). The bursal wedge commonly had a fibrous leading edge (Fig. 6b,c) and occasional specimens showed evidence of inflammatory infiltrates. A meniscal fold of varying length was sometimes present between the Achilles tendon and the calcaneus (Fig. 6d). It originated from the most proximal part of the enthesis.

Discussion

We suggest that movement of the calcaneal bursal wedge of Kager's fat pad minimizes pressure changes

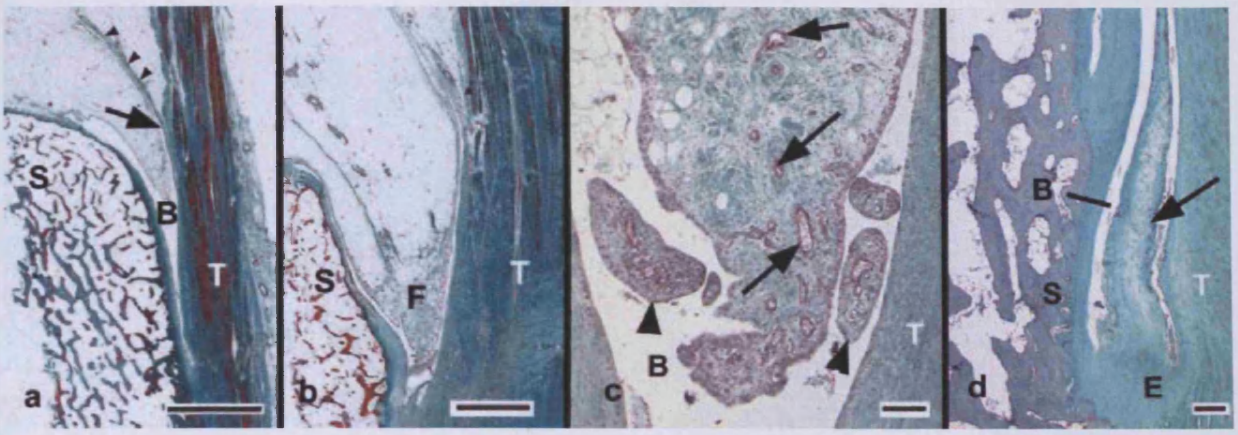

Fig. 6 Sagittal histological sections of the bursal wedge of Kager's fat pad stained with Masson's trichrome. (a) A low-power view showing the tip of the fat pad protruding into the bursa (B) between the Achilles tendon (T) and the superior tuberosity of the calcaneus (S). Note the deep synovial invagination which promotes the mobility of this region of Kager's pad (arrow), and the fibrous tissue associated with it (arrowheads). Scale bar = 3 mm. (b) The fibrous tip (F) of the bursal wedge. Scale bar = 2 mm. (c) A higher power view of the fibrous tip of the bursal wedge than that shown in (b). Note the numerous small blood vessels (arrows) and dense fibrous connective tissue in its core, and the small synovial villi at its tip (arrowheads). Scale bar = 100 μm. (d) A tapering, fibrocartilaginous meniscal fold (arrow) protruding into the retrocalcaneal bursa (B) at the proximal end of the enthesis (E) of the Achilles tendon. Scale bar = 500 μm.

in the retrocalcaneal bursa, when the insertional angle between the Achilles tendon and the calcaneus increases on plantarflexion. Because the deep fascia and paratenon in Kager's triangle create an air-tight seal, the pressure within the bursa would change, were it not for the fat pad acting as a 'variable plunger', moving in and out of the bursa with ankle movements (Canoso et al. 1988). As changes in pressure have been associated with synovial ischaemia and hypoxia in synovial joints (James et al. 1990), the lubricating function of the bursa could be affected by altered fat pad movements. The enclosure of much of the Achilles part of Kager's fat pad within the paratenon (i.e. the 'false' tendon sheath) directs movements of the calcaneal wedge of fat towards the bursa during plantarflexion, by restricting medial–lateral and anterior movements. The Achilles tendon itself prevents posterior movements and fibrous anchors stop the fat from moving proximally.

There would seem to be three mechanisms that could account for the movement of the bursal wedge as the insertional angle between the Achilles tendon and the bone increases during plantarflexion: (1) the movement is a passive consequence of an upward displacement of the calcaneus; (2) the fatty wedge is 'sucked' (i.e. pulled) into the bursa to minimize pressure changes; and (3) the fat is pushed into the bursa by muscle contraction, i.e. the muscle belly of FHL acts as a 'fat pad motor unit'. Certainly, the upward motion of the calcaneus that occurs on plantarflexion and the opening of the insertional angle of the Achilles tendon must move the bursa towards the bursal wedge – rather than vice versa. The calcaneal movement lifts Kager's fat pad, so that it contacts both the hard posterior surface of the tibia and the rigid, contracted muscle belly of FHL. This increases the efficiency of this passive system. However, the US movie files showed that the upward movement of the calcaneus was also accompanied by a downward movement of the bursal wedge. Consequently, one or both of the other mechanisms must also occur. This idea is supported by the observation that the excursional range of the bursal wedge was greater during active plantarflexion under load. It is difficult to account for this by the calcaneal movement theory alone. The retraction of the bursal wedge during dorsiflexion is likely to be a passive consequence of a decreasing insertional angle. Either the fat gets squeezed out as the surfaces become apposed or it moves out as a consequence of increased bursal pressure.

The significance of the muscle belly of FHL to the mechanics of fat pad movement could explain the characteristic distal prominence of the muscle belly of FHL at a level where other muscles acting upon the foot (e.g. flexor digitorum longus and tibialis posterior) are tendinous (Standring, 2004). It also highlights an

additional way in which tendon/tendon sheath disorders and anomalies of FHL could result in posteromedial heel pain (Narvaez et al. 2000) and emphasizes the importance during surgery within Kager's triangle of minimizing the risk of adhesions which would compromise fat pad movements. The role of FHL could be important to consider when evaluating injuries to this tendon that occur in ballet dancers *en pointe*, or in soccer players (ball-kicking results in forced plantarflexion) or in athletes engaged in downhill running (Lo et al. 2001). Although fluid accumulation is well recognized around the tendon of FHL either as a sign of pathology or as a consequence of a direct continuation between the synovial sheath of FHL tendon and the ankle joint cavity (Bureau et al. 2000; Lo et al. 2001; Lohman et al. 2001), the consequence of this on fat pad mechanics is currently overlooked. It is striking, for example, that the oedema illustrated by Lo et al. (2001) in a 38-year-old woman with FHL-entrapment associated with an enlarged os trigonum is precisely in the region of FHL-associated fat and this would be expected to influence the ultimate movements of the bursal wedge of Kager's pad.

The wedge shape of the tip of Kager's fat pad ensures that it moves progressively into the bursa as the foot is plantarflexed and its fibrous leading edge could minimize the risk of damage that accompanies the movement. This idea is supported by the observation that a long, thin wedge of fat with a fibrous tip was most typical of specimens with a prominent superior tuberosity. Where the tuberosity was less obvious, the fat was less fibrous. Equally, the length of meniscal folds also varied with the size of the superior tuberosity – folds were most prominent where the tuberosity was large. It is possible that such folds serve to modify contact stresses between tendon and bone when the surfaces are apposed in dorsiflexion. Whether the movements of Kager's fat pad are altered after resection of the calcaneal superior tuberosity in patients with Haglund's deformity is unclear. However, this could have a bearing on the poor outcome that has been reported with this procedure (Schneider et al. 2000) or emphasize the importance of choosing the most appropriate angle at which the calcaneus is resected (Sella et al. 1998). At least in the initial postoperative period, the synovial membrane which covers the bursal wedge may be in danger of being torn by exposed cancellous bone.

The partial enclosure of Kager's fat pad within the paratenon surrounding the Achilles tendon protects and stabilizes the blood vessels passing through the fat into the tendon and their tortuosity is a further adaptation to minimizing the effects of movement. This again emphasizes the importance of maintaining fat pad integrity at surgery and highlights the possibility that oedema within the fat (associated, for example, with inflammation) could temporarily diminish blood flow to the tendon. The confinement of the Achilles-associated fat within the tendon sheath accounts for the localized nature of the oedema reported by Ly & Bui-Mansfield (2004) in a patient with a partial Achilles tendon tear.

We suggest that Kager's fat pad as a whole is designed in a manner which promotes the movement of one part (its bursal wedge) while minimizing movement in another part (its Achilles-associated part). The synovial invaginations which partly isolate the bursal wedge from the rest are clearly an adaptation for encouraging the independent mobility of the wedge. Collectively, the variety of functions which may be associated with Kager's fat pad add fuel to the debate about the use of local corticosteroids to treat retrocalcaneal pain (Hugate et al. 2004), for one of the common side-effects of corticosteroids is fat atrophy (Cole & Schumacher, 2005). To what extent (if any) the mechanics of Kager's fat pad are altered in patients with an accessory soleus muscle belly, which may obliterate the fat pad in radiographs (Peterson et al. 1993), or altered by the surgical excision of this muscle (Brodie et al. 1997) is unclear.

In summary, we have shown that Kager's fat pad has three distinct regions that are associated with each of the three borders of Kager's triangle. The highly mobile, bursal-associated wedge of fat that is closely related to the calcaneus is moved both passively and actively into the retrocalcaneal bursa during plantarflexion. The more stable, Achilles-associated part protects blood vessels passing through it to supply the Achilles tendon, and all three regions of fat probably contribute to reducing the risk of tendon kinking on plantarflexion. Kager's fat pad should thus be seen as an important part of the Achilles tendon enthesis organ (Benjamin et al. 2004).

Acknowledgement

We thank Dr Simon Blease for his helpful comments on the manuscript.

References

Benjamin M, Moriggl B, Brenner E, Emery P, McGonagle D, Redman S (2004) The 'enthesis organ' concept: why

enthesopathies may not present as focal insertional disorders. *Arthritis Rheum* **50**, 3306–3313.

Brodie JT, Dormans JP, Gregg JR, Davidson RS (1997) Accessory soleus muscle. A report of 4 cases and review of literature. *Clin Orthop Relat Res* **337**, 180–186.

Bureau NJ, Cardinal E, Hobden R, Aubin B (2000) Posterior ankle impingement syndrome: MR imaging findings in seven patients. *Radiology* **215**, 497–503.

Canoso JJ, Liu N, Traill MR, Runge VM (1988) Physiology of the retrocalcaneal bursa. *Ann Rheum Dis* **47**, 910–912.

Cole BJ, Schumacher HR Jr (2005) Injectable corticosteroids in modern practice. *J Am Acad Orthop* **13**, 37–46.

Hugate R, Pennypacker J, Saunders M, Juliano P (2004) The effects of intratendinous and retrocalcaneal intrabursal injections of corticosteroid on the biomechanical properties of rabbit Achilles tendons. *J Bone Joint Surg* **86A**, 794–801.

James MJ, Cleland LG, Rofe AM, Leslie AL (1990) Intraarticular pressure and the relationship between synovial perfusion and metabolic demand. *J Rheumat* **17**, 521–527.

Lo LD, Schweitzer ME, Fan JK, Wapner KL, Hecht PJ (2001) MR imaging findings of entrapment of the flexor hallucis longus tendon. *Am J Roentgenol* **176**, 1145–1148.

Lohman M, Kivisaari A, Vehmas T, Kallio P, Malmivaara A, Kivisaari L (2001) MRI abnormalities of foot and ankle in asymptomatic, physically active individuals. *Skeletal Radiol* **30**, 61–66.

Ly JQ, Bui-Mansfield LT (2004) Anatomy of and abnormalities associated with Kager's fat Pad. *Am J Roentgenol* **182**, 147–154.

Narvaez JA, Narvaez J, Ortega R, Aguilera C, Sanchez A, Andia E (2000) Painful heel: MR imaging findings. *Radiographics* **20**, 333–532.

Peterson DA, Stinson W, Carter J (1993) Bilateral accessory soleus: a report on four patients with partial fasciectomy. *Foot Ankle* **14**, 284–288.

Schneider W, Niehus W, Knahr K (2000) Haglund's syndrome: disappointing results following surgery – a clinical and radiographic analysis. *Foot Ankle Int* **21**, 26–30.

Sella EJ, Caminear DS, McLarney EA (1998) Haglund's syndrome. *J Foot Ankle Surg* **37**, 110–114; discussion 173.

Standring S (2004) *Gray's Anatomy: the Anatomical Basis of Clinical Practice*. Edinburgh: Elsevier/Churchill Livingstone.

B.1.3 The Lubrication Regime of the Contact between Fat and Bone in Bovine Tissue

Theobald, P., Byrne, C., Oldfield, S. F., Dowson, D., Benjamin, M., Dent, C., Pugh, N. and Nokes, L. D. M. The Lubrication Regime of the Contact between Fat and Bone in Bovine Tissue. *Proc Inst Mech Eng [H]*, Submitted for publication.

The Lubrication Regime of the Contact between Fat and Bone in Bovine Tissue

P.Theobald [1*], C.Byrne[1], S.F.Oldfield[2], D.Dowson[1], M.Benjamin[2], C.Dent[1], N.Pugh[1] and L.D.M.Nokes[1]

[1] Institute of Medical Engineering and Medical Physics, Cardiff University, Queens Building, The Parade, PO Box 925, Cardiff, CF24 0YF.

[2] School of Biosciences, Cardiff University, Museum Avenue, PO Box 911, Cardiff CF10 3US.

*Corresponding author: Institute of Medical Engineering and Medical Physics, Cardiff University, Queens Building, The Parade, PO Box 925, Cardiff, CF24 0YF.

Email: TheobaldPS@Cardiff.ac.uk

Abstract:

Fat pads are masses of encapsulated adipose tissue located throughout the human body. Whilst a number of studies describe these soft tissues anatomically, little is known about their biomechanics and surgeons may excise them arthroscopically, if they hinder the visual inspection of the joint or bursa. By measuring the coefficient of friction between - and performing Sommerfeld analysis of - the surfaces approximating the in vivo conjuncture, this contact has been shown to have a coefficient of friction of order 0.01. The system appears to be lubricated hydrodynamically, thus possibly promoting low levels of wear. It is suggested that one of the functions of fat pads associated with subtendinous bursae and synovial joints is to generate a hydrodynamic lubricating layer between the opposing surfaces.

1, Introduction

The coefficient of friction between two mating surfaces is the ratio of the frictional force and the applied load. Three distinct modes of lubrication have previously been identified; boundary, mixed and fluid-film. In boundary lubrication, the coefficient of friction is relatively high - typically about 0.1 - with the layer of lubricant covering the conjoining surfaces being of insufficient thickness to achieve complete surface separation. Thus, wear at the conjuncture is expected. Optimum fluid-film lubrication can yield coefficients of friction as low as 0.001. Synovial fluid typically provides this layer in the synovial joint **[1, 2]**, thus minimal wear is expected at such a conjuncture. The mixed lubrication regime has properties between these two extremes.

Previous studies of friction within biological systems have concentrated on studies of natural and total replacement joints **[3-6]**. The former work has revealed the fundamental nature of the remarkable bearing characteristics of healthy natural synovial joints, while the latter has been dedicated to an effort to decrease wear and thus increase the longevity of prostheses. Related studies have been concerned with efforts to improve the comfort of both clothing **[7, 8]** and grooming **[9, 10]**. Despite the need for information regarding in vivo surface contacts for improving clinical practise and advancing orthopaedic designs, such studies are limited by difficulties associated with ethical considerations, tissue acquisition and manufacturing limitations. While extensive studies of synovial joints **[6, 11, 12]** have been published, little is known about soft tissue lubrication **[12].** There appear to be no previous accounts of the lubrication mechanisms associated with the presence of fat pads both in synovial joints and in subtendinous bursae **[13]**.

Fat pads are masses of adipose tissue that have been given relatively little attention by clinicians, though the significance of Hoffa's pad in the knee in association with knee pain is well documented **[14, 15]**. Some fat pads form compression-resisting devices which may act as effective shock absorbers; others are a prominent feature of synovial joints or subtendinous bursae **[13]**. The former include the heel pad on the plantar surface of the foot which bears approximately 70% of the body weight **[16]** on heel strike and absorbs 90% of the energy generated **[17]**. The latter includes Kager's fat pad, situated in Kager's triangle, between the Achilles tendon, flexor hallucis longus, and the calcaneus. Kager's fat pad is a highly mobile structure which protrudes into the retrocalcaneal bursa on plantarflexion **[18]**, sliding over the periosteal fibrocartilage covering the calcaneus. As its tip has a synovial membrane that secretes

synovial fluid into the bursa, the tribological role of this fat pad is likely to be significant.

The current lack of knowledge of fat pad biomechanics is likely to be a key factor in the decision of many surgeons to excise parts of this tissue if it obscures the arthroscopic view of a synovial joint. Several decades ago, a similar lack of understanding of function lead to what is now widely recognised as an inappropriate excision of knee joint menisci **[19]**. Menisci are now known to have important functions as load-bearing surfaces and the current surgical preference is to preserve rather than to remove them. Thus, the purpose of the present study is to highlight the potential importance of fat pads in the lubrication mechanisms of joints and bursae by estimating their coefficient of friction.

2, Materials and Methods

The fat pad situated immediately proximal to the phalanges was harvested from four skinned bovine legs, 18 months old and obtained fresh from an abattoir. In addition, synovial fluid was aspirated from the medial and lateral sides of the metacarpophalangeal (MCP) joint cavities, using a 20ml gauge syringe and needle. The apparatus, shown diagrammatically in Figure 1, consisted of an aluminium tube (A) (wall thickness 5mm, outer diameter 25mm, length 300mm), pivoted and freely rotating on a pillar with specially modified light bearings and suspended over either a glass or Perspex disc (D).

This apparatus was successfully validated by comparing the positive gradient of the data-points obtained when measuring bovine synovial membrane (Figure 2) to that achieved by Cooke *et al.* **[12]** (dotted line, Figure 2) when examining similar tissue. Both indicative of fluid-film lubrication, the slight offset of the results may be caused by a number of factors, including the viscosity of the synovial fluid – which can vary 4-fold depending upon the health of the joint **[1]**. The coefficient of friction lying predominantly between 0.001-0.01 is further evidence of this lubrication regime, and thus of successful validation **[20, 21]**.

The mean average roughness, Ra, of 4 measurements (Form Talysurf Series 2, Taylor-Hobson Ltd., UK) of each of the surfaces was calculated. The fat pad was then attached to the specimen holder (H) at the end of the arm using Dermabond tissue adhesive (Ethicon Inc., US), before being positioned upon the disc. A counter-balance (M) ensured zero net loading. Excess synovial fluid was used to lubricate the conjunction between the rotating glass/Perspex disc and the fat pad.

The specimen was vertically loaded against the rotating disc in the range 0.5N – 10N. The deflection of the arm promoted by friction between the fat pad and the rotating disc was resisted by a spring (S) of known stiffness (k=0.02N/mm). The in vivo speed of movement of Kager's fat pad was measured in four volunteers using dynamic ultrasound during the gait cycle at a gentle cadence. It was estimated as reaching 15mm/s, and thus the minimum experimental speed that was achievable (16mm/s) was used throughout the current work. Although the maximum experimental speed (140mm/s) almost certainly exceeded the fat pad speed during running, predicted to be approximately two and a half times greater than that during gentle cadence, it was

nevertheless used to increase the range of test conditions. To ensure that high quality data was achieved, the disc was ramped up to the desired speed for approximately 10 seconds, before the arm was allowed to settle. The deflection of the arm was then logged for 10 seconds, with ten readings per second being recorded on a PC via a datalogger (Pico Technology Ltd, UK.). The mean deflection during the recording period was calculated and recorded. The coefficient of friction was then calculated and the results were plotted against the ratio of (sliding speed/load). This ratio is representative of the Sommerfeld number for a given viscosity and geometry. Comparison of the resulting trace against the Stribeck curve (Figure 3) - and the calculated levels of friction against known values – enabled the dominant lubrication regime between the fat pad and bone to be determined.

3, Results:

The results obtained from the fat pad-rotating disc conjunction are summarised in Figures 4-5 for the glass and Perspex discs respectively. These graphs show how the coefficient of friction of the fat pad on the two surfaces depended on the ratio of speed to load and hence upon the Sommerfeld number.

The glass disc results clearly show a positive gradient, indicative of fluid film lubrication. The Perspex disc results displayed in Figure 4 exhibit similar levels of friction coefficient to those obtained with the glass disc. However, the rising trend of the coefficient of friction as the Sommerfeld number was reduced in the lower range of values suggests that the conjunction was encountering some mixed lubrication.

4, Discussion

The values of coefficient of friction presented in Figures 3 and 4 are relatively low and representative of fluid-film lubrication conditions. The presence of this mode of lubrication can be supported by considering 3 different criteria:

(i) Comparison of the shapes of the relationships (i.e. the rising trend) between coefficient of friction and the reduced form of the Sommerfeld number represented by the ratio (sliding speed/load) with the distinct form of Figure 2 is indicative of fluid-film lubrication.

(ii) The majority of the data-points lying within the coefficient of friction range 0.001 - 0.01; it is well recognised that fluid-film lubrication predominates within these boundaries **[20, 21]**.

(iii) Mixed lubrication is also evident – in particular in Figure 5 – which occurs when the fluid film lubrication breaks down at lower speeds and higher loads.

Whilst the well defined positive gradient obtained for the interaction between fat pad and glass shown in Figure 4 clearly reflects hydrodynamic lubrication, comparing Figure 5 with the Stribeck curve indicates that there was a transition from fluid-film to mixed lubrication at lower speeds or higher loads. This characteristic has been reported earlier for synovial joints **[2, 22-25]**. As the hydrodynamic layer broke down at slower speeds, some surface contact was expected between opposing asperities, since the surface roughness of the Perspex (Ra = 0.297μm) was greater than that of

glass (Ra = 0.034μm). Since similar coefficients of friction were detected between fat pad and glass or Perspex, it seems clear that fluid-film lubrication regimes predominated at the contacts with both surfaces. However, it is possible that this mode of lubrication could have developed due to differences in fat pad characteristics rather than the change in the counterface alone **[26]**.

The viscosity of the lubricant, synovial fluid, is significant in determining the lubrication regime. In this study it was assumed that the viscosity of the shear thinning lubricant was constant, since little is known about the variation of synovial fluid viscosity with the high shear rates **[2]** likely to have been encountered in these tests.

It is also well known that temperature affects the viscosity of synovial fluid **[1]**. The experiments reported here were conducted under atmospheric, laboratory conditions, but no attempt was made to measure the temperature in the lubricated conjunction. The mean laboratory temperature of 18°C remained reasonably constant and it is therefore unlikely that changes in ambient temperature would have had a significant effect upon the major features of the results. The problems of measuring the viscosity of synovial fluid have been reported by others **[12, 26]**, but it was felt to be inappropriate to include this parameter in the reduced Sommerfeld number adopted in Figures 4 and 5.

Whilst the area of contact at the experimental conjuncture was similar to that in vivo, the shape of the tissues did vary. Physiologically, the wedged-shape of Kager's fat pad is more likely to encourage the formation of a lubricating layer of synovial fluid

than the shapeless bovine fat pad used experimentally. In contrast, the formation of a hydrodynamic film is likely to have been encouraged experimentally by the flatter profile of the disc in comparison to that of the in-vivo bone geometry. As the magnitude of loading at the physiological conjuncture is unknown, the accuracy of the loading environment applied at the experimental conjuncture is unclear. In addition, whilst the approximation of glass and Perspex to fibrocartilage (the articulating tissue covering the bone) has never been reported, these surfaces have been favourably compared to articular cartilage **[12, 26]**, which is functionally similar. The experiments were carried out under steady rotation of the disc, whilst the more physiologically-correct motion is that of reciprocation. No attempt was been made to introduce oscillation into the disc motion at this stage, but in similar experiments on synovial membrane, disc oscillation was reported to be insignificant **[26]**. Consistent experimental conditions were achieved by controlling the extent of arm deflection through adjustment of the spring position.

Since hydrodynamic lubrication appears to operate in relation to bovine fat pads, it is suggested that the fat itself may be influential in maintaining a hydrodynamic film in vivo. If the present findings can be extrapolated to human fat, then the Kager's fat pad, which protrudes into the synovial fluid-containing retrocalcaneal bursa, may serve to prevent gravity from pooling fluid at the lowest point in the bursa and thus reduce the risk of the contacting surfaces becoming dry. Fat pads may play a role analogous to that of menisci in spreading synovial fluid **[19]**. It should be recalled that a 20% increase in friction has been reported within the knee following meniscectomy **[19, 27, 28]**. Hence, an understanding of the biomechanical properties

of fat pads is important and further studies are planned to explore their frictional and load bearing characteristics.

5, Conclusion

It has been established that both contacts approximating the fat pad-fibrocartilage conjuncture are lubricated hydrodynamically, with a coefficient of friction of about 0.01. These initial results must be viewed with some caution, since they relate to bovine rather than human fat pads. However, they do suggest that a structure such as Kager's fat pad, which has been shown in previous studies to move in and out of the retrocalcaneal bursa according to foot position **[18]**, could play a role analogous to that of the menisci in the knee.

6, Acknowledgements:

We thank Mr Ajay Dhulipalla & Professor Ray Snidle for their assistance in measuring the roughness of the counterface surfaces, and Mr David Hobbs & Mr Alan Griffiths for their technical support.

7, References

1 Cooke, A. F., Dowson, D. and Wright, V. The rheology of synovial fluid and some potential synthetic lubricants for degenerate synovial joints. *Engng Med*, 1978, 7, 66-72.

2 McCutchen, C. W. Why did nature make synovial fluid slimy? *Clin Orthop Relat Res*, 1969, **64**, 18-20.

3 Scholes, S. C., Unsworth, A., Hall, R. M., et al. The effects of material combination and lubricant on the friction of total hip prostheses. *Wear*, 2000, **241** (2), 209-213.

4 Graindorge, S., Ferrandez, W., Jin, Z., et al. Biphasic surface amorphous layer lubrication of articular cartilage. *Med Eng Phys*, 2005, **27** (10), 836-844.

5 Unsworth, A., Dowson, D. and Wright, V. The frictional behaviour of human synovial joints - Part II. Artificial joints. *J Lubric Tech-T ASME*, 1975, **97** (3), 377-382.

6 Weightman, B. O., Paul, I. L., Rose, R. M., et al. A comparative study of total hip replacement prostheses. *J Biomech*, 1973, **6** (3), 299-306.

7 Zhang, M. and Mak, A. F. In vivo friction properties of human skin. *Prosthet Orthot Int*, 1999, **23** (2), 135-141.

8 Kenins Influence of fibre type and moisture on measured fabric-to-skin friction. *Textile Res J*, 1994, **64** (12), 722-728.

9 Bhushan, B., Wei, G. and Haddad, P. Friction and wear studies of human hair and skin. *Wear*, 2005, **259** (7-12), 1012-1021.

10 El-Shimi, A. F. In vivo skin friction measurements. *J Soc Cosmet Chem*, 1977, **28**, 37-51.

11 Jones, E. S. Joint Lubrication. *Lancet*, 1936, **227** (5879), 1043-1045.

12 Cooke, A. F., Dowson, D. and Wright, V. Lubrication of synovial membrane. *Ann Rheum Dis*, 1976, **35** (1), 56-59.

13 Standring, S. *Gray's Anatomy: the Anatomical Basis of Clinical Practice*. 2005, Edinburgh: Elsevier/Churchill Livingstone.

14 Hoffa, A. Influence of adipose tissue with regard to the pathology of the knee joint. *JAMA*, 1904, **43** (795-796),

15 Magi, M., Branca, A., Bucca, C., et al. Hoffa disease. *Ital J Orthop Traumatol*, 1991, **17** (2), 211-216.

16 Jorgensen, U. and Ekstrand, J. Significance of heel pad confinement for the shock absorption at heel strike. *Int J Sports Med*, 1988, **9** (6), 468-473.

17 Cavanagh, P. R. and Lafortune, M. A. Ground reaction forces in distance running. *J Biomech*, 1980, **13** (5), 397-406.

18 Theobald, P., Byrne, C., Oldfield, S. F., et al. The Lubrication Regime of the Contact between Fat and Bone in Bovine Tissue. *Proc Inst Mech Eng [H], Submitted for consideration*,

19 MacConaill, M. A. The function of intra-articular fibrocartilages, with special reference to the knee and inferior radio-ulnar joints. *J Anat*, 1932, **66**, 210-227.

20 Dowson, D. New joints for the Millennium: wear control in total replacement hip joints. *Proc Inst Mech Eng [H]*, 2001, **215** (4), 335-358.

21 O'Kelly, J., Unsworth, A., Dowson, D., et al. A study of the role of synovial fluid and its constituents in the friction and lubrication of human hip joints. *Engng Med*, 1978, 7 (2), 72-83.

22 Forster, H. and Fisher, J. The influence of loading time and lubricant on the friction of articular cartilage. *Proc Inst Mech Eng [H]*, 1996, **210** (2), 109-119.

23 Longfield, M. D., Dowson, D., Walker, P. S., et al. "Boosted lubrication" of human joints by fluid enrichment and entrapment. *Biomed Eng*, 1969, **4** (11), 517-522.

24 Walker, P. S., Dowson, D., Longfield, M. D., et al. "Boosted lubrication" in synovial joints by fluid entrapment and enrichment. *Ann Rheum Dis*, 1968, **27** (6), 512-520.

25 Unsworth, A., Dowson, D. and Wright, V. The frictional behaviour of human synovial joints - Part I. Natural joints. *J Lubric Tech-T ASME*, 1975, **97** (3), 369-376.

26 Cooke, A. F. Lubrication of synovial membrane. 1981, In *Introduction to the Biomechanics of Joints and Joint Replacement* (Ed. D. Dowson and V. Wright), London: Mechanical Engineering Publications Ltd.154-158

27 MacConaill, M. A. Studies in the mechanics of synovial joints II. Displacements on articular surfaces and the significance of saddle joints. *Ir H Med Sci*, 1946, **6**, 223-235.

28 MacConaill, M. A. The movements of bones and joints; the synovial fluid and its assistants. *J Bone Joint Surg Br*, 1950, **32-B** (2), 244-252.

8, Figures:

Figure 1. Diagrammatic representation of apparatus. A= Arm; B= Bearing; D= Rotating disc; H= Specimen holder; M= Counterbalance mass; P= Pillar; S= Spring;
Arrow = Direction of rotation.

Figure 2. Variation of the coefficient of friction of bovine synovial membrane against a Perspex disc in the presence of bovine synovial fluid with reduced Sommerfeld number. The apparatus was successfully validated following comparison of the results to those of Cooke et al. **[12]** (dotted line).

Figure 3. Representation of the Stribeck diagram relating coefficient of friction to Sommerfeld number.

Figure 4. Variation of the coefficient of friction of bovine fat pads against a glass disc in the presence of bovine synovial fluid with reduced Sommerfeld number.

Figure 5. Variation of the coefficient of friction of bovine fat pads against a Perspex disc in the presence of bovine synovial fluid with reduced Sommerfeld number.

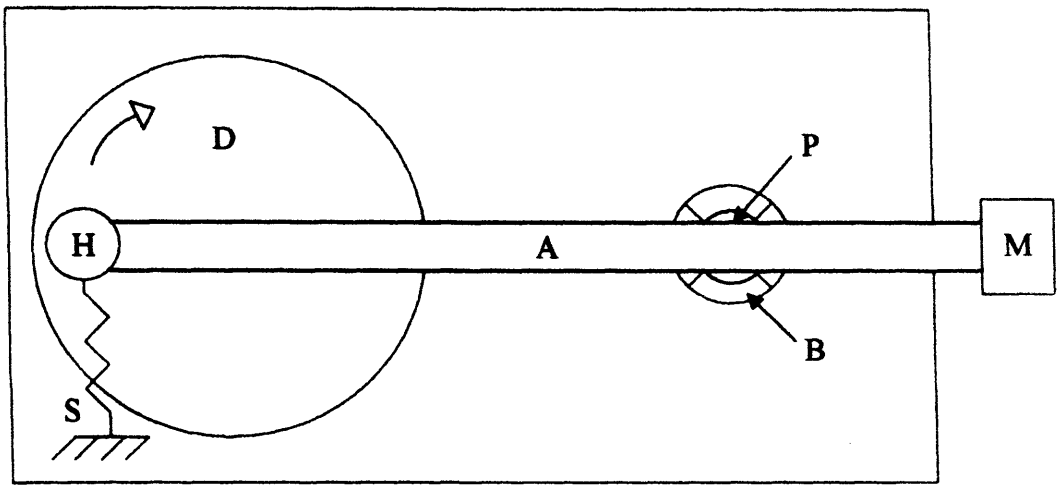
D
P
H
A
M
B
S

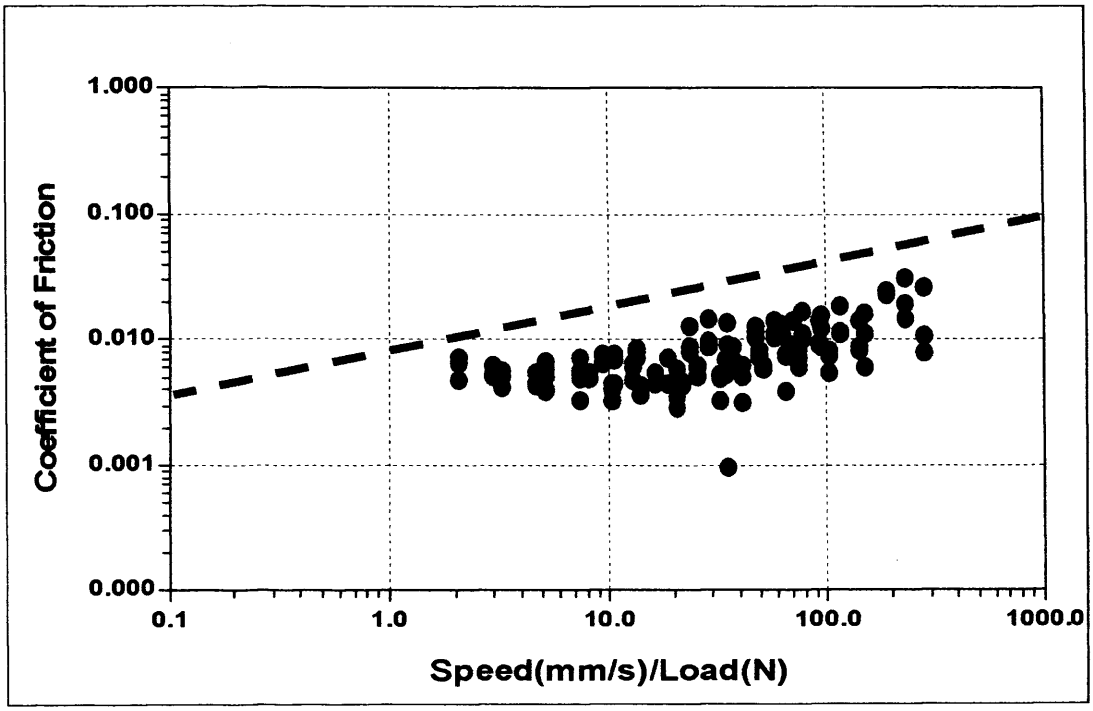
1.000
0.100
0.010
0.001
0.000
Coefficient of Friction
0.1
1.0
10.0
100.0
1000.0
Speed(mm/s)/Load(N)

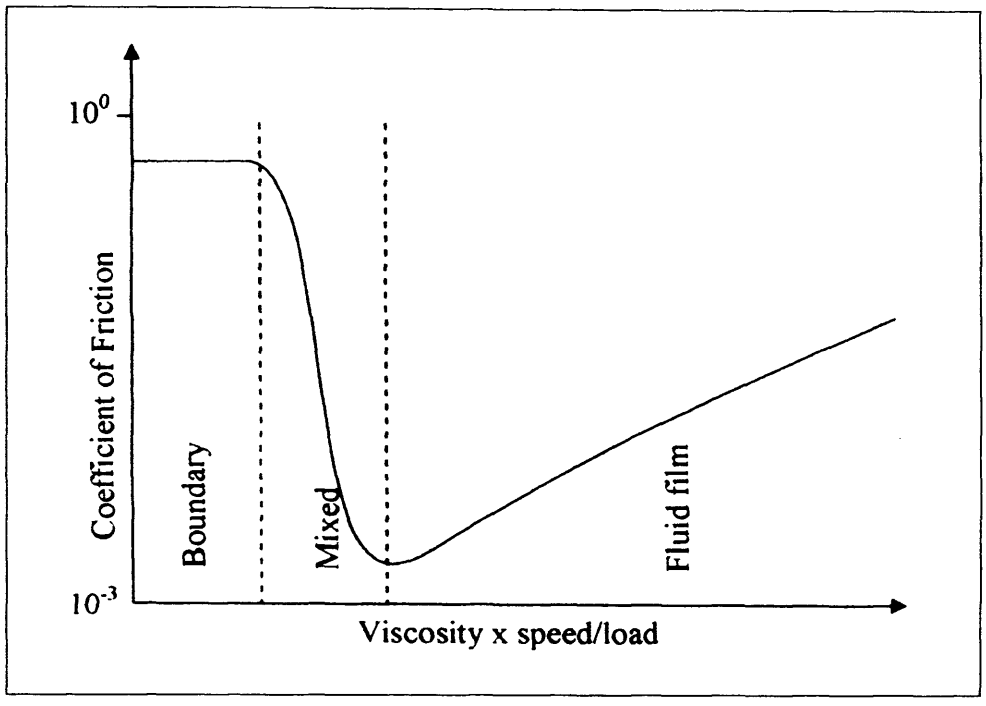
10^0
10^{-3}
Coefficient of Friction
Boundary
Mixed
Fluid film
Viscosity x speed/load

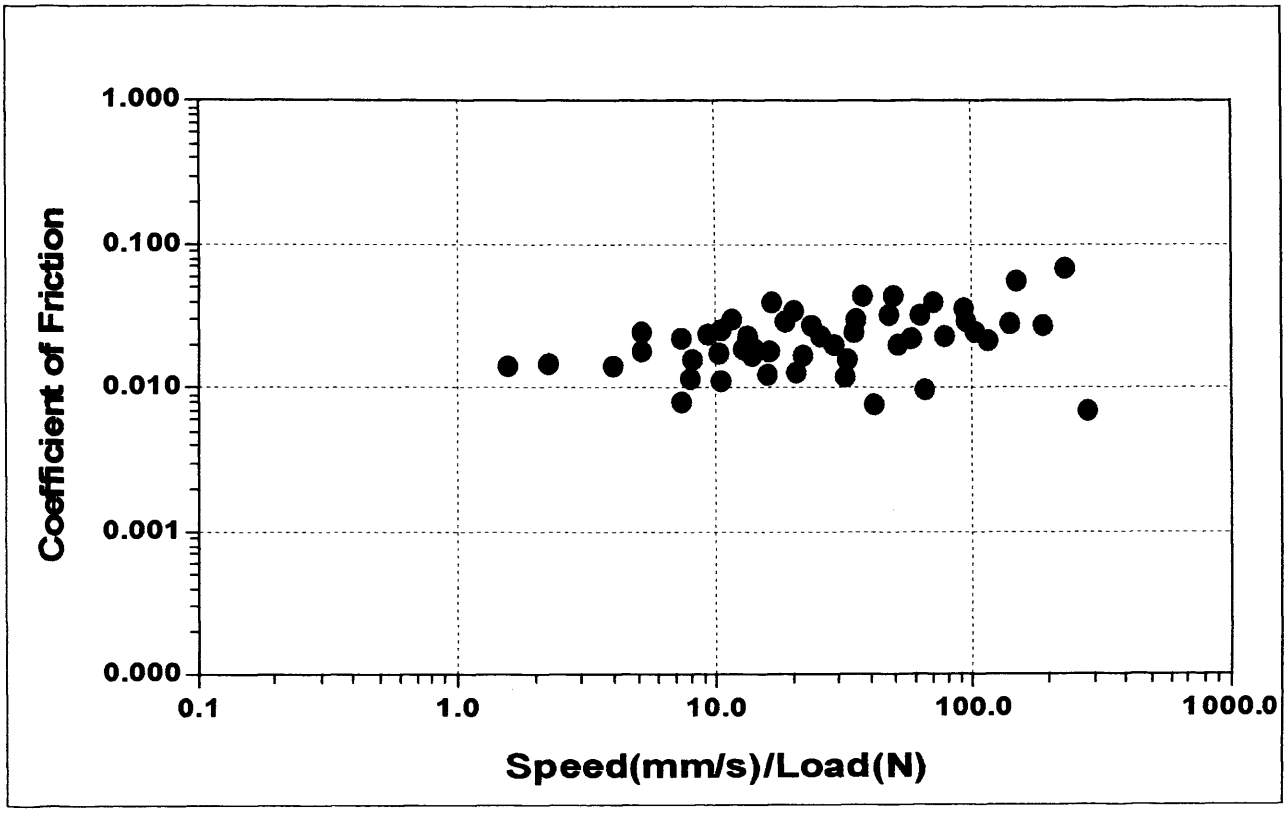
1.000
0.100
0.010
0.001
0.000
Coefficient of Friction
0.1
1.0
10.0
100.0
1000.0
Speed(mm/s)/Load(N)

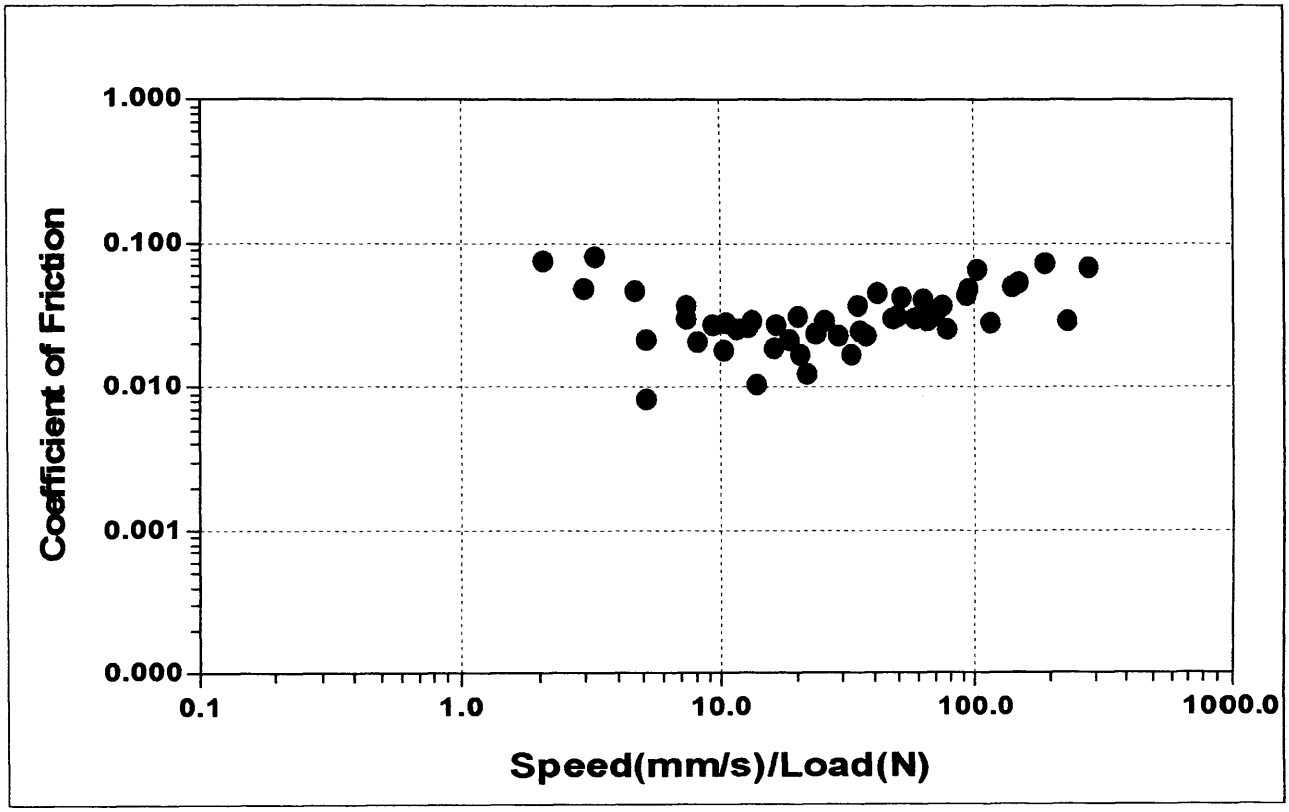
1.000
0.100
0.010
0.001
0.000
Coefficient of Friction
0.1
1.0
10.0
100.0
1000.0
Speed(mm/s)/Load(N)

B.2 Conference Abstracts

B.2.1 Variation in Periosteum Thickness in relation to Tuberosity-Tendon Contact Area

Theobald, P., Benjamin, M., Dent, C. and Nokes, L. Variation in Periosteum Thickness in relation to Tuberosity-Tendon Contact Area. *J Bone Joint Surg Br*, In press.

MEETING OF THE BRITISH ORTHOPAEDIC RESEARCH SOCIETY
THE UNIVERSITY OF MANCHESTER
13-14 SEPTEMBER 2004

Abstract deadline: 1 June 2004

Title Variation in Periosteum Thickness in relation to Tuberosity-Tendon Contact Area

Authors Peter Theobald, Colin Dent, Michael Benjamin, Len Nokes.
Corresponding author Peter Theobald.
Address of corresponding author Cardiff School of Engineering, Cardiff University, Queen's Buildings, PO Box 925, Cardiff, CF24 0YF.

Email address of corresponding author TheobaldPS@Cardiff.ac.uk

Abstract (font Times New Roman 12pt – no paragraphs; justified text; 300 words)

This study aimed to explore the relationship between the geometry of the tuberosity located superior to the Achilles tendon enthesis and the thickness of its fibrocartilaginous periosteum. The tuberosity acts as a pulley for the tendon during dorsiflexion of the foot and is thus compressed by the overlying tendon. This can result in pressure-related injuries which account for a significant number of Achilles-related problems among sportsmen or women. We postulated that variations in the contact area between the tendon and the tuberosity (and consequently the pressure exerted by the tendon) affects the periosteum thickness. Here, we report four methods of portraying the two dimensional geometry of the superior tuberosity. Material was obtained from 10 elderly dissecting room cadavers donated to the Cardiff University for anatomical examination and prepared for routine histology. Serial sagittal sections were collected at 1 mm intervals, and stained with Masson's trichrome, toluidine blue and haematoxylin & eosin. In the first method, the area of the bursal cavity was measured between the deep surface of the tendon and the tuberosity within a 9mm radius of the proximal part of the attachment site. The second technique was similar, though used the long axis of the tendon as a reference, rather than its deep surface. The third technique measured the area of the tuberosity within 20 degrees of the tendon long axis. The final technique measured the cumulative gradient of the first 5 mm of the tuberosity, with reference to the tendon long axis. The periosteum thickness was measured at 500 μm intervals from the proximal part of the enthesis and mean values calculated. A good correlation was seen between all techniques, with the tuberosities having the most localised area of contact with the tendon, showing the thickest periosteum.

B.2.2 The functional significance of Kager's fat pad in relation to the Achilles tendon

Theobald, P., Bydder, G., Nokes, L., Pugh, N. and Benjamin, M. The functional significance of Kager's fat pad in relation to the Achilles tendon. *J Anat*, 2006, **208** (3), 407-408.

(vastus medialis – VM, vastus lateralis – VL, rectus femoris – RF, semitendinosus/semimembranosus – ST/SM, biceps femoris – BF and tensor fasciae latae – TFL) were recorded using surface electromyography. MVCs were 157 ± 47 Nm for knee extension, 84 ± 35 Nm for flexion, 11 ± 3 Nm for lateral rotation, and 8 ± 1 Nm for medial rotation. Compared with slow isokinetic strengths of the nonsurgical knee of male tendon transfer patients (Osternig et al. *Arch.Phys. Medical Rehab.* 62, 1981), the female subjects had strengths that were 97% (flexion), 63% (extension), 24% (lateral rotation) and 21% (medial rotation). The relatively weak knee rotatory muscles could be a factor that contributes to the high incidence of noncontact knee ligament injuries in female sports. At 50% MVC, the muscles that were most active during single degree of freedom tasks were VM (ext. 40% Max EMG), VL (ext. 45% Max EMG) and BF (flex. 55% Max EMG), while others were most active during dual degree of freedom tasks; RF (ext. + lat. rot. 55% Max EMG), ST/SM (flex. + med. rot. 70% Max EMG) and TFL (ext. + lat. rot. 30% Max EMG). Generally, levels of muscle activation increased when isolated flexion-extension oscillating tasks were performed, in comparison to the static isometric tasks. However, activity levels tended to decrease during oscillating 2-degree of freedom tasks, such as oscillating lateral/medial rotation with a constant extension or flexion torque.

P5

The effect of mechanical strain on hyaluronan metabolism in synovial cells from osteoarthritic knees

R. Williams, G. P. Dowthwaite, A. S. Williams and C. Archer

School of Biosciences, Cardiff University, UK

During osteoarthritis friction-free articulation of the joint is reduced leading to a loss of mechanical stimuli as the joint becomes painful to move. An important component of the synovial fluid within the joint cavity is hyaluronan which acts as a lubricating molecule and helps to maintain a constant synovial fluid volume. Previously, differential hyaluronan synthesis at the presumptive joint line has been shown to be mediated by mechanical stimuli and it is likely that continued mechanical stimuli and subsequent HA synthesis is required to maintain friction-free articulation of the joint. Indeed, a number of studies have already highlighted the benefits of combined walking, aerobic and muscle strengthening exercise in improving the flexibility of the joint and in reducing joint pain. The synovium and synovial fluid from OA knees show alterations in HA synthesis and decreases in HA concentration respectively which could be a result of the loss of mechanical stimuli. Thus this study aimed to examine the *in vitro* effects of mechanical stimuli on synovial cells from osteoarthritic human knees to try and understand their response to short periods of mechanical stimuli in terms of media HA concentration and differential *HAS* gene expression.

Cells were subjected to 10 min of strain using a 4-point bending mechanical loading jig to apply a defined and controlled mechanical stimulus to the cells. The physiological strain of 4000με increased media HA concentrations 24 h post strain whereas a higher strain of 6000με did not maintain increased media HA concentrations. QPCR data showed significant increases in all 3 *HAS* gene mRNA expression 24 h post strain.

The data from this study demonstrates an important role for mechanical stimuli in generating the necessary signals to synthesise HA in OA synovial cells. These data suggest that the development of exercise based therapies engendering defined physiological strains could prove beneficial in the non-invasive treatment of OA.

P6

A re-investigation of the clinical anatomy of the iliotibial tract

K. Hayashi,[1] H. Toumi,[1] M. Benjamin,[1] G. Bydder[2] and J. Fairclough[3]

[1]*School of Biosciences and* [3]*Department of Orthopaedics, Cardiff University, UK; and* [2]*Department of Radiology, University of California San Diego, USA*

Iliotibial band (ITB) syndrome is a common cause of knee pain, particularly among runners and cyclists. It is viewed as an overuse injury caused by repetitive friction of the iliotibial tract (ITT) as it 'rolls over' the lateral femoral epicondyle during knee flexion and extension. Here, we reinvestigate ITT anatomy and propose an alternative theory. Gross anatomical observations, both on dissecting room cadavers and on the knees of younger individuals at surgery, together with magnetic resonance imaging studies have demonstrated the universal presence of strong fibrous connections that pass from the ITT, through a layer of fat to the lateral aspect of the femur – including the epicondyle. This conflicts with the view that any fibrous links are pathological adhesions between the ITT and the femur. Histological studies showed that the fibrous tissue both attached to and traversed the periosteum, and that the epicondyle was covered by fibrocartilage. As the ITT is not a discrete structure, but a region of increased tension in the fascia lata that is anchored to the femur as well as the tibia, we suggest that it cannot roll over the epicondyle. It creates the illusion of doing so, because stress levels shift between anterior and posterior fibres during knee flexion and extension. Our finding that a bursa was absent between the ITT and the epicondyle in all knees is in line with our theory and challenges the suggestion that oedema in individuals with ITB syndome necessarily indicates an inflamed bursa. We suggest that ITB syndrome has more in common with enthesopathies and may be associated with degenerative change at a fibrous connection between the ITT and the femur. Our findings also challenge the concept that the ITT can be stretched along its length from tensor fasciae latae to Gerdy's tubercle. Part of the stretching load must be dissipated through the fibrous links.

P7

The functional significance of Kager's fat pad in relation to the Achilles tendon

P. Theobald[1], G. Bydder[2], L. Nokes[1], N. Pugh[3] and M. Benjamin[4]

[1]*School of Engineering, Cardiff University, UK;* [2]*Department of Radiology, University of California, San Diego, USA; and* [3]*Department of Medical Physics and* [4]*School of Biosciences, Cardiff University, UK*

Kager's (pre-Achilles) fat pad is a prominent mass of adipose tissue lying anterior to the distal portion of the Achilles tendon. Proximally

it relates to the region where the tendon is commonly ruptured and distally it protrudes into the retrocalcaneal bursa. This is a region implicated in insertional tendinopathies. We report the findings of an anatomical, magnetic resonance imaging and ultrasound study which lead us to suggest that the fat pad has a mechanical role in protecting the Achilles tendon and its blood supply from injury. Ultrasound studies show that the fat pad is moved passively during plantarflexion and dorsiflexion of the foot by the muscular contractions of flexor hallucis longus (FHL): the movement is most obvious during weight-bearing. By recording ultrasound movies, we have detected a J-shaped line of force transmission through the fat pad, which allows contractions of the muscle belly of FHL to drive fat distally into the retrocalcaneal bursa during plantarflexion. Lateral movements of Kager's pad are minimised by the deep fascia but distal movements are promoted by the wedge-shaped, fibrous tip of the pad with its deep synovial infolds. As the plantarflexed foot returns to the anatomical position, the fatty wedge is retracted from the bursa. The deep fascia plays an important role in limiting lateral movements of the fat pad (but maximising distal movements), and fibrous connections linking the fat to the Achilles tendon, anchor and stabilise the fat more proximally. We suggest that the mobility of the wedge-shaped tip of Kager's pad reduces kinking of the Achilles tendon during plantarflexion of the foot and that the relative stability of the more proximal fat, protects the blood vessels coursing through it to supply the Achilles tendon.

P8

Metaplastic skeletal development: an unusual example from *Alligator mississippiensis* (Crocodylia, Reptilia)

M. K. Vickaryous and B. K. Hall

Department of Biology, Dalhousie University, Halifax, Canada

The direct transformation of one tissue type into another – metaplasia – is an uncommon mode of skeletogenesis under normal (non-pathological) circumstances. As part of a larger study on the evolutionary developmental biology of the amniote exoskeleton (dermoskeleton), we investigated the development of skeletal plates (osteoderms) within the dermis of *Alligator mississippiensis*. Osteoderm development is considerably delayed compared with the rest of the skeleton. Prior to osteoderm formation, the dermis is already well structured. Towards the hypodermis, large bundles of collagen form orthogonal or herring bone horizons that demonstrate strong positive reactions for various connective tissue stains, albeit not Alcian blue. Towards the epidermis, the collagen bundles are thinner, more poorly stratified, and stain less intensely. Incipient centres of ossification develop within the keels, dorsal to the thick collagen network, beginning around one year in age. Incipient osteoderms do not demonstrate a regular periosteum, nor is there any sign of osteoid or cartilage. Compared with other dermal elements there are relatively few skeletogenic cells, most of which resemble fibroblasts (fusiform morphology). Osteoderms also demonstrate Sharpey-like fibres, suggesting the incorporation of preexisting collagen matrix of dermis into the mineralization front. The unusual pattern of osteoderm development is best characterized as tissue metaplasia.

This work was supported by a Jurassic Foundation Grant to MKV and an NSERC Operating Grant to BKH.

P9

Sulfasalazine results in the formation of immature neutrophil leucocytes in patients with rheumatoid arthritis

J. M. Delieu,[1] D. E. Bax[2] and R. W. Horobin[3]

[1]School of Radiography, University of Wales, Bangor; [2]Dept of Rheumatology, Royal Hallamshire Hospital, Sheffield; and [3]Division of Neuroscience and Biomedical Systems, Institute of Biomedical and Life Sciences, Glasgow University, UK

This investigation evaluated the sub-clinical abnormality of increased numbers of immature neutrophils observed in patients with rheumatoid arthritis treated with enteric coated sulfasalazine. Neutrophil maturity of patients and controls was compared, by determining mean nuclear lobularity in peripheral blood smears. Immaturity was defined as a decreased nuclear lobation. White blood cell and neutrophil counts were also made. Subjects were patients medicated with sulfasalazine ($n = 27$). Controls ($n = 20$) were healthy, non-medicated clinical and academic staff. Determination of mean lobe number involved assessment of 300 neutrophils per individual. For subject and control groups, means of mean lobe numbers, mean white cell and neutrophil counts were determined. Means for each group were compared using the Mann–Whitney U test; variances using F ratios. Means of mean of lobe numbers of the patient population were significantly different ($P < 0.0001$) from controls. 89% of patients had mean lobe numbers below the control range, but total white cell and neutrophil counts in patients and controls did not differ significantly. Thus patients medicated with sulfasalazine typically have increased immature neutrophils, but have normal white cell and neutrophil counts compared with controls. For one patient, mean lobe numbers were obtained before and after sulfasalazine medication commenced, and the mean lobe number decreased with treatment. Consequently this effect is probably drug-induced. The mean lobe number is used here as a measure of a patients response to such drug-induced sulfasalazine treatment and possible toxicity.

P10

The distribution of cell clusters related to developing chick spinal and cranial nerve roots

O. O'Donoghue, P. Dockery and J. Fraher

Department of Anatomy, BioSciences Institute, University College Cork, Ireland

Previous studies investigated cellular relationships of the presumptive motor exit points (MEP) and sensory entry zones (SEZ) of both spinal and cranial nerves of the developing rat neural tube (O'Donoghue et al. *Journal of Anatomy* 4, 2004; *Int J Develop Neurosci* 22, 2004). They showed that presumptive MEPs are not prefigured by the presence of any cells apposed to the presumptive glia limitans. In this they differ from presumptive SEZs, at which cell clusters (Boundary Caps) are found, apposed to the glia limitans. These cells have possible roles in the guidance and segregation of centripetal dorsal rootlet axons (Golding & Cohen, *Mol Cell Neurosci* 9, 1997; Niederländer & Lumsden, *Development* 122, 1976).

This study examines corresponding areas of the developing chick neural tube. Transverse semithin sections of E2 to E4 chick neural tubes

B.3 Book Chapters

B.3.1 The Anatomy of the Achilles Tendon.

Benjamin, M., Theobald, P., Suzuki, D. and Toumi, H. The anatomy of the Achilles tendon. In Press, In *The Achilles tendon* (Ed. N. Maffulli and L. Almekinders), New York: Springer -Verlag.

The anatomy of the Achilles tendon

M Benjamin

P Theobald

D Suzuki

H Toumi

School of Biosciences, Cardiff University, Museum Avenue, Cardiff CF10 3US, UK

Correspondence to Professor M Benjamin School of Biosciences, Cardiff University, Museum Avenue, Cardiff CF10 3US, UK

Email: Benjamin@cardiff.ac.uk

Tel/Fax +44 (0)29 20875041

Acknowledgements: The work of Dr D Suzuki was supported by grants from the ITOH foundation and Sapporo Medical University Academic Foundation, Japan

INTRODUCTORY COMMENTS

The Achilles tendon (tendo calcaneus) is the strongest and thickest tendon in the body and serves to attach the triceps surae (soleus and the two heads of gastrocnemius) to the calcaneus (Fig. 1). It is a highly characteristic feature of Man's anatomy and it has even been suggested that the tendon has helped to shape human evolution. Bramble & Liebermann (1) have argued that the emergence of Man is critically linked to his ability to run and that his unique combination of moderate speed and exceptional endurance has been underestimated. They view the Achilles tendon as having been a "key player" in the natural selection process and hypothesize that as in modern apes, an Achilles tendon was absent from *Australopithecus* (a genus widely recognized as ancestral to the genus *Homo*) and probably originated in *Homo* more than 3 Myr ago.

Several unique functional demands are placed upon the Achilles tendon which adds to its vulnerability to injury.

1. The upright stance of Man dictates that the foot is at right angle to the leg in the anatomical position and that the Achilles tendon approaches the back of the foot tangentially and generates heavy torque. Man thus has one of largest angles between the long axis of the tibia and the calcaneus in any mammal.

2. The muscles contributing to the formation of the tendon have different functions and different physiological properties. Soleus plantar flexes the ankle joint and contains a high proportion of type I (slow-twitch) fibers which facilitates its role as a postural muscle, preventing the body from falling forwards when standing (2). However, gastrocnemius also flexes the knee joint and contains a greater number of type IIB fibers (fast twitch). These promote the vigorous propulsive movements that occur in sprinting and jumping.

3. As the Achilles tendon attaches to the calcaneus, it acts on the subtalar as well as the knee and ankle joints. Because the axis of the subtalar joint typically passes upwards and medially from the posterolateral corner of the calcaneus (3), the triceps surae also supinates the foot (4). Thus stress concentration between the medial and lateral sides of the Achilles tendon enthesis can be non-uniform.

4. The rotation of the limb bud that occurs during development, means that the adult Achilles tendon is twisted upon itself, so that the fibers derived from gastrocnemius are attached to the lateral part of the calcaneal insertion site and those derived from soleus are attached medially (5,6). Thus, when the tendon is under load, it is subject to a "wringing" action. Because gastrocnemius crosses the knee joint and a flexed knee can rotate, the part of the Achilles tendon which is derived from the tendon of gastrocnemius can be variably twisted relative to the tendon of soleus – i.e. the one tendon can exert a sawing action on the other (4). This complex rotatory action is further compounded by

the shape of the talus. This shape such that there is a subtle change in the position of the axis of the ankle joint relative to the Achilles tendon during dorsi- and plantar flexion. Slight passive rotation occurs (7).

5. Finally, the Achilles tendon transmits forces that are approximately seven times the body weight during running (8). This represents an enormous increase on the forces which act during standing (which are roughly half the body weight ; 8).

GROSS ANATOMY

The formation of the Achilles tendon from the gastrocnemius and soleus muscles has been described in detail by Cummins et al. (6). The medial and lateral heads of gastrocnemius arise from the femoral condyles and their contribution to the Achilles tendon commences as a wide aponeurosis at the lower ends of these muscular bellies (Fig 1a). In 2.9-5.5% of people, there is a third head of gastrocnemius, most commonly associated with the medial head (9). Occasionally plantaris can effectively form a third head – i.e. when it joins gastrocnemius at the point of convergence of its medial and lateral heads (9). It should also be noted that lateral head of gastrocnemius can sometimes be reduced to a fibrous cord (9).

Soleus arises entirely below the knee, largely from the tibia and fibula and its tendinous contribution to the Achilles is thicker but shorter (6). Occasionally the tibial "head" of soleus can be absent or an accessory soleus muscle present between the soleus tendon and flexor hallucis longus (9). An accessory soleus can contribute

to the formation of the Achilles tendon, attach independently on the calcaneus or fuse with the medial collateral ligament of the ankle joint (9). Typically, a broad sheet of connective tissue begins on the posterior surface of the soleus muscle belly, at a position more proximal than the start of the aponeurosis of gastrocnemius (Fig 1h). Consequently, where the soleus and gastrocnemius muscle bellies are in contact with each other (i.e. are subject to mutual pressure), the two bellies are separated by dense fibrous connective tissue on the surface of the muscles (Fig 1h) and by a thin film of loose connective tissue between them. There is a similar arrangement in quadriceps femoris, where the anterior surface of vastus intermedius is aponeurotic and overlain by rectus femoris – but separated from it by areolar connective tissue. Such a tissue probably promotes independent movement.

The sheet of connective tissue on the posterior surface of soleus is attached to the gastrocnemius aponeurosis by fascia at a variable point near the middle of the calf (Fig 1h). The combined aponeurosis continues to run distally over the posterior surface of soleus, receiving further tendinous contributions from the muscle as it descends. In addition, there is a narrow intramuscular tendon within soleus (promoting a bipennate arrangement of muscle fibers) which merges with the principal tendon distally (10; Fig 1g). Typically, full incorporation of the soleus and gastrocnemius tendons into the Achilles is evident 8-10 cm above the calcaneal attachment site, but occasionally the tendon of soleus can remain separate from that of gastrocnemius as far as the insertion itself (11). Sometimes, the two heads of gastrocnemius remain separate and the tendons which arise from them attach independently (both from each other and from the tendon of soleus) on the calcaneus (9). Such anatomical variations can give a false impression of a pathologically-

thickened Achilles tendon. When viewed from behind, a typical soleus muscle belly is covered proximally by gastrocnemius, but distally it protrudes either side of the tendon of gastrocnemius, making this a convenient site for biopsy or electromyography (10).

As the tendon fibers derived from gastrocnemius descend, they converge so that the Achilles tendon narrows. However, the fibers also rotate around those of soleus, so that they ultimately come to be attached to the calcaneus laterally, whereas those of soleus (which also rotate) attach more medially (6). The degree of rotation is variable, so that in addition to contributing to the lateral part of the calcaneal attachment site in all individuals, the gastrocnemius tendon contributes to its posterior part in some people and to its anterior part in others (6). This rotation becomes more obvious in the terminal 5 - 6 cm of the tendon (Fig 1j). Where the twisting of the tendon is marked, it is easier to trace the individual contributions of the soleus and gastrocnemius tendons to the Achilles tendon than it is where rotation is slight (4). The spiralling of the tendon fascicles results in less fibre buckling when the tendon is lax and less deformation when the tendon is under tension. This reduces both fibre distortion and inter-fibre friction (12).

A variable proportion of the superficial fibers of the Achilles tendon do not attach to the calcaneus at all, but pass under the heel to become continuous with the fibers of the plantar fascia. Such soft tissue continuity is particularly marked in younger individuals (13) and is in line with a general principle that relatively few tendons attach to bone in isolation – most fuse with adjacent structures or attach at more than a single site, so as to dissipate stress concentration (14). Myers (15) has greatly

expanded on the related concept of myofascial continuities via an endless fascial "web" in the body, in his intriguing book "Anatomy Trains".

The shape of the Achilles tendon varies considerably from proximal to distal and the changes are illustrated in Fig. 1b-f. As with many tendons elsewhere in the body, the Achilles tendon flares out as it nears its bony attachment site and this contributes to the marked anterior-posterior flattening, and slight anterior concavity of the tendon, that is evident at the level of its enthesis (Fig. 1f). These features are also seen radiologically (11). Typically, the distal part of the tendon does not exceed 7 mm in thickness and anything greater than that is suggestive of pathology (16). At the insertion site itself, where the tendon is extremely flattened, it is approximately 3 cm wide and 2-3 mm thick (17).

The Achilles tendon lacks a true synovial tendon sheath but has a false sheath or "paratenon" (Fig 2a) that forms an elastic sleeve permitting the tendon to glide relative to adjacent structures (18). The paratenon essentially consists of several closely-packed, membranous sheets of dense connective tissue that separate the tendon itself from the deep fascia of the leg. It is rich in blood vessels and nerves and together with the epitenon which adheres to the surface of the tendon itself, it is sometimes referred to as the peritenon. According to Myerson et al. (19), it can stretch 2-3 cm as the tendon moves.

Relationships: The deep fascia of the leg is immediately superficial to the sheath of the Achilles tendon (Fig 1j), fuses with the tendon sheath near the calcaneus and serves as an unheralded retinaculum for the tendon. It thus contributes to the

slight anterior curvature of the tendon (20,21) and prevents the tendon from bowstringing in a plantar flexed foot. We thus suggest that it plays an important role in minimizing insertional angle changes that occur at the enthesis during foot movements. This in turn reduces wear and tear.

The sural nerve lies in close contact with the Achilles tendon sheath (Fig 1a,j) and commonly crosses its lateral border approximately 10 cm above the tendon enthesis (22). The vestigial muscle belly of plantaris arises adjacent to the lateral head of gastrocnemius and its long tendon runs along the medial side of the Achilles tendon to end in a variable fashion. Usually, it attaches to the calcaneus on the medial side of the Achilles tendon (47% of cases according to Cummins et al. 6), but in 36.5% of the 200 specimens with a plantaris tendon examined by these authors, the tendon inserts slightly anterior to the medial aspect of the Achilles. Intriguingly, in such individuals, the enthesis of the plantaris tendon serve to support the anteromedial part of the retrocalcaneal bursa. In the third variation of the plantaris insertion reported in 12.5% of cases by Cummins et al. (6), the tendon fans out distally to invest the posterior and medial aspects of the Achilles tendon. Finally, in 4% of individuals, the plantaris tendon fuses with the Achilles tendon proximal to the calcaneal attachment site of the latter (6).

Near its calcaneal insertion site, the Achilles tendon is flanked by two bursae (23). There is a superficial bursa between the skin and the tendon which promotes skin movement and a deep (retrocalcaneal) bursa between the tendon and the superior calcaneal tuberosity that promotes tendon movement (Fig 1i). Protruding into the retrocalcaneal bursa is a wedge-shaped, fatty, synovial-covered fold that represents

the distal tip of Kager's fat pad, a mass of adipose tissue between flexor hallucis longus muscle and the Achilles tendon (Fig 1i). Intriguingly, the relative size of this fat pad differs between the foot of the newborn child and the adult (24), though the significance of this is unclear. Latex molds of the bursa show that it is disc-shaped and has two extensions ("legs") that are directed proximally (see Fig. 4 in 24). It is molded over the posterosuperior surface of the calcaneus, like a cap with an anterior concavity (24). A healthy bursa has a smooth outline and 1-1.5 ml of contrast medium can be injected into it (24). However, leakage of contrast material over time into the superficial bursa suggests that the bursae communicate with each other (24). The magnetic resonance imaging (MRI) studies of Bottger et al (25) also confirm that the retrocalcaneal bursa normally contains fluid which gives a high-signal-intensity. The aspiration studies of Canoso et al. (26) show that the bursa is filled with a clear, viscous fluid and MRI studies by the same group (27) have lead to the suggestion that in a healthy individual, the tip of Kager's fat pad moves in and out of the bursa in plantar and dorsiflexion respectively. This has been confirmed by ultrasound (M Benjamin, P Theobald, L Nokes and N Pugh unpublished observations). Canoso et al. (27) have suggested that this may influence the insertional angle of the Achilles tendon in different foot positions. Although the retrocalcaneal bursa is enlarged in symptomatic patients, paradoxically, less contrast material can be injected into it (23).

Blood supply: The Achilles tendon receives a blood supply from vessels running in the paratenon which are largely derived from the posterior tibial artery (12, 28, 29). The vessels enter the tendon via a structure that is comparable to a mesotenon (4). The mid region of the tendon is the most poorly vascularized and this may contribute to the vulnerability of the tendon to rupture, 2-6 cm above the calcaneus. The proximal

part of the tendon receives an additional supply from the muscle bellies that continues into the tendon via the endotenon, though this contribution is not believed to be significant (12, 30-32). The distal region of the tendon also receives vessels from an arterial periosteal plexus on the posterior aspect of the calcaneus (33). This supply starts at the margin of the insertion and extends up the endotenon for approximately 2cm proximally (12, 30, 32, 34). It is pertinent to note that a healthy fibrocartilaginous enthesis is avascular so that vessels do not normally pass directly from bone to tendon at the osteotendinous junction (35, 36).

Innervation: There is no single comprehensive study of the innervation of the Achilles tendon from its myotendinous junction to its enthesis. Nevertheless, the sensory nerve supply of the tendon and its sheath is of nociceptive and proprioceptive significance. The integrity of the nerve supply to the tendon may also play a key role in promoting its repair as peripheral denervation in rats reduces the load to failure of healing, transected Achilles tendons by 50% within two weeks (37).

The Achilles tendon is supplied by sensory nerves from the contributing muscles and via twigs from neighboring cutaneous nerves, notably the sural nerve (38). The paratenon is more richly innervated than the tendon itself and according to Lang (39) it contains Pacinian corpuscles, which are presumably important in proprioception. Both Golgi tendon organs and muscle spindles have been demonstrated in association with the Achilles tendon of the cat (40). The former lie in the muscle itself, close to the myotendinous junction, but the latter are located more distally in the tendon.

According to Ackermann et al. (41), there is an opioid system in the rat Achilles tendon that may contribute to a peripheral inhibition of pain. Some of the sensory nerves (probably C fibers) immunolabel for the delta opioid receptor (DOR). Labeling is largely restricted to the endotenon and epitenon, where it typically occurs in association with blood vessels, and to the paratenon, where a vascular association is less obvious. The DOR labeling co-localizes with that for enkephalins, suggesting that the latter act as receptors. Ackermann et al. (41) have suggested that enkephalins acting on DOR inhibit the nociceptive action and the pro-inflammatory response of sensory neuropeptides. The authors raise the possibility that there is normally a fine balance between the expression of opioids in muscle-tendon units and the expression of sensory neuropeptides that could change with tendon pathology.

It is difficult to reconcile what we know of the innervation of the Achilles tendon with the pain associated with tendinopathy. Fenwick et al. (42) have made the interesting suggestion that tendon pain may be linked to vascular changes. A common feature of tendinopathy is the proliferation of blood vessels either in the tendon itself or its sheath (43-45) and injured tendons may show an ischaemic response (42).

STRUCTURE OF THE TENDON MIDSUBSTANCE

As with all tendons, the Achilles tendon is dominated by type I collagen which accounts for its considerable tensile strength (46). According to Viidik (47) and Williams et al. (10), this is of the order of 50-100N/mm. However, this may well be an underestimate because of the general difficulty of clamping tendons, which by

their very nature consist of large numbers of partly independent fibers (49). The type I collagen is organized into heterotypic fibrils in association with types III and V collagens (46) and these minor collagens play a role in regulating fibril diameter (48). Western blot analyses of Achilles tendons from elderly individuals, show that the β and γ forms of type I collagen are conspicuous – probably reflecting the increased formation of cross links with age (46).

The type I collagen fibrils are grouped successively into fibers, fiber bundles and fascicles, so that a tendon is analogous to a multistranded cable (49). It is important to recognize that individual fibrils do not run the length of a tendon and thus stress must be transferred between them (49). This is a function of the amorphous matrix in which the fibrils are embedded and it has been suggested that type VI collagen (a non-fibrillar collagen) and decorin (a leucine-rich repeat proteoglycan) are important. Both these molecules, along with fibromodulin, biglycan, lumican and versican are present in the Achilles tendon (46) and have a relatively high turnover (50).

It is a feature of tendons in general that the fibrils within them run a wavy course i.e. are "crimped" with an axial periodicity of approximately 100 μm (49). Such "pre-buckling" is thought to contribute to their flexibility along with the partial independence of fibrils and fascicles that derives from the low compressive stiffness of the extracellular matrix (49). Of key importance here is the endotenon that separates adjacent fascicles and is continuous with the epitenon on the surface of the tendon. The endotenon forms vascularized and innervated layers of loose connective tissue that promote independent movement between fascicles.

The cells in the mid-substance of the Achilles tendon are fibroblasts which are arranged in longitudinal rows and have a highly complex shape. In the mid-substance of tendons, there are a number of broad, flat cell processes which extend laterally from the cell bodies and partition the collagen fibers into bundles (51). There are also more elongated and thinner cell processes that extend longitudinally within a tendon. In both cases, where processes of adjacent tendon cells meet, the cells communicate by means of gap junctions (51). Communication is established between cells both within rows and between rows. Consequently, there is a 3-dimensional network of interlinking cell processes in the Achilles tendon that is ever bit as impressive as the better known network of osteocytic cell processes permeating the extracellular matrix (ECM) of bone. Gap junctional communication (involving connexins 32 and 43) could form the basis for a co-coordinated response of tendon cells to mechanical load (51). Connexin 32 junctions occur predominantly between cells within a row (and is thus along the lines of principal tensile loading), while gap junctions characterized by connexin 43 link cells between rows as well (51). Waggett et al. (52) have thus suggested that the two different gap junctions have distinctive roles in ECM synthesis when tendon cells are subject to mechanical loading. They have shown that connexin 43 gap junctional communication inhibits collagen synthesis whereas that involving connexin 32 is stimulatory.

THE ENTHESIS AND THE ENTHESIS ORGAN:

The Achilles tendon attaches to a rectangular area in the middle third of the posterior surface of the calcaneus – with a greater surface area of the tendon attached medially than laterally (53). According to Kolodziej et al. (54), the average height of the insertion (i.e. the distance between the superior and inferior limits of the tendon attachment) is 19.8 mm, and the average width is 23.8 mm superiorly and 31.2 mm inferiorly. Thus, the tendon flares out considerably at its enthesis, dissipating the region of stress concentration. Although it is unlikely that the increased surface area of the tendon at this site is associated with a greater number of collagen fibres, the nature of the packing tissue has not been firmly established. In other tendons, fat accumulation near the osteotendinous junction is an important contributory factor (55).

As with other tendons in the body, the direction in which the Achilles tendon approaches its insertion site is kept relatively constant in different positions of the foot and leg. When the foot is dorsiflexed, the superior tuberosity of the calcaneus (Fig 2a) acts as a guiding pulley, but during plantar flexion, simple inspection suggests that it is the deep crural fascia which must primarily be responsible for controlling the insertional angle (4). It is in connection with pronation and supination movements of the calcaneus, that comparable guiding control mechanisms for maintaining constancy of bone-tendon position are less obvious. Although continuity of the crural fascia with the periosteum on the medial and lateral aspects of the calcaneus is likely to be a factor, the fibrocartilagous nature of the enthesis is probably also important. The "enthesis fibrocartilage" (Fig 2a-c) balances the differing elastic moduli of the tendon

and bone and reduces stress concentration at the insertion site (56). Effectively, it stiffens the tendon at the hard-soft tissue interface and plays a role analogous to that of a grommet where a lead joins an electrical plug (57). It ensures that any bending of the collagen fibres of the tendon is not all concentrated at the hard-soft tissue interface, but is gradually dissipated into the tendon itself, reducing the risk of wear and tear.

It is important however to recognize that the task of reducing stress concentration at the Achilles enthesis does not all relate to mechanisms at the tendon-bone junction. In a dorsiflexed foot, the adjacent anterior surface of the tendon presses against the superior tuberosity of the calcaneus (Fig 2a) and this reduces stress concentration at the enthesis itself. What never seems to be acknowledged in accounts of the surgical treatment of Haglund's deformity, is the increase in stress concentration at the enthesis that inevitably follows any removal of bone from the superior tuberosity. The extent to which the stress concentration is increased, depends on the prominence of the tuberosity. Such considerations may be particularly important when contemplating surgery on elite athletes in whom the Achilles tendon may periodically be heavily loaded.

The intermittent contact between the tendon and the superior tuberosity is associated with structural specialisations at both surfaces because of the mutual compression of the tissues. Thus, the calcaneus is covered by a thick fibrocartilaginous periosteum and the deep surface of the tendon is lined by a "sesamoid fibrocartilage" (58; Fig 2a, c,d). The latter term was coined because this fibrocartilage lies within the substance of the tendon itself – i.e. it is comparable to a sesamoid bone. The free movement of

the opposing surfaces is promoted by the retrocalcaneal bursa into which a tongue-like, downward extension of Kager's fat pad extends in a plantar flexed foot. The enthesis itself, the periosteal and sesamoid fibrocartilages, bursa and fat pad collectively constitute an "enthesis organ" (14, 36; Fig 2a). This is a collection of tissues that all contribute to the common function of reducing stress concentration and the risk of failure at the osteotendinous junction.

At the distal tip of the retrocalcaneal bursa, there is no synovial lining, for the walls of the bursa are formed directly by the sesamoid and periosteal fibrocartilages (36,58). While it may surprise some readers to learn that part of the bursa is not lined by synovium, it is logical when one remembers that the bursa has much in common with a synovial joint (36, 59). The sesamoid and periosteal fibrocartilages serve effectively articular cartilages and are thus subject to compression (in a dorsiflexed foot). Consequently, like classical articular cartilage, they cannot be covered with a vascular synovial membrane – this is therefore restricted to the more proximal parts of the bursa (Fig 2a). Degenerative changes paralleling those seen in osteoarthritic articular cartilage (in particular fissuring and chondrocyte clustering) are common in elderly people (58). Detachment of tissue fragments into the bursa is also frequently seen and Rufai et al. (58) have suggested that the inflammatory changes characteristic of retrocalcaneal bursitis may be a secondary consequence of what is primarily an issue of fibrocartilage degeneration.

Four zones of tissue have been described at the enthesis itself – dense fibrous connective tissue, uncalcified fibrocartilage, calcified fibrocartilage and bone (36,58). Between the zones of calcified and uncalcified fibrocartilage is a tidemark, which

marks the outer limit of calcification (Fig 2b). In a healthy tendon, the tidemark is remarkably straight, for it serves as the mechanical boundary between hard and soft tissues. However, it is *not* the tissue boundary – i.e. the *exact* location of the tendon-bone junction. This boundary is the highly irregular interface between the zone of calcified enthesis fibrocartilage and the subchondral bone (Fig 2c). The complex interdigitation of the two tissues in three dimensions is pivotal in securing the tendon to the bone, for little anchorage is provided by the direct continuation of collagen fibres from tendon to bone (60). Thus, the mechanical and tissue boundaries of the tendon are spatially distinct. Conflicting functional demands means that they cannot coincide exactly. The mechanical boundary must be straight in a healthy enthesis so that the tendon is not damaged by jagged edges of bone as the tendon moves. However, the tissue boundary must be highly irregular to promote firm anchorage of tendon to bone. The mechanical paradox is solved in the adult tendon at least, by the presence of a thin coating of calcified fibrocartilage on the bone surface (Fig 2c). This can be visualized as analogous to a layer of cement applied over rough cast brickwork. It is the presence of this layer which accounts for the smooth marking left by the Achilles tendon on a dried bone. The soft tissues fall away from the bone at the level of the tidemark after maceration (61).

As with other fibrocartilaginous entheses, Sharpey's fibres are not a prominent feature of the Achilles tendon insertion. This reflects both the development of the enthesis and the paucity of compact bone in the subchondral plate (Fig. 1a). The study by Gao et al. (62) of the rat Achilles tendon shows that the enthesis fibrocartilage develops by metaplasia of fibroblasts in the dense fibrous connective tissue of the tendon near its bony interface. Thus the fibrocartilage cells are arranged in longitudinal rows (Fig 2b)

simply because the fibroblasts from which they develop also have this arrangement. The fibrocartilage probably develops in response to mechanical stimuli shortly after birth. It is important to recognize that the tissue acts as a "mini growth plate" for the bone (62). As tendon fibroblasts turn into fibrocartilage cells on one side of the enthesis (i.e. the border between the zones of dense fibrous connective tissue and uncalcified fibrocartilage), bone replaces fibrocartilage at the other, by a process analogous to endochondral ossification in the growth plate of a long bone (62).

Enthesis fibrocartilage is not equally obvious over the entire osteotendinous junction. It is more conspicuous superiorly (i.e. in the deep part of the tendon, Fig 2a) than inferiorly - where the enthesis is more fibrous. Curiously, it is in the postero-inferior part that bony spurs most typically develop. The wedge shape of the enthesis fibrocartilage may enable it to act as soft tissue pulley by virtue of its viscoelasticity (60). This complements the action of the more obvious bony pulley that is formed by the superior tuberosity. However, such a soft tissue pulley can only compensate slightly for a marked decrease in the moment arm of the Achilles tendon that inevitably occurs when the foot is dorsiflexed. Quigley & Chaffin (63) have calculated that the distance from the Achilles tendon to the axis of rotation of the ankle joint (i.e. the moment arm) decreases by 40% at 35° of dorsiflexion. This means that greater muscular effort is needed to rise onto the toes and thus greater load is transferred from muscle to tendon and from tendon to bone.

Finally, little attention has been paid to the bone beneath the Achilles tendon enthesis. As stated above, there is a striking absence of any substantial layer of cortical bone (Fig 2a). However, there is a highly ordered array of trabeculae orientated along the

long axis of the Achilles tendon, linking the tendon enthesis to that of the plantar fascia (60). The trabecular pattern suggests there is a line of force transmission within the bone, linking these two soft tissues. In younger individuals in particular, there can also be soft tissue continuity between the Achilles tendon and the plantar fascia (13). The situation is thus analogous to that in the patellar tendon where again there are parallel trabeculae in the anterior region of the patella, and tendon fibres that pass over the anterior surface to establish direct continuity between the patellar and quadriceps tendons (M Benjamin, unpublished observations). In both cases, this presents a classic example of the "myofascial" continuity concept promoted by Myers (15) to emphasize the endless web that is formed by connective tissue throughout the body.

REFERENCES

1. Bramble DM, Lieberman DE. Endurance running and the evolution of *Homo*. *Nature* 2004; 432: 345-352
2. Schepsis AA, Jones H, Haas AL Achilles tendon disorders in athletes - Current Concepts. *Am J Sports Med* 2002; 30:287-305
3. Manter JT. Movements of the subtalar and transverse tarsal joints. *Anat Rec* 1941; 80: 397-410
4. Barfred T. Achilles tendon rupture. *Acta Orthop Scand* 1973; Suppl 152: 7-126
5. White JW Torsion of the Achilles tendon: its surgical significance. *Arch Surg* 1943; 46:784-787
6. Cummins EJ, Anson BJ, Carr BW, Wright RR, Hauser EDW. The structure of the calcaneal tendon (of Achilles) in relation to orthopedic surgery. *Surg Gynecol Obstet* 1946; 83: 107-116
7. Hicks JH. The mechanics of the foot. *J Anat* 1953; 87: 345-357
8. Ker RF, Bennett MB, Bibby SR, Kester RC, Alexander RM. The spring in the arch of the human foot. *Nature* 1987; 325: 147-149.
9. Bergmann RA, Afifi AK, Miyauchi R. *Illustrated Encyclopedia of Human Anatomic Variation*. http://www.uh.org/Providers/Texbooks/AnatomicVariants/AnatomyHP.html2002
10. Williams PL, Warwick R, Dyson M, Bannister LH. *Gray's Anatomy*. 37th Ed. Churchill Livingstone 1989

11. Mellado J, Rosenberg ZS, Beltran J. Low incorporation of soleus tendon: a potential diagnostic pitfall on MR imaging. *Skeletal Radiol* 1998; 27: 222-224

12. Ahmed IM, Lagopoulos M., McConnell P, Soames RW, Sefton GK. Blood supply of the Achilles tendon. *J Orthop Res* 1998; 16: 591-596

13. Snow SW, Bohne WH, DiCarlo E, Chang VK. Anatomy of the Achilles tendon and plantar fascia in relation to the calcaneus in various age groups. *Foot Ankle Int* 1995; 16: 418-421

14. Benjamin M, Moriggl B, Brenner E, Emery P, McGonagle D, Redman S. The "enthesis organ" concept. Why enthesopathies may not present as focal insertional disorders. *Arth Rheum* 2004; 50: 3306-3313.

15. Myers TW. *Anatomy trains. Myofascial meridians for manual and movement therapists.* Edinburgh: Churchill Livingstone, 2001

16. Sadro C, Delinka M. Magnetic resonance imaging of the tendons of the ankle and foot. *Uni Pennsylvania Orthop J* 2000; 13: 1-9

17. Koch S, Tillmann B. Structure of the gastrocnemius tendon. *Orthop Traumatol* 1995; 4: 184-185.

18. Józsa, Lászl Ki ó G. *Human tendons : anatomy, physiology, and pathology.* Champaign, IL : Human Kinetics, 1997.

19. Myerson MS, McGarvey W. Disorders of the Achilles tendon insertion and Achilles tendonitis. *Instr Course Lect* 1998; 48:211-218

20. Loetzke HH. Uber die Achillessehne mit ihnen Fascienverhaltnissen beim Menschen und dem Subcutannraum im Bereich der Wadenmuskulatur. *Anat Anz* 1956; 103: 287-304

21. Schnorrenberg G Uber die Gefassversorgung der Achillessehne. *Morph Jb* 1962; 103: 428-456

22. Webb J, Moorjani N, Radford M. Anatomy of the sural nerve and its relation to the Achilles tendon. *Foot Ankle Int* 2000; 21: 475-477

23. Frey C, Rosenberg Z, Shereff MJ, Kim H. The retrocalcaneal bursa: anatomy and bursography. *Foot Ankle* 1992; 13: 203-207

24. Fritsch H. Sectional anatomy of connective tissue structures in the hindfoot of the newborn child and the adult. *Anat Rec* 1996; 246:147-154

25. Bottger BA, Schweitzer ME, El-Noueam KI, Desai M. MR imaging of the normal and abnormal retrocalcaneal bursae. *Am J Roentgenol.* 1998; 170:1239-1241

26. Canoso JJ, Wohlgethan JR, Newberg AH, Goldsmith MR. Aspiration of the retrocalcaneal bursa. *Ann Rheum Dis* 1984; 43:308-312

27. Canoso JJ, Liu N, Traill MR, Runge VM. Physiology of the retrocalcaneal bursa. *Ann Rheum Dis* 1988; 47: 910-912

28. Carr AJ, Norris SH. The blood supply of the calcaneal tendon. *J Bone Joint Surg* 1989; 71:100-101

29. Schmidt-Rohlfing B, Graf, J., Schneider, U., Niethard, F.U.: The blood supply of the Achilles tendon. *Int Orthop* 1992;16:29-31

30. Lagergren C, Lindholm A. Vascular distribution in the Achilles tendon. *Acta Chir Scand* 1958-59; 116: 491-495

31. Langberg H, Bulow J, Kjaer M. Blood flow in the peritendinous space of the human Achilles tendon during exercise. *Acta Physiol Scand* 1998; 163:149-153

32. Zantop T, Tillmann, B., Petersen, W.,Tillmann B, Petersen W. Quantitative assessment of blood vessels of the human Achilles tendon: an immunohistochemical cadaver study. *Arch Orthop Trauma Surg*: 2003; 123: 501-504

33. Edwards DAW. The blood supply and lymphatic drainage of tendons. *J Anat* 1946; 80: 147-152

34. Karcz MJ, Skawina, A., Gorczyca, J., Danilewicz, M. The arterial vascularisation of the human calcaneus (Achilles) tendo during the prenatal development. *Folia Morphol (Warsz)* 1996; 55:306-308

35. Astrom M, Westlin N. Blood flow in the human Achilles tendon assessed by laser doppler flowmetry. *J Orthop Res* 1994; 12: 246-252

36. Benjamin M, McGonagle D. The anatomical basis for disease localisation in seronegative spondyloarthropathy at entheses and related sites. *J Anat* 2001; 199: 503-526

37. Aspenberg P, Forslund C. Bone morphogenetic proteins and tendon repair. *Scand J Med Sci Sports* 2000; 10: 372-375

38. Stilwell DL Jr. The innervation of tendons and aponeuroses. *Am J Anat* 1957; 100: 289-317

39. Lang J. Uber das Verschiebegewebe der Achillessehne. *Anat Anz* 1960; 108: 225-237

40. Marchand R, Bridgman CF, Shumpert E, Eldred E. Association of tendon organs with spindles in muscles of the cat's leg. *Anat Rec* 1971;169:23-32

41. Ackermann PW, Spetea M, Nylander I, Ploj K, Ahmed M, Kreicbergs A. An opioid system in connective tissue: a study of Achilles tendon in the rat. *J Histochem Cytochem* 2001; 49: 1387-1395

42. Fenwick SA, Hazleman BL, Riley GP. The vasculature and its role in the damaged and healing tendon. *Arth Res* 2002; 4: 252-260

43. Yu JS, Popp JE, Kaeding CC, Lucas J. Correlation of MR imaging and pathologic findings in athletes undergoing surgery for chronic patellar tendonitis. *Am J Roentgenol* 1995; 165:115-118

44. Astrom M, Rausing A. A survey of surgical and histopathologic findings. *Clin Orthop* 1995; 316:151-164

45. Kvist M, Jozsa L, Jarvinen MJ, Kvist H: Chronic Achilles paratenonitis in athletes: a histological and histochemical study. *Pathology* 1987; 19:1-11

46. Waggett AD, Ralphs JR, Kwan AP, Woodnutt D, Benjamin M. Characterization of collagens and proteoglycans at the insertion of the human Achilles tendon. *Matrix Biol* 1998; 16: 457-470

47. Viidik A. Tensile strength properties of Achilles tendon systems in trained and untrained rabbits. *Acta Orthop Scand* 1962; 10: 261-272

48. Birk DE, Fitch JM, Babiarz JP, Doane KJ, Linsenmayer TF (1990). Collagen fibrillogenesis in vitro: interaction of types I and V collagen regulates fibril diameter. *J Cell Sci* 95:649-657.

49. Ker RF. The implications of the adaptable fatigue quality of tendons for their construction, repair and function. *Comp Biochem Physiol* 2002; 133A: 987-1000

50. Ireland D, Harrall R, Curry V, Holloway G, Hackney R, Hazleman B, Riley G. Multiple changes in gene expression in chronic human Achilles tendinopathy. *Matrix Biol* 2001; 20:159-169

51. McNeilly CM, Banes AJ, Benjamin M, Ralphs JR. Tendon cells in vivo form a three dimensional network of cell processes linked by gap junctions. *J Anat* 1996; 189: 593-600

52. Waggett AD, Benjamin M, Ralphs JR. Gap junctions comprising connexion 32 and 43 differentially regulate tendon fibroblast response to cyclic mechanical load. *Matrix Biol* 2005 (submitted).

53. Chao W, Deland JT, Bates JE, Kenneally SM. Achilles tendon insertion: an in vitro anatomic study. *Foot Ankle Int.* 1997; 18:81-84.

54. Kolodziej P, Glisson RR, Nunley JA. Risk of avulsion of the Achilles tendon after partial excision for treatment of insertional tendonitis and Haglund's deformity: a biomechanical study. *Foot Ankle Int* 1999; 20: 433-437

55. Benjamin M, Redman S, Milz S, Buttner A, Amin A, Moriggl B, Brenner E, Emery P, McGonagle D, Bydder G. Adipose tissue at entheses: the rheumatological implications of its distribution. A potential site of pain and stress dissipation? *Ann Rheum Dis* 2004b; 63: 1549-1555

56. Benjamin M, Kumai T, Milz S, Boszczyk BM, Boszczyk AA, Ralphs JR. The skeletal attachment of tendons - tendon entheses. *Comp Biochem Phys A Mol Integr Physiol* 2002; 133:931-945

57. Schneider H. Zur Struktur der Sehnenansatzzonen. *Z. Anat* 1956; 119: 431-456

58. Rufai A, Ralphs JR, Benjamin M. Structure and histopathology of the insertional region of the human Achilles tendon. *J Orthop Res* 1995; 13: 585-593.

59. Canoso JJ. The premiere enthesis. *J Rheumatol* 1998; 25: 1254-1256

60. Milz S, Rufai A, Buettner A, Putz R, Ralphs JR, Benjamin M. Three dimensional reconstructions of the Achilles tendon enthesis in Man. *J Anat* 2002; 200: 145-152

61. Benjamin M, Evans EJ, Copp L. The histology of tendon attachments in man. *J Anat* 1986; 149: 89-100

62. Gao J, Messner K, Ralphs JR, Benjamin M. An immunohistochemical study of enthesis development in the medial collateral ligament of the rat knee joint. *Anat Embryol* 1996; 194: 399-406

63. Quigley BM, Chaffin DB. A computerized biomechanical model applied to analysis of skiing. *Med Sci Sports*. 1971; 3: 89-96

LEGENDS

Fig 1. Gross anatomy of the Achilles tendon. (a) A posterior view of the right Achilles tendon indicating with horizontal yellow lines, the levels at which the transverse sections featured in b-f are taken. Note the close relationship of the Achilles (TA) and gastrocnemius (TG) tendons to the sural nerve (SN). MG, muscle belly of gastrocnemius. (b-f) Transverse sections of the Achilles tendon to show the change in shape of the tendon from proximal to distal. Figures b-f inclusive correspond (from above down) to the 5 horizontal lines shown in 'a'. Note that the gastrocnemius tendon is very broad and flat (b), that the Achilles tendon in the region vulnerable to ruptures is oval (c) and that the tendon flares out again (d-f) as it approaches the calcaneus (C). Sections taken at levels d-e pass through the pre-Achilles fat pad (F) and the retrocalcaneal bursa (B) into which the fat pad protrudes. At the enthesis itself (f), the extremely flattened Achilles tendon has a marked anterior curvature. (g) Here, both gastrocnemius and soleus have been partly removed so as to demonstrate the intramuscular tendon of soleus (arrow). MS, muscle belly of soleus. (h) The union of the tendons of soleus (TS) and gastrocnemius that form the Achilles tendon at mid calf level. (i) A sagittal section through the calcaneus to show the Achilles tendon enthesis (E) and the prominent pre-Achilles fat pad (F). The tip of the fat pad is quite distinctive from the rest and protrudes into the retrocalcaneal bursa (B) between the Achilles tendon and the superior tuberosity of the calcaneus (ST). (j) A posterior view of the Achilles tendon to show its associated paratenon (P). A rectangular window has been cut into the paratenon exposing the underlying Achilles tendon in which a slight obliquity of the tendon fascicles can be noted (arrow).

Fig. 2 Microscopic anatomy of the Achilles tendon 'enthesis organ'. (a) Low power view of a sagittal section of the enthesis organ. The enthesis itself is characterised by a prominent enthesis fibrocartilage (EF), which is thickest in the deepest part of the attachment site (arrowheads). Immediately proximal to the osteotendinous junction, the deep surface of the tendon is related to the superior tuberosity (ST) of the calcaneus, but is separated from it by the retrocalcaneal bursa (RB). Protruding into the bursa is the pre-Achilles fat pad (FP) that is covered with a synovial membrane (arrows). The most distal part of the bursa is lined directly by sesamoid (SF) and periosteal fibrocartilages (PF). The former lies in the deep surface of the Achilles tendon, immediately adjacent to the enthesis, and the latter covers the superior tuberosity in a dorsiflexed foot. These fibrocartilages are shown in further detail in figure d. Note the epitenon (E) on the posterior surface of the tendon with several blood vessels (BV) visible within it and the paucity of a subchondral bone plate at the enthesis. (b) A high power view of the enthesis fibrocartilage in the region either side of the tidemark (TM). Note the longitudinal rows of fibrocartilage cells (arrows) in the zone of uncalcified fibrocartilage (UF) and the zone of calcified fibrocartilage (CF) which lies immediately deep to the tidemark. (c) A high power view of the enthesis fibrocartilage in the region either side of the tidemark, showing the complex interdigitations of the zone of calcified fibrocartilage with the underlying bone (B). (d) A high power view of the lfibrocartilaginous lining of the distal part of the retrocalcaneal bursa showing sesamoid fibrocartilage in the deep surface of the tendon and a periosteal fibrocartilage covering the bone. Note that neither fibrocartilage is covered with synovium. Scale bars a = 2mm; b-d = 100 μm. Figure c is of a specimen stained with toluidine blue, all the other sections are stained with Masson's trichrome.

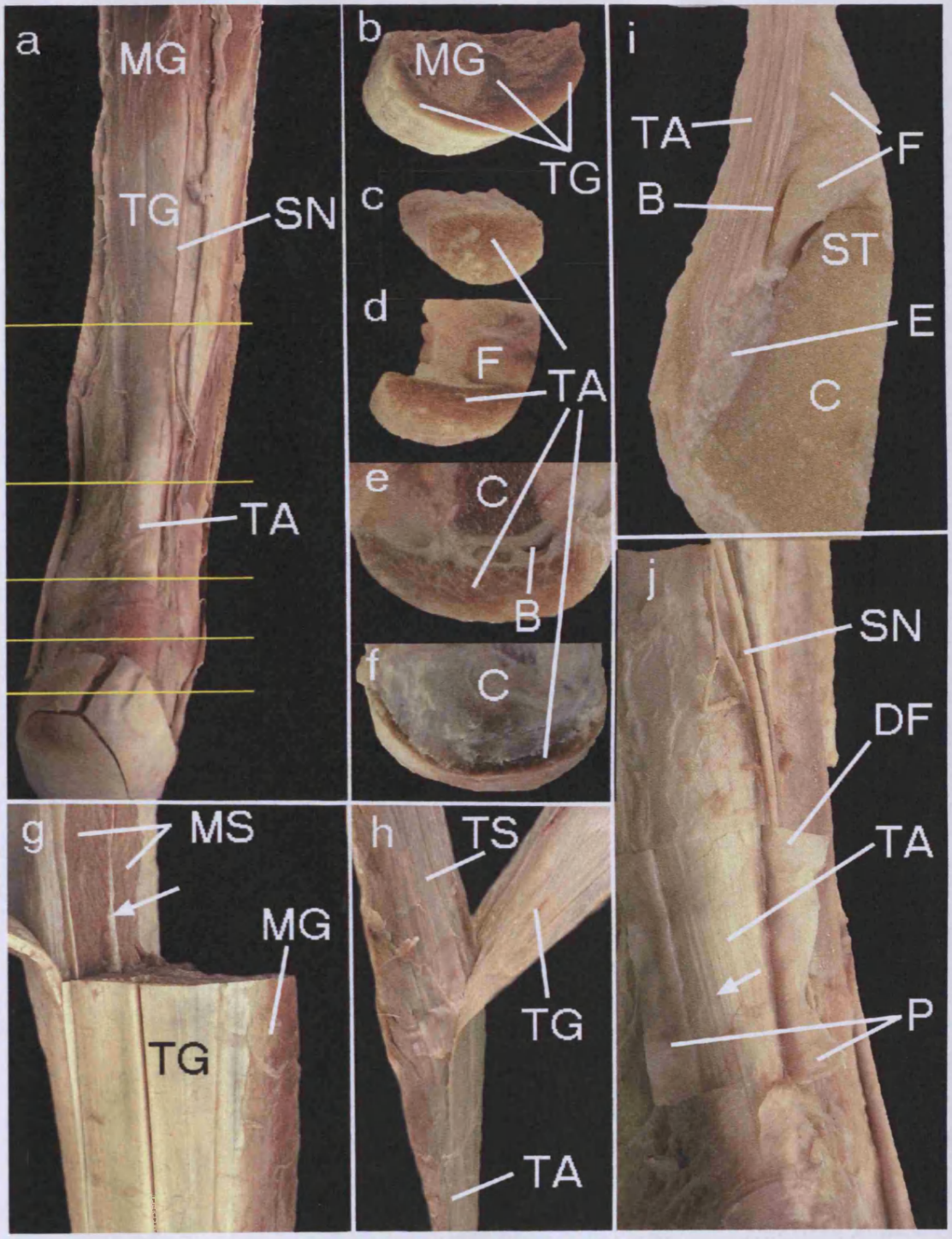
a
MG
TG
SN
TA
b
MG
TG
c
d
F
TA
e
C
B
f
C
i
TA
F
B
ST
E
C
j
SN
DF
TA
P
g
MS
MG
TG
h
TS
TG
TA